UTS UNIVERSITY OF TECHNOLOGY SYDNEY

DEVELOPMENT, MECHANICAL BEHAVIOUR AND IMPACT RESISTANCE OF SUSTAINABLE STEEL FIBRE-REINFORCED DRY ULTRA-HIGH PERFORMANCE CONCRETE (DUHPC)

by Ruizhe Shao

Thesis submitted in fulfilment of the requirements for the degree of

DOCTOR OF PHILOSOPHY

under the supervision of

Principal Supervisor:	Professor Chengqing Wu
Co-Supervisor:	Doctor Jun Li

University of Technology Sydney
Faculty of Engineering and Information Technology

June 2023

Certificate of Original Authorship

I, Ruizhe Shao, declare that this thesis, is submitted in fulfilment of the requirements for the award of Doctor of Philosophy, in the School of Civil and Environmental Engineering at the University of Technology Sydney.

This thesis is wholly my own work unless otherwise referenced or acknowledged. In addition, I certify that all information sources and literature used are indicated in the thesis.

This document has not been submitted for qualifications at any other academic institution.

This research is supported by the Australian Government Research Training Program.

Signature: Production Note:
Signature removed prior to publication.

Date: 15 June 2023

Acknowledgement

This study and degree are smoothly completed under the careful guidance of my supervisors, Prof. Chengqing Wu and Dr. Jun Li. Their serious scientific attitude, rigorous academic spirit, and efficient work style have deeply encouraged and infected me. They not only gave me meticulous guidance in academics, but also showed me the thoughtful care in my life. Here I would like to express my sincere gratitude and high respect to them. Moreover, I particularly thank Prof. Zhongxian Liu, Dr. Yu Su, Dr. Shenchun Xu, Dr. Pengtao Wu and Dr. Xuejie Zhang for their help and convenience in my study and life during COVID-19. I also would like to acknowledge the postgraduate students Changle Liu, Ying Han, Zhouxu Sun and Xueyan Zhang for their assistance and support with the experiments performed.

I would particularly like to heartfeltly thank all staffs at UTS Mortar and Concrete Lab, especially Mr. Rami Haddad, Mr. Mulugheta Hailu and Miss Ann Yan. The specialized knowledge, rigorous attitude, team-work spirit and warm-hearted help you provided and presented will be of great help to my future academic work.

I would extremely grateful to my parents and wife. It is your constant love, concern and encouragement that makes me not afraid of the setbacks and failures, and renders me more mature and go further on the road of my life.

Lastly, I would like to acknowledge UTS International Research Scholarship and UTS President's Scholarship for providing the financial support for my PhD study.

List of Publications

1. Shao, R., Wu, C., Li, J., 2022. A comprehensive review on dry concrete: Application, raw material, preparation, mechanical, smart and durability performance. *Journal of Building Engineering*, 55, 104676.

2. Shao, R., Wu, C., Li, J., Liu, Z., 2022. Development of sustainable steel fibre-reinforced dry ultra-high performance concrete (DUHPC). *Journal of Cleaner Production*, 337, 130507.

3. Shao, R., Wu, C., Li, J., Liu, Z., 2022. Investigation on the mechanical characteristics of multiscale mono/hybrid steel fibre-reinforced dry UHPC. *Cement and Concrete Composites*, 133, 104681.

4. Shao, R., Wu, C., Li, J., Liu, Z., Wu, P., Yang, Y., 2023. Mechanical behaviour and environmental benefit of eco-friendly steel fibre-reinforced dry UHPC incorporating high-volume fly ash and crumb rubber. *Journal of Building Engineering*, 65, 105747.

5. Shao, R., Wu, C., Li, J., Liu, Z., 2023. Repeated impact resistance of steel fibre-reinforced dry UHPC: Effects of fibre length, mixing method, fly ash content and crumb rubber. *Composite Structures*. Accepted.

Table of Contents

Certificate of Original Authorship i

Acknowledgement ii

List of Publications iii

List of Figures ix

List of Tables xix

List of Abbreviations xxii

Abstract xxvii

Chapter 1 Introduction 1

1.1 Background 1

1.2 Objectives 4

1.3 Outline 6

Chapter 2 Literature Review 9

2.1 Raw material and preparation method 9

2.1.1 Cementitious material 9

2.1.2 Aggregate 11

2.1.3 Chemical additive and fibre 12

2.1.4 Preparation method 13

2.2 Mixture basic performance 14

2.2.1 Adiabatic temperature rising 14

2.2.2 Consistency and unit weight 16

2.3 Static mechanical property 18

2.3.1 Strength behaviour 18

2.3.2 Modulus of elasticity 32

2.4 Dynamic mechanical performance 34

2.5 Summary and discussion 38

Chapter 3 Development of Sustainable Steel Fibre-Reinforced DUHPC 41

3.1 Introduction 41

3.2 Materials and proportioning design 43

3.2.1 Raw materials 43

3.2.2 Proportioning design method 46

3.3 Specimen preparation, curing and testing 48

3.3.1 Specimen preparation 48

3.3.2 Curing regime 49

3.3.3 Test procedure 50

3.4 Results and discussion 52

3.4.1 Orthogonal experiment results 52

3.4.2 DUHPC experimental results 62

3.4.3 Microstructure analysis (SEM) 81

3.5 Environmental impact of developed DUHPC 83

3.6 Conclusion 86

Chapter 4 Mechanical Characteristic of Multiscale Mono and Hybrid Steel FR-DUHPC 88

4.1 Introduction 88

4.2 Materials, mix proportion and preparation 90

4.2.1 Raw materials and proportioning 90

4.2.2 Preparation and curing regime 93

4.3 Testing program 95

4.4 Results and discussion 97

4.4.1 Compression behaviour 99

4.4.2 Flexure behaviour 107

4.4.3 Split-tension behaviour 116

4.4.4 Discussion 120

4.5 Multivariate regression analysis 124

4.6 Conclusion 132

Chapter 5 Mechanical Behaviour and Environmental Benefit of Eco-Friendly

Steel FR-DUHPC Containing HVFA and Crumb Rubber 135

5.1 Introduction 135

5.2 Experimental programme 137

5.2.1 Raw materials 137

5.2.2 Mix proportions 140

5.2.3 Preparation and curing regime 142

5.2.4 Test setup 143

5.3 Results and discussion 145

5.3.1 FR-DUHPC incorporating HVFA 145

5.3.2 FR-DUHPC incorporating HVFA and CR 163

5.4 Eco-friendly assessment 181

5.4.1 Cost analysis 181

5.4.2 Environmental impact analysis 183

5.5 Conclusion 187

Chapter 6 Repeated Impact Resistance of Steel FR-DUHPC: Effects of Fibre Length, Mixing Method, FA Content and CR Addition 190

6.1 Introduction 190

6.2 Experimental programme 193

6.2.1 Materials and sample preparation 193

6.2.2 Testing procedure 197

6.3 Results and discussion 200

6.3.1 Flexural impact behaviour 200

6.3.2 Weibull distribution analysis 221

6.4 Conclusion 225

Chapter 7 Conclusions and Recommendations 228

7.1 Conclusions 228

7.2 Recommendations for future work 232

References 235

List of Figures

Fig. 1.1. RCC engineering applications of (a) dams [24] and (b) pavements [25]. 3

Fig. 1.2. DCC prefabricated units of (a) sewer pipes [28] and (b) paving blocks [34]. 4

Fig. 2.1. Preparation methods for fresh dry concrete: (a) mechanical consolidation and vibration [30]; (b) vibrating table compaction [6] and (c) roller compaction [94]. 14

Fig. 2.2. Relationships between rubber content and (a) density decrease as well as (b) Vebe time of RCC [42]. 17

Fig. 2.3 Relationships between mechanical strength behaviour and FA content of RCC in which FA substitutes partial (a, c and e) cement and (b, d and f) aggregate [99]. 24

Fig. 2.4. SEM images of ITZ between EAF slag and paste under 200 and 1000 magnifications [73]. 27

Fig. 2.5. Cracking and volume expansion of rubberized DCC paving blocks [2]. 27

Fig. 2.6. Crack trajectory envelope for different mono/hybrid FRCC samples under Mode I applied loading [88]. 30

Fig. 2.7. Typical flexural failure patterns and crack bridging by fibres of fibre-reinforced DCC pipe [30]. 31

Fig. 2.8. (a) MOE variation and (b) its relationship with compressive strength of DCC blocks containing various contents of waste marble and types of cement [117]. 34
Fig. 2.9. Seismic response of RCCD after Wenchuan earthquake: (a) downstream view; (b) upstream view; (c) left abutment and (d) right abutment [118]. 38
Fig. 3.1. PSD curves of raw materials used in dry-cast cement mortar and DUHPC. 45
Fig. 3.2. Preparation process of FR-DUHPC samples for static mechanical tests. 49
Fig. 3.3. Dry-cast mortar of (a) cubic, (b) beam and (c) cylindrical samples after curing. 50
Fig. 3.4. Split-tension test setup (left) and failure pattern (right) of the mortar sample. 52
Fig. 3.5. Effects of various factors on unit weight of dry-cast cement mortar.....54
Fig. 3.6. Effects of various factors on compressive strength of dry-cast cement mortar. 56
Fig. 3.7. Effects of various factors on rupture modulus of dry-cast cement mortar. 58
Fig. 3.8. Effects of various factors on split-tensile strength of dry-cast cement mortar. 60
Fig. 3.9. Effects of initial curing temperature and fibre dosage on density of DUHPC. 64

Fig. 3.10. Effects of initial curing and fibre dosage on compressive strength of DUHPC. 66

Fig. 3.11. Development of various strength values for DUHPC under different initial curing temperatures: (a) 0.5%; (b) 1.0%; (c) 1.5% and (d) 2.0% fibre dosage. 67

Fig. 3.12. Typical 28-day compressive test data of DUHPC samples under various initial curing temperatures: (a) 0.5%; (b) 1.0%; (c) 1.5% and (d) 2.0% fibre dosage. 68

Fig. 3.13. (a) 28-day static MOE and (b) its relationship with compressive strength of DUHPC reinforced with different fibre dosages. 69

Fig. 3.14. Effects of curing temperature and fibre dosage on flexural strength of DUHPC. 71

Fig. 3.15. Typical 28-day flexural test data of DUHPC samples under various initial curing temperatures: (a) 0.5%; (b) 1.0%; (c) 1.5% and (d) 2.0% fibre dosage. 72

Fig. 3.16. Typical flexural-tensile failure patterns of (a) 0.5%; (b) 1.0%; (c) 1.5% and (d) 2.0% FR-DUHPC samples after bending tests. 73

Fig. 3.17. Effects of initial curing and fibre dosage on split-tensile strength of DUHPC. 75

Fig. 3.18. Typical 28-day split-tensile test data of DUHPC samples under various initial curing temperatures: (a) 0.5%; (b) 1.0%; (c) 1.5% and (d) 2.0% fibre dosage. 76

Fig. 3.19. (a) Typical split-tensile failure and (b) delamination of FR-DUHPC samples. 77

Fig. 3.20. Relationships between compressive and flexural strength of 0.5-2.0 Vol-% FR-DUHPC samples after (a) 1 day of moist/steam curing and (b) following 7/28 days of normal-temperature water curing. 80

Fig. 3.21. Relationships between compressive and split-tensile strength of 0.5-2.0 Vol-% FR-DUHPC samples after (a) 1 day of moist/steam curing and (b) following 7/28 days of normal-temperature water curing. 80

Fig. 3.22. Microstructure for DUHPC mixtures after 1 day of (a) 30 ℃; (b) 40 ℃; (c) 50 ℃ and (d) 60 ℃ moist/steam curing based on SEM. 83

Fig. 4.1. Main chemical compositions of cementitious materials for FR-DUHPC. 91

Fig. 4.2. Preparation procedures of FR-DUHPC samples and the observed fibre agglomeration upon stirring. 94

Fig. 4.3. (a) Moist/steam curing device and typical (b) prism and (c) cylinder FR-DUHPC samples before testing. 95

Fig. 4.4. Schematic diagrams of FR-DUHPC samples under (a) bending and (b) splitting-tensile loads. 97

Fig. 4.5. Compressive strength of mono FR-DUHPC samples after 1, 7 and 28-day curing: (a) 6-mm fibre; (b) 10-mm fibre; (c) 13-mm fibre and (d) 28-day strength comparison regarding control samples. 100

Fig. 4.6. Effects of hybrid fibre reinforcement on compressive strength of DUHPC. 102

Fig. 4.7. Typical 28-day compressive stress-strain curves of (a-c) mono and (d) hybrid FR-DUHPC samples. 103
Fig. 4.8. Compressive total energy absorption and toughness index of (a) control; (b) mono and (c) hybrid FR-DUHPC samples after 1, 7 and 28-day curing. ... 105
Fig. 4.9. (a) 28-day static MOE and (b) its relationship with compressive strength of mono and hybrid FR-DUHPC samples. 106
Fig. 4.10. Flexural strength of mono FR-DUHPC samples after 1, 7 and 28-day curing: (a) 6-mm fibre; (b) 10-mm fibre; (c) 13-mm fibre and (d) 28-day strength comparison regarding control samples. 108
Fig. 4.11. Effects of hybrid fibre reinforcement on flexural strength of DUHPC. 109
Fig. 4.12. Typical 28-day flexural load-deflection curves of (a-c) mono and (d) hybrid FR-DUHPC samples. 112
Fig. 4.13. Flexural cracking strength and its ratio to the ultimate strength of (a) mono and (b) hybrid FR-DUHPC samples after 28-day curing. 114
Fig. 4.14. Flexural toughness (FT) and toughness indexes (FTI) of (a) mono and (b) hybrid FR-DUHPC samples after 28-day curing. 115
Fig. 4.15. Split-tensile strength of mono FR-DUHPC samples after 1, 7 and 28-day curing: (a) 6-mm fibre; (b) 10-mm fibre; (c) 13-mm fibre and (d) 28-day strength comparison regarding control samples. 117
Fig. 4.16. Effects of hybrid fibre reinforcement on split-tensile strength of DUHPC. 118

Fig. 4.17. Typical 28-day split-tensile load-displacement curves of (a-c) mono and (d) hybrid FR-DUHPC samples. 119
Fig. 4.18. Fibre distribution within the fracture surface of 0.5-2.0% FR-DUHPC samples after bending tests. 124
Fig. 4.19. Standardized residual and normal probability of (a-b) compressive, (c-d) flexural and (e-f) split-tensile strengths related using best-fit models. 128
Fig. 4.20. Comparisons between the experimental and predicted results of (a-b) flexural and (c-d) split-tensile strengths related using Model 7 and Model 8#..132
Fig. 5.1. Appearance of silica fume, FA, GGBS, CR particles and steel fibres. 140
Fig. 5.2. Water curing and typical FR-DUHPC samples containing CR aggregate. 143
Fig. 5.3. Schematics of (a) uniaxial compression and (b) four-point bending test. 144
Fig. 5.4. Effect of FA substitution level on hardened density of FR-DUHPC....146
Fig. 5.5. Effect of FA substitution level on compressive strength of FR-DUHPC. 148
Fig. 5.6. Effect of FA substitution on compressive specific strength of FR-DUHPC. 151
Fig. 5.7. Contribution rate of FA effect to compressive strength of FR-DUHPC. 152
Fig. 5.8. Typical (a) 28-day and (b) 60-day compressive stress-strain relationships of FR-DUHPC incorporating various contents of FA. 153

Fig. 5.9. (a) 28/60-day static MOE and (b) its relationship with compressive strength of FR-DUHPC incorporating various contents of FA. 154
Fig. 5.10. Effect of FA substitution level on flexural strength of FR-DUHPC....156
Fig. 5.11. Effect of FA substitution on flexural specific strength of FR-DUHPC. 157
Fig. 5.12. Contribution rate of FA effect to flexural strength of FR-DUHPC. 158
Fig. 5.13. Typical (a) 28-day and (b) 60-day flexural load-deflection relationships of FR-DUHPC incorporating various contents of FA. 160
Fig. 5.14. (a) Flexural cracking strength and (b) its ratio to the ultimate strength of 20-60% FA-incorporated FR-DUHPC after 28- and 60-day curing. 160
Fig. 5.15. (a) Strength ratio at various ages and (b) relationship between compressive and flexural strengths of FR-DUHPC incorporating various contents of FA. 162
Fig. 5.16. Correlation between FA content and (a) compressive as well as (b) flexural strengths of FR-DUHPC. 162
Fig. 5.17. Effects of CR substitution and fibre dosage on density of FR-DUHPC. 165
Fig. 5.18. Effects of CR substitution and fibre volume dosage on compressive strength of FR-DUHPC. 167
Fig. 5.19. Microstructure images in terms of ITZs between CR aggregate and (a) cement paste as well as (b) steel fibres of rubberized dry concrete based on SEM. 167

Fig. 5.20. Typical (a) 28-day and (b) 60-day compressive stress-strain relationships of 1.5% FR-DUHPC incorporating various contents of CR aggregate. 169
Fig. 5.21. Typical (a) 28-day and (b) 60-day compressive stress-strain relationships of 0.5-1.5% FR-DUHPC incorporating various contents of CR aggregate. 170
Fig. 5.22. (a) 28/60-day static MOE and (b) its relationship with compressive strength of 0.5-1.5% FR-DUHPC incorporating various contents of CR aggregate. 171
Fig. 5.23. Effects of CR substitution and fibre dosage on flexural strength of FR-DUHPC. 173
Fig. 5.24. Typical (a) 28-day and (b) 60-day flexural load-deflection relationships of 1.5% FR-DUHPC incorporating various contents of CR aggregate. 176
Fig. 5.25. Typical (a) 28-day and (b) 60-day flexural load-deflection relationships of 0.5-1.5% FR-DUHPC incorporating various contents of CR aggregate. 176
Fig. 5.26. (a) Flexural cracking strength and (b) its ratio to the ultimate strength of 0.5-1.5% FR-DUHPC incorporating various contents of CR aggregate after 28- and 60-day curing. 178
Fig. 5.27. Correlation between hardened density and (a) compressive as well as (b) flexural strengths of FR-DUHPC incorporating CR aggregate. 180
Fig. 5.28. (a) Strength ratio at various ages and (b) relationship between compressive and flexural strengths of FR-DUHPC incorporating CR aggregate. 180

Fig. 5.29. Estimated cost of FR-DUHPC incorporating various contents of (a) FA and (b) CR aggregate. 183
Fig. 5.30. Embodied CO_2 emission of FR-DUHPC incorporating various contents of (a) FA and (b) CR aggregate. 185
Fig. 5.31. Embodied CO_2 index of FR-DUHPC incorporating various contents of (a) FA and (b) CR aggregate. 185
Fig. 5.32. Comparisons of embodied CO_2 emission of the developed 20-60% FA-mixed FR-DUHPC and other self-compacting FR-UHPC or FR-dry concrete. 186
Fig. 6.1. Appearances of the major raw materials of FA, CR aggregate and steel fibre. 194
Fig. 6.2. (a) Detailed preparation flow and (b) typical FR-DUHPC beam samples prior to impact test. 197
Fig. 6.3. Low-speed drop-weight impact test: (a) testing machine overview and (b) setup schematic diagram. 198
Fig. 6.4. Judgment basis for (a) initial cracking and (b) ultimate damage of samples. 199
Fig. 6.5. Schematic of four-point bending residual strength test setup. 200
Fig. 6.6. Impact number of (a) initial crack and (b) ultimate failure of mono/hybrid FR-DUHPC after 1, 7 and 28-day curing. 205
Fig. 6.7. Impact number of (a) initial crack and (b) ultimate failure of HVFA-/CR-mixed FR-DUHPC after 1, 7 and 28-day curing. 207
Fig. 6.8. Impact ductility of (a) mono/hybrid and (b) HVFA-/CR-mixed FR-DUHPC after 1, 7 and 28-day curing. 209

Fig. 6.9. Typical impact force-time curves at (a) initial cracking and (b) final failure of FR-DUHPC samples. 211

Fig. 6.10. Time histories of impact force of mono/hybrid FR-DUHPC at (a) initial cracking and (b) ultimate failure. 212

Fig. 6.11. Time histories of impact force of (a) HVFA50- and (b) CR-mixed FR-DUHPC at initial cracking and ultimate failure. 213

Fig. 6.12. Typical ultimate failure patterns of (a-c) mono and (d-k) hybrid FR-DUHPC beam samples after repeated drop-weight impacts. 215

Fig. 6.13. Ultimate failure patterns of (a) HVFA50- and (b) CR-mixed FR-DUHPC beam samples after repeated drop-weight impacts along with (c) microstructure image of prepared CR-mixed dry concrete. 217

Fig. 6.14. Residual flexural strength and capacity ratio of mono/hybrid FR-DUHPC samples after impact tests. 219

Fig. 6.15. Residual flexural strength and capacity ratio of HVFA-/CR-mixed FR-DUHPC samples after impact tests. 221

Fig. 6.16. 28-day linear regressions of ultimate failure impact numbers (N_d) for (a) mono/hybrid and (b) HVFA-mixed FR-DUHPC in Weibull distribution. 223

Fig. 6.17. Predicted 28-day impact numbers at ultimate failure of (a) mono; (b) hybrid and (c) HVFA-mixed FR-DUHPC in terms of different levels of reliability. 225

List of Tables

Table 2.1 Effects of alternative materials (AM) on strength behaviour of dry concrete from literature (Increase: ↑, Decrease: ↓).....19

Table 2.2 Effects of various fibres on strength behaviour of dry concrete from literature (Increase: ↑, Decrease: ↓).....21

Table 3.1 Components and physical characteristics of silica fume, FA and GGBS. 44

Table 3.2 Factors and levels of the orthogonal experiments. 47

Table 3.3 Orthogonal experiments for mortar mixtures and the relevant test results. 47

Table 3.4 Response table for unit weight of dry-cast cement mortar. 54

Table 3.5 ANOVA table for unit weight of dry-cast cement mortar. 54

Table 3.6 Response table for compressive strength of dry-cast cement mortar. 56

Table 3.7 ANOVA table for compressive strength of dry-cast cement mortar. ...56

Table 3.8 Response table for rupture modulus of dry-cast cement mortar. 58

Table 3.9 ANOVA table for rupture modulus of dry-cast cement mortar.....58

Table 3.10 Response table for split-tensile strength of dry-cast cement mortar. 59

Table 3.11 ANOVA table for split-tensile strength of dry-cast cement mortar.....60

Table 3.12 Testing results of optimal mix proportion for dry-cast cement mortar. 62

Table 3.13 Summary of density and mechanical property test results of prepared FR-DUHPC. 63

Table 3.14 Correlation models between compression and flexure/split-tension for FR-DUHPC. 80

Table 3.15 Comparisons of ASCMs content and strength values (28 days) of UHPC and developed DUHPC. 85

Table 4.1 Mixture proportions of mono and hybrid FR-DUHPC. 92

Table 4.2 Quasi-static testing approaches and studied parameters of mono/hybrid FR-DUHPC. 97

Table 4.3 Summary of static mechanical test results of mono FR-DUHPC samples. 98

Table 4.4 Summary of static mechanical test results of hybrid FR-DUHPC samples. 98

Table 4.5 Deflection ductility index of mono and hybrid FR-DUHPC samples. 112

Table 4.6 Regression results of strength behaviour for mono FR-DUHPC. 126

Table 4.7 ANOVA and individual influencing factor results based on Model 1. 129

Table 4.8 Regression results of flexural tensile strength for mono FR-DUHPC (considering X_{fc}). 130

Table 5.1 Main chemical compositions of cementitious materials for FR-DUHPC. 139

Table 5.2 Physical characteristics and composition of CR aggregate. 139

Table 5.3 Mixture proportions of eco-friendly FR-DUHPC by weight. 141

Table 5.4 Density and mechanical test results of FR-DUHPC incorporating HVFA. 145

Table 5.5 Compressive strength increment at different time intervals. 149

Table 5.6 Flexural strength increment at different time intervals.....156

Table 5.7 Density and mechanical results of FR-DUHPC containing HVFA and CR. 163

Table 6.1 Mixture proportions of studied FR-DUHPC by weight. 195

Table 6.2 Summary of drop-weight test results of mono/hybrid FR-DUHPC. ..201

Table 6.3 Summary of drop-weight test results of HVFA-/CR-mixed FR-DUHPC. 202

Table 6.4 Static and dynamic residual flexural results of mono/hybrid FR-DUHPC. 218

Table 6.5 Static and dynamic residual flexural results of HVFA-/CR-mixed FR-DUHPC. 220

Table 6.6 Weibull regression parameters of the studied FR-DUHPC at final failure. 224

List of Abbreviations

ACI	American Concrete Institute
AMs	Alternative Materials
AFt	Al_2O_3-Fe_2O_3-Trisulfate
ANOAV	Analysis of Variance
AS	Australian Standard
ASCMs	Alternative Supplementary Cementitious Materials
ASTM	American Society for Testing and Materials
BBA	Biomass Bottom Ash
BFA	Biomass Fly Ash
CCB	Crushed Clay Brick
CCR	Coarse Crumb Rubber
CEBC	Compressive Energy Absorption before Cracking
CFBC	Circulating Fluidized Bed Combustion
CNY	Chinese Yuan
CR	Crumb Rubber
CRT	Cathode Ray Tube
C-S-H	Calcium Silicate Hydrates
CSS	Coarse Silica Sand
CTE	Compressive Total Energy Absorption
CTI	Compressive Toughness Index

CTWP	Ceramic Tile Waste Powder
CWA	Coal Waste Ash
CWP	Coal Waste Powder
DCC	Dry-Cast Concrete
DIF	Dynamic Increase Factor
DOF	Degree of Freedom
DUHPC	Dry Ultra-High Performance Concrete
D-W	Durbin-Watson
EAF	Electric Arc Furnace
ECO_2	Embodied CO_2
FA	Fly Ash
FEM	Finite-Element Method
FR-DUHPC	Fibre-Reinforced Dry Ultra-High Performance Concrete
FR-UHPC	Fibre-Reinforced Ultra-High Performance Concrete
FT	Flexural Toughness
FTI	Flexural Toughness Index
GGBS	Ground Granulated Blast Furnace Slag
GP	Graphite Nanoplatelet
HPC	High Performance Concrete
HSF	Hybrid Steel Fibre
HVFA	High-Volume Fly Ash
IS	Indian Standards

ITZ	Interfacial Transition Zone
IVs	Independent Variables
LSP	Limestone Powder
LVDTs	Linear Variable Displacement Transducers
LWC	Lightweight Concrete
MCR	Medium Crumb Rubber
MK	Metakaolin
MOE	Modulus of Elasticity
MS_A	Mean Squares
M-Sand	Manufactured Sand
MSS	Medium Silica Sand
MSWI	Municipal Solid Waste Incineration
NI	National Instrument
OPC	Ordinary Portland Cement
PP	Polypropylene
PVA	Polyvinyl Alcohol
RAP	Reclaimed Asphalt Pavement
RC	Reinforced Concrete
RCA	Recycled Concrete Aggregate
RCC	Roller-Compacted Concrete
RCCD	Roller-Compacted Concrete Dam
RCCP	Roller-Compacted Concrete Pavement

RDVs	Response Dependent Variables
RHA	Rice Husk Ash
RP	Replacement Percentage
SCMs	Supplementary Cementitious Materials
SEM	Scanning Electron Microscope
SHPB	Split Hopkinson Pressure Bar
SLF	Silica Fume
SP	Silica Powder
SS_A	Sum of Squares
TEBTs	Three-Edge Bearing Tests
UCE	Unit Compaction Energy
UHPC	Ultra-High Performance Concrete
VBT	Vebe Time
WCBPD	White Cement by Pass Dust
b	Width of Prismatic Sample
d_s	Steel Fibre Diameter
f_c	Compressive Strength
f_r	Rupture Modulus or Flexural Strength
f_{rr}	Residual Flexural Strength
f_{ts}	Split-Tensile Strength
h	Depth of Prismatic Sample
w/b	Water-Binder Ratio

α	Shape Parameter of Weibull Distribution
u	Scale Parameter of Weibull Distribution
$\dot{\varepsilon}$	Strain Rate
δ_{cr}	Cracking Deflection
H	Hot-Water Bath Curing
L	Clear Span between Support Rollers
L_N	Survival Function of Weibull Distribution
L_s	Steel Fibre Length
M	Moist/Steam Curing
N	Stochastic Variable of Weibull Distribution
N_c	Impact Cracking Resistance Factor
N_d	Impact Failure Resistance Factor
N_f	Predicted Failure Impact Number
P	Peak Load
R^2	Goodness of Fit
R_{FA}	Strength Contribution Rate of Fly Ash Effect
SD	Standard Deviation
SP_{Con}	Concrete Specific Strength
SP_{CSG}	Concrete Specific Strength except Fly Ash Effect
SP_{FA}	Fly Ash Effect Specific Strength
Vol-%	Steel Fibre Volume Fraction
W	Normal-Temperature Water Curing

Abstract

Dry concrete is defined as the fresh mixture having no flowability with a very small slump value. Dry concrete technology has been widely used in many engineering fields by virtue of its remarkable advantages. Dry ultra-high performance concrete (DUHPC), developed and studied in this thesis, is a promising building material with better mechanical performance and excellent eco-friendly benefit.

Chapter 1 introduces the background, application and advantages of dry concrete, and presents the motivation and outline of this study.

Chapter 2 provides a detailed literature review of the representative dry concrete mixtures named roller-compacted concrete (RCC) and dry-cast concrete (DCC). It was shown that the preparation method and raw material played the dominant role in the performance of dry concrete. Dynamic material tests revealed that dry concrete was a strain rate sensitive material.

In Chapter 3, the mechanical performance of steel fibre-reinforced DUHPC (FR-DUHPC) was experimentally investigated. It was concluded that the inclusion of steel fibres contributed more positive impact to the flexural performance, and 50 ℃ moist/steam curing was suggested considering the early/long-term strength.

The influences of multiscale mono/hybrid steel fibre reinforcements on the static mechanical performance were studied in Chapter 4. The results showed that the mixtures with hybrid 10-/13-mm fibres as well as hybrid 6-/10-/13-mm ones were suggested to be used for DUHPC structures/units that were mainly subjected to static loads. The proposed multivariate regression models could well predict both

the flexural and split-tensile properties.

Chapter 5 explores the feasibility of introducing the recycled wastes into DUHPC. The findings illustrated that the contribution of fly ash to the strength was evidently increased owing to the moist/steam curing. For rubberized FR-DUHPC, the use of finer rubber particles caused the most evident decrease in concrete properties at all ages, whereas the adverse effect was less serious on flexural strength. The developed lightweight dry concrete can be used in eco-friendly constructions.

Chapter 6 evaluates the impact resistance of FR-DUHPC by conducting the low-velocity drop-weight test. The results revealed that the impact performance was markedly improved with fibre length, but significantly deteriorated with fly ash and rubber addition. Moreover, the use of 6-mm fibres to substitute partial longer ones could not restrain the microcracks rapid development. The two-parameter Weibull distribution could well predict the failure hit number of FR-DUHPC under repeated impact.

Chapter 7 summarizes the findings of this study and proposes some suggestions and ideas for the future research of DUHPC.

Chapter 1

Introduction

1.1 Background

Concrete is the widely used building material owing to its several advantages of broad source of raw materials, low cost and energy consumption, simple process and good fire resistance. Based on the difference in the mixture's flowability and appearance, concrete can be simply divided into two types, namely dry concrete and self-compacting concrete. Generally speaking, dry concrete is defined as its fresh mixture having no flowability when the mixing is completed and the slump value is very small of no more than 25 mm [1]. Compared with self-compacting concrete, dry concrete has a lower moisture and cementitious material content in which part of the cement is commonly substituted by alternative supplementary cementitious materials (ASCMs). These characteristics hence contribute to fast hardening speed and high early strength, and the low workability allows the rapid demoulding after compaction, or even without any formwork operation during the preparation [2-4]. Roller-compacted concrete (RCC) and dry-cast concrete (DCC) are two types of dry concrete with different casting and fabrication methods [5]. The moulding of RCC is commonly achieved by repeated steel and rubber-tired rolling compaction, and it is generally applied to the engineering areas of dams and pavements [5-8]. As for DCC, mechanical consolidation and vibration are greatly required to cast the pre-fabricated components like segmental retaining wall, masonry units and pipes [5, 9, 10]. Additionally, when concrete mixes are

utilized in the engineering aspects of normal pavements and concrete masonry products where strength is not the primary concern, many industrial by-products that do not meet the requirements of raw materials of conventional concrete are still feasible to substitute a large amount of ingredients in dry concrete mixtures [11, 12].

For RCC, the most important engineering applications are RCC dams (RCCD) and RCC pavements (RCCP) as indicated in Fig. 1.1. Fresh mixtures with zero slump used in roller-compacted method of RCCD/RCCP are favourable to obtain the sufficient compaction during the laying. The construction process of RCCD is simpler and faster than conventional concrete dams [13], and the laying process as well as machines and equipment used for RCCP are essentially the same as those of asphalt pavements with no formwork [3]. It is reported that for RCCD, the layered roller-compacted placement of dry concrete mixtures may cause poor adhesion between the layers, which in turn significantly attenuate the horizontal strength and increase the permeability at the construction interfaces and joints of the dam body [7, 14]. In addition, thermal stress and temperature cracking due to cement hydration and poor thermal conductivity of the super-volume structures are another primary unfavourable factors affecting the durability and long-term serviceability of RCCD [15, 16]. Data from several experiments have indicated that the early-age strength of the mixture whose cement or aggregate is partially substituted by ASCMs or recycled aggregates is significantly reduced, causing a decline in the early-age abrasion and fatigue resistance of concrete [17-19]. It is

therefore, for RCCP, important to choose appropriate materials and dosage when RCC is laid as the outermost layer which needs to withstand the repeated vehicle loads, especially in the heavy-duty pavements. It is noteworthy that the rough and uneven surface of RCC without grinding renders it unsuitable for paving the rapid transit pavements, and the loose state of the dry mixture makes the transportation volume of the ready-mix truck much smaller [20]. Finally, due to the large surface area and low moisture content of either RCCD or RCCP, improper curing regime considerably accelerates the evaporation of water within the mixture, making strengths and durability of the structure unable to be guaranteed [21-23].

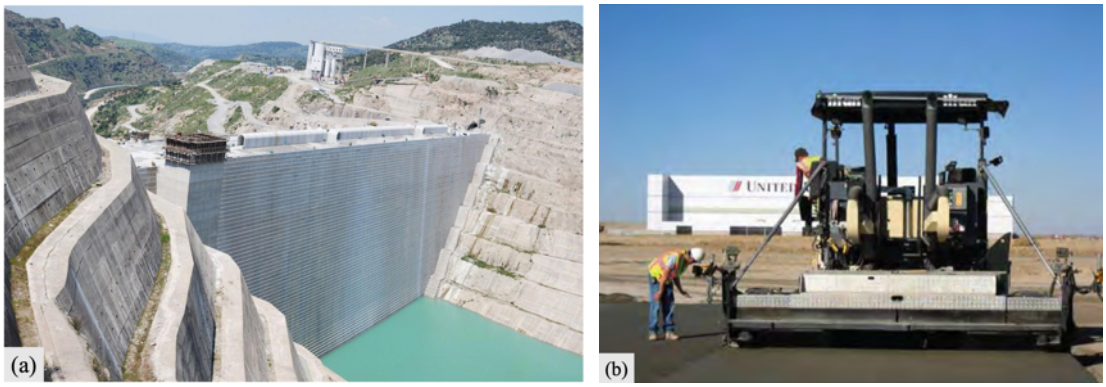

Fig. 1.1. RCC engineering applications of (a) dams [24] and (b) pavements [25].

In terms of DCC, its widespread use in the precast concrete industry is profited from its time efficiency and effectiveness [26]. Some published literatures pointed out that the lean or very low-slump mixtures utilized to manufacture DCC sewer pipes were not particularly suitable to the fibre dispersion as well as the interfacial interactions between the mixture and steel cages or fibres [27, 28]. During the casting, fresh mixture needs to be poured into the mould with steel cages fixing on the bottom ring to prevent the brittle failure and help the early demoulding of

pipes. Moreover, appropriate consistency is positively beneficial to disperse fibres and improve the vibration efficiency when preparing fibre-reinforced DCC pipes [28-30]. Unlike RCC, DCC is more used to fabricate smaller concrete units like concrete bricks, blocks, sewer pipes and paving stones (Fig. 1.2). The casting moulds can be removed immediately once the mixture is formed, and therefore prominently increase the turnaround speed of moulds [27, 31, 32]. Steam curing is generally adopted following the rapid demoulding to accelerate the hardening rate and improve the early mechanical properties of mixtures. In addition, it was illustrated by Willis [33] that the application of DCC in the construction of the site-cast precast panels, supported slabs and concrete brick set made it possible to save approximately 35%, 10% and 25% of the cost, even without considering the multiple advantages such as reduced working time and higher early strength.

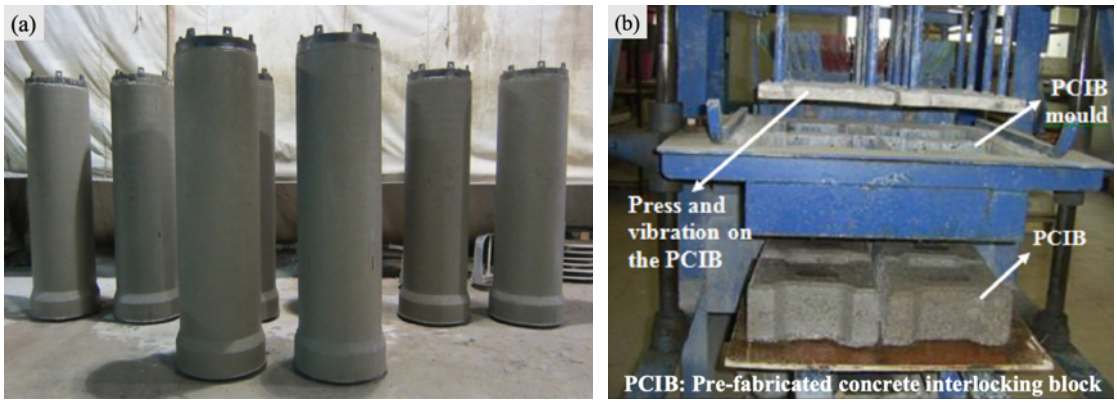

Fig. 1.2. DCC prefabricated units of (a) sewer pipes [28] and (b) paving blocks [34].

1.2 Objectives

Dry concrete technology has been extensively utilized in many engineering fields thanks to its remarkable high early strength, fast hardening and low production cost. However, its strength and durability are undesirable owing to the addition of

coarse aggregate and a large amount of recycled materials, which constrain the adaptation and popularization in the widespread range of applications. Dry ultra-high performance concrete (DUHPC) is a great promising concrete material that effectively addresses the defects of traditional dry concrete, offering exceptional characteristics such as extremely high strength, outstanding crack resistance and superior durability. Furthermore, the addition of steel fibres and rubber aggregate into DUHPC can significantly enhance its resistance to brittle failure induced by bending and impact loads, which are frequently encountered during the service life of its structures and units. To this end, this study investigates the development, mechanical behaviour and impact resistance of sustainable steel fibre-reinforced DUHPC (FR-DUHPC) containing varying proportions of steel fibres and recycled materials. The primary objectives are presented as follows:

1) Determine the benchmark mix proportion of DUHPC; study the effect of curing regime and fibre dosage on the mechanical performance, microstructure and damage of FR-DUHPC; select an appropriate curing regime/temperature and fibre dosage considering the cost, preparation and mechanical properties for practical applications.
2) Investigate the effect of multiscale mono/hybrid steel fibre reinforcements on the static mechanical properties of DUHPC; explore the impact of the adopted layered fabrication on the reinforcement effect of different fibre combinations; suggest the optimal steel fibre hybridization in view of the main application field along with the effect of fibre distribution, dosage and length on static behaviour;

propose the multivariate regression model to estimate the strength of DUHPC with mono steel fibre reinforcement.

3) Evaluate the influence of high-volume fly ash and waste crumb rubber on the mechanical performance and environmental benefit of steel FR-DUHPC; study the contribution of fly ash pozzolanic effect on strength behaviour; investigate the microstructure morphology of rubberized FR-DUHPC; suggest the optimal fly ash and rubber content in view of the sustainable development in resources as well as their impacts at various ages; compare the mixture's carbon footprint with other self-compacting UHPC and conventional dry concrete.
4) Study the impact of steel fibre length, mixing method, fly ash content and the addition of rubber aggregate on the impact resistance of FR-DUHPC; analyse the impact force time history and failure patterns of FR-DUHPC samples under impact loads; evaluate the residual flexural performance of FR-DUHPC after the multiple drop-weight impacts; explore the correlation between the ultimate failure blow number and the empirical survival function of FR-DUHPC samples utilizing Weibull distribution.

1.3 Outline

Chapter 1 presents the research background, objectives and outline of this study. Chapter 2 presents the literature review on the current study of two representative dry concrete mixtures, roller-compacted concrete (RCC) and dry-cast concrete (DCC), in terms of the raw material, preparation technology, mixture performance, static and dynamic mechanical behaviour, and application.

In Chapter 3, a promising material named dry ultra-high performance concrete (DUHPC) was developed utilizing a high-efficiency orthogonal test method. Then, the mechanical properties including compressive and indirect tensile behaviour of steel fibre-reinforced DUHPC (FR-DUHPC) were experimentally investigated based on the determined benchmark mix proportion. Different steel fibre dosages (0.5-2.0%) and curing regimes (normal-temperature water curing, moist/steam curing and hot-water bath curing) were used to explore their impacts on DUHPC performance. Finally, the environmental impact was evaluated considering the total amount of cement and CO_2 emissions.

In Chapter 4, the impacts of multiscale mono and hybrid steel fibre reinforcements on the static mechanical property of DUHPC were further studied based on the mixing ratio and optimal curing regime obtained from Chapter 3. The optimal steel fibre hybridization was suggested after comprehensively considering the primary application fields as well as the influence of fibre distribution, dosage, length and mixing method on the performance of DUHPC. Finally, the multivariate regression models were proposed to estimate the strength values of mono FR-DUHPC at a given range of steel fibre length, volume dosage and curing age.

In Chapter 5, the mechanical behaviour and environmental benefit of steel FR-DUHPC containing high-volume recycled waste materials were evaluated still on the basis of the sustainable FR-DUHPC developed in Chapter 3. To this end, two categories of wastes, namely fly ash and crumb rubber, were selected as the renewable materials to partially replace the cement and natural sand in concrete

mixes, respectively. Mixtures were assessed based on the results of compressive and flexural property, as well as the cost and environmental impact. Finally, the comparisons of embodied CO_2 emission between the high-volume fly ash-mixed FR-DUHPC and other self-compacting FR-UHPC as well as conventional FR-dry concrete were performed.

In Chapter 6, the impact resistance of steel FR-DUHPC was evaluated in detail via using the modified low-speed drop-weight impact test, drawing on the test methods used by other researchers for fibre-reinforced self-compacting concrete. The effects of steel fibre length, mixing method, fly ash content (used to replace partial cement) and the inclusion of crumb rubber (used to replace partial silica sand) on the cracking/failure impact number, residual bending performance, peak impact force and failure pattern were studied. Finally, the correlation between the damage impact number and the empirical survival function of tested concrete samples was explored via the Weibull distribution analysis.

Chapter 7 summarizes the overall findings of this study and presents some issues and suggestions for future research.

Chapter 2

Literature Review

2.1 Raw material and preparation method

2.1.1 Cementitious material

It is well known that cement is a major and important powdery cementing material applied to civil engineering national defence and other engineering applications. The slurry formed by mixing with water can bond various aggregates and fibres together. At present, Portland cement complying with ASTM C150-05 (TYPE Ⅰ) [8, 32, 35], ASTM C150 (TYPE Ⅱ) [12, 30, 36, 37], IS4031 [38-40] and CEM Ⅱ 42.5N [41, 42] is the most commonly used cement type in the mix design of dry concrete. Additionally, Portland cement of type GU [9, 43] and type HE [31] are also employed as cementing materials for preparing dry concrete. The specific gravity and Blaine surface area of the above cement are around 3.15 g/cm^3 and 300-450 m^2/kg, respectively, and the initial and final setting time is approximately 155 and 225 min, respectively. The primary chemical composition of the reported cement includes CaO, SO_2, Al_2O_3, Fe_2O_3, MgO and SO_3. It should be noted that compared with self-compacting concrete, TYPE III Portland cement is impractical for the preparation of the most dry concrete structures and units due to its faster early hardening and higher thermal evolution rate, which evidently shortens the available cast/fabrication time and increase the possibility of thermal cracking of dry concrete mixtures [3].

Fly ash (FA) is a kind of industrial by-product produced by pulverized coal

combustion during the thermal power generation. Considering the perspectives of the environmental sustainability along with the filling, lubricating, reactivating and dispersing functions, a certain amount of FA is usually introduced into dry concrete mixtures substituting partial cement (commonly up to approximately 50% by weight) or aggregate to achieve the purpose of saving cost, improving fresh concrete workability and enhancing long-term performance [43-45]. Additionally, the effect of introducing FA to reduce temperature rising and initial cracking, and further improve the structural durability illustrates particularly important when dry concrete is used to construct RCCD or RCCP [46-49].

Silica fume is an ultrafine siliceous powder material produced in the smelting of the ferroalloy and industrial silicon. Its main constituent is SiO_2 and it possesses a specific surface area of 20000 m^2/kg and an average particle size of 0.1-1 μm. These features render silica fume possess excellent pozzolanic activity and a desired effect on increasing the low early-age strength of the hardened mixture caused by the partial replacement utilizing ASCMs [23, 36, 50, 51]. Generally, the improvement of silica fume to concrete cementing system is mainly achieved via the filling, pozzolanic activity, rheological and solution chemical effects [52].

In addition to FA and silica fume introduced above, some other waste materials and by-products like industrial coal waste, ground granulated blast furnace slag (GGBS), rice husk ash (RHA), municipal solid waste incineration (MSWI) bottom ash, white cement by pass dust (WCBPD), trass and glass powder [9, 12, 19, 22, 31, 53-59] are also added to dry concrete mixtures to partially substitute cement,

in considerations of raw material cost and severe environmental issues. These materials are therefore called ASCMs. It is noteworthy that a promising ASCM called sludge ash has been utilized to prepare self-compacting concrete blocks relying on its higher pozzolanic reactivity and the ability to accelerate the early hydration reaction [60, 61]. The proper incorporation of sludge ash is therefore very beneficial to dry concrete since most of ASCMs mentioned above will reduce the early-age performance which is very important for dry concrete structures and components. In addition, nanoscale material, such as nano-silica, has been used as a supplementary cementitious material (SCM) in dry concrete mix to densify the internal micro-structure and improve the physical-mechanical properties of hardened mixtures [62-64].

2.1.2 Aggregate

Aggregate, which accounts for more than half of the mass fraction of the mix proportion, is the main component of the concrete mixture, and its characteristics have a vital impact on concrete technical properties and economic benefit [65]. The aggregate utilized to cast dry concrete is basically the same as conventional concrete composing of fine and coarse aggregate and sand. The particle size gradation is particularly important since the total dosage of cement paste utilized to fill the aggregate voids is reduced, owing to the lower moisture content of dry concrete by nature. Moreover, the size and category of aggregate are related to the practical applications, such as crushed limestones with larger dimensions are generally utilized to improve the abrasion resistance of RCCP [66, 67], and the

mixture with fine sand is utilized to cast the surface layer of paving blocks [2]. Additionally, in order to reduce the raw material cost and in line with the aim of protecting environment and saving resources, a variety of recyclable aggregate like manufactured sand (M-sand) [38, 39, 68], reclaimed asphalt pavement (RAP) aggregate [19, 69, 70], recycled concrete aggregate (RCA) [41, 71, 72], electric arc furnace (EAF) slag [73], circulating fluidized bed combustion (CFBC) ash [35], polyethylene polymer pellets [31] and recycled cathode ray tube (CRT) glass [74] are used to replace partial natural sand or aggregate in dry concrete mix without high strength requirement. In addition, rubber particles shredded by waste rubber products like tyres and slippers is another kind of reclaimed material substituting the partial fine and coarse aggregate, and the prepared concrete is usually called rubberized concrete [4, 30, 36, 75-77].

2.1.3 Chemical additive and fibre

High-performance polycarboxylates water-reducing agent (superplasticizer) and air-entraining agent are two commonly-used chemical additives in the preparation of dry concrete structures and components. Superplasticizer has a considerable effect on increasing the mixture consistency and various strengths, especially for fibre-reinforced dry concrete with poor workability [28, 78, 79]. Incorporating air-entraining agent can be beneficial for concrete against freeze-thaw damages [44, 55, 57, 80]. Furthermore, the addition of steel, polypropylene (PP) and polyvinyl alcohol (PVA) fibres is another effective method frequently utilized to improve the bending and ductility performance of dry concrete [27, 28, 81-83]. Additionally,

some treated “ecological green” fibres (recycled glass, plastic, steel and PP fibre) recovered from waste materials are also used as the reinforcement considering both mechanical performance and cost [84-87].

2.1.4 Preparation method

Although the raw materials of dry concrete are roughly the same as conventional concrete and the properties/performance are closely related to the mix proportion, the different appearance of fresh concrete renders the preparation likewise have a great impact on dry concrete performance. At present, the commonly utilized fabrication method for DCC precast units is the mechanical consolidation with plant compaction or hand ramming, and vibration is also considered in some cases to disperse the mixture evenly [2, 26]. For RCC samples, vibrating table [42, 46, 88] and vibrating hammer [48, 54, 89] compaction, respectively in accordance with ASTM standards C1176/C1176M [90] and C1435/C1435M [91], are widely used laboratory preparation techniques. The former method utilizes a certain mass of surcharge compacting the fresh concrete to achieve the final form on the vibrating table, and the latter employs a steel tamping plate to uniformly distribute the vibrated compaction energy generated by hammer on each layer of the mixture. In addition, roller compaction using vibratory roller drum and rubber-tired roller is employed in the engineering constructions of RCCD and RCCP, and this method is also used in RCC behaviour studies to simulate real construction conditions [89, 92-94]. Fig. 2.1 exhibits the typical preparation methods reported above, and all of which aim to compact the mixture to reduce the void content

and obtain the dense concrete structure.

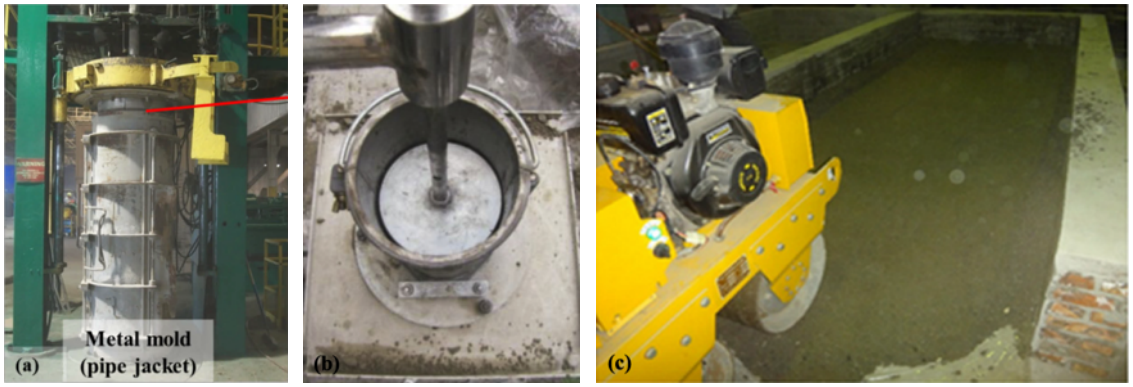

Fig. 2.1. Preparation methods for fresh dry concrete: (a) mechanical consolidation and vibration [30]; (b) vibrating table compaction [6] and (c) roller compaction [94].

2.2 Mixture basic performance

2.2.1 Adiabatic temperature rising

The adiabatic temperature rising of concrete mainly relies on the amount and rate of the cement hydration heat. When cement is mixed with water, unbalanced compounds in the high-energy state react with water and the hydration products are formed with stable low-energy state, that is, cement hydration is a continuous energy-released (exothermic) process [95]. RCCD, as a typical structure of the large-volume concrete application reported above, its quick construction process and poor thermal conductivity cause the internal temperature to rise rapidly and the volume expansion occurs due to the cement hydration. Consequently, the thermal stress and resulting surface cracks appear on account of the lower initial strength of the matrix, along with the combined action of the large temperature gradient and surface tensile stresses [16]. The cracks will further develop into the penetration cracks once the following curing is inappropriate, leading to serious

damage as well as unguaranteed serviceability and durability of RCCD structure. To control and reduce the temperature cracking caused by the thermal stress, it is usually realized by adjusting the cement ratio in concrete mix [47] and adopting some new technical approaches such as superficial thermal insulation [15, 96]. In terms of adjusting the cement ratio within concrete mixes, RCCD is advantaged with better temperature cracking resistance compared with conventional concrete dams, by virtue of the natural characteristics of dry concrete with low cement addition as well as a large amount of ASCMs added to substitute partial cement, as elaborated in Section 2.1.1. This, therefore, provides potential and advantages for the wide use of RCCD in practical engineering. In addition, it is noteworthy that the finite-element simulation is an effective analysis technique for assessing the adiabatic temperature rising and thermal stress of RCCD. For instance, Zhang et al. [96] studied the impact of superficial thermal insulation on the RCCD superficial temperature in cold regions by performing simulation and analysis. It was indicated that the existence of the superficial insulation notably raised the surface temperature and effectively reduced the surface temperature difference and maximum tensile stress, and therefore limited the formation of temperature cracking of RCCD. For another instance, Jaafar et al. [97] numerically evaluated the effect of placing season on temperature responses of RCCD by introducing the technology of element's birth and death, which could effectively decrease the volume of the input data. It was demonstrated that the location of the maximum temperature zone could be optimized by changing the placing schedule, and the

seasons with lower temperatures were more favourable to reduce the tensile stresses within the critical zone.

2.2.2 Consistency and unit weight

In order to achieve a sufficient compaction of dry concrete mixture and provide a good appearance as it is compacted, good workability is particularly important. Further, it is conductive to minimize the compaction energy during preparation. Generally, the performance of fresh dry concrete is indicated by the consistency and unit weight, and Vebe time (VBT) is utilized to characterize the consistency since the slump of fresh dry concrete is closed to zero [8, 45, 85]. VBT is the time interval expressed in seconds from when Vebe apparatus starts to vibrate to a complete mortar ring appears between the surcharge and the container wall [98]. However, the proper consistency obtained through the laboratory test may not be fully applicable to engineering practice. Chhorn et al. [92] noted that the range of VBT should be expanded to 30-75 s to improve the practicality. Additionally, the proper consistency of the mixture, that is, whether the paste is cohesive enough, should also be determined by specific concrete applications applied in the actual projects. The universality of much published research has drawn conclusions that several factors like moisture content, aggregate type and gradation, cementitious material dosage and additives have a considerable impact on the unit weight and consistency of RCC mixtures. For instance, Karadelis et al. [79] and Kolase et al. [82] pointed out that the addition of steel and PP fibres in RCC mixtures resulted in bad workability, whereas using superplasticizer with a dosage of 2.5% and 1.0%

could effectively improve the workability and mechanical properties of FR-RCC. Fig. 2.2 depicts the relationships between the rubber content and the density or VBT of fresh RCC concluded by Meddah et al. [42] who used shredded rubber tire to partially replace the natural crushed aggregate. As can be observed that the unit weight lightens as the rubber addition increased within the mix, but the consistency tends to increase as the replacement ratio changes from 0 to 30%, which was attributed to the low water absorption of rubber particles, and the free water within the mixture is hence increased. Similar increase in VBT was also observed in the fabrication of pedestrian DCC blocks by Sukontasukkul et al. [4]. Lessard et al. [43] concluded that an evident workability loss can be observed when the biomass FA and bottom ash were respectively used to replace cement and sand in DCC mixtures, and the compacted energy required to achieve the prescribed consolidation indices was therefore increased. In addition, the partial substitution of cement by glass powder [57] and aggregate by electric arc furnace (EAF) slag [73] both increase the unit weight of fresh RCC.

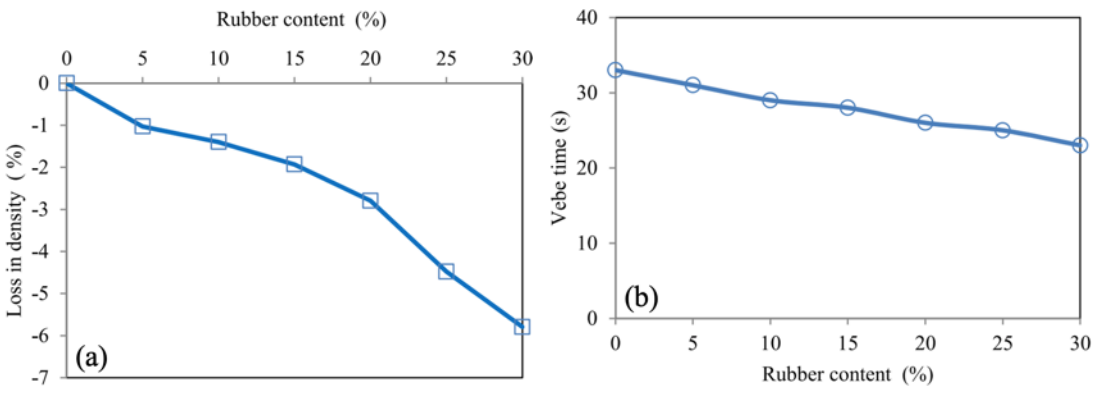

Fig. 2.2. Relationships between rubber content and (a) density decrease as well as (b) Vebe time of RCC [42].

2.3 Static mechanical property

2.3.1 Strength behaviour

It is well known that the compressive and tensile strengths are the most critical and frequently-used indicators for the static performance assessment of various concrete, especially for dry concrete which is characterized by fast hardening speed and high early strength. Even though the ingredients of dry concrete are similar as those of conventional concrete as introduced above, its static strength behaviour and research focus are quite different due to the evident distinctions in composition ratio, moulding method and application field, as well as more ASCMs and less moisture content. Tables 2.1 and 2.2 respectively show the influences of various alternative materials (AM) and fibres on the strength behaviour of dry concrete obtained by organizing the relevant literature. Then, the mechanical performance is elaborated in detail from above two aspects.

In the research team of Rao et al. [38-40, 68], they conducted experimental study on mechanical properties of RCC with cement (295 kg/m^3) and river sand (801 kg/m^3) being partially substituted by FA, GGBS and M-sand, respectively. Test results indicated that when cement was substituted by FA (0-60%), the strengths were deteriorated with increasing FA substitution, especially at early ages. As an illustration, the compressive and flexural strengths of RCC (60% FA substitution), respectively, reduced by 67.9% and 65.8% at 3-day age as compared to those of the control case without FA addition, and, respectively, diminished by 49.9% and 36.1% at 90 days. For RCC with cement partially substituted by GGBS (10-60%),

Table 2.1

Effects of alternative materials (AM) on strength behaviour of dry concrete from literature (Increase: ↑, Decrease: ↓).

Researchers	AM (substituted content)	Replaced material	Compressive strength	Flexural strength	Split-tensile strength
Aghabaglou et al. [99]	FA (20-60%)	Cement (wt. R)	20-60%↓	20-60%↓	20-60%↓
		Agg. (vol. R)	20-60%↑	20-60%↑	20-60%↑
Adamu et al. [18]	FA (50-70%)	Cement (vol. R)	3-28d↓, 90d-365d↑	7-90d↓	3-90d↓
Atis [100]	FA (50%, 70%)	Cement (wt. R)	50% 28-365d↑, 70%↓	50%↑, 70%↓	50%↑, 70%↓
Rao et al. [40]	GGBS (10-60%)	Cement (wt. R)	3d↓, 7-90d↑	3d↓, 7-90d↑	3d↓, 7-90d↑
Madhkhan et al. [78]	GGBS, FA (15%, 30%)	Cement (wt. R)	15%↓, 30%↓	15%↓, 30%↓	---
Ashteyat et al. [54]	WCBPD (10-40%)	Cement (wt. R)	0-10%↑, 10-40%↓	---	0-10%↑, 10-40%↓
Ghahari et al. [55, 56]	Trass (15-25%)	Cement (wt. R)	15-25%↓	---	15-25%↓
Modarres et al. [19]	RHA (3%, 5%)	Cement (wt. R)	3%120d↑, 5%↓	3%120d↑, 5%↓	---
	RAP (100%)	Coarse/Fine Agg. (wt. R)	Coarse↓, Fine↓	Coarse↓, Fine↓	---
Omran et al. [57]	Glass powder (20%)	Cement (wt. R)	7d↓, 28-91d↑	7d↓, 28-91d↑	1.18 Years↑
Lessard et al. [43, 45]	BFA (10-30%)	Cement (wt. R)	10-30%↓	10-30%↓	10-30%↓
	BBA (50%, 100%)	Sand (vol. R)	50%↓, 100%↓	50%↓, 100%↓	50%↓, 100%↓
Rao et al. [39]	M-sand (50%, 100%)	River sand (wt. R)	50%↑, 100%↓	50%↑, 100%Variable	---

Researchers	AM (substituted content)	Replaced material	Compressive strength	Flexural strength	Split-tensile strength
Settari et al. [101]	RAP (50%, 100%)	Coarse/Fine Agg. (wt. R)	Coarse↓, Fine↓	---	50%Coarse+Fine↑
Debbarma et al. [17]	RAP (50%, 100%)	Coarse/Fine Agg. (wt. R)	Variable	Coarse↓, Fine↓	Coarse↓, Fine↓
Rooholamini et al. [102]	EAF slag (25%, 50%)	Coarse/Fine Agg. (vol. R)	Coarse↓, Fine↓	Coarse↓, Fine↓	Coarse↑, Fine↓
Lopez et al. [41]	RCA (50%, 100%)	Coarse Agg. (vol. R)	50%↓, 100%↓	50%↓, 100%↓	50%↓, 100%↓
Poon et al. [72]	CCB (25%, 50%, 75%)	RCA (wt. R)	25-75%↓	25-75%↓	25-75%↓
Ling [2]	Crumb rubber (10-30%)	Sand (vol. R)	0-10%↑, 10-30%↓	0-10%↑, 10-30%↓	---
Sukontasukkul et al. [4]	Crumb rubber (10%, 20%)	Coarse/Fine Agg. (wt. R)	10-20%↓	10-20%↓	---
Fakhri et al. [36]	Waste rubber (5-35%)	Sand (vol. R)	0-10%↑, 10-35%↓	0-5%↑, 5-35%↓	---
Meddah et al. [42]	Shredded rubber (5-30%)	Coarse Agg. (vol. R)	5-30%↓	5-30%↓	5-30%↓
Mohammed et al. [103]	Crumb rubber (10-30%)	Fine Agg. (vol. R)	0-10%↑, 10-30%↓	0-20%↑, 20-30%↓	0-10%↑, 10-30%↓

Notes: “FA” denotes fly ash; “M-sand” denotes manufactured sand; “GGBS” denotes ground granulated blast furnace slag; “WCBPD” denotes white cement by pass dust; “RHA” denotes rice husk ash; “RAP” denotes recycled asphalt pavement; “BFA” denotes biomass fly ash; “BBA” denotes biomass bottom ash; “EAF” denotes electric arc furnace; “RCA” denotes recycled concrete aggregate; “CCB” denotes crushed clay brick; “d” denotes curing age; “Agg.” denotes aggregate; “wt. R” denotes weight replacement; “vol. R” denotes volume replacement and “---” denotes unstudied.

Table 2.2

Effects of various fibres on strength behaviour of dry concrete from literature (Increase: ↑, Decrease: ↓).

Researchers	Fibre type (volume fraction)	Compressive strength	Flexural strength	Split-tensile strength
Rooholamini et al. [8]	Twisted PP (0.25%, 0.5%)	Not significant	0.25-0.5%↑	---
Algin et al. [83]	Twisted/Mesh PP (0.2%, 0.4%, 0.6%)	0.2-0.6%↑	0.2-0.6%↑	---
Kolase et al. [82]	Triangular PP (0.25%, 0.5%, 0.75%)	0.25-0.75%↓	0.25-0.75%↑	Variable
Yazici et al. [104]	Mesh PP (0.25%, 0.5%, 0.75%)	0.25-0.75%↓	0.25-0.75%↓	0.25-0.5%↑, 0.75%↓
Ashteyat et al. [54]	Virgin PP (0.25%, 0.5%)	0.25%↑, 0.5%↑	---	0.25%↑, 0.5%↑
LaHucik et al. [105]	Embossed/Smooth PP (0.2%, 0.4%)	0.2%↑, 0.4%↑	0.2%↓, 0.4%↓	0.2%↑, 0.4%↑
	Hooked end steel (0.2%, 0.4%)	0.2%↑, 0.4%↓	0.2%↑, 0.4%↓	0.2%↑, 0.4%↑
Madhkhan et al. [78]	Hooked end steel (0.4%, 0.6%, 0.8%)	0.4-0.8%↑	Variable	---
Karadelis et al. [79]	Straight steel (1.0%, 1.5%, 2.0%)	Not significant	1.0-2.0%↑	---
Mohamed et al. [29]	Hooked end steel (0.25%, 0.5%, 0.75%)	0.25-0.75%↑	0.25-0.75%↑	0.25-0.75%↑
Peyvandi et al. [27]	Polyvinyl alcohol (0.8%)	0.8%↓	0.8%↑	---
Yildizel et al. [84]	Glass (1.0%, 1.5%, 2.0%)	1.0-2.0%↓	1.0-1.5%↓, 2.0%↑	---
Sobhan et al. [86]	Plastic (0.25%, 0.5%)	0.25%↓, 0.5%↓	Variable	0.25%Variable, 0.5%↑

Notes: “PP” denotes polypropylene and “---” denotes unstudied.

the strengths also reduced with GGBS content at 3 days but improved to varying degrees at 7-90 days. Moreover, the use of M-sand at 50% replacement yielded higher strengths, but the complete replacement caused a decrease in strengths, ultrasonic pulse velocity and dynamic elastic modulus. It is noteworthy that for normal-strength self-compacting concrete with higher cement (340 kg/m^3) and lower sand (737 kg/m^3) addition, its strengths under the same FA substitutions (10-60%) showed significantly less decline, and the long-term strengths even increased to some extents [106]. For instance, the compressive strength of the foregoing concrete (60% FA substitution) decreased by 34.8% at 3-day age in comparison with the control case, while increased by 4.3% and 18.6% at 56 and 91 days, respectively. The reason might be that at a higher FA substitution, the hydration degree of dry concrete mixture with low cement addition was reduced, causing an evident decrease in its mechanical properties at early ages. Then, a small amount of continuously generated hydration products like $Ca(OH)_2$ could not fully react with FA and hence affected the later strength development. Above views regarding the negative impact of FA replacing cement were supported by other researchers [43, 45, 99], but meanwhile the positive influence on improving strength performance was also observed when FA content was appropriate and the curing age was extended [18, 100, 107]. The activation effect of FA and GGBS is realized via the formation of the cementing products during the crystallization as well as the pozzolanic reaction between cement hydration products and active components of FA and GGBS, in the middle and later stages of concrete curing

period [40, 68, 108]. Interestingly, the strength showed a significant enhancement when compared with control cases as the material replaced by FA was changed from cement to aggregate (Fig. 2.3), which was attributed to more cementitious material content and higher compatibility [99]. In addition to FA and GGBS, a certain amount of literature has been published on mechanical properties of dry concrete using some other ASCMs to replace partial cement participating in the hydration and secondary hydration reaction. As an illustration, Hesami et al. [12] and Modarres et al. [53] jointly carried out the experimental research on strength, toughness and microstructure of RCCP containing limestone powder (LSP), coal waste powder (CWP) and its ash (CWA). It was illustrated that the utilization of 5% CWP and up to 10% CWA as the cement substitution into mixtures expressed comparable strength values as compared to control case. The hybrid of CWA with 7% LS outperformed the mechanical behaviour of RCCP attributed to denser and homogenous microstructure which observed in SEM images. Again for instance, Zhang et al. [9] explored the feasibility of mixing MSWI bottom ash (MSWI-BS) as an ASCM in DCC. The common expansion cracking appeared in high-slump concrete was not observed in DCC containing MSWI-BS. The use of MSWI-BS replacing Portland cement enhanced the early cement hydration and pozzolanic reactivity, and 20% addition exhibited up to 18% higher strength at 90 days as compared to the control ones. In some cases, even if a high amount of cement substitution causes a notable decrease in strength values, the minimum strength requirements of standards and practical engineering are still met [19, 45, 74].

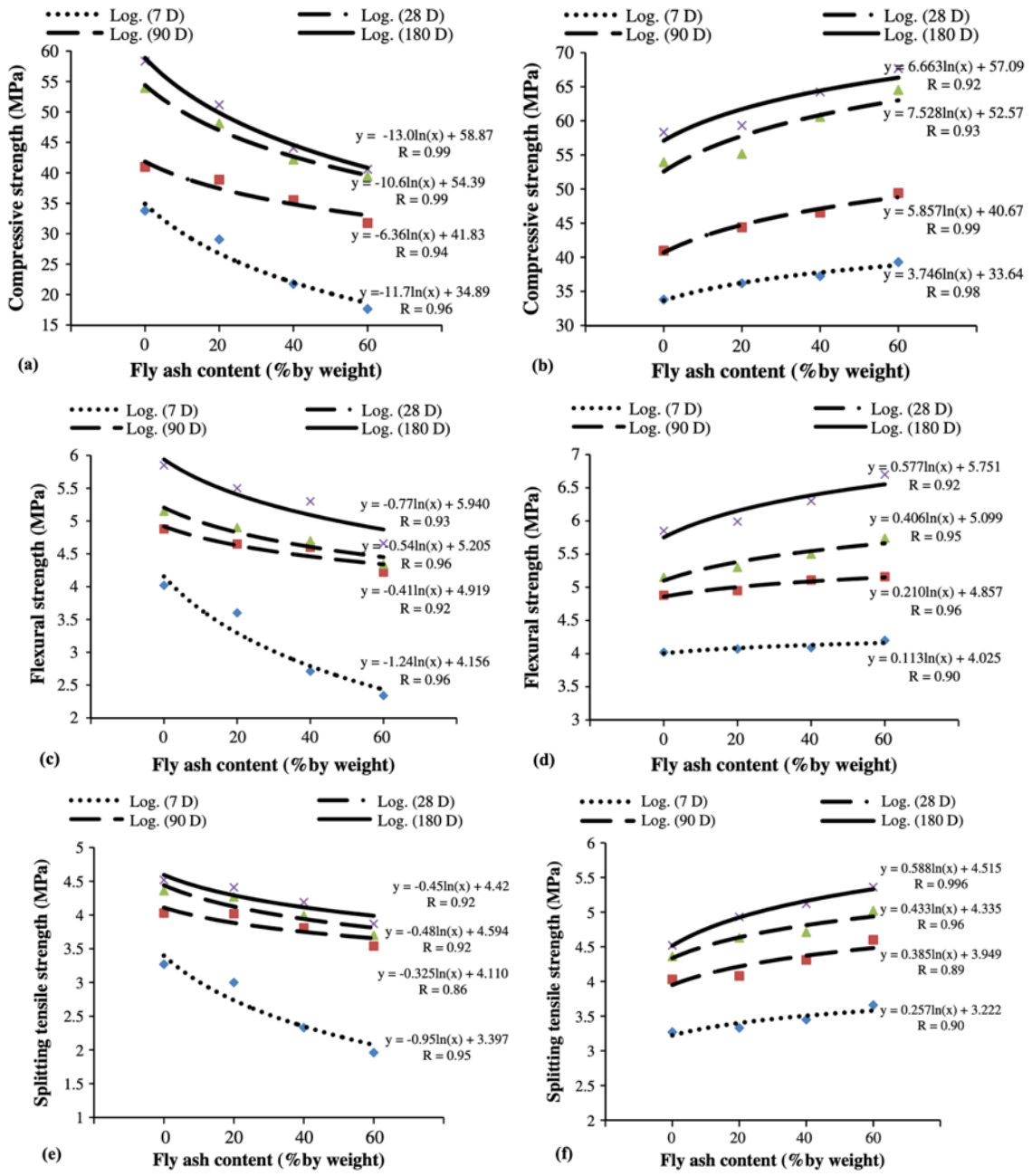

Fig. 2.3 Relationships between mechanical strength behaviour and FA content of RCC in which FA substitutes partial (a, c and e) cement and (b, d and f) aggregate [99].

Aggregate plays an important role in affecting the strength behaviour of hardened concrete, and several researches examining the relationship between aggregate replacement and mechanical characteristics of dry concrete have been carried out with pertinence. At present, recycled aggregate including RAP [17, 19, 69,

101] and RCA [41, 72] is one of the major AMs for natural sand and aggregate appeared in research papers to investigate the replacement effect. The strength properties of hardened RCC with coarse and fine RAP materials (without bitumen extraction) substituting 50% and 100% coarse and fine natural aggregate were evaluated by Settari et al. [101]. It was indicated that all the substitution ratios caused a regularly strength reduction in compression and tension, except that 50% RAP replacement contributed to higher tensile strength. The reason might be that RAP materials were at the virgin state and thus their surfaces were covered with untreated bitumen, resulted in poor adhesion between RAP particles and slurries [70]. Similar conclusions had also been drawn from other studies conducted by Modarres et al. [19] and Debbarma et al. [17], but they also obtained a useful achievement that the mixture incorporating RAP aggregate reached the minimum requirements of compressive (27.6 MPa) and bending strengths (3.7 MPa) at 28 days for RCCP constructions. Poon et al. [72] studied the density, compressive and indirect tensile strengths of DCC paving blocks containing RCA and crushed clay brick (CCB). It was concluded that the above properties gradually reduced as CCB substitution level increased, but the incorporation of 25% and 50% still respectively conformed the paving block requirements for traffic and pedestrian areas. Moreover, Debieb et al. [71] found that although the chloride ion content seemed to have less impact on RCC properties, the contaminated RCA could be reused in reinforced concrete without any corrosion concern since their surface chloride content could be leached into the water. Apart from recycled aggregate,

EAF slag [73, 102] and crumb rubber particles [2, 4, 42, 75, 76] are another two commonly utilized AMs of natural aggregate for preparing dry concrete. Lam et al. [73] conducted mix design and mechanical property studies of RCCP made of EAF slag pre-treated with spraying water to ensure the volume stability of slag aggregate. It was pointed out that the replacement of crushed stone aggregates utilizing EAF slag slightly weakened the compressive and split-tensile strength due to the bad interfacial transition zones (ITZs) between EAF slag and cement paste as indicated in Fig. 2.4. In contrast, the combination of slag aggregate and 20% FA addition could prepare good-quality RCCP that met the requirements of exposed wearing surfaces. The mechanical behaviour of RCC containing crumb rubber and nano-silica was evaluated by the research team of Adamu et al. [18, 75, 103]. It was concluded that the substitution of fine aggregate with up to 20% rubber particles contributed to higher flexural strength values and ductility index as compared to the control case, but the compressive and split-tensile strengths evidently decreased when the substitution exceeded 10%. The inclusion of up to 2% nano-silica evidently mitigated the 28-day strength loss in compression and split-tension, and the optimum addition was 1.0%. The main principle is that nano-silica with high pozzolanic reactivity accelerates the cement hydration rate and increases the quantity of C-S-H gel [64]. The microstructure and ITZs between cement paste and rubber particles are thus both densified, which in turn improve the strengths of rubberized concrete while possessing great flexural toughness, crack resistance and longer service life. In addition, the behaviour of DCC paving

blocks considering various consolidation methods and rubber replacement ratios of sand was explored by Ling [2]. The findings reported that the delamination and cracking may appear on fresh block samples when the rubber content exceeded 20%, and the volume and dimensions were easily changed when the samples were demoulded (Fig. 2.5), causing the rejection rate increased. Inclusion of soft rubber particles of no more than 10% slightly enhanced the samples' strengths, but observably improved the deformability and toughness at all substitution ratios. In the practical viewpoint, plant-made compaction method is more recommended for rubberized paving blocks as compared to hand-ramming method.

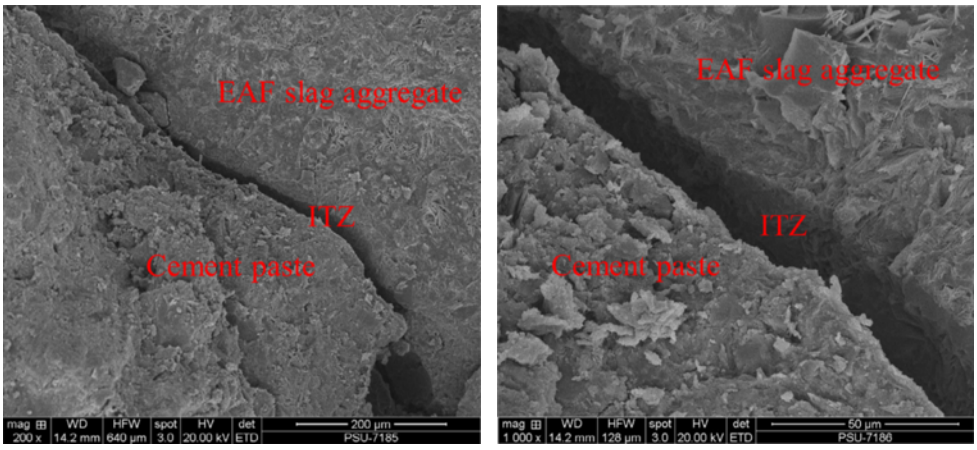

Fig. 2.4. SEM images of ITZ between EAF slag and paste under 200 and 1000 magnifications [73].

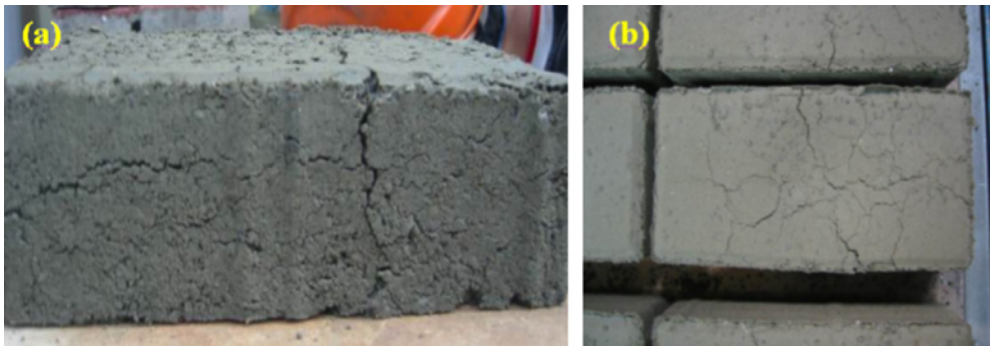

Fig. 2.5. Cracking and volume expansion of rubberized DCC paving blocks [2].

Since one of the most critical criteria for evaluating the RCCP and DCC pipes is whether they have an excellent tensile performance, researchers in their studies pay particular attention to the impacts of fibre type and dosage on the strength behaviour, especially the flexural tensile strength. Rooholamini et al. [8] assessed the effects of twisted bundle polyethylene fibres on pre-cracking RCCP properties including the flexural strength and fracture energy by carrying out the notched three-point bending test. According to the laboratory test results, conspicuous influence of fibre addition on compressive strength was not concluded, whereas a promising potential in increasing the flexural and residual strength was obtained and the post-cracking behaviour showed great ductility in high-flexural-strength RCCP. They further investigated the Mode I plain-strain cracking toughness of different mono/hybrid steel/PP fibre-reinforced RCC using revised two-parameter model in another research [88]. It can be seen from Fig. 2.6 that the change in fibre type, stiffness and aspect ratio (R_1, R_2 and H, respectively, denote mono PP, mono steel and hybrid fibre reinforcement) had less impact on the appearance of possible kinked cracks during the stable growth in comparison with control RCC without fibre reinforcement (N). The hybrid of copper-coated steel and macro PP fibres demonstrated the excellent fracture toughness in all cases (H_1, H_2 and H_3) benefitted from the effects of steel fibres on preventing the crack development and providing wider contact surface area. Karadelis et al. [79] conducted detailed experimental tests on flexural behaviour and fibre efficiency of polymer modified (PM) RCC with steel fibre reinforcement. It was concluded that the PM RCC

containing 1.5% steel fibres presented very high flexural strength (15.2 MPa) and great bonding with old concrete, which was very beneficial for the rehabilitation of worn pavements. In addition, Mohamed et al. [29] explored the structural and mechanical properties of full-size steel FR-DCC pipes via performing three-edge bearing tests (TEBT). Not surprisingly, the engineering characteristics including strength and modulus of elastic of the hardened mixture were improved with fibre addition, which endowed fibre-reinforced pipes with higher ultimate strength and superior post-cracking performance. Collated hooked end steel fibres were more effective on enhancing the flexural and tensile strength of pipe specimens, and dispersed steel fibres with minimum dosage of 20 kg/m^3 could be used to replace the conventional steel cages and met the reinforcement specification for Class V precast concrete pipes. Similar fibre toughening effect was also achieved by other researchers who employed PP and PVA fibres in the fabrication of DCC precast pipes [28, 30, 109]. Whether DCC mixtures were reinforced with mono or hybrid fibres, it had a remarkable impact on enhancing the pipe strength and ductility, along with holding cracks and preventing the collapse. Fig. 2.7 shows the typical crack patterns of fibre-reinforced DCC pipe after the TEBTs. Except for the four main cracks, no other serious damage was found, and the majority of steel fibres remained intact bridging the cracks and pipe matrix. In terms of fibre efficiency, Shao et al. [110] reported that the addition of steel fibres (within the range of 0.5-2.0 %) into dry concrete mixtures contributed more positive impact to the flexural strength rather than the compression, owing to the adopted preparation method

of the layered compaction endowed fibres with a longer anchorage length when the matrix was cracked under bending loads. As compared to self-compacting concrete with similar fibre size and dosage, the prepared dry concrete exhibited higher compressive and flexural strengths at 28 days of age, that is, steel fibres demonstrated a greater fibre efficiency. In addition, considering the higher fibre cost and the purpose of increasing the recycling ratio of waste materials, several types of sustainable fibres are mixed in concrete mixes to improve their properties. For instance, Haghnejad et al. [85] studied the mechanical responses of recycled PP FR-RCCP against the freeze-thaw and fatigue damage; Sobhan et al. [86] conducted laboratory experiments to study the strength behaviour of RCCP with incorporation of waste plastic fibres, and Angelakopoulos et al. [111] explored the compressive and bending performance of RCC reinforced with reused tyre fibres.

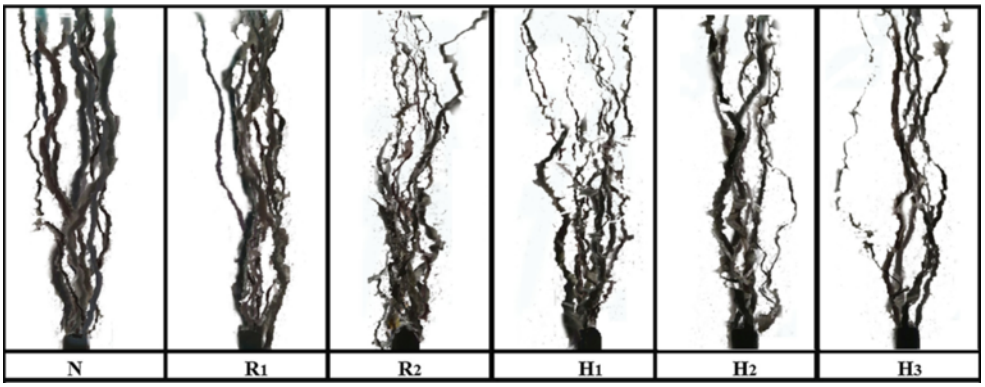

Fig. 2.6. Crack trajectory envelope for different mono/hybrid FRCC samples under Mode I applied loading [88].

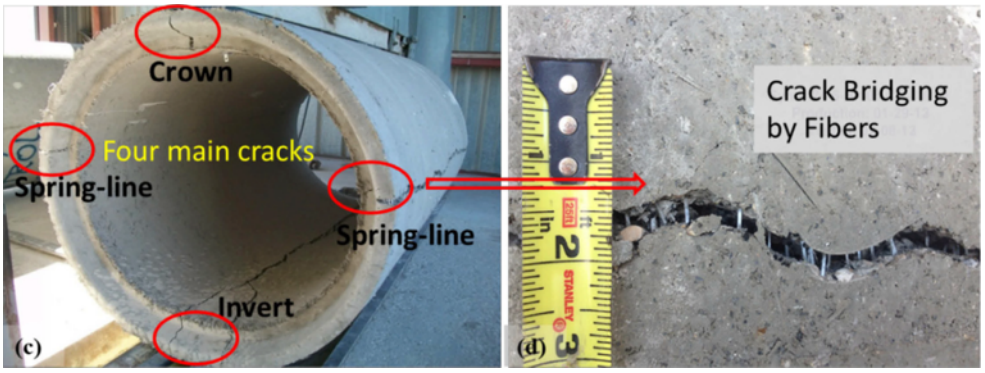

Fig. 2.7. Typical flexural failure patterns and crack bridging by fibres of fibre-reinforced DCC pipe [30].

It is noteworthy that since the main laying method of RCC is roller compaction layer by layer, the research into the interlayer performance of RCC is especially important. Liu et al. [112] investigated the influences of time interval and interlayer treatment on the interlayer shear strength of RCC. It was shown that the ultimate shear strength of RCC interlayer reduced with time intervals, especially after the final setting. In addition, the treatments of the expansion agent and nano-silica with mortar were proved to be more effective to improve the shear strength than the mortar alone. Zhu et al. [113] also studied the effects of the treatment (cement mortar with double expansion agents) on the properties of RCC interlayer, and it was demonstrated that the appropriate addition of double expansion agents could increase the shear strength, cohesive strength and frictional coefficient. The use of interlayer treatment materials could solve the permeation and bonding quality issues of RCCD structures. For the bond strength of RCC interlayer, Madhkhan et al. [114] investigated the influences of different normal pressures by carrying out the experimental investigation utilizing interlayer cement grout. Test results

illustrated that the use of cement grout, the increase in normal pressure and the decrease in moisture content of cement grout all improved the bond strength of RCC interlayer. In addition to the shear and bonding strength of RCC interlayer, the impact of the compaction quality was also very important for RCC interlayer performance. Liu et al. [115] evaluated the compaction quality of RCC matrix and interface by using the real-time monitoring quality index (unit compaction energy, UCE). Based on the data collected from laboratory compaction tests, a density regression and a shear strength regression models of RCC matrix and interface were developed to determine the control criteria of UCE. Moreover, a UCE-based real-time monitoring software was established for practical quality control, which could provide the quality assurance for RCC constructions.

2.3.2 Modulus of elasticity

The modulus of elasticity (MOE) is an essential and commonly used mechanical index for evaluating the ability of concrete material against the elastic deformation. Similar to conventional concrete, the MOE of dry concrete is commonly achieved by calculating the slope of the linear elasticity within the compressive stress-strain curve of a cylindrical specimen. Therefore, the variation law of MOE is closely similar to that of compressive behaviour [116]. It can also be said that most of the factors affecting the compressive strength, such as cementitious material content, aggregate type, water-binder ratio and curing period, may cause a fluctuation of MOE of dry concrete. Adamu et al. [18] found that the high-volume FA (HVFA) replacing cement markedly decreased the MOE of RCC at early ages originated

from the lagging pozzolanic reactivity of FA, and they further obtained 9-51% reduction in MOE at 28 days in the cases of 10-30% fine aggregate replacement with crumb rubber. This was attributed to the high deformation and low MOE of crumb rubber incorporated, and hence the mixtures had less rigidity as compared to control ones. Besides, a logarithmic correlation between compressive strength and MOE of HVFA RCC (MOE = 28166lnf_c - 83485) was developed possessing a better goodness of fit in comparison with ACI 318 model. Similar conclusions had also been drawn in other investigations where shredded rubber was added into RCC mixtures, and the factors such as higher porosity and poor adhesion between rubber particles and cement matrix were likewise considered to be other reasons for reducing the MOE of rubberized dry concrete [12, 42, 103]. Moreover, when natural aggregates were partially substituted by waste marble, RCA, RAP, EAF slag and plastic aggregate, the MOE of dry concrete demonstrated varying degrees of declination due to the weak bonding between the slurries and waste aggregates [31, 41, 73, 101, 117]. For example, the MOE of DCC blocks gradually diminished with the substitution level of waste marble increased from 0 to 40% (from A/B0 to A/B4), while the higher strength grade of cement (A-CEM Ⅱ 32.5N, B-CEM Ⅱ 42.5N) contributed to greater MOE and a reliable linear relationship existed between the compressive strength and MOE as presented in Fig. 2.8 [117]. Data in Table 2.2 demonstrated that the impact of various fibres on the compressive strength of dry concrete was inconclusive, and the MOE fluctuated as the inclusion of steel, PP and waste glass fibres increased [29, 54, 84, 104,

105]. The reason may be that the upper limit of MOE measurement was 40% of the ultimate compressive strength, i.e., the fibres' reinforcement and toughening effect had not yet been fully exerted [29].

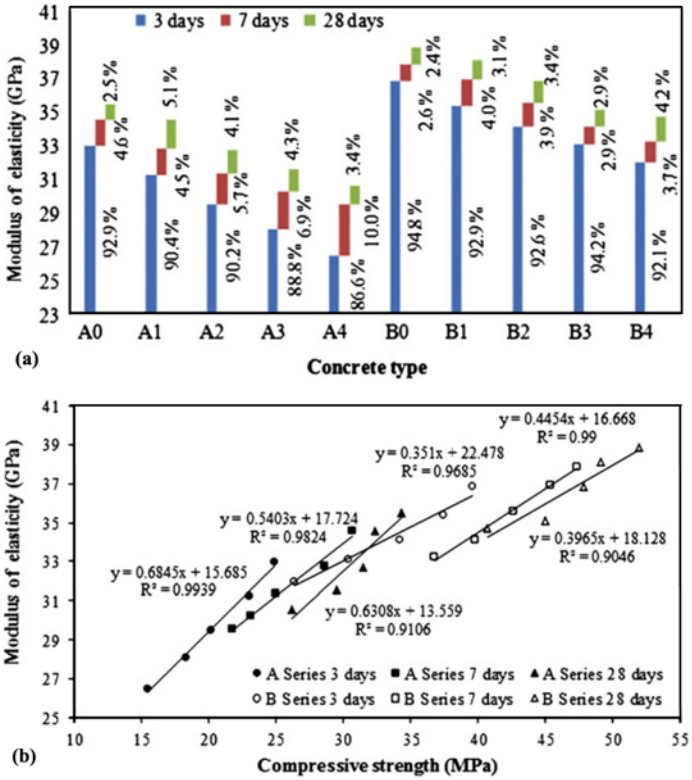

Fig. 2.8. (a) MOE variation and (b) its relationship with compressive strength of DCC blocks containing various contents of waste marble and types of cement [117].

2.4 Dynamic mechanical performance

It is well known that the mechanical performance of concrete structures under dynamic loads, such as seismic, impact and blast, are dramatically different from those under static/quasi-static conditions. It is, hence, essential to carry out the dynamic behaviour investigation of concrete structures. However, very scare literature is available on above dynamic property of dry concrete, and many of published papers pay particular attention to the dynamic compressive behaviour

of RCC mixtures under impact loads, as well as the seismic responses of RCC gravity dams under earthquake loads [93, 94, 118-121]. The research team of Wang et al. [93, 120, 121] studied the compressive behaviour and constitutive model of RCC under impact loads (SHPB with strain rate $\dot{\varepsilon}$ up to 120 s^{-1}) with consideration of the vertical stratification and initial damage. Moreover, considering that the poor interlayer bonding would significantly affect the mechanical and durability property of RCC layered structures like dam and pavement, the stress wave travelling across interlayers within RCC under SHPB impact loads was also analysed concretely [94]. Similar to conventional concrete, RCC was a strain rate sensitive material, but its dynamic increase factor (DIF) under different strain rates had a smaller fluctuation owing to the densified microstructure along with less water viscosity effect [120]. The derived DIF empirical formulae for the prepared RCC with respect to the compressive strength are given below:

$$DIF_{\dot{\varepsilon}} = 0.02669 \cdot (\log\dot{\varepsilon}) + 1.09872, \ (0.0001\ s^{-1} < \dot{\varepsilon} \leq 30\ s^{-1}) \quad (2.1)$$

$$DIF_{\dot{\varepsilon}} = 2.39591 \cdot (\log\dot{\varepsilon})^2 - 7.09013 \cdot (\log\dot{\varepsilon}) + 6.336, \ (30\ s^{-1} < \dot{\varepsilon} \leq 80\ s^{-1}) \quad (2.2)$$

Under the action of viscous/inertia effect at high strain rates and variation in MOE between cement paste and aggregate, RCC specimens were broken into several large fragments at lower strain rates ($\dot{\varepsilon} \leq 40\ s^{-1}$) and pieces were crushed into powders at higher strain rates ($\dot{\varepsilon} \geq 60\ s^{-1}$). The dynamic responses (strength and toughness) of RCC, along with the discrete degree of these values all increased

with strain rate, and the initial damage would result in a signal attenuation in the aforementioned properties at a higher strain rate [93, 121]. As an illustration, the decrease in dynamic compressive strength of damaged samples were 28.2% and 35.2% at the strain rates of 40 s^{-1} and 120 s^{-1}, respectively. Furthermore, in the analysis of the stress wave propagation within RCC interlayers under impact load, it was indicated that the existence of poor interlayers could effectively resist the propagation of stress waves, and the attenuation degree of stress waves within concrete samples was much weaker at higher strain rates [94]. The theoretical transmitted wave could well interpret the foregoing phenomenon. In terms of the seismic responses under earthquake loads, Wieland et al. [122] carried out a qualitative assessment to study the behaviour of RCCD under strong earthquake and pointed out that the dynamic stability of RCCD was reliable since the cracks developed along the horizontal interfaces. Based on a spot survey, the hazards and seismic responses of RCC arch dam (132 m) and concrete-faced rock-fill dam (156 m) following Wenchuan 8.0 earthquake were exhaustively evaluated by Lin et al. [118]. Research findings indicated that even though the earthquake loading suffered by RCCD was far greater than its design intensity of 7 and the extensive collapse was observed on both sides of mountains, the dam structure remained intact and was still safe after the mighty shaking without any visible cracking (Fig. 2.9(a-b)). The maintenance of the arch resistant effect of RCCD was effectively ensured by the mutual anchoring between the abutment slopes and granite, as depicted in Fig. 2.9(c-d). In addition to the field study, the finite-

element method (FEM) was another effective method in exploring some specific details on the seismic performance of RCCD. For instance, Kartal et al. [24, 119] studied the earthquake responses of RCCD under strong ground shaking via using FEM along with considering different reservoir lengths (0.5h-10h, h was the height of the dam). It was reported that the horizontal displacement significantly increased under hydrodynamic pressure, and the seismic properties were greatly affected by nonlinear responses as well as the dam reservoir length. Furthermore, Yazici et al. [104] evaluated the impact resistance of PP fibre-reinforced RCC (0.25-0.75% fibre volume dosage) by performing low-speed drop-weight tests on cylinder samples with a height of 64 mm and a diameter of 150 mm. As expected, fibre-reinforced samples were able to resist more drop impacts (increased from 134 to up to 141) and showed better fracture toughness by virtue of the evidently improved matrix brittleness, even though their mechanical properties reduced by approximately 20% in comparison with the plain concrete.

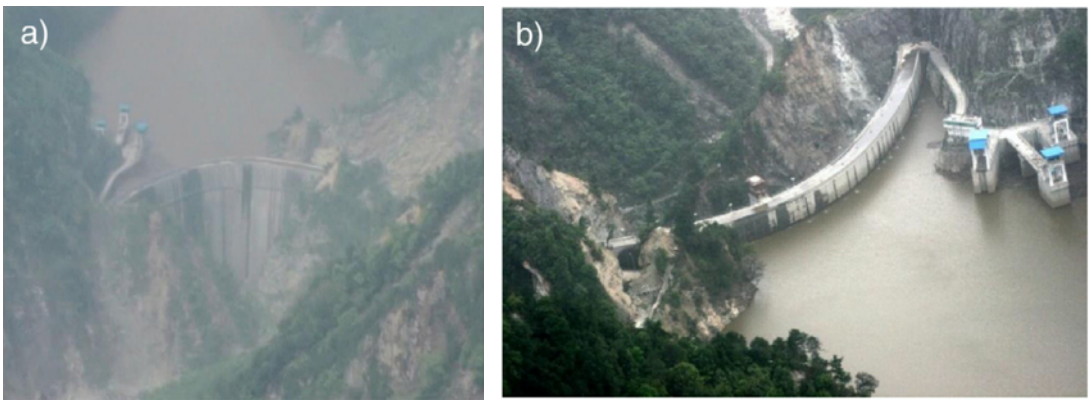

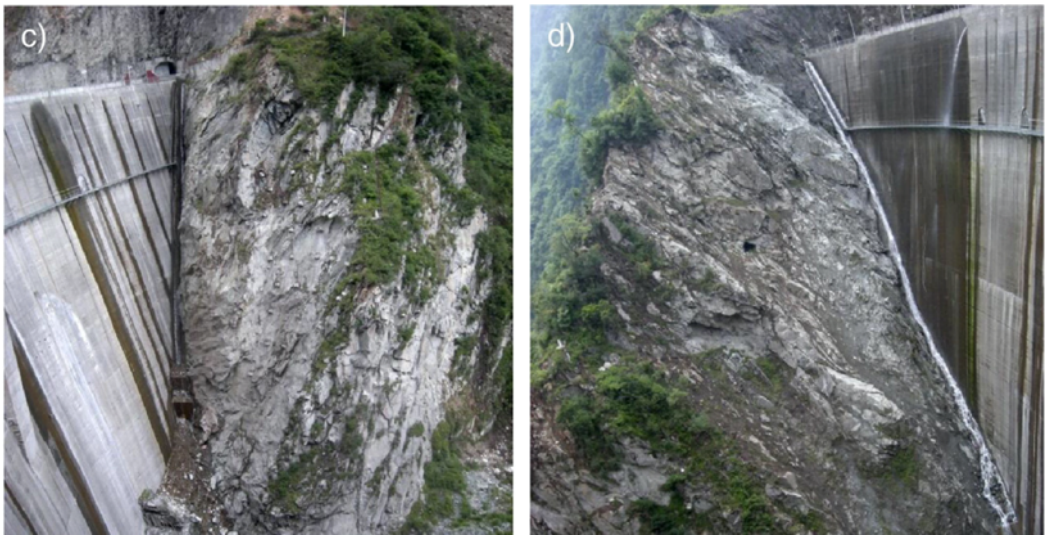

Fig. 2.9. Seismic response of RCCD after Wenchuan earthquake: (a) downstream view; (b) upstream view; (c) left abutment and (d) right abutment [118].

2.5 Summary and discussion

By collating a large number of published literature, this chapter reviews the raw material, preparation method, mixture performance and mechanical behaviour of dry concrete in detail. Based on the summary and discussion reported above, the conclusions can be drawn as follows:

1) As compared to the conventional self-compacting concrete, dry concrete has basically the same material composition but lower moisture and cementitious material content. Based on different casting and fabrication techniques, RCC and DCC are two most representative mixtures of dry concrete.
2) Preparation technique takes a dominant part in the properties of dry concrete. The commonly used fabrication method for DCC precast unit is mechanical consolidation and vibration, and that for RCCD/RCCP is roller compaction with vibratory drums and rollers. For RCC samples, compaction with vibrating

table and hammer is widely used laboratory preparation method in line with ASTM standards.

3) Thermal stress and the resulting surface cracks result in serious damage, unguaranteed service and durability of RCCD. Adjusting the cement addition, increasing the SCM content and adopting appropriate curing regime are of great help in controlling and reducing the temperature cracking.
4) The type and content of AMs, aggregate gradation and fibre are the most vital factors affecting the mechanical properties of dry concrete. Some industrial by-products are feasible to be extensively added to dry concrete mixtures of normal pavements and masonry products where the strength is not the main concern. Moreover, the bending performance and fracture toughness can be evidently improved by mixing rubber particles and most types of fibres.
5) Most of the factors affecting the compressive strength may cause a fluctuation of dry concrete MOE. The incorporation of waste aggregate instead of natural aggregate resulted in a decrease in MOE in different levels due to the weak bonding between the slurries and waste aggregate. The influence of fibres on MOE of dry concrete is inconclusive since the fibre reinforcement is not fully activated.
6) Dry concrete is a strain rate sensitive material with a smaller fluctuation of DIF under different strain rates. Based on a spot survey, RCCD remained intact and was still safe without any visible cracking even though the seismic loading suffered by dams was far greater than the specification design limit.

Dry concrete technology has been extensively employed in the construction of various concrete structures and the fabrication of prefabricated units owing to its excellent high early strength, fast construction speed and low production cost. However, its several shortcomings such as the low flexural tensile strength, poor toughness and susceptible to crack under stress and temperature also render the safety and service life of the concrete structures unable to be effectively ensured, due to the introduction of coarse aggregate and a large amount of AMs. Therefore, a sustainable dry ultra-high performance concrete (DUHPC), which combines the characteristics of conventional dry concrete with UHPC (ultra-high strength and great toughness/ductility), is necessary to be developed to expand dry concrete to more application fields. In addition, the influences of steel fibre reinforcement (different fibre dosages and combinations), curing regime (different temperatures) and recycled materials (HVFA and waste crumb rubber) on the static and dynamic behaviour, as well as the environmental benefit of the developed DUHPC are needed to be further explored and investigated.

Chapter 3

Development of Sustainable Steel Fibre-Reinforced DUHPC

3.1 Introduction

Concrete is a multi-phase heterogeneous composite building material constituted principally with cement, aggregate, chemical additives and water. In line with the evident distinctions in mixture flowability and the following fabrication method, concrete may be simply divided into two types, namely self-compacting concrete and dry concrete. In accordance with the definition of ACI 211.2 [1], dry concrete is considered as the hardened mixture having a low moisture and cementitious material content, and its fresh consistency with slump value of no more than 25 mm is significantly higher than that of ordinary Portland cement (OPC) concrete. During the mixing and casting, the fresh mixture needs to be moist enough to facilitate the slurry to fill the gap between the aggregates but viscous enough to support rollers or withstand the compaction load until the final form. RCC and DCC are two typical dry concrete mixtures with different fabrication methods and application areas [5, 123].

Based on the primary application fields of literatures introduced dry concrete, its structures and members are susceptible to damage caused by flexural-bending load, abrasion and penetrated erosion during their service. Unfortunately, the mechanical properties of the existing or developed dry concrete are unsatisfying due to its inherent features, such as low cement addition, and a large amount of recycled materials used to substitute partial OPC (FA, RHA, waste glass powder, alkali-activated slag, etc.) [19, 48, 56, 57, 124, 125] and aggregate (recycled CRT

funnel glass powder, EAF slag, CFBC ash, RCA, rubber, etc.) [18, 35, 41, 73, 74]. Therefore, numerous experimental studies have been conducted to enhance the mechanical properties of dry concrete and prolong its service life. These studies have demonstrated the potential use of some recycled materials in the production of high-performance concrete (HPC), leveraging their various advantages [3].

Adamu et al. [18] explored the compressive/flexural/split-tensile strength, MOE and abrasion resistance of HVFA RCC mixed with rubber aggregate and nano-silica. It was indicated that the foregoing properties reduced as the ratio of rubber particles replacing fine aggregate increased, but nano-silica could mitigate these adverse impacts by virtue of its great pozzolanic effect on densifying the micro-structure and ITZ of concrete matrix. In addition, the authors pointed out that the inclusion of nano-silica could contribute to better fatigue, shrinkage and creep resistance of crumb rubber-incorporated RCC with and without HVFA [62, 63]. Rooholamini et al. [8] explored the impact of twisted PP fibre on the consistency and mechanical property of RCCP by conducting three-point bending test on pre-cracking beams and using response surface method. Test results indicated that although the inclusion of PP fibres would diminish the mixture consistency and thus increase the compaction energy, it markedly contributed to flexural strength and fracture energy in addition to the compressive strength. Moreover, to further study the effect of mono/hybrid (PP and steel) fibres on RCCP fracture behaviour, a modified two-parameter model was developed to assess the fracture toughness considering the possible kinked cracks [88]. Mohamed et al. [29] studied the

mechanical behaviour of steel fibre-reinforced DCC to explore the possibility of utilizing the developed DCC to replace conventional RC for fabricating the pipes. It was concluded that the dispersed steel fibres with 20 kg/m^3 volume addition reached the reinforcement requirements for Class V pipes as per ASTM C76, and could be adopted to replace regular steel cages inside pre-cast concrete pipes. Additionally, researchers who mixed PP and PVA fibres into mixtures came to the similar conclusions of fibre's toughening effect on DCC pipe properties [28, 30, 109]. In addition to steel, PP and PVA fibres reported above, different recycled fibres, such as reused tyre [87, 111], waste plastic [86] and glass fibres [84], were also added to dry concrete to improve its target performance.

This study aims to develop a sustainable DUHPC, which not only possesses the characteristics of fast hardening as well as rapid demoulding of conventional dry concrete, but also has the advantages of ultra-high strength and great toughness of UHPC. Subsequently, the influences of different curing regimes and steel fibre volume additions on the mechanical behaviour of steel fibre-reinforced DUHPC (FR-DUHPC) were further explored. Finally, the environmental impact of DUHPC was evaluated via considering the total amount of ASCMs and CO_2 emissions.

3.2 Materials and proportioning design

3.2.1 Raw materials

Like conventional concrete, the properties of dry concrete are associated with the type, mixing ratio and moisture content of its matrix raw materials. It is therefore important to use appropriate raw materials and carry out mix design for fresh

mixture workability as well as strength and durability of hardened concrete. To ensure the consistency of dry-cast cement mortar and steel FR-DUHPC, the cement used was composite Portland cement (42.5 Grade) complying with the Chinese standard GB175-2020. The ultra-fine industrial waste silica fume was selected as an ASCM to densify the matrix microstructure in consideration of its excellent pozzolanic activity and micro-aggregate filling effect. Moreover, in order to improve the mixture internal microstructure, interfacial properties, workability and reduce its early hydration heat, as well as enhance the long-term strength of dry concrete (based on the pozzolanic reaction), FA and GGBS were added to concrete mixtures as a partial substitute for cement. The main components and physical characteristics of silica fume, FA and GGBS are listed in Table 3.1. It is noteworthy that the incorporation of the foregoing ASCMs can likewise minimize the amount of cement utilized and cut down the environmental wastes generated, which is in line with green and sustainable concrete concepts.

Table 3.1

Components and physical characteristics of silica fume, FA and GGBS.

Components/Properties	Silica fume	FA	GGBS
Al_2O_3 (%)	--	29.09	21.71
SiO_2 (%)	93.91	53.36	34.43
CaO (%)	1.85	8.27	33.16
Other components	MgO, Fe_2O_3, K_2O, Na_2O	MgO, Fe_2O_3, K_2O	MgO, Fe_2O_3, SO_3
Loss ignition (%)	0.30	2.48	1.01
Fineness (Blaine, m^2/kg)	--	359	385
Specific gravity	2.20	2.55	2.83

As for aggregate, natural quartz sand with an aggregate size ranged between 0.12 mm and 1.18 mm was used to substitute the traditional gravel aggregate inside the concrete mixture in favour of good particle packing and cementitious materials with the aggregate bond. Its specific gravity and packing density were, respectively, 2.63 and 1.65 g/cm^3, and the water absorption was 0.58%. The particle size distribution (PSD) curves of natural quartz sand, cement, silica fume, FA and GGBS mixed in dry-cast mortar and DUHPC mixtures are plotted in Fig. 3.1. Moreover, smooth and copper-coated steel micro-fibres with diameter of 0.12 mm, length-diameter ratio of 83.33 and tensile strength of more than 4000 MPa were added to DUHPC mixes to upgrade its mechanical properties. The volume dosage of the fibre addition was 0.5%, 1.0%, 1.5% and 2.0%, respectively. Since the moisture content of dry concrete was limited and the presence of steel fibres would reduce the workability of fresh mixtures, polycarboxylate superplasticizer with early-strength ingredients and a water-reducing rate of 27% was added to all mixtures to achieve a satisfied consistency and good workability.

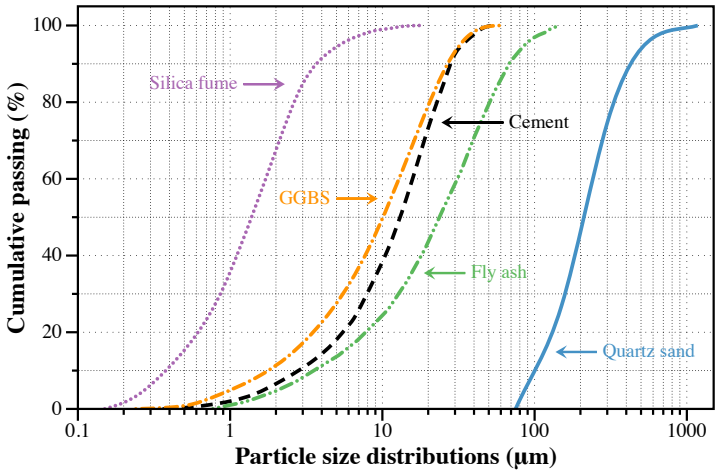

Fig. 3.1. PSD curves of raw materials used in dry-cast cement mortar and DUHPC.

3.2.2 Proportioning design method

For the purpose of determining the benchmark mix proportion of FR-DUHPC as well as exploring the effects of water-binder ratio (w/b) and the substitution ratio of cement using silica fume, FA and GGBS on the behaviour of dry-cast cement mortar, a high-efficiency orthogonal test method was utilized in the current study. Orthogonal test adopts orthogonal table to arrange parameters and levels, and selects representative tests from all combinations to perform range and variance analysis, and finally the optimal scheme can be obtained [126]. Based on the preliminary trials, the fractions of the total cementitious materials, aggregate and superplasticizer were set to predetermined values, and the mass ratio of these three materials was 1: 1.85: 0.02. L16 (4^5) orthogonal table with an error column was selected, and the parameters and levels of the orthogonal experiments are detailly listed in Table 3.2, in which the percentage indicates the replacement ratio of the corresponding ASCMs for cement. Finally, 16 dry-cast mortar mixes with the combination of four levels of A, B, C and D and an error column were prepared without any significance. The mix combinations are given in Table 3.3. After the optimal mix proportion of dry-cast cement mortar was determined, steel fibres with volume dosage ranged between 0.5% and 2.0% were added to the matrix to study their effect on the performance of FR-DUHPC.

Table 3.2

Factors and levels of the orthogonal experiments.

Factors		Level 1	Level 2	Level 3	Level 4
Water-binder ratio	A	0.15	0.16	0.17	0.18
Silica fume	B	0%	5%	10%	15%
FA	C	0%	10%	15%	20%
GGBS	D	0%	5%	10%	15%

Table 3.3

Orthogonal experiments for mortar mixtures and the relevant test results.

Mix	W/b	SLF	FA	GGBS	Error	Density (kg/m^3)		f_c (MPa)		f_r (MPa)		f_{ts} (MPa)	
	(A)	(B)	(C)	(D)	(E)	Fresh	Har.	3-d	7-d	3-d	7-d	3-d	7-d
L1	1	1	1	1	1	2170	2173	30.1	31.7	6.6	9.6	3.3	3.5
L2	1	2	2	2	2	2208	2211	38.9	41.0	5.8	10.1	4.2	4.9
L3	1	3	3	3	3	2277	2302	49.9	58.0	7.6	11.7	4.3	5.7
L4	1	4	4	4	4	2322	2326	54.6	66.8	9.7	12.9	4.6	6.5
L5	2	1	2	3	4	2226	2229	30.2	31.8	4.9	7.3	3.6	3.9
L6	2	2	1	4	3	2310	2314	53.9	55.1	11.2	11.9	5.0	5.4
L7	2	3	4	1	2	2299	2283	61.9	87.8	15.3	16.3	6.1	8.4
L8	2	4	3	2	1	2290	2288	60.7	79.5	12.8	14.8	6.2	7.4
L9	3	1	3	4	2	2242	2245	42.2	44.4	5.2	7.2	3.3	3.6
L10	3	2	4	3	1	2259	2252	61.5	63.8	9.3	11.1	3.8	4.8
L11	3	3	1	2	4	2303	2304	73.5	78.0	10.5	14.7	5.8	7.2
L12	3	4	2	1	3	2267	2269	67.1	76.8	9.9	13.3	5.2	6.7
L13	4	1	4	2	3	2273	2275	50.2	61.2	6.7	7.5	3.0	3.7
L14	4	2	3	1	4	2259	2261	72.4	82.1	9.5	12.0	4.1	6.9
L15	4	3	2	4	1	2268	2271	70.6	74.6	6.8	10.4	4.6	6.3
L16	4	4	1	3	2	2304	2307	77.6	82.8	9.5	11.5	5.9	7.4

Notes: “SLF” denotes silica fume and “Har.” denotes hardened density.

3.3 Specimen preparation, curing and testing

3.3.1 Specimen preparation

During the preparation of dry-cast cement mortar, well-graded quartz sand and powder materials which consisted of cement, silica fume, FA and GGBS were dry mixed using a laboratory concrete mixer for 5 mins prior to any water introduction. Additionally, steel fibres were evenly dispersed into the mixer within the 5 mins of dry mixing when FR-DUHPC mixtures was being mixed. Then, the weighed water (superplasticizer pre-blended) was slowly poured into dry materials and mixed for another 7 mins and fibres were evenly distributed and the desired consistency was observed. Subsequently, the fresh mixture was poured into steel and plastic variform moulds and compacted in three layers via utilizing a concrete shaking table with a frequency of 48 Hz and an amplitude of 0.3-0.6 mm. The vibrating duration was between 20-35 s per layer and the slurry ring would appear in the previous layer prior to starting to prepare the next layer. Surcharges with different cross-sectional dimensions and shapes, based on different tests, were used to distribute the vibrated-compaction energy. Finally, a plastic film that prevented the evaporation of water was employed to wrap the mould. It is noteworthy that the low moisture content and steel fibre addition affected the consistency of FR-DUHPC. Hence, extra attention was paid once the water was added. Short wet stirring time could not adequately mix dry materials with water, whereas the water evaporation inside the mixture would increase with long mixing period, causing attenuated concrete performance. Fig. 3.2 shows the preparation process of FR-

DUHPC samples and the used moulds (surcharges) respectively for compression, bending and split-tension tests.

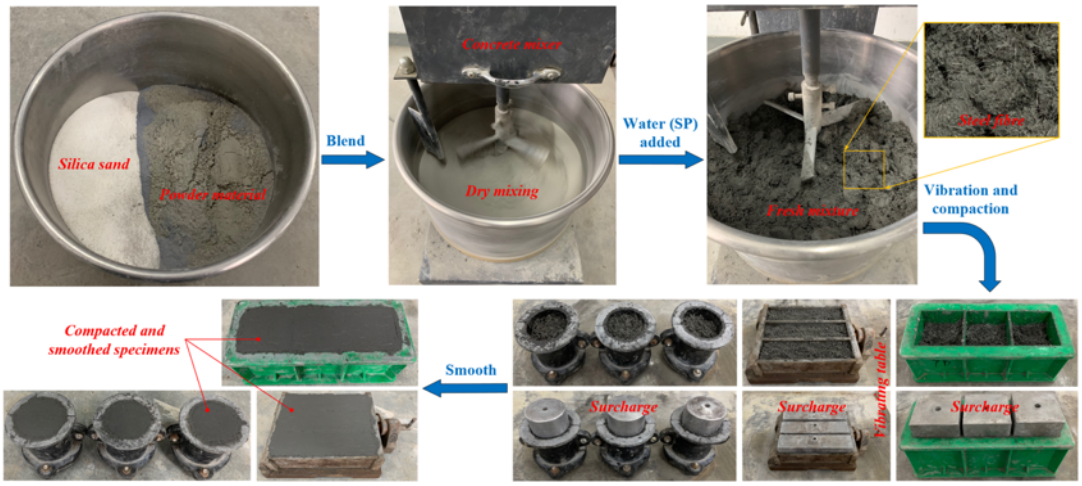

Fig. 3.2. Preparation process of FR-DUHPC samples for static mechanical tests.

3.3.2 Curing regime

The curing regimes including room-temperature water curing (20 ℃), moist/steam curing (30-60 ℃) and hot-water bath curing (90 ℃) were employed to explore the effect of curing regime on the behaviour of FR-DUHPC. Moist/steam curing is a high efficiency curing method in common use for pre-cast concrete components, and another two are universally accepted concrete curing methods in laboratories, especially for preparing UHPC. After compaction, moist/steam curing samples were placed in an insulated container at corresponding temperatures for 24 h, and the samples under the other two curing conditions were cured in a humid room (20 ± 2 ℃) for 24 h first. All samples were then in turn demoulded and cured in normal-temperature water until they were tested. For hot-water bath samples, they were cured in hot water for another 24 h before put in 20 ℃ water. For dry-cast mortar samples, room-temperature water curing was used until the testing.

Concrete samples cured in water were provided with a curing environment for the continuous hydration of cementing materials upon demoulding, and the moisture loss of concrete matrix due to surface evaporation could also be effectively prevented, which was beneficial for dry-cast cement mortar and DUHPC with low moisture content. Fig. 3.3 exhibits the cubic, beam and cylinder mortar samples after the water curing.

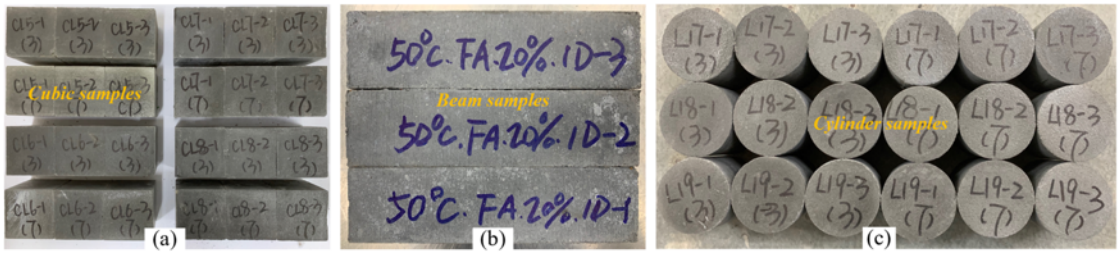

Fig. 3.3. Dry-cast mortar of (a) cubic, (b) beam and (c) cylindrical samples after curing.

3.3.3 Test procedure

Quasi-static uniaxial compression tests, as per Chinese standards GB/T50081-2019 and CECS13-89, were performed on dry-cast cement mortar and DUHPC samples using a computer-controlled hydraulic testing machine with a capacity of 100 tons. The dimensions of cubic samples were 40 × 40 × 40 mm and their compacted surfaces were set as the load-bearing direction. All the samples were centrally put between the upper and lower rigid plates and loaded at a constant rate of 0.2 mm/min until failure. On both sides of the support plate, two LVDTs were symmetrically fixed to measure/record the axial displacement of samples. In total there were 321 cubic samples tested, including 105 dry-cast mortar and 216 FR-DUHPC samples.

Quasi-static bending tests, conforming to Chinese standards GB/T50081-2019 and CECS13-89, were carried out on beam samples with dimensions of 40 × 40 × 160 mm by utilizing a 5-ton universal testing machine. The flexural behaviour of beam samples without notch was explored via utilizing a three-point flexural bending configuration, and the clear span between the two roller supports was 100 mm. Similarly, two symmetrical LVDT sensors were fixed at each side of the mid-span to record the vertical deflection of the samples. To obtain the sample's complete force-deflection relationship, a displacement loading of 0.05 mm/min was adopted. The compacted surface was also set as the load-bearing surface, and a total of 105 cement mortar and 216 FR-DUHPC samples were prepared and tested.

Splitting-tension tests, in accordance with Chinese standards GB/T50081-2019 and CECS13-89, were carried out on cylindrical dry-cast mortar and FR-DUHPC samples with dimensions of 50 mm in diameter and height via utilizing a 10-ton universal testing machine. Cylindrical samples were horizontally fixed between the support and loading plates via two upper and lower plywood with a width of 4 mm. Then, the compression load was slowly applied along the height of samples at a rate of 0.05 mm/min. Tests stopped when the cylinder samples were split into two parts along the loading direction as depicted in Fig. 3.4, and this damage pattern was caused by the indirect tensile stress from the Poisson's effect. Finally, a total of 321 dry-cast samples with 105 cement mortar and 216 FR-DUHPC were laboratorial prepared and tested.

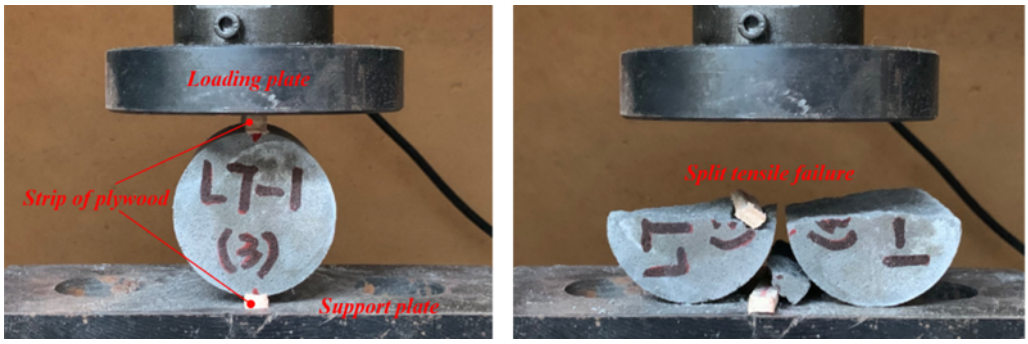

Fig. 3.4. Split-tension test setup (left) and failure pattern (right) of the mortar sample.

3.4 Results and discussion

3.4.1 Orthogonal experiment results

According to the orthogonal experimental scheme, a total of 16 groups of mix proportion tests were carried out. Three identical dry-cast mortar samples were prepared for each group. The results of the orthogonal experiments are listed in Table 3.3, where f_c is the uniaxial compressive strength, f_r is the rupture modulus (flexural strength for FR-DUHPC) and f_{ts} is the splitting-tensile strength. All of the mortar samples were tested for the strength behaviour at 3 and 7 days after 20 ℃ water curing. It should be noted that high compactness was a significant feature of UHPC, the unit weight of the mixtures in both fresh and hardened states was therefore considered an important indicator for evaluating the performance of the prepared dry-cast mortar. Then, the benchmark mixing proportion of FR-DUHPC was determined in view of the analysis on these orthogonal test results.

3.4.1.1 Unit weight of cement mortar

The range analysis of the unit weight and the influences of each factor in the orthogonal experiments are, respectively, shown in Table 3.4 and Fig. 3.5, where

Delta (Δ) is the difference between the maximum and minimum values. The fresh unit weight corresponded to the state of mixtures after vibrated compaction and prior to curing, and the hardened unit weight referred to the state of mortar after they were demoulded. As can be observed from the range analysis, interestingly, the unit weight of cement mortar under both fresh and hardened conditions was more affected by the replacement percentage of silica fume and FA rather than water-binder ratio. During the mixing, it can be noticed that under the same water-binder ratio, the consistency was evidently improved with increasing FA content substituted for cement. This maybe that the FA with a micro-spherical appearance enhanced the movement and permeability of the paste across aggregate cracks and hence improving the interface bonding performance between the aggregates and slurries. The increased amount of micro-spheres after the equivalent mass replacement of cement further enhanced this effect. Furthermore, the increase in silica fume content also densified the microstructure of mortar and improved its unit weight. The results of analysis of variance (ANOVA) for unit weight of dry-cast cement mortar are presented in Table 3.5 in detail, in which SS_A is the sum of squares, DOF is the degrees of freedom, MS_A is the mean squares for each variation source and F-value is used to test whether the result can represent the truth scale of the sample population. It was indicated that all the sources had no significant effect on both fresh and hardened unit weight since the F-value was less than 9.28 ($F_{0.05}$). After considering the cost and unit weight of dry-cast mortar, the optimal combination is A2B3C4D4.

Table 3.4

Response table for unit weight of dry-cast cement mortar.

Levels	Fresh mixture unit weight (kg/m^3)					Hardened mixture unit weight (kg/m^3)				
	A	B	C	D	E	A	B	C	D	E
1	2244	2227	2272	2249	2247	2248	2230	2275	2251	2251
2	2281	2259	2243	2269	2263	2284	2262	2245	2271	2266
3	2268	2287	2267	2267	2282	2270	2289	2271	2270	2285
4	2276	2296	2288	2285	2278	2279	2299	2291	2289	2280
Delta (△)	37.0	68.0	46.0	36.0	35.0	36.0	69.0	47.0	38.0	34.0
Rank	3	1	2	4	5	4	1	2	3	5

Table 3.5

ANOVA table for unit weight of dry-cast cement mortar.

Source	Fresh mixture unit weight				Hardened mixture unit weight			
	SS_A	DOF	MS_A	F-value	SS_A	DOF	MS_A	F-value
W-b ratio	3207.188	3	1069.063	1.067^{NS}	3036.500	3	1012.167	1.036^{NS}
Silica fume	11283.188	3	3761.063	3.753^{NS}	11326.500	3	3775.500	3.864^{NS}
FA	4345.188	3	1448.396	1.445^{NS}	4345.000	3	1448.333	1.482^{NS}
GGBS	2709.688	3	903.229	0.901^{NS}	2929.500	3	976.500	0.999^{NS}
Error	3006.190	3	1002.063	---	2931.500	3	977.167	---

Notes: “W-b ratio” denotes water-binder ratio and “NS” denotes no significant.

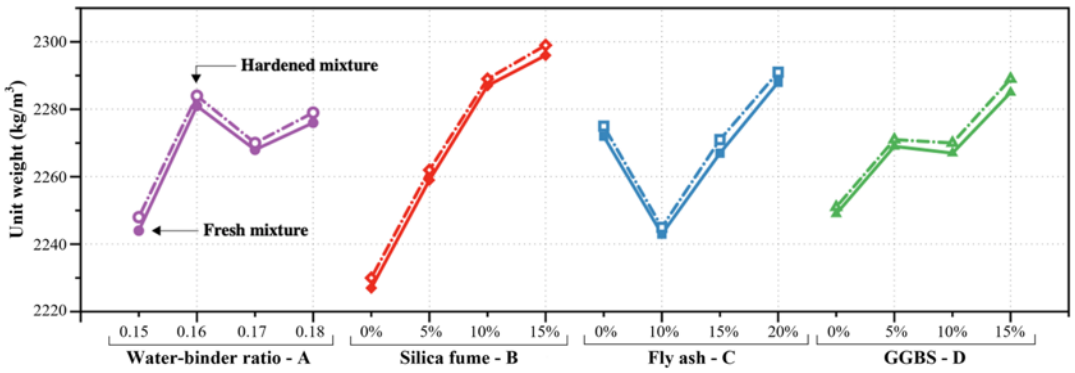

Fig. 3.5. Effects of various factors on unit weight of dry-cast cement mortar.

3.4.1.2 Compressive strength of cement mortar

The range analysis for dry-cast cement mortar in compressive strength and the effects of each factor in orthogonal experiments are, respectively, shown in Table 3.6 and Fig. 3.6. Data and curves clearly illustrated that the order of the effect of various factors on 3 and 7-day compressive strength was the same, i.e., silica fume content > water-binder ratio > FA content > GGBS content. The 3 and 7-day compressive strength of mortar samples increased as the water-binder ratio and silica fume content increased. But the strength growth rate slowed down observably when the replacement ratio of silica fume exceeded 10%. Moreover, the impact of FA and GGBS addition on 3-day compression behaviour was not evident. However, the 7-day strength was gradually enhanced as the FA addition increased from 10% to 20%, which was attributed to the continuous secondary hydration provided by FA with great pozzolanic activity. Table 3.7 illustrates the significance of various variation sources on the compressive strength of dry-cast cement mortar. The results indicated that the water-binder ratio and silica fume content were highly significant as expressed by F-value greater than 29.5 ($F_{0.01}$), while the GGBS and FA addition were only, respectively, significant and highly significant for 7-day compressive strength, which were consistent with the range analysis results. Therefore, the optimal mix proportion regarding the compression performance of cement mortar is A4B3C4D2.

Table 3.6

Response table for compressive strength of dry-cast cement mortar.

Levels	3-day compressive strength (MPa)					7-day compressive strength (MPa)				
	A	B	C	D	E	A	B	C	D	E
1	43.4	38.2	58.8	57.9	55.7	49.4	42.3	61.9	69.6	62.4
2	51.7	56.7	51.7	55.8	55.2	63.6	60.5	56.1	64.9	64.0
3	61.1	64.0	56.3	54.8	55.3	65.8	74.6	66.0	59.1	62.8
4	67.7	65.0	57.1	55.3	57.7	75.2	76.5	69.9	60.2	64.7
Delta (△)	24.3	26.8	7.1	3.1	2.5	25.8	34.2	13.9	10.5	2.3
Rank	2	1	3	4	5	2	1	3	4	5

Table 3.7

ANOVA table for compressive strength of dry-cast cement mortar.

Source	3-day compressive strength				7-day compressive strength			
	SS_A	DOF	MS_A	F-value	SS_A	DOF	MS_A	F-value
W-b ratio	1362.937	3	454.312	82.647^{**}	1363.523	3	454.508	101.453^{**}
Silica fume	1851.117	3	617.039	112.250^{**}	3004.223	3	1001.408	223.529^{**}
FA	109.502	3	36.501	6.640^{NS}	421.067	3	140.356	31.330^{**}
GGBS	21.737	3	7.246	1.318^{NS}	277.282	3	92.427	20.631^{*}
Error	16.490	3	5.497	---	13.440	3	4.480	---

Notes: “W-b ratio” denotes water-binder ratio, “NS” denotes no significant, “*” denotes significant and “**” denotes highly significant.

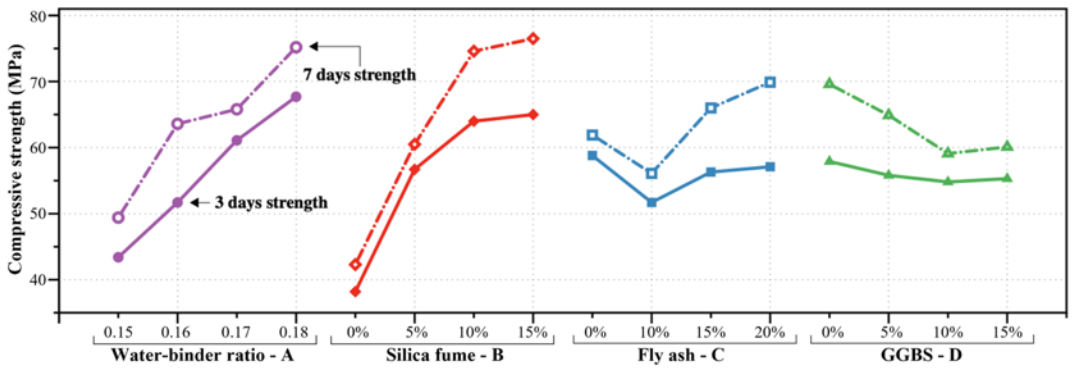

Fig. 3.6. Effects of various factors on compressive strength of dry-cast cement mortar.

3.4.1.3 Rupture modulus of cement mortar

The range analysis of the rupture modulus for cement mortar and the impacts of each factor from the orthogonal experiments are, respectively, exhibited in Table 3.8 and Fig. 3.7. No surprisingly, the content of silica fume exhibited the greatest impact on both 3 and 7-day rupture modulus of mortar samples. The influence of water-binder ratio and FA addition on 3-day rupture modulus was ranked second and third with little difference, whereas the other three parameters excluding silica fume addition had no marked difference on 7-day rupture modulus. The rupture modulus was not continuously increased with water content, which was different from its impact on compressive performance. An optimal water-binder ratio was found, and beyond/below which the rupture modulus would be reduced. Moreover, when the proportion of FA substituting partial cement was within the range of 10-20%, its positive influence on rupture modulus was less evident than that against the compressive strength. Table 3.9 exhibits the results of ANOAV for the rupture performance of mortar samples and it was shown that all the control factors had remarkable significance when the testing age was 3 days. But for 7-day rupture modulus, the influences of FA content and water-binder ratio/GGBS content were downgraded to inapparent and normal significant, respectively. Thus, the optimal mix combination for rupture behaviour of cement mortar is A2B3C4D2.

Table 3.8

Response table for rupture modulus of dry-cast cement mortar.

Levels	3-day rupture modulus (MPa)					7-day rupture modulus (MPa)				
	A	B	C	D	E	A	B	C	D	E
1	7.4	5.9	9.5	10.3	8.9	11.1	7.9	11.9	12.8	11.5
2	11.1	9.0	6.9	9.0	9.0	12.6	11.3	10.3	11.8	11.3
3	8.7	10.1	8.8	7.8	8.9	11.6	13.3	11.4	10.4	11.1
4	8.1	10.5	10.3	8.2	8.7	10.4	13.1	12.1	10.6	11.7
Delta (△)	3.6	4.6	3.4	2.5	0.3	2.2	5.4	1.8	2.4	0.6
Rank	2	1	3	4	5	3	1	4	2	5

Table 3.9

ANOVA table for rupture modulus of dry-cast cement mortar.

Source	3-day rupture modulus				7-day rupture modulus			
	SS_A	DOF	MS_A	F-value	SS_A	DOF	MS_A	F-value
W-b ratio	29.642	3	9.881	147.478^{**}	10.477	3	3.492	12.041^{*}
Silica fume	52.357	3	17.452	260.478^{**}	75.027	3	25.009	86.238^{**}
FA	25.297	3	8.432	125.851^{**}	7.377	3	2.459	8.479^{NS}
GGBS	14.502	3	4.834	72.149^{**}	14.962	3	4.987	17.197^{*}
Error	0.200	3	0.067	---	0.870	3	0.290	---

Notes: “W-b ratio” denotes water-binder ratio, “NS” denotes no significant, “*” denotes significant and “**” denotes highly significant.

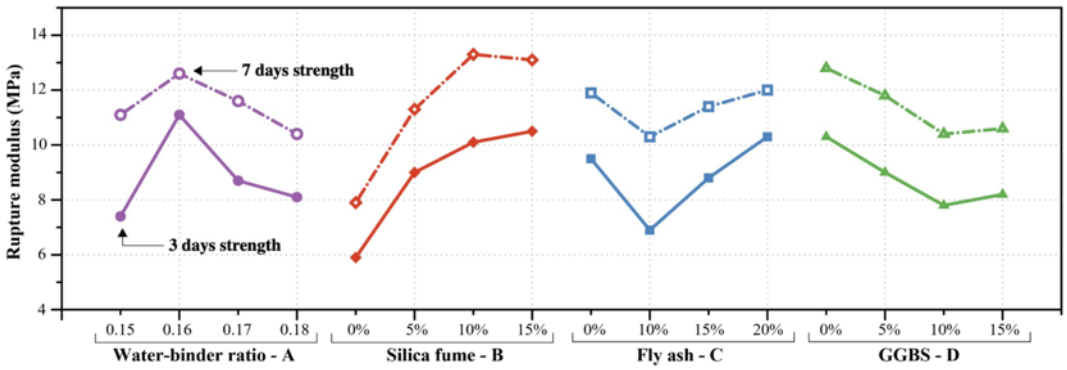

Fig. 3.7. Effects of various factors on rupture modulus of dry-cast cement mortar.

3.4.1.4 Split-tensile strength of cement mortar

The range analysis for dry-cast cement mortar in split-tensile strength and the influences of each factor from the orthogonal experiments are exhibited in Table 3.10 and Fig. 3.8, respectively. Since the flexural bending and split-tension tests were two commonly used means to measure the tensile behaviour of concrete members, the effect of four factors on split-tensile strength was similar to that on rupture modulus. The introduction of silica fume substituting partial cement and the water-binder ratio were two prominent factors affecting the early split-tensile behaviour of cement mortar, but the other two parameters presented a smaller influence. The obtained ANOVA results listed in Table 3.11 further confirmed the above findings and only silica fume content was conspicuous for 3-day splitting-tensile strength. Finally, the optimal proportion combination considering the split-tensile performance is A2B3C4D2, which is the same as that of rupture modulus.

Table 3.10

Response table for split-tensile strength of dry-cast cement mortar.

Levels	3-day split-tensile strength (MPa)					7-day split-tensile strength (MPa)				
	A	B	C	D	E	A	B	C	D	E
1	4.1	3.3	5.0	4.7	4.5	5.2	3.7	5.9	6.4	5.5
2	5.2	4.3	4.4	4.8	4.9	6.3	5.5	5.4	5.8	6.1
3	4.5	5.2	4.5	4.4	4.4	5.6	6.9	5.9	5.5	5.4
4	4.4	5.5	4.4	4.4	4.5	6.1	7.0	5.9	5.5	6.1
Delta (△)	1.1	2.2	0.6	0.4	0.5	1.1	3.3	0.5	0.9	0.7
Rank	2	1	3	5	4	2	1	5	3	4

Table 3.11

ANOVA table for split-tensile strength of dry-cast cement mortar.

Source	3-day split-tensile strength				7-day split-tensile strength			
	SS_A	DOF	MS_A	F-value	SS_A	DOF	MS_A	F-value
W-b ratio	2.722	3	0.907	4.774^{NS}	3.082	3	1.027	1.720^{NS}
Silica fume	11.662	3	3.887	20.458^{*}	29.007	3	9.669	16.196^{NS}
FA	1.043	3	0.348	1.832^{NS}	1.547	3	0.516	0.864^{NS}
GGBS	0.522	3	0.174	0.916^{NS}	2.287	3	0.762	1.276^{NS}
Error	0.570	3	0.190	---	1.790	3	0.597	---

Notes: “W-b ratio” denotes water-binder ratio, “NS” denotes no significant and “*” denotes significant.

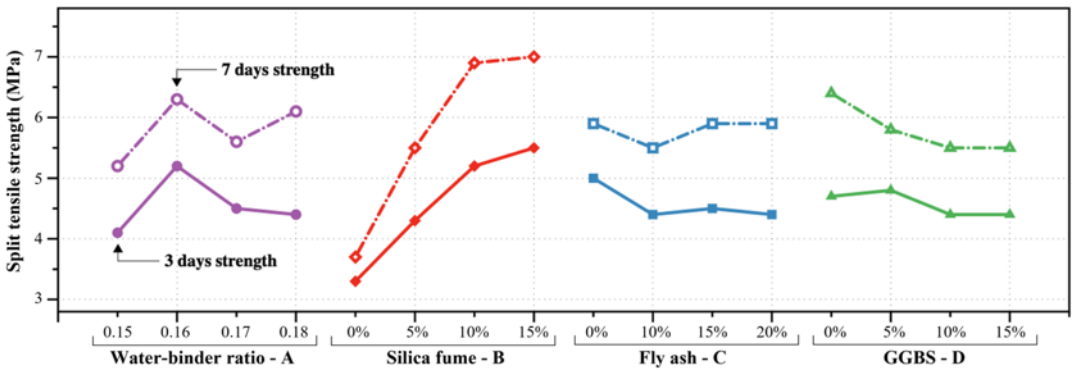

Fig. 3.8. Effects of various factors on split-tensile strength of dry-cast cement mortar.

3.4.1.5 Optimal mix proportion of cement mortar

It can be clearly illustrated through the foregoing analysis that the proportions of silica fume and FA replacing partial cement are the principal factors determining the unit weight of cement mortar. However, the influences of both FA and GGBS addition on its mechanical performance are inconspicuous, which are not quite identical to what other researchers have reported [18, 40, 43, 123]. The reason

might be that the high-strength cement mortar contained evidently more cement in comparison with traditional normal-strength dry concrete, and meanwhile the amounts of cement-substitution with FA and GGBS were within a lower range in this study. The active ingredient in these materials had not fully participated in the pozzolanic reaction at early stages, and they mainly played a micro-aggregate filling effect in the concrete mixture. Hence, the impact of their content change on mortar strength was less prominent than that of silica fume and moisture content. In addition, owing to the fact that concrete mechanical properties are the decisive factors affecting its proportion design and also dry concrete structures and units are more vulnerable to the flexural tensile loads during their service life, the mix design should give priority to its impact on the bending property of dry concrete. Also, since the water-binder ratio exceeding the optimal moisture content notably diminished the flexural and splitting-tensile strengths of cement mortar, the mix proportion combination was ultimately determined as A2B3C4D2, i.e., the water-binder ratio was 0.16 and the percentages of utilizing silica fume, FA and GGBS instead of partial cement were, respectively, 10%, 20% and 5%. High-strength dry-cast cement mortar mixed with optimum mix proportions were subsequently prepared and tested for 3, 7 and 28-day mechanical properties, and the results are summarized in Table 3.12.

Table 3.12

Testing results of optimal mix proportion for dry-cast cement mortar.

Density (kg/m^3)		f_c (MPa)			f_r (MPa)			f_{ts} (MPa)			MOE (GPa)
Fresh	Hardened	3-d	7-d	28-d	3-d	7-d	28-d	3-d	7-d	28-d	28-d
2,284	2,276	65.9	79.8	92.6	9.2	14.1	16.2	4.5	5.2	6.9	35.8

3.4.2 DUHPC experimental results

FR-DUHPC mixtures were prepared by mixing the above-determined benchmark mix proportion and steel fibres. The mass ratio of the incorporated cement, silica fume, FA, GGBS, aggregate, water and superplasticizer were 1: 0.15: 0.31:0.08: 2.84: 0.25: 0.03, and smooth fibres with 0.5%, 1.0%, 1.5% and 2.0% volume fractions of the total mixture volume were used for reinforcing the concrete matrix. Three different curing regimes including 20 ℃ normal-temperature water curing (W), 30-60 ℃ moist/steam curing (M) and 90 ℃ hot-water bath curing (H) were used, and FR-DUHPC were tested for density and mechanical performance after 1 day (M), 3 (W and H), 7 and 28 days of curing. The test results for density and various strength properties based on the average of three identical FR-DUHPC samples are listed in detail in Table 3.13.

Table 3.13

Summary of density and mechanical property test results of prepared FR-DUHPC.

Samples		Density (kg/m^3)		f_c (MPa)			f_r (MPa)			f_{ts} (MPa)		
Fibre (%)		7-d	28-d	1/3-d	7-d	28-d	1/3-d	7-d	28-d	1/3-d	7-d	28-d
0.5	W20	2,359	2,343	72.8[3]	98.4	110.8	10.3[3]	15.8	19.0	5.0[3]	6.1	8.5
	M30	2,348	2,334	52.9[1]	84.4	107.7	8.7[1]	13.1	17.9	3.5[1]	5.7	8.4
	M40	2,328	2,331	69.4[1]	90.6	106.5	10.6[1]	13.8	16.4	4.4[1]	6.3	8.2
	M50	2,335	2,310	86.9[1]	95.9	102.6	12.4[1]	15.1	15.5	5.1[1]	7.2	8.1
	M60	2,326	2,323	93.8[1]	102.6	105.8	13.4[1]	15.2	15.9	6.2[1]	7.8	8.4
	H90	2,336	2,349	109.9[3]	117.2	120.4	18.0[3]	19.7	20.5	8.2[3]	9.5	10.3
1.0	W20	2,383	2,389	94.6[3]	117.5	139.3	16.9[3]	22.1	25.3	5.6[3]	8.7	10.4
	M30	2,395	2,406	64.4[1]	94.1	140.9	9.8[1]	17.4	25.0	4.1[1]	7.1	10.0
	M40	2,406	2,423	77.9[1]	98.4	135.3	11.9[1]	18.3	24.3	5.3[1]	7.6	9.8
	M50	2,388	2,394	89.3[1]	104.1	133.7	15.3[1]	19.4	23.7	6.4[1]	8.5	9.9
	M60	2,356	2,376	102.9[1]	115.6	130.4	18.4[1]	21.7	25.0	7.7[1]	9.2	10.2
	H90	2,373	2,388	120.7[3]	133.9	141.9	22.9[3]	26.5	28.5	9.8[3]	10.9	11.5
1.5	W20	2,415	2,432	110.5[3]	128.1	162.6	26.1[3]	28.5	32.2	8.2[3]	10.4	13.1
	M30	2,437	2,432	70.7[1]	108.6	152.9	10.9[1]	22.2	30.3	4.9[1]	9.1	12.9
	M40	2,413	2,432	98.8[1]	120.9	144.4	19.9[1]	25.5	29.1	7.5[1]	10.5	12.8
	M50	2,417	2,429	124.8[1]	132.0	144.6	24.9[1]	26.7	29.2	9.1[1]	10.9	12.6
	M60	2,414	2,433	129.7[1]	141.1	147.0	26.9[1]	29.7	30.7	10.4[1]	11.5	13.3
	H90	2,431	2,455	146.3[3]	155.6	163.3	32.0[3]	34.6	36.5	12.1[3]	13.1	14.0
2.0	W20	2,441	2,472	115.2[3]	125.3	168.9	27.0[3]	30.0	36.6	9.6[3]	12.0	14.2
	M30	2,434	2,448	78.9[1]	121.2	163.7	15.2[1]	29.3	35.8	5.2[1]	10.1	13.8
	M40	2,452	2,468	123.1[1]	137.8	167.7	25.6[1]	32.3	36.0	8.9[1]	11.2	13.5
	M50	2,438	2,435	129.3[1]	142.4	159.3	28.1[1]	32.2	33.2	11.4[1]	12.0	13.4
	M60	2,425	2,451	135.6[1]	139.3	154.6	29.5[1]	30.8	32.7	12.5[1]	13.1	14.3
	H90	2,436	2,471	150.3[3]	159.5	167.6	35.2[3]	36.8	38.3	12.8[3]	13.8	14.6

3.4.2.1 Density of DUHPC mixtures

The density variations in FR-DUHPC under different initial curing temperatures and fibre dosages are plotted in Fig. 3.9. As exhibited in the figure and Tables 3.12 and 3.13, changes in temperature from 20-90 ℃ had a little impact on FR-DUHPC density, while the average unit weight increased from 2276 to 2448 kg/m^3 as the volume dosage of steel fibres increased from 0 to 2.0%. Compared with other raw materials, the addition of steel fibres with higher density increased the mass of fresh concrete per unit volume and squeezed the free water space within the mixture under the combined conditions of the constant moisture content and vibrated-compaction work. As a result, the mixture's porosity was reduced and its compactness was enhanced, thereby evidently improving the density and various properties of FR-DUHPC.

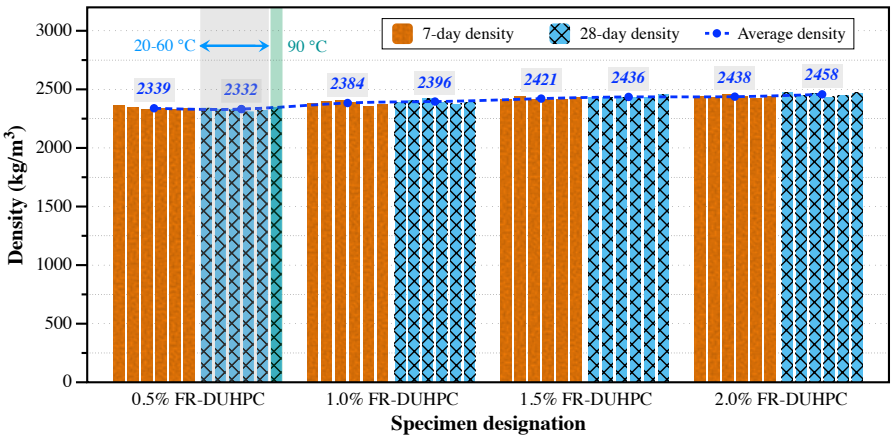

Fig. 3.9. Effects of initial curing temperature and fibre dosage on density of DUHPC.

3.4.2.2 Compressive performance

The results for the impacts of initial curing temperature and fibre dosage on the compressive strength of DUHPC are illustrated in Fig. 3.10. As can be visually

observed from the figure and Tables 3.12 and 3.13 that the 28-day strength was increased from 92.6 MPa for dry-cast cement mortar to 168.9 MPa for 2.0 Vol-% FR-DUHPC (W20) samples. Moreover, the average strength values of DUHPC at 28-day age were, respectively, 109.0 (0.5 Vol-%), 136.9 (1.0 Vol-%), 152.5 (1.5 Vol-%) and 163.6 (2.0 Vol-%) MPa without considering the influence of different initial curing temperatures, and the increments were calculated as 25.6% (0.5-1.0 Vol-%), 11.4% (1.0-1.5 Vol-%) and 7.3% (1.5-2.0 Vol-%). When the curing temperature and testing age were the same, the compressive strength was also enhanced markedly with fibre addition. It was noteworthy that the raise in curing temperature via adopting moist/steam curing caused a downtrend in compression under the same fibre dosage, especially for samples at 28 days. As an illustration, the compressive strength of 1.5% FR-DUHPC samples at 28-day age decreased by 6.0%, 11.2%, 11.1% and 9.6% as the initial temperature increased from 20 to 30, 40, 50 and 60 ℃, respectively. The degradation in final strength when raising temperatures was due to the decrease in moisture content within the mixes as well as the denser, heterogeneous and coarser distribution of hydration products [23, 127, 128]. However, the compressive strength development for DUHPC with 0.5-2.0% fibre reinforcements, as shown in Fig. 3.11, was improved as the initial curing temperature increased from 30 to 60 ℃ at early ages, especially when the temperature reached 40 ℃ and above. Better early compressive performance is particularly important for enhancing the early abrasion resistance of dry concrete structures and components. In addition, it could be noticed that for all FR-DUHPC

samples, they exhibited notably higher compressive strength after being cured in hot-water bath in comparison with the same-age samples of the other two curing methods. The 3-day strength value (H90) was greater than or close to the 28-day strength values (W20-M60) for 0.5% samples, and also for 1.0-2.0% FR-DUHPC, their 3-day strength (H90) were all higher than the corresponding samples' 7-day strength (W20-M60). The primary reason was that the high-temperature water bath not only improved the reaction rate and the degree of cement hydration, but also fully activated the compound pozzolanic effect of silica fume, FA and GGBS, which markedly increased the amount of hydration products inside the cementing system and densified the microstructure of the matrix [129].

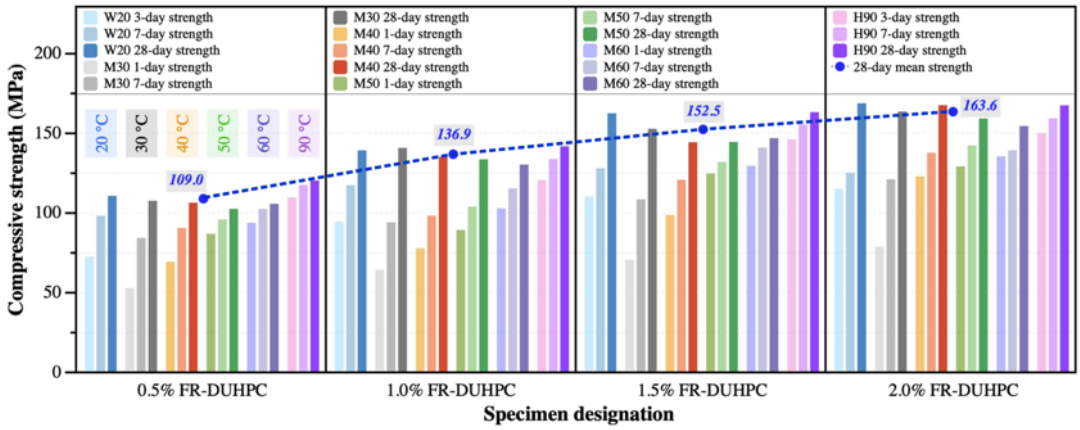

Fig. 3.10. Effects of initial curing and fibre dosage on compressive strength of DUHPC.

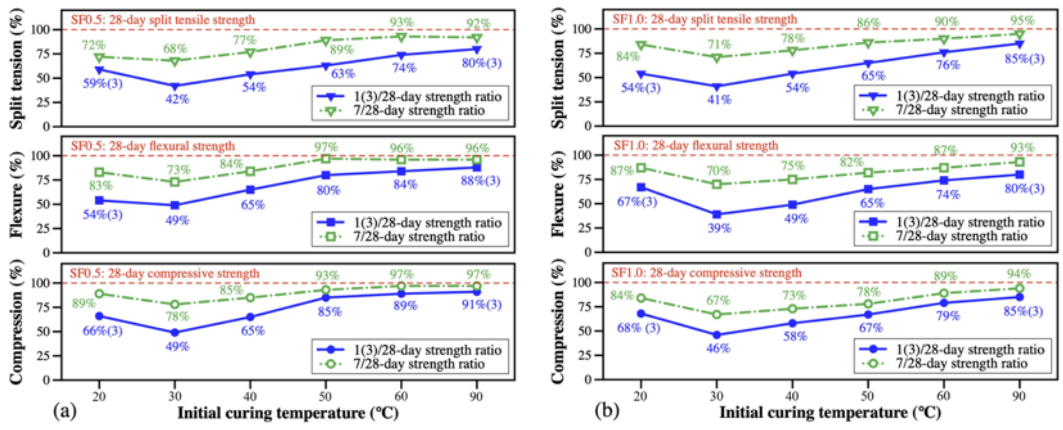

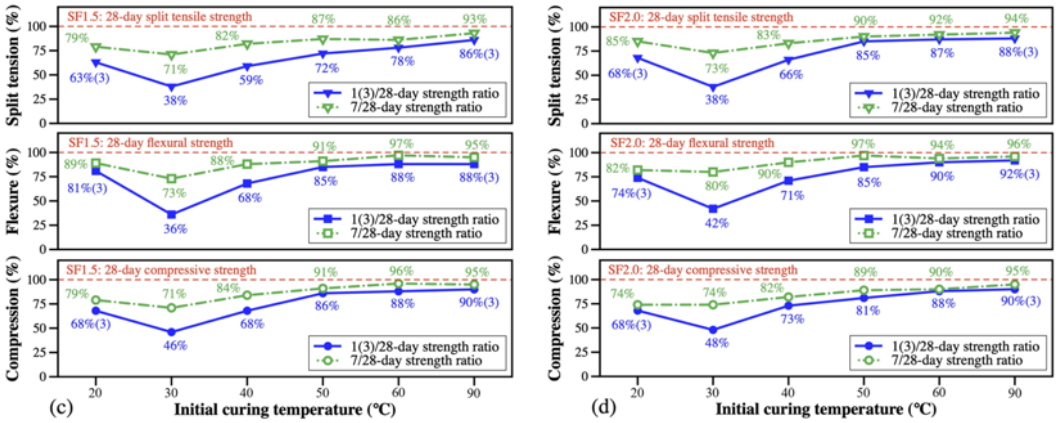

Fig. 3.11. Development of various strength values for DUHPC under different initial curing temperatures: (a) 0.5%; (b) 1.0%; (c) 1.5% and (d) 2.0% fibre dosage.

The typical and complete compressive stress-strain relationships for 28-day-age 0.5-2.0 Vol-% FR-DUHPC samples with various initial curing regimes are plotted in Fig. 3.12. Curves indicated that the compression bearing capability enhanced markedly with fibre volume dosage, and the corresponding peak strain presented the same increasing trend. For the tested DUHPC samples mixed with different fibre volume dosages, the change in the initial curing temperature seemed to have no obvious regularity in the effect of the strain at the peak stress. Moreover, as could be noted that when the fibre dosage was gradually increased and 90 ℃ water curing was used, the contour of stress-strain curves became plumper and the descending sections were smoother with better extensibility. The increase in fibre addition rendered more “fibre nets” formed inside concrete and meanwhile the accelerated cement hydration and pozzolanic reaction rate enhanced the bonding performance of steel fibres with the matrix, thus effectively restrained the concrete lateral deformation and improved their post-cracking behaviour when they were subjected to compression loads.

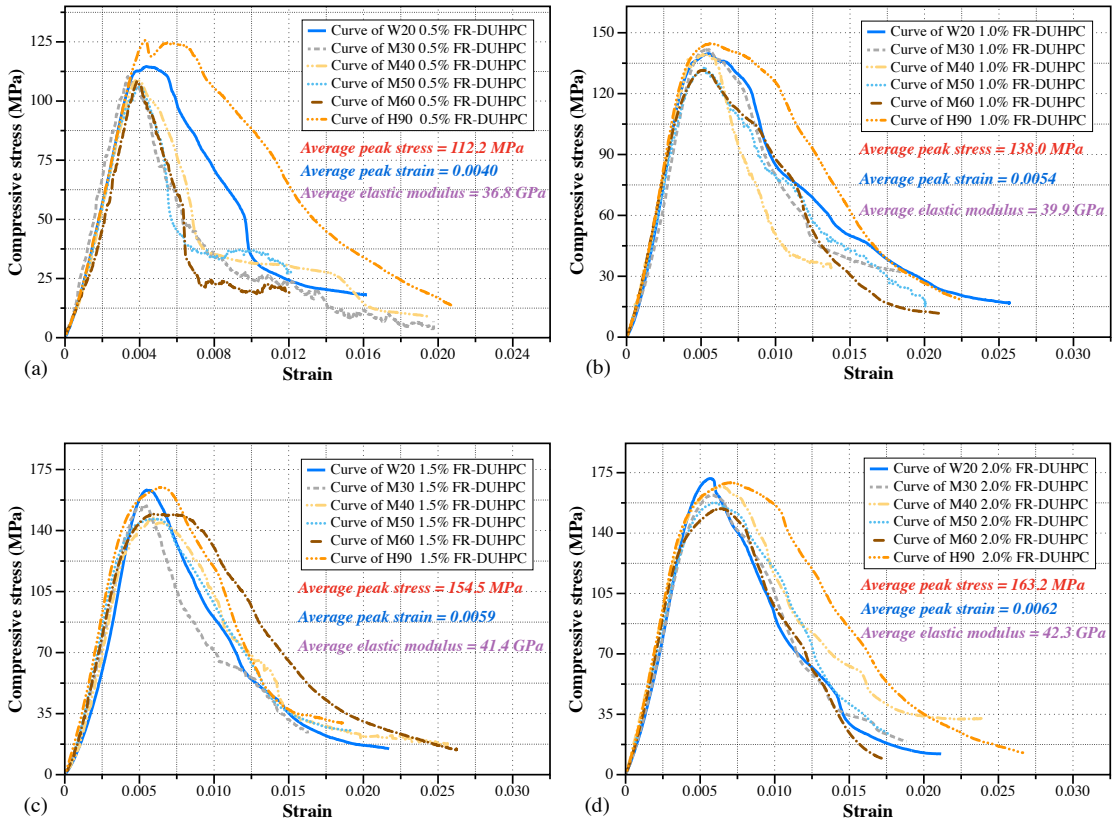

Fig. 3.12. Typical 28-day compressive test data of DUHPC samples under various initial curing temperatures: (a) 0.5%; (b) 1.0%; (c) 1.5% and (d) 2.0% fibre dosage.

The 28-day static MOE, calculated from the compression test data, for 0.5-2.0 Vol-% FR-DUHPC samples at different initial curing temperatures are presented in Fig. 3.13(a). Wang et al. [130] pointed out that the proportional elastic limit within the rising part of compressive stress-strain curves for UHPC was about 83-95% of the ultimate load ascribed to its dense and homogeneous microstructure, which was significantly broader than that for OPC concrete (40-50%). Thus, 85% of the peak compressive stress was considered as the elastic branch to calculate the static MOE of FR-DUHPC. As can be observed that the 28-day mean MOE increased from 36.8 to 42.3 GPa with steel fibre addition, whereas the variation in initial curing temperature presented little impact on the static MOE. Moreover,

by comparing the 28-day MOE of 2.0 Vol-% FR-DUHPC (W20, 42.8 GPa) and dry-cast cement mortar (35.8 GPa) samples exhibited in Table 3.12, the change in fibre inclusion from 0 to 2.0% increased the MOE by 19.6% attributed to the enhancement of steel fibres for compressive performance. Fig. 3.13(b) presents the developed function relationship between FR-DUHPC 28-day compressive strength and MOE without considering the impact of the initial curing temperature. As shown, the increase in compressive strength led to a logarithmic improvement in static MOE, as expected, and a strong correlation (MOE = 14,152·lnf_c - 44,028) existed between these two variables with R^2 greater than 0.98.

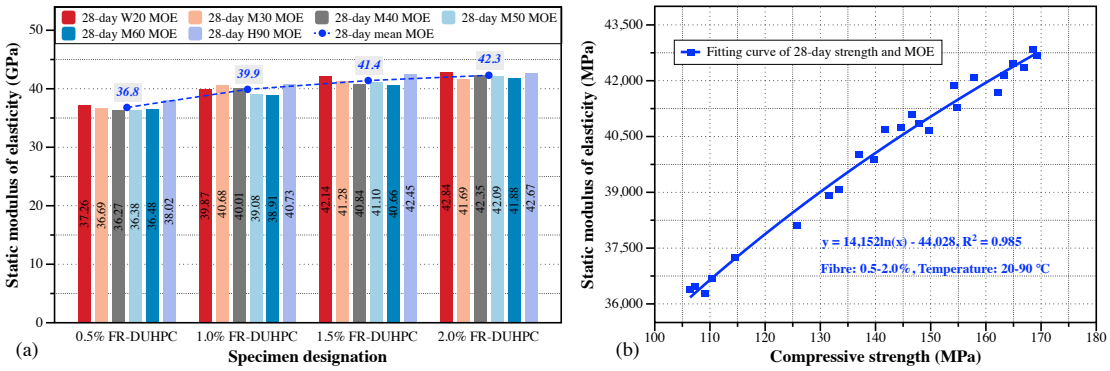

Fig. 3.13. (a) 28-day static MOE and (b) its relationship with compressive strength of DUHPC reinforced with different fibre dosages.

3.4.2.3 Flexural performance

The variations in the flexural strength of DUHPC with different initial temperatures and fibre dosages are shown in Fig. 3.14. As expected, the final strength values after 28 days of 20 ℃ normal-temperature water curing were improved from16.2 (cement mortar) to 19.0 (0.5 Vol-%), 25.3 (1.0 Vol-%), 32.2 (1.5 Vol-%) and 36.6 (2.0 Vol-%) MPa, and the corresponding improvements were, respectively, 17.3%,

33.2%, 27.3% and 13.7%. Additionally, the increments in 28-day mean flexural strength for DUHPC samples with 0.5-2.0% fibre reinforcements were obtained as 44.6%, 23.7% and 13.1%, which indicated that the inclusion of steel fibres contributed more positive effect to flexural behaviour rather than the compression. This was extremely beneficial for dry concrete structures and units that are mainly subjected to bending loads during their serviceability. Furthermore, it should be pointed out that an improvement effect on flexural behaviour better than that on compression was found when DUHPC samples were cured in 90 ℃ water after being completely hardened. The 7-day flexural strengths (H90) of the samples reinforced with all fibre additions were greater than their 28-day strengths under other curing conditions, which was mainly attributed to the formation of the dense and uniform C-S-H gels derived from the accelerated hydration and secondary hydration reaction, as well as the higher interfacial bond strength existed between steel fibres and matrix [129].

The development of flexural strength with initial temperature changes is shown in Fig. 3.11. As an accelerated degree of hydration and the increased amount of hydration products, the raise in temperatures (30-60 ℃) markedly increased the strength evolution kinematics, especially after 40 ℃ and the fibre dosage reached 1.5 Vol-%. For instance, 85% and 97% of final values of flexural strength were, respectively, achieved for 2.0% samples after 1 day of 50 ℃ moist/steam curing and the following 7 days of 20 ℃ room-temperature water curing, whereas the 28-day strength was only diminished by 9.3%. Therefore, even though a similar

phenomenon of the strength attenuation was obtained when comparing the 28-day flexural strength of FR-DUHPC cured with moist/steam regime to those with room-temperature water, it was greatly advantageous for some applications that had special requirements for early flexural strength, such as paving blocks, pipes, pavements and roof tiles.

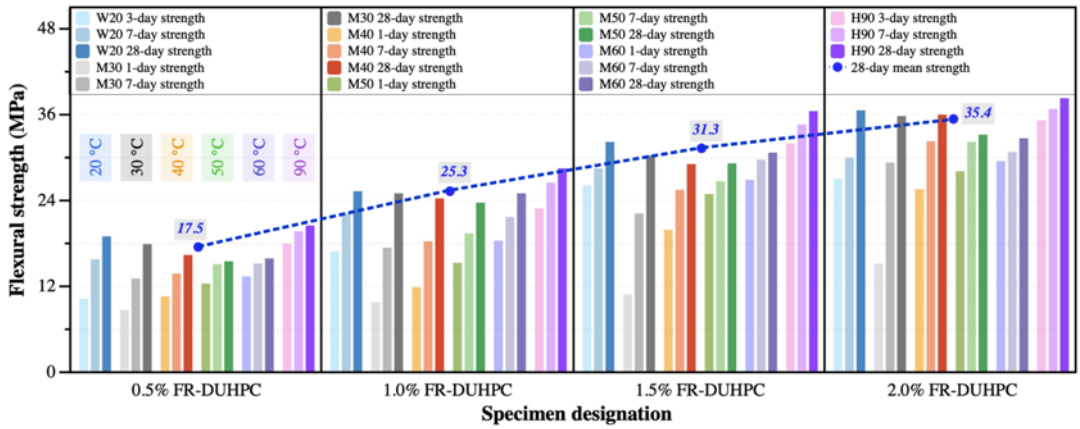

Fig. 3.14. Effects of curing temperature and fibre dosage on flexural strength of DUHPC.

The typical and complete 28-day flexural stress-midspan displacement curves of 0.5-2.0 Vol-% FR-DUHPC samples cured with different initial temperatures are displayed in Fig. 3.15. As illustrated, the midspan deflection of the beam samples subjected to bending load increased linearly before the initial cracks appeared and it was directly proportional to the bearing load. Then, the deflection extended plastically up to the peak stress. For 0.5 Vol-% FR-DUHPC, samples cured with different initial temperatures all presented slight brittle failure after reaching the peak stress, but meanwhile they still had a certain plastic deformation ability after the carried loads dropped suddenly, which was attributed to the presence of a small amount of steel fibres. However, the brittle failure disappeared under the

condition of higher fibre additions and the samples' ductility was improved visibly. Moreover, the average midspan deflection corresponding to the peak stress was likewise extended from 0.493 to 0.657 mm ascribed to the enhanced toughening effect derived from the increased fibre dosage.

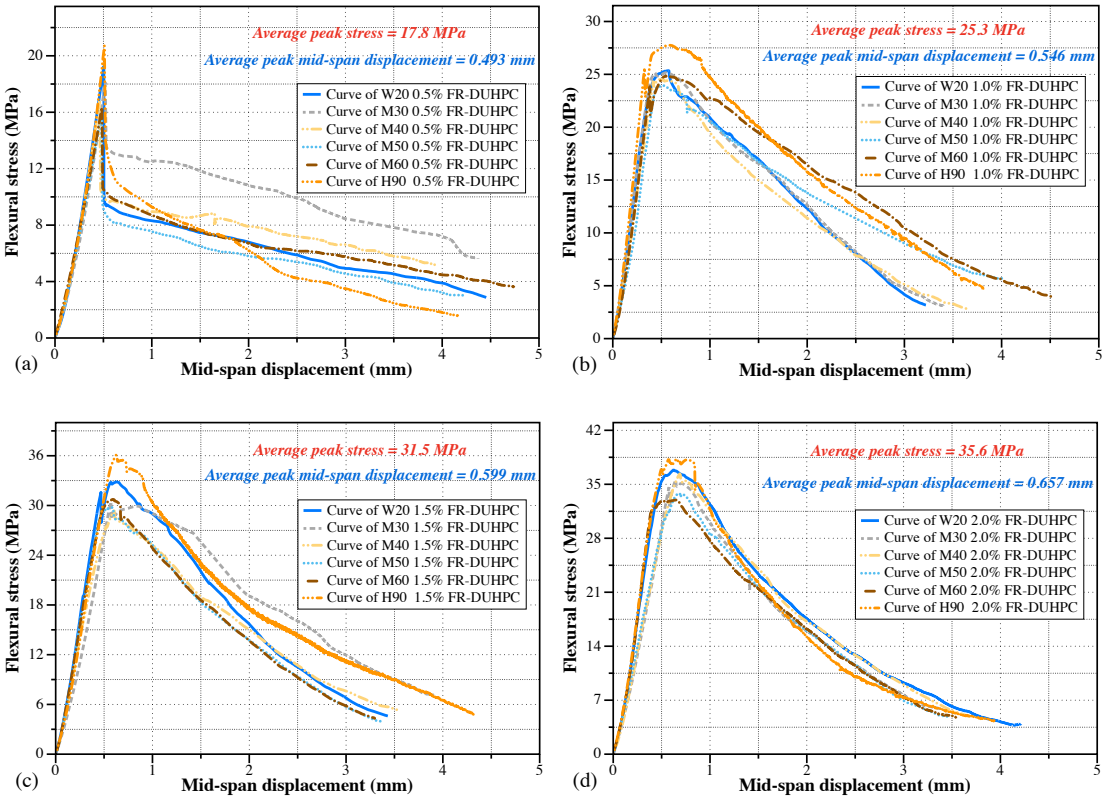

Fig. 3.15. Typical 28-day flexural test data of DUHPC samples under various initial curing temperatures: (a) 0.5%; (b) 1.0%; (c) 1.5% and (d) 2.0% fibre dosage.

Fig. 3.16 presents the pictures of the typical failure patterns of 0.5-2.0 Vol-% FR-DUHPC samples after the three-point bending tests. It was noticed that a principal fracture crack propagating from the bottom to the load location occurred in beam samples under the flexural-tensile stress. All samples remained intact when the ultimate was reached, even when the fibre dosage was lower, that is, they still possessed a good load bearing capacity. In addition, part of the fibres pulled out

and remaining fibres bridging the matrix on both sides of the crack could be observed within the fracture surface. This phenomenon was especially evident when the fibre addition was higher. During the inception of loading, the stress was mainly borne by the matrix concrete. As the strain increased, the load carried by steel fibres became larger. Upon the cracking, the stress between cracks was redistributed and the stress originally borne by the matrix was transferred to fibres. Then fibres that had not been pulled out transmitted the load to concrete on both sides of the crack, which rendered the samples still to remain the load bearing capacity and simultaneously retarded the crack propagation. When the number of fibres across the fracture surface increased, the duration of the stable crack propagation was prolonged and the ultimate tensile stress reached was also improved. This was the main reason for the significant difference between FR-DUHPC and OPC concrete in terms of flexural-tensile failure patterns.

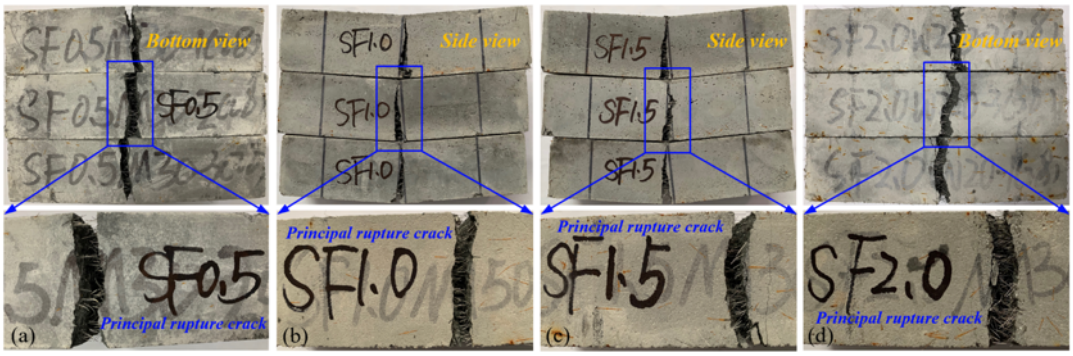

Fig. 3.16. Typical flexural-tensile failure patterns of (a) 0.5%; (b) 1.0%; (c) 1.5% and (d) 2.0% FR-DUHPC samples after bending tests.

3.4.2.4 Split-tensile performance

Fig. 3.17 shows the effects of initial curing temperature and fibre volume dosage on the split-tensile strength of DUHPC after having been cured for 1 day as well

as 3, 7 and 28 days. Under the normal-temperature water curing, the variation trend of the strength in split-tension was basically the same as that in flexure, that is, the strength increased from 6.9 MPa to more than doubled 14.2 MPa with fibre dosage changed from 0 to 2.0%. The largest percentage improvement in 28-day mean strength of 27.2% was observed when the fibre volume addition increased from 1.0% to 1.5%. However, on the contrary, the insignificant effect of 6.9% enhancement (from 13.1 to 14.0 MPa) occurred when the volume ratio exceeded 1.5%, which was attributed to fibre agglomeration within the mix and the visible reduction in workability. In addition, a relatively large difference from compressive performance was that the 28-day split-tensile behaviour was modest affected by the changes in initial curing temperature except for 90 ℃. For example, for 0.5 Vol-% FR-DUHPC samples, the 28-day strength values were, respectively, 8.5, 8.4, 8.2, 8.1 and 8.4 MPa when the temperature increased from 20 to 60 ℃, whereas for 1.5% and 2.0% FR-DUHPC samples, their 28-day strength values at 60 ℃ were even higher. As expected, the samples after having been cured in hot water had evidently higher 3 and 7-day strength values.

Fig. 3.11 also presents the percentage ratios of the split-tensile strength at 1 day, 3 and 7 days as compared to 28 days under different initial curing temperature and fibre dosage conditions. Although the temperature changes (excluding 90 ℃) exhibited lesser impact on 28-day split-tensile behaviour of DUHPC, its strength development ratios at the corresponding age were also increased evidently with temperatures (30-60 ℃), especially when the curing temperature reached 40 ℃

and above. In addition, compared with the 60 ℃ moist/steam curing method, high-temperature water bath curing exhibited a better promoting effect on early split-tensile strength for DUHPC samples reinforced with 0.5-1.5 Vol-% fibre additions.

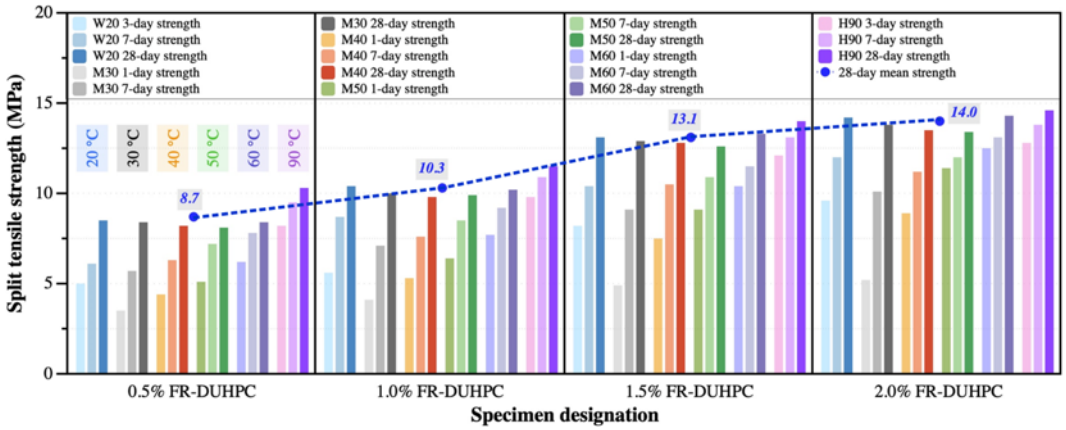

Fig. 3.17. Effects of initial curing and fibre dosage on split-tensile strength of DUHPC.

The typical 28-day split-tensile stress-displacement curves of 0.5-2.0 Vol-% FR-DUHPC samples adopting various initial curing methods are exhibited in Fig. 3.18. As could be observed that the extent of the sudden drop in split-tensile stress when failure occurred was effectively controlled with fibre addition. The ultimate split-tensile stress of DUHPC samples was determined as the first point where the bearing capacity was insufficient due to crack initiation, and the subsequent load carried by samples after the failure was considered to be more from the reinforcement effect of steel fibres rather than the improvement of tensile strength of the material itself. Compared with 0.5-1.0% FR-DUHPC, samples with 1.5% and 2.0% fibre reinforcements showed higher peak stress and better ductility, and the average vertical displacement corresponding to the ultimate splitting-tensile strength was extended from 0.851 to 0.923 and 0.943 mm.

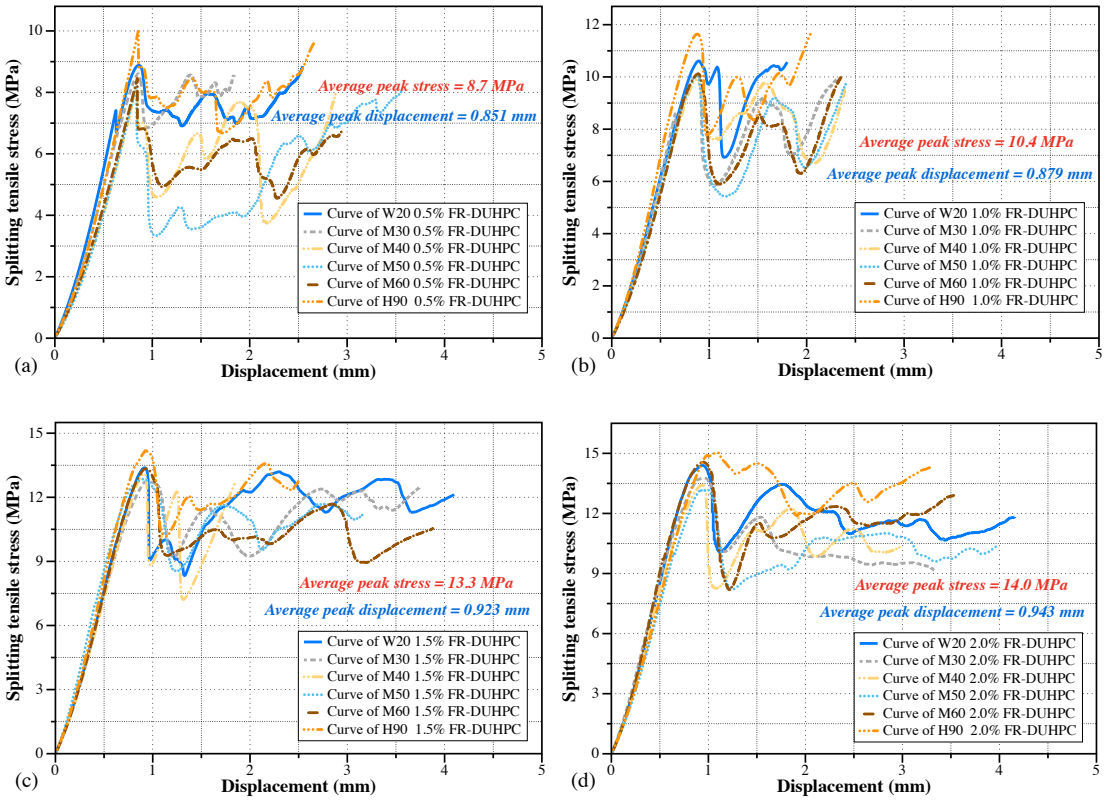

Fig. 3.18. Typical 28-day split-tensile test data of DUHPC samples under various initial curing temperatures: (a) 0.5%; (b) 1.0%; (c) 1.5% and (d) 2.0% fibre dosage.

Fig. 3.19 exhibits the typical failure modes of 0.5-2.0% FR-DUHPC samples after the splitting-tensile tests. As it could be noticed from Fig. 3.19(a) that cylindrical samples were not split into two pieces under the splitting load, and there were still a large number of fibres bridging the concrete matrix on both sides within the split section. Additionally, the width of the principal crack was visibly decreased owing to the enhancement of the restraint effect of steel fibres on macro-cracks development. It should be noticed that after individual split-tensile tests, a small part of cylindrical samples were damaged into the upper, middle and lower parts as depicted in Fig. 3.19(b) in addition to the principal splitting crack. The foremost reason was that the adopted preparation method of layered vibrated compaction

rendered the steel fibres distribute along the horizontal direction of the compacted surface, which resulted in insufficient fibre anchoring between layers.

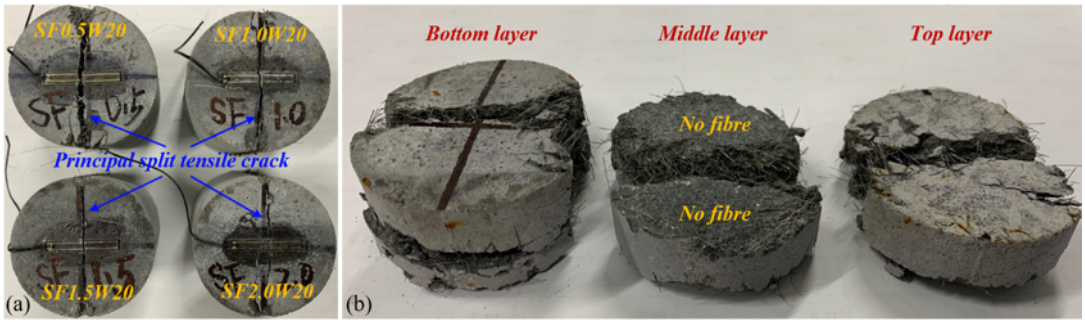

Fig. 3.19. (a) Typical split-tensile failure and (b) delamination of FR-DUHPC samples.

3.4.2.5 Strength development kinematics

As reported in Sections 3.4.2.2 to 3.4.2.4, Fig. 3.11 exhibits the percentage ratios of the strength development in compression, flexure and split-tension for 0.5-2.0 Vol-% FR-DUHPC samples at various initial curing temperatures. It was shown that the evolution kinematics of all strengths were quickened when moist/steam and hot-water bath curing methods were used at early ages, especially when the curing temperature reached 40 ℃ and above. The lower curing temperature could not contribute to desirable early-age mechanical behaviour, and the lowest 1-day percentage of the sample's strength development was 36% of the corresponding 28-day strength value while the highest could only reach 49%. Compared with other fibre dosages, the strength evolution rate of 0.5% FR-DUHPC was relatively sluggish when adopting normal-temperature water curing, but as the temperature increased, the difference between its strength development kinematics and other 1.0-2.0% FR-DUHPC samples was gradually smaller. The reason might be that the early strength of DUHPC was greatly affected by fibre dosage when the initial

temperature was lower, whereas increasing the curing temperature accelerated the formation of hydration products and weakened the effect of fibre dosage on the strength. Furthermore, it should be particularly noted that the hot-water bath curing not only markedly enhanced the ultimate strength in compression, flexure and split-tension, but also signally speeded up the early evolution rate of various strength properties of FR-DUHPC. For example, the 3 and 7-day compressive strength could be achieved up to 91% and 97% of 28-day strength; for the flexural strength, the values were up to 92% and 96%, and for the split-tensile strength, the maximum strength percentages could reach 88% and 95%. In general, the prepared FR-DUHPC possessed excellent mechanical performance while having fast hardening along with early-age strength characteristics, irrespective of which curing regime was adopted.

3.4.2.6 Relationship between strength behaviour

Taking into account that dry concrete structures and units are more susceptible to flexural tensile loads during their service life, as well as the complexity of the indirect tensile tests and the discreteness of the results, it is therefore necessary and meaningful to predict the indirect tensile behaviour through the material's compressive property. Figs. 3.20 and 3.21 respectively displays the relationships between compression and flexure/split-tension of 0.5-2.0% FR-DUHPC samples under moist/steam curing (30-60 ℃). Each set of correlations was divided into 1-day (4 data points) and 7/28-day (8 data points) models since the 1-day strength was greatly affected by the change in initial curing temperature as reported above.

Good relationships were observed existing between compressive and another two strength property with R^2 greater than 0.9, except for 7/28-day compressive-split-tensile relationship of 2.0% FR-DUHPC samples (R^2 = 0.822) as presented in Fig. 3.21(b). The various models with respect to the strength behaviour are summarized in Table 3.14 in detail. It could be clearly found that enhancing the compressive strength resulted in a power functional improvement in two indirect tensile performance, but the development of the split-tensile strength under the same fibre dosage was slower than that of the flexural strength. In addition, the positive impact of fibre dosage on flexural performance was also notably stronger than its impact on split-tension. The main reason was that the preparation method of the layered vibration/compaction rendered FR-DUHPC cylinder samples lack sufficient fibre bonding between the layers, as shown in Fig. 3.19(b), which in turn led to the samples to be more prone to damage when subjected to splitting loads. It can also be observed from Fig. 3.21 that the incorporation of 2.0% steel fibres had a slightly remarkable impact on improving the split-tensile behaviour under the same compressive strength values, and this enhancement effect became evident when the curing age was longer, and the fibre dosage was also extended to 1.5%. Nevertheless, the split-tensile strength values of samples mixing with 2.0% fibre addition were more discrete (with the minimum goodness of fit) owing to the potential fibre agglomeration and delamination failure. Thus, in the case of comprehensive consideration of the cost and mechanical property of FR-DUHPC, dosage of 1.5% was proposed as the most suitable fibre addition in this study.

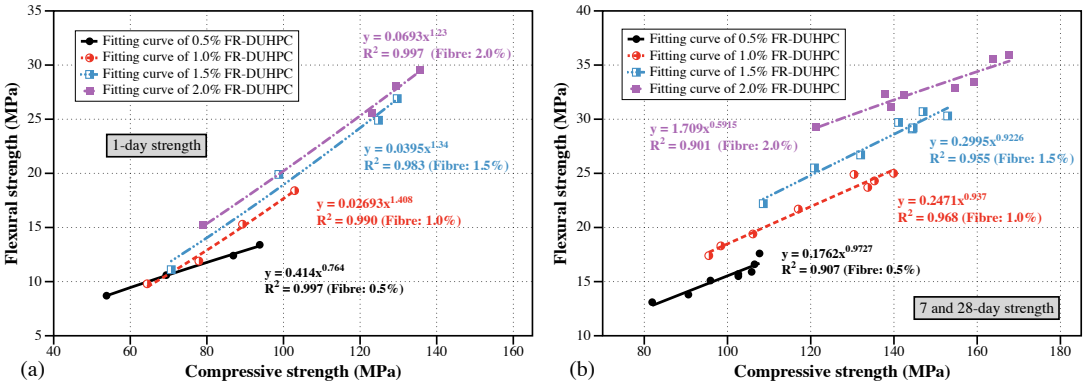

Fig. 3.20. Relationships between compressive and flexural strength of 0.5-2.0 Vol-% FR-DUHPC samples after (a) 1 day of moist/steam curing and (b) following 7/28 days of normal-temperature water curing.

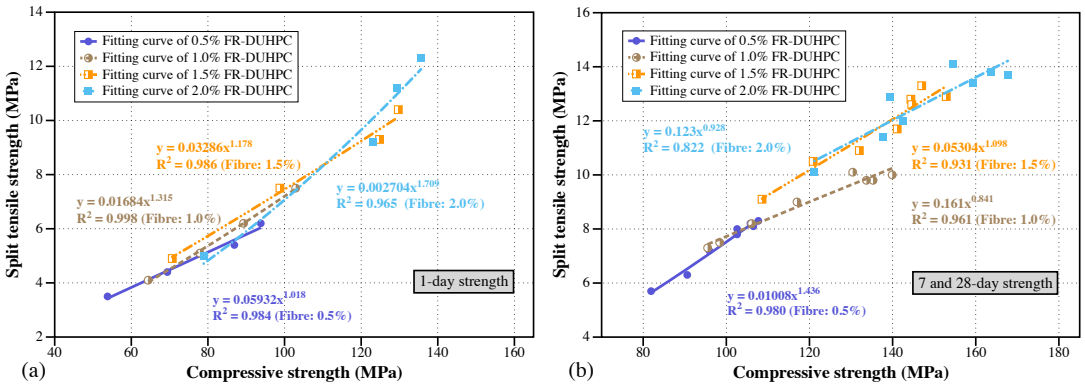

Fig. 3.21. Relationships between compressive and split-tensile strength of 0.5-2.0 Vol-% FR-DUHPC samples after (a) 1 day of moist/steam curing and (b) following 7/28 days of normal-temperature water curing.

Table 3.14

Correlation models between compression and flexure/split-tension for FR-DUHPC.

Fibre dosage	Correlation models of compressive-flexural behaviour	
	1-day curing age	7 and 28-day curing age
0.5%	$f_r = 0.414 \cdot f_c^{0.764}$, $R^2 = 0.997$	$f_r = 0.176 \cdot f_c^{0.973}$, $R^2 = 0.907$
1.0%	$f_r = 0.027 \cdot f_c^{1.408}$, $R^2 = 0.990$	$f_r = 0.247 \cdot f_c^{0.937}$, $R^2 = 0.968$
1.5%	$f_r = 0.040 \cdot f_c^{1.340}$, $R^2 = 0.983$	$f_r = 0.300 \cdot f_c^{0.923}$, $R^2 = 0.955$
2.0%	$f_r = 0.069 \cdot f_c^{1.230}$, $R^2 = 0.997$	$f_r = 1.709 \cdot f_c^{0.592}$, $R^2 = 0.901$

Fibre content	Correlation models of compressive-split-tensile behaviour	
	1-day curing age	7 and 28-day curing age
0.5%	$f_{ts} = 0.059 \cdot f_c^{1.018}$, $R^2 = 0.984$	$f_{ts} = 0.010 \cdot f_c^{1.436}$, $R^2 = 0.980$
1.0%	$f_{ts} = 0.017 \cdot f_c^{1.315}$, $R^2 = 0.998$	$f_{ts} = 0.161 \cdot f_c^{0.841}$, $R^2 = 0.961$
1.5%	$f_{ts} = 0.033 \cdot f_c^{1.178}$, $R^2 = 0.986$	$f_{ts} = 0.053 \cdot f_c^{1.098}$, $R^2 = 0.931$
2.0%	$f_{ts} = 0.003 \cdot f_c^{1.709}$, $R^2 = 0.965$	$f_{ts} = 0.123 \cdot f_c^{0.928}$, $R^2 = 0.822$

3.4.3 Microstructure analysis (SEM)

As reported above, the moist/steam curing is generally utilized to accelerate the hardening rate of dry concrete mixtures and increase the turn-around speed of moulds. Therefore, to further explore the effect of moist/steam curing on the early performance of DUHPC, the 1-day microstructure patterns for the mixtures under different moist/steam curing temperatures were studied utilizing SEM technique, which could intuitively exhibit the mixture's microstructure and the distribution of hydration products upon heating [131]. The typical morphological images were exhibited in Fig. 3.22. It can be clearly observed from Fig. 3.22(a) that when the initial curing temperature was 30 ℃, the degree of cement hydration was lower and the hydration process of SCMs was still within the preliminary stage. Large amount of needle-bar ettringite (AFt) phase as well as unreacted spherical FA and silica fume particles were embedded/interlaced in C-S-H gels, which were derived from the cementing materials hydration. Besides, the crystalline $Ca(OH)_2$ in the form of laminated shapes could also be visually recognized owing to the slow pozzolanic reaction of FA and GGBS at early ages [132]. As expected, the increase in initial curing temperature contributed to increased cement hydration

rate along with the consumption of $Ca(OH)_2$, as a result of accelerated secondary hydration process of SCMs, and produced more gels filling up the pores in the mixtures [133] and consequently rendered DUHPC matrix more dense as shown in Figs. 3.22(b-c). However, the higher temperatures during the early moist/steam curing also speeded up the migration of surface water into concrete matrix and formed a denser shell on the surface of cement particles, which in turn attenuating the later hydration of cement clinker [134]. After a long period of high temperature curing, the hydration products and the interface between aggregates and matrix presented varying degrees of micro-cracks, which were not conductive to long-term strength development. As the temperature increased to 60 ℃, the foregoing adverse impacts became more evident, accompanied by uneven-distributed and coarse-crystallized hydration products, as well as visibly increased porosity and ITZ thickness as shown in Fig. 3.22(d). Combining the microstructure patterns of DUHPC mixture at different curing temperatures and their mechanical behaviour obtained from Section 3.4.2, 50 ℃ was considered the most suitable moist/steam curing temperature for DUHPC in this study.

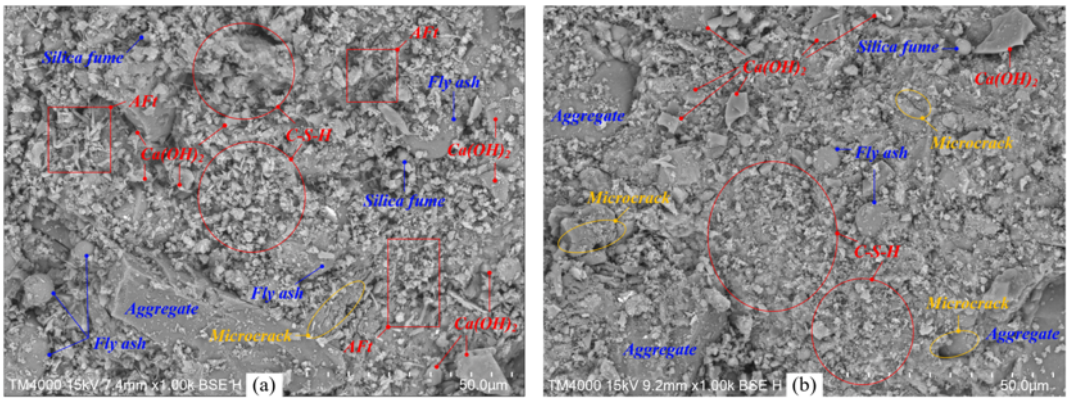

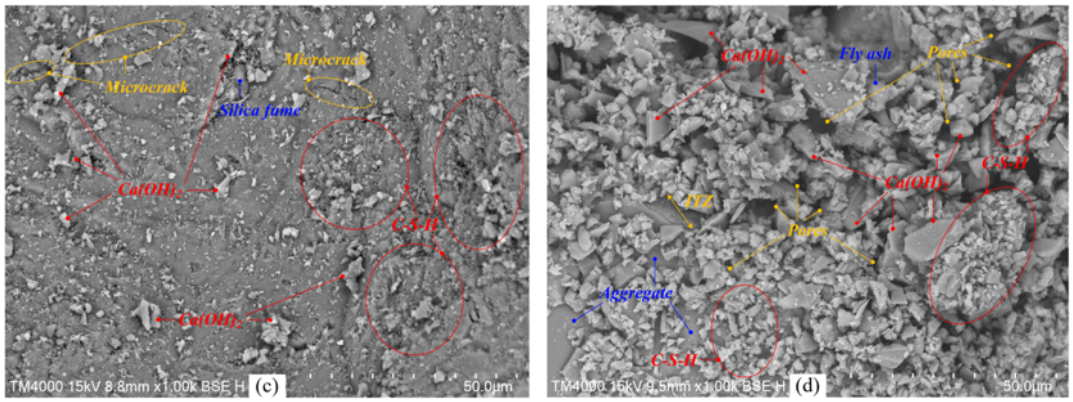

Fig. 3.22. Microstructure for DUHPC mixtures after 1 day of (a) 30 ℃; (b) 40 ℃; (c) 50 ℃ and (d) 60 ℃ moist/steam curing based on SEM.

3.5 Environmental impact of developed DUHPC

In order to prepare UHPC with high strength, low porosity and excellent durability, gravel aggregates are generally removed from concrete mix proportion and more cement is introduced (800-1000 kg/m^3). However, the huge cement consumption releases a large amount of CO_2 in production and consumes a lot of resources and energy. As reported above, dry concrete contains lower cement and moisture content in comparison with conventional OPC concrete, and a variety of waste materials and by-products can be introduced as ASCMs to replace partial cement. Table 3.15 exhibits the comparisons of the content of cement and ASCMs, as well as the replacement percentage and 28-day strength in compression and flexure of straight steel fibre-reinforced UHPC and the developed DUHPC in this study. All samples were tested after 28-day room-temperature water curing. It is evident that with less cement incorporation and comparable replacement percentage (RP) of cement, the developed DUHPC still demonstrated superior strength behaviour. As an illustration, Yu et al. [135] used 610 kg/m^3 cement and 33% substitution of

cement to prepare UHPC and the compressive (f_c) and flexural (f_r) strengths at 28-day age were obtained as around 140 and 26.5 MPa, respectively. However, the corresponding strengths of the developed DUHPC could, respectively, reach around 169 and 36.5 MPa with only 560 kg/m^3 cement and lower fibre addition. Furthermore, the embodied CO_2 (ECO_2) of the developed FR-DUHPC, which was calculated using the expression $ECO_2 = \sum_{i=1}^{n} \left(M_i \times ECO_{2_i}\right)$ (i is the number of factors affecting the ECO_2 in the mix, M_i is the content (kg/m^3) of the foregoing i-th factor, and ECO_{2i} is the equivalent CO_2 emission (CO_2-kg/kg) corresponding to the i-th factor), is approximately 658 kg/m^3 based on the CO_2 emission indexes of various raw materials provided by references [136, 137]. Therefore, it can be concluded that the DUHPC developed in this study not only has the advantages of conventional dry concrete and self-compacting UHPC, but also contains low cement addition and considerable cement replacement, which is consistent with the principles of sustainable development along with the energy conservation and emission reduction.

Table 3.15

Comparisons of ASCMs content and strength values (28 days) of UHPC and developed DUHPC.

References	Cementitious materials (kg/m^3)			Steel fibre reinforcement		Sample size	f_c	f_r
	Cement	ASCMs	RP (%)	Fibre size (mm)	Vol-%	(mm)	(MPa)	(MPa)
Yu et al. [135]	~ 610	LSP+SP, ~ 305	33	L_s = 13, d_s = 0.2	2.5	40×40×160	~ 140	~ 26.5
Song et al. [138]	~ 750	FA+SLF, ~ 344	31	L_s = 13, d_s = 0.2	3.0	40×40×160	~ 170	~ 33.5
Wu et al. [139]	~ 785	SLF, ~ 260	25	L_s = 13, d_s = 0.2	3.0	40×40×160	~ 160	~ 38.0
Xu et al. [140]	---	CTWP, ---	35	L_s = 13, d_s = 0.2	2.0	40×40×160	~ 135	~ 19.0
Brito et al. [141]	~ 570	MK+SLF, ~ 305	35	L_s = 12.5, d_s = 0.5	5.0	40×40×160	~ 118	~ 36.5
Yu et al. [142]	~ 700	FA+SP, ~ 200	22	L_s = 13, d_s = 0.2	2.5	40×40×160	---	~ 25.0
This study	**~ 560**	**FA+SLF+GGBS, ~ 305**	**35**	**L_s = 10, d_s = 0.12**	**2.0**	**40×40×160**	**~ 169**	**~ 36.5**

Notes: only in this table, “RP” denotes replacement percentage, “SLF” denotes silica fume, “LSP” denotes limestone powder, “SP” denotes silica powder, “CTWP” denotes ceramic tile waste powder, “MK” denotes metakaolin, “L_s” denotes fibre length, “d_s” denotes fibre diameter and “---” denotes unmentioned.

3.6 Conclusion

In this chapter, the mechanical property of FR-DUHPC was investigated after a benchmark mix proportion of dry-cast mortar was determined via the orthogonal tests. Different steel fibre additions and curing regimes were used to explore their influences on the mechanical behaviour of DUHPC. With the results presented above, several conclusions can be drawn as follows:

1) The inclusion of silica fume and FA as a partial substitute for cement were identified as the most significant factors influencing the unit weight of dry-cast cement mortar, whereas the water-binder ratio and silica fume content were the predominant factors affecting its compression, rupture modulus and split-tension performance.
2) The various mechanical properties of DUHPC were improved visibly with steel fibre dosage at all ages. The increments of compressive and flexural strength of DUHPC with 0.5-2.0% fibre reinforcements at 28-day age were respectively 25.6%, 11.4%, 7.3% and 44.6%, 23.7%, 13.1%, indicating that the addition of steel fibres contributed better impact to the flexural rather than compressive behaviour, which is extremely beneficial for dry concrete structures/units that are mainly subjected to flexural-bending loads during their serviceability.
3) The increase in initial curing temperature via using moist/steam curing regime led to an attenuation trend in various strengths of DUHPC under the identical fibre dosage, especially at 28-day period. However, its strength development kinematics improved evidently as the initial curing temperature raised at early

ages. Up to 90% and 97% of final values of flexural strength were obtained after 1-day moist/steam curing and the following 7-day normal-temperature water curing. 50 ℃ moist/steam curing was suggested for consolidating the pre-fabricated DUHPC units based on the microstructure analysis performed.

4) Strong power functional relationships existed between the compressive and flexural as well as split-tensile strength. The development of flexural strength under the identical fibre addition was faster than that of split-tensile strength owing to the potential delamination failure. After comprehensively considering the cost and mechanical performance of the developed FR-DUHPC, a volume dosage of 1.5% was determined to be the most suitable steel fibre addition in the current study.

Chapter 4

Mechanical Characteristic of Multiscale Mono and Hybrid Steel FR-DUHPC

4.1 Introduction

Dry concrete, with RCC and DCC as its representative hardened mixtures, is an engineering composite material containing less moisture and cement content but more incorporation of aggregate. In practical applications, for the purpose of reducing the material cost, some waste materials, such as ASCMs and recycled aggregates, are commonly utilized as a partial substitute for cement [43, 53, 54, 78] and natural aggregate [17, 41, 42, 74]. Therefore, some early age properties that are important for dry concrete may be deteriorated and its long-term durability cannot be guaranteed.

The addition of fibres into the mixture can significantly improve the mechanical property of dry concrete, via reducing the micro-cracks induced by the shrinkage of matrix as well as delaying their propagation at the initial stage of loading, and finally becoming the main carrier of the external loads [27, 28, 104, 143, 144]. In addition, some researchers pointed out that dry concrete with fibre reinforcement showed better fibre efficiency than OPC concrete, which mainly attributed to the enhanced anchorage friction between the fibres and cement matrix due to the denser internal structure [79, 88]. Sharbatdar et al. [143] explored the strength behaviour and impact resistance of RCCP with incorporation of different types of fibres. It was concluded that steel fibres exhibited a better effect on improving the

various strength characteristics, followed by synthetic and plastic fibres, while for impact resistance of RCCP, steel and synthetic fibres exhibited the comparable enhancement of 270% and 290%. Another type of the synthetic fibre, namely PVA fibre, was considered by Peyvandi et al. [27, 28] to evaluate its influence on the structural and durability performance of industrial-scale DCC pipes with addition of modified graphite nanoplatelets (GP). The findings illustrated that the foregoing performance including the crack resistance, carrying capability and toughness, as well as the abrasion and acid resistance of PVA FR-DCC pipes were improved evidently, especially in combination of modified GP. Similar strengthening and toughening effects were likewise obtained from other studies in which steel and synthetic fibres were used to manufacture DCC pipes [29, 30, 109]. What needs extra focus here is that the research for the effects of crumb rubber, PP and steel fibres on the structure behaviour of practical full-scale DCC pipes conducted by Park et al. [30]. In addition to the findings that the shredded rubber caused a reduction in the load-carrying ability of DCC pipes whereas this negative effect could be remedied after fibres were added separately, hybrid fibre reinforcement was more effective in improving the strength and ductility. Higher fibre efficiency was a joint result of the high-strength steel fibres and the enhanced adhesive strength of synthetic fibres, owing to their hackly appearance in the rubberized mixture. Generally, hybrid fibres with different shapes or dimensions and types can restrain the development of multiscale cracks. Short and ductile fibres (micro-fibres with a diameter of no more than 5 μm) are active in controlling the initiation and propagation of micro-cracks by virtue of their better dispersibility and quantity

advantages. As for long and stiff fibres (macro-fibres with a diameter greater than 100 μm) at the same volume addition, by virtue of the size advantages and higher friction with cement matrix, they can provide effective bridging mechanism across macro-cracks and restrain their rapid development [145, 146].

By collating and analyzing the state of the art, several researches on mechanical behaviour and durability of dry concrete with fibre reinforcement and addition of recycled materials have been conducted. However, the strength (especially the early strength behaviour) of dry concrete developed in those investigations was relatively low despite fibre reinforcement was used. In this chapter, the effects of multiscale mono and hybrid steel fibre reinforcements on the static mechanical properties of DUHPC were further investigated based on the research findings obtained from Chapter 3.

4.2 Materials, mix proportion and preparation

4.2.1 Raw materials and proportioning

In the current study, the primary raw materials utilized to prepare FR-DUHPC comprised the Portland cement, silica fume, FA, GGBS, quartz sand, steel fibre, polycarboxylate superplasticizer and water. FA, silica fume and GGBS, which served as the SCMs, were utilized as the partial replacement for cement to improve the mixture consistency and densify the microstructure of the matrix. The main components of the cement and SCMs are exhibited in Fig. 4.1. In terms of steel fibres, considering their toughening effect and the dispersibility in mixtures, copper-coated straight fibres with an identical diameter of 0.12 mm but different

lengths of 6, 10 and 13 mm were used to achieve the multiscale reinforcement. The aspect ratios of these three lengths of steel fibres were, respectively, 50.0, 83.3 and 108.3, and their elastic modulus and tensile strength were 200 and more than 4 GPa, respectively. In addition, owing to the lower moisture content of dry concrete and the addition of fibres, high-efficiency SP with a water reduction of 30% was used. Furthermore, considering that the incorporated cement contained admixtures and the secondary hydration (pozzolanic reaction) process of FA and GGBS lagged behind, an additional 2% early-strength component was added to SP to obtain better early properties of hardened dry concrete.

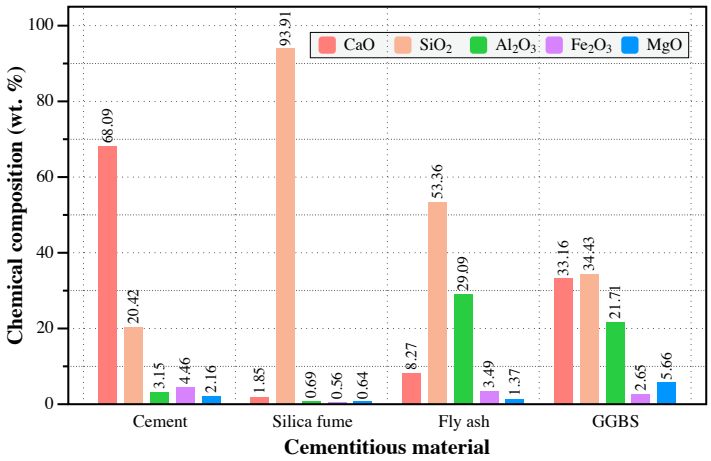

Fig. 4.1. Main chemical compositions of cementitious materials for FR-DUHPC.

Based on previous laboratory experiments reported in Chapter 3, DUHPC with a water-binder ratio of 0.16, superplasticizer dose of 3% by the mass of cement, and cement replacement ratios of 10%, 20% and 5% by mass via using silica fume, FA and GGBS, could achieve a satisfied mixture consistency and concrete properties. Thus, mixtures mixed with the above materials and three lengths of steel fibres were used in this study to assess the impact of multiscale mono/hybrid

fibre reinforcement on the mechanical behaviour of DUHPC. In the case of mono reinforcement, the fibre dosage was selected as 0.5-2.0% to investigate the effect of three lengths of fibres under different dosages. For hybrid reinforcement, the fibre dosage was selected as 1.5% to assess the effect of various hybridizations at the optimal fibre addition obtained in Chapter 3. The detailed mix proportion of mono and hybrid fibre reinforcements are given in Table 4.1. For the naming of different mixtures, F05-20 represents the fibre dosage of the mixture, and S, M and L, respectively, indicate 6-mm short fibre, 10-mm medium fibre and 13-mm long fibre. For example, F20M corresponds to the mixture incorporating 2.0% 10-mm medium-length fibres, and F05S10L corresponds to the mixture incorporating 0.5% 6-mm short-length and 1.0% 13-mm long-length steel fibres. Totally twenty groups of DUHPC mixtures including a control case without fibre reinforcement, twelve cases with a mono fibre reinforcement and seven cases with hybrid fibre reinforcements were prepared.

Table 4.1

Mixture proportions of mono and hybrid FR-DUHPC.

Sample	Cement	SLF	FA	GGBS	Sand	Water	Fibre (%)	Fibre proportion
Control	1.00	0.15	0.31	0.08	2.84	0.25	0.0	---
Mono	1.00	0.15	0.31	0.08	2.84	0.25	0.5-2.0	F05-20S, F05-20M, F05-20L
Hybrid	1.00	0.15	0.31	0.08	2.84	0.25	1.5	F05S10M, F10S05M, F05S10L, F10S05L, F05M10L, F10M05L, F05SML

Notes: “SLF” denotes silica fume.

4.2.2 Preparation and curing regime

Owing to the lower moisture content of FR-DUHPC, its mixing procedures were slightly different from those of self-compacting UHPC. The preparation processes were as follows: (i) the weighed sand and powdery cementitious materials were first put into a concrete mixer and stirred at a speed of 60 rpm for 2 mins; (ii) dispersed steel fibres were gently introduced into the blended materials and dry stirring continued for 4 mins; (iii) water with pre-blended superplasticizer was added and the mixtures were stirred for another 6 mins; (iv) mixture was poured into cube/prism/cylinder moulds and vibration-compacted to final form by using surcharges and a shaking table. The moulding of cubic and beam samples was 3-layer compaction, while 2-layer compaction for cylinder split-tensile samples. It was noteworthy that prior to the casting, all groups of fresh mixtures were tested for their consistency, expressed in Vebe time (VBT), with results ranging from 16 s (control mixtures without fibre reinforcement) to 43 s (mixtures with 2.0% 13-mm fibre reinforcement). That is, the incorporation of longer steel fibres and an increase in fibre dosage significantly deteriorated the workability of dry concrete mixtures. Nonetheless, all the prepared concrete mixtures possessed effective workability since the obtained VBT fell within the appropriate range of the VBT (30-75s) given by ACI 325.10R guidelines [147] and Ref. [92] for practical practicality. It should pointed out that the mixture's mixing time after water added should not be too long to diminish the water evaporation within the mixes and prevent the balling effect of fibres. However, the fibre cohesive agglomeration

could also be observed when fibre dosage reached 2.0%, especially when 13-mm fibres were incorporated. Fig. 4.2 depicts the preparation procedures of FR-DUHPC samples described above and the observed agglomeration of steel fibres during the mixing.

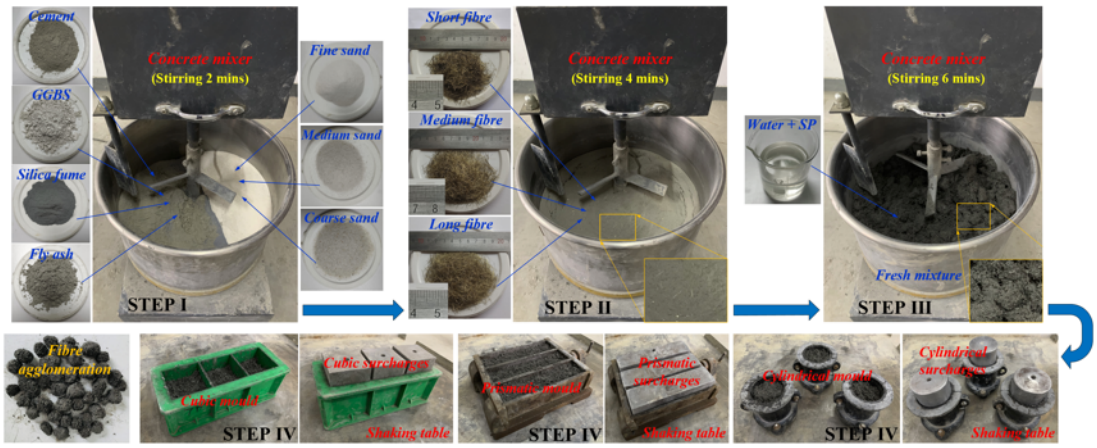

Fig. 4.2. Preparation procedures of FR-DUHPC samples and the observed fibre agglomeration upon stirring.

Early high-temperature curing is considered as an effective method to accelerate the consolidation of fresh concrete and enhance the early property of hardened mixtures. Thus, moist/steam curing regime with closed ambient temperature of 50 ℃ was used in this study according to the experimental findings reported in Chapter 3. Upon vibrated compaction, all samples covered with plastic film were first left in natural environment for 3 h. Afterwards, they were put in an insulated water tank and moist/steam cured at 50 ℃ for another 21 h. They were later demoulded and immersed in the normal-temperature water for continuous curing until the testing ages. Fig. 4.3 shows the moist/steam curing device employed and the typical samples upon the curing, in which strain gages were attached to

the surface of the beam and cylindrical samples to achieve the accurate test data. In total, there were 540 FR-DUHPC samples were prepared and cured for quasi-static tests at different testing ages.

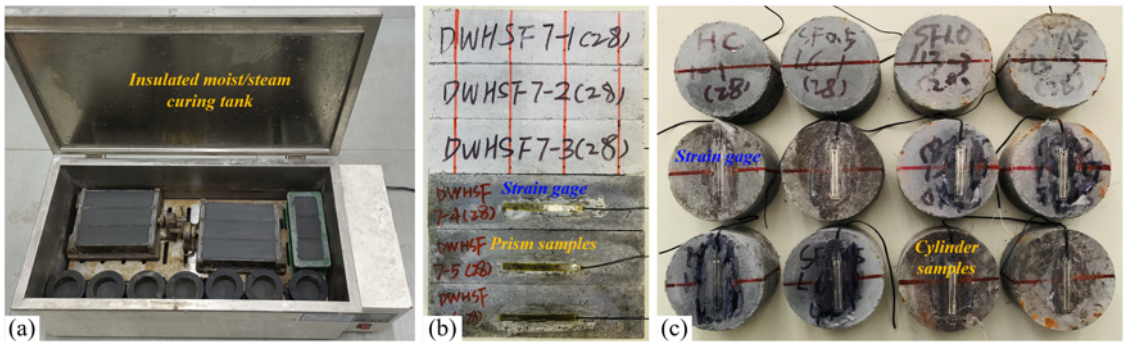

Fig. 4.3. (a) Moist/steam curing device and typical (b) prism and (c) cylinder FR-DUHPC samples before testing.

4.3 Testing program

At the end of 1, 7 and 28-day curing, the quasi-static mechanical performance of mono and hybrid FR-DUHPC including compressive, flexural and split-tensile behaviour were investigated complying with the Chinese national standards. The uniaxial compression tests were performed on cubic samples via using a micro-computer-controlled hydraulic test machine with a loading capacity of 50 tons. The bending and split-tensile tests were, respectively, conducted on beam and cylindrical concrete samples via utilizing a 10-ton computer-controlled universal testing machine. In order to obtain the concrete samples' ultimate strength data and complete stress-strain along with load-displacement curves, all tests were loaded using the constant displacement control, respectively, with 0.2 mm/min for compression and 0.05 mm/min for four-point bending and splitting-tensile tests.

Moreover, two symmetrical laser LVDTs were fixed between the platens of the machine and on both sides of the sample to record the displacement (deflection) along the load direction. For beam samples, strain gauges were likewise affixed to their bottom tension area to record the accurate flexural cracking strength. In addition, for samples subjected to compression and bending loads, tests would be terminated when the residual bearing capacity dropped to 10% of the peak load, while for samples subjected to split-tension, tests would be terminated when the displacement in the loading direction exceeded 2 mm. It should be pointed out that the samples' loading direction in the bending and split-tensile tests was a bit different, due to the preparation method of the layered vibrated-compaction as well as the setting of the bearing surface of prism and cylinder samples. As shown in Fig. 4.4, the casting surface (represented by dashed purple lines) of the samples was defined as the X-Y plane and the Z-axis directed to the multiplied casting layers. For prismatic samples in the bending test, the Z- and X-axis corresponded to the direction of the loading and resulting flexural-tensile stress, respectively. For cylindrical samples in the split-tensile test, the loading direction was switched to the Y-axis and the split-tensile stress was generated along the X-direction. Different loading directions and cracking modes would significantly affect the failure behaviour of FR-DUHPC by virtue of its inherent anisotropy characteristic caused by the layer-by-layer preparation method reported above. In addition, the quasi-static testing programs and research parameters involved are listed in Table 4.2.

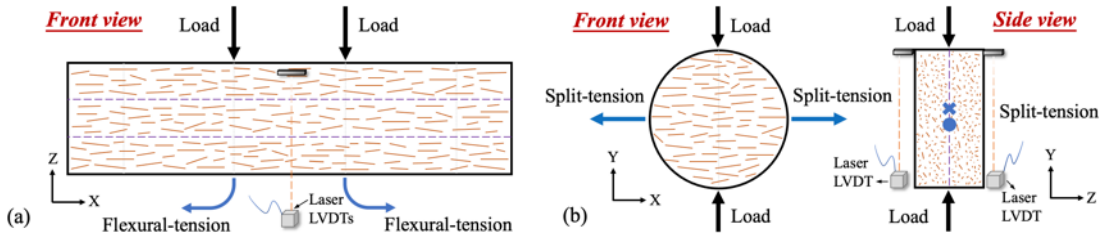

Fig. 4.4. Schematic diagrams of FR-DUHPC samples under (a) bending and (b) splitting-tensile loads.

Table 4.2

Quasi-static testing approaches and studied parameters of mono/hybrid FR-DUHPC.

Tests	Standards	Dimensions (mm)	Quantity	Parameters studied
Compression (Uniaxial compression)	GB/T50081-2019 [148] CECS13-89 [149] GB/T17671-2021 [150]	40 × 40 × 40 Cube	180	Compressive strength Stress-strain curve Modulus of elasticity Toughness index
Flexure (Four-point bending)	GB/T50081-2019 [148] CECS13-89 [149] GB/T17671-2021 [150]	40 × 40 × 160 Prism	180	Flexural strength Load-deflection curve Deflection hardening Toughness index
Split-tension	GB/T50081-2019 [148]	50 × 25 Cylinder	180	Split-tensile strength Load-displacement curve

4.4 Results and discussion

As introduced in Section 4.3, the static mechanical tests including compression, flexure and split-tension were performed on FR-DUHPC samples after they were cured for 1 day, 7 and 28 days. Tables 4.3 and 4.4, respectively, present the obtained ultimate strength values (averages of three identical samples) of mono and hybrid FR-DUHPC samples at different curing ages, in which f_c, f_r and f_{ts} are, respectively, the uniaxial compressive, flexural and split-tensile strength.

Table 4.3

Summary of static mechanical test results of mono FR-DUHPC samples.

Samples No.		f_c (MPa)			f_r (MPa)			f_{ts} (MPa)		
(Fibre length)		1-d	7-d	28-d	1-d	7-d	28-d	1-d	7-d	28-d
Control (No fibre)		72.3	82.2	90.8	9.3	11.7	12.9	4.4	5.5	6.4
6 mm	F05S	86.3	95.9	104.8	11.2	13.1	14.8	5.4	6.3	7.2
	F10S	93.2	104.1	113.1	15.8	19.7	22.0	6.2	7.2	8.2
	F15S	107.6	112.4	126.2	20.7	24.1	28.2	7.2	8.4	9.6
	F20S	117.9	122.0	135.3	23.5	27.8	31.9	7.8	9.1	10.1
10 mm	F05M	88.1	98.3	106.1	13.7	16.2	17.9	6.1	7.0	7.7
	F10M	98.5	109.3	120.4	19.2	23.5	27.1	7.0	7.8	9.0
	F15M	124.8	132.5	141.3	26.1	31.4	35.0	7.9	9.3	10.9
	F20M	130.4	142.0	152.3	29.4	35.3	39.6	8.6	10.2	11.7
13 mm	F05L	91.3	101.1	108.3	16.9	20.1	22.7	7.1	7.9	8.5
	F10L	105.3	117.8	128.9	21.1	27.2	32.5	7.7	8.6	9.7
	F15L	130.2	142.3	153.3	31.3	36.3	40.6	8.7	9.9	11.2
	F20L	133.2	148.7	162.7	32.1	37.2	42.2	9.4	10.7	12.1

Table 4.4

Summary of static mechanical test results of hybrid FR-DUHPC samples.

Samples No.		f_c (MPa)			f_r (MPa)			f_{ts} (MPa)		
(Hybridization)		1-d	7-d	28-d	1-d	7-d	28-d	1-d	7-d	28-d
Double	F05S10M (HSF1)	122.5	128.0	139.9	23.1	27.7	32.8	7.7	9.0	10.4
	F10S05M (HSF2)	110.8	121.9	133.3	21.8	26.0	30.1	7.3	8.5	9.9
	F05S10L (HSF3)	123.2	133.7	144.9	27.4	30.9	35.2	8.1	9.2	10.6
	F10S05L (HSF4)	112.6	124.1	135.8	25.3	29.7	33.0	7.6	8.8	10.1
	F05M10L (HSF5)	127.8	138.5	148.4	30.1	34.4	38.6	8.5	9.8	11.2
	F10M05L (HSF6)	126.2	136.6	145.2	29.5	33.0	37.5	8.6	10.0	11.4
Ternary	F05SML (HSF7)	124.4	135.6	144.4	27.1	31.4	35.9	8.0	9.3	11.1

Notes: items in parentheses denote the hybrid fibre numbers labelled on samples' surface.

4.4.1 Compression behaviour

The development of the compressive strength with curing age and fibre dosage when different lengths of steel fibres are separately mixed into concrete mixtures is shown in Fig. 4.5. Compared with control samples without fibre reinforcement, the single addition of any length of steel fibres notably increased the compressive strength of DUHPC at all ages, which was consistent with the research findings reported in Chapter 3. As an illustration, the average strength values at 28 days increased from 90.8 (control) to 126.2 (F15S), 141.3 (F15M) and 153.3 (F15L) MPa when the fibre dosage was 1.5%, and the enhancements were 39.0%, 55.6% and 68.8%, respectively. The highest strength value was achieved as 162.7 MPa at 28 days for F20L samples. It should be noted that the increase rate of strength started to slow down after the fibre dosage exceeded 1.5%, especially for cases mixing with 10- and 13-mm fibres. This was associated with the phenomenon of the fibre agglomeration during the stirring shown in Fig. 4.2. Additionally, little difference in compressive strength of DUHPC reinforced with three single lengths of fibres was discerned (such as 86.3, 88.1 and 91.3 MPa at 1 day of age) at low fibre addition of 0.5%, but the difference gradually manifested with fibre dosage, as can be clearly found from Fig. 4.5(d). This was mainly because when the fibre volume addition was low, short fibres could form a relatively dense fibre nets within the matrix by virtue of their quantity advantage. However, the number of longer fibres increased remarkably with dosage, demonstrating a more effective reinforcement in conjunction with their size effect. The largest 28-day strength

differences, in comparison with 6-mm FR-DUHPC samples, were 12.6% for 10-mm FR-DUHPC (F20M, 135.3-152.3 MPa) and 21.5% for 13-mm FR-DUHPC (F15L, 126.2-153.3 MPa) samples.

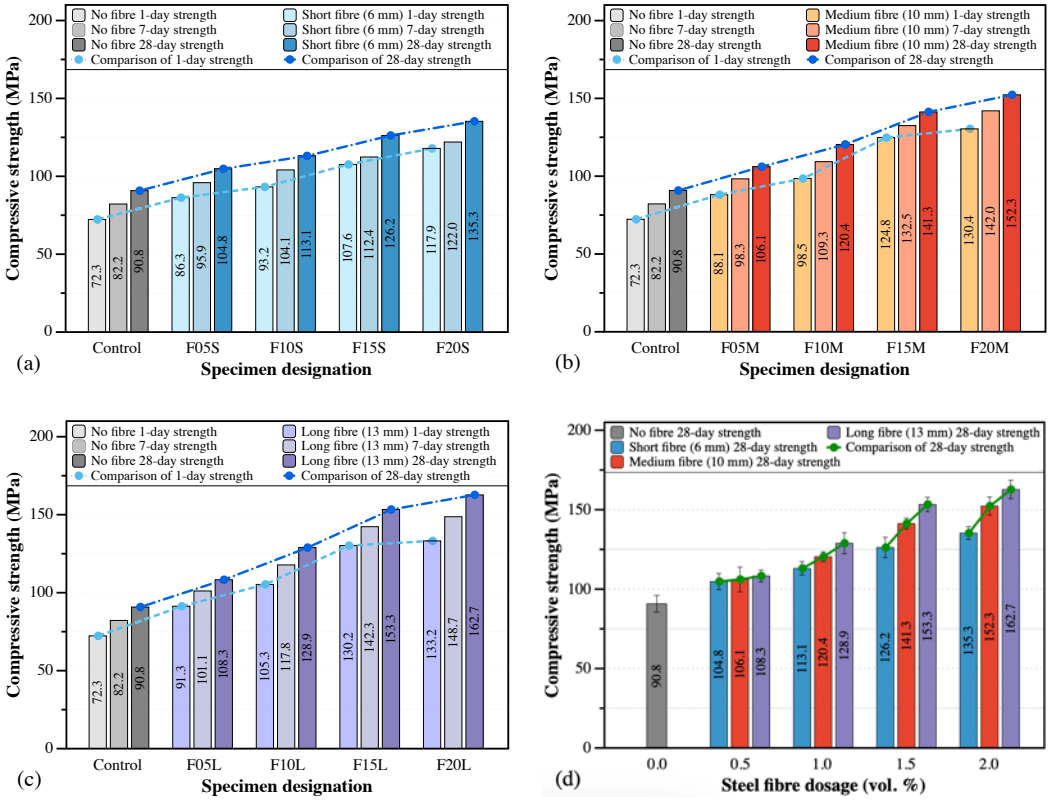

Fig. 4.5. Compressive strength of mono FR-DUHPC samples after 1, 7 and 28-day curing: (a) 6-mm fibre; (b) 10-mm fibre; (c) 13-mm fibre and (d) 28-day strength comparison regarding control samples.

Fig. 4.6 shows the effects of hybrid fibre reinforcement (1.5%) on the compressive strength of DUHPC up to 28 days of age. Of all ages tested, the concrete sample with the highest compressive strength was F05M10L, followed by F10M05L and F05SML. Under the same fibre dosage and double hybrid conditions, the addition of shorter steel fibres to substitute part of the initial size ones attenuated the

compressive strength to a certain extent. As an illustration, the 28-day ultimate strengths of F05S10M and F10S05M samples were reduced by 2.9% and 7.5%, respectively, compared with F15M samples. The marked reduction occurred in the case where 13-mm fibres were partially replaced by 6-mm short fibres, with the maximum decrease up to 12.4% (F10S05L, 131.6 MPa). The foremost reason was that while short fibres could restrain the development of micro-cracks, longer steel fibres were able to bridge the macro-cracks which were critical to the peak compressive strength [151-153]. The weakness derived from the short fibres was further magnified as the replacement gradually increased. Another reason for the attenuation in strength might be that in the case of double hybridization, a “size jump” existed between 6- and 13-mm fibres. That is, short fibres mainly mitigated the appearance and development of the micro-cracks under loads [154], but long fibres could not effectively restrict the further propagation of cracks due to their smaller quantity and scattered distribution. If a length of fibre reinforcement acting as a “transition size” was incorporated into the mix between the short and long steel fibres, the foregoing “size jump” would be avoided, rendering the multiscale cracks being more targeted by the hybrid reinforcement system. Therefore, the compressive strength of DUHPC with ternary hybrid fibre reinforcement (F05SML) at different ages was only 3.6-4.8% lower than that of F15L samples, but signally higher than F15S samples by 13.4-20.4%, at the same fibre dosage. In addition, as can be observed that substituting partial 13-mm fibres with medium-sized ones had little impact on compressive strength.

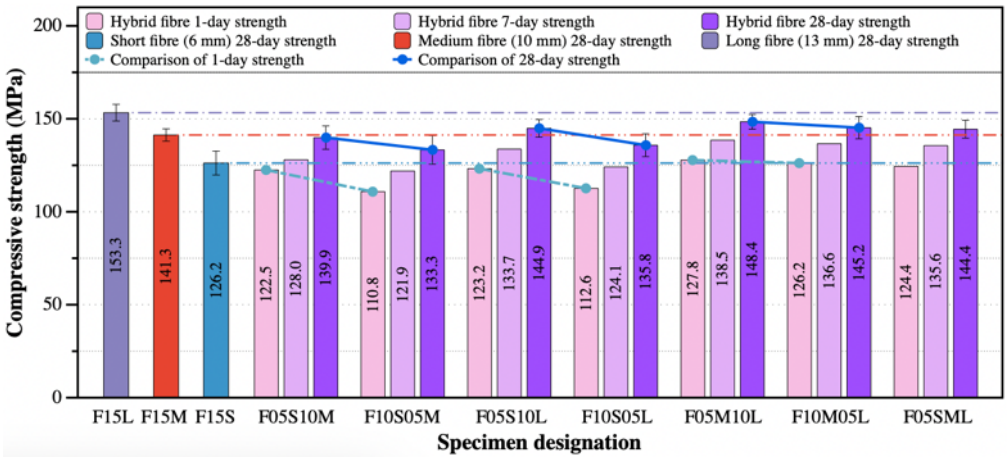

Fig. 4.6. Effects of hybrid fibre reinforcement on compressive strength of DUHPC.

Fig. 4.7 illustrates the typical compressive stress-strain relationships of DUHPC samples reinforced with mono and hybrid steel fibres after 28 days of curing, and the correlation curve for control samples is also depicted. Compared with control samples without fibre reinforcement, the addition of steel fibres could evidently transform the failure mode of DUHPC under compressive loads from brittleness to ductility, irrespective of the fibre length, dosage and mixing method (mono and hybrid). For mono samples, the peak stress and strain (corresponding to the peak stress) were increased with fibre addition, respectively in the ranges of 102.6-136.0 MPa and 0.0036-0.005, 106.4-150.9 MPa and 0.0036-0.0056, and 109.1-163.7 MPa and 0.0035-0.0058 when 6-, 10- and 13-mm steel fibres were mixed. Besides, the samples with higher fibre dosages and longer fibre lengths exhibited better ductility and energy absorption performance (would be analyzed in detail in the following section), which was manifested in that the post-cracking contour of the curves was more plump and the samples had a higher residual strength under the same strain. Moreover, compared with 6-mm steel fibres, the dosage

exceeding 1.5% had less evident effect on enhancing the bearing capability of samples with longer steel fibre reinforcements than improving their post-cracking behaviour. For hybrid samples exhibited in Fig. 4.7(d), the use of shorter fibres instead of partial longer ones showed little impact on the peak strain, while the proportion of longer steel fibres still dominated the post-cracking behaviour of the samples and the plumpness of the curves.

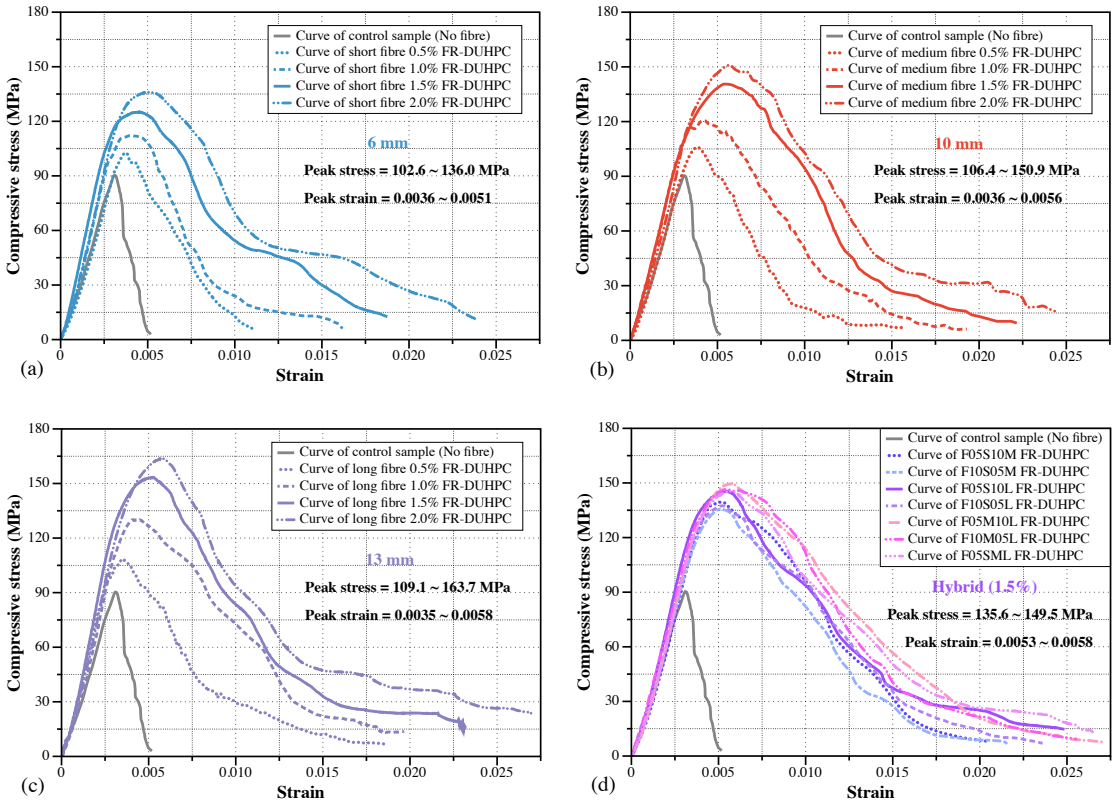

Fig. 4.7. Typical 28-day compressive stress-strain curves of (a-c) mono and (d) hybrid FR-DUHPC samples.

The toughness of concrete material is a very important parameter reflecting its deformability under external loads [155]. Fig. 4.8 compares the compressive total energy absorption (CTE) and toughness index (CTI) of control and FR-DUHPC samples at different testing ages. CTE is considered as the total area under the

compressive stress-strain curves shown in Fig. 4.7 corresponding to the residual strength at 10% of the ultimate stress, while CTI is the ratio of CTE to the energy absorption before cracking (CEBC), i.e., the area enclosed by the curves from zero to the ultimate stress [145, 156]. As can be broadly observed that the energy absorption ability and toughness of DUHPC improved notably with the addition of mono and hybrid fibres, which could be increased by 115-892% for CTE and 70-114% for CTI, in comparison with control samples. Additionally, the value of CTE gradually increased with steel fibre length under the same dosage, especially at higher volume fractions of 1.0-2.0%, as depicted in Fig. 4.8(b). However, it is noteworthy that the CTI of the samples with 2.0% short fibre reinforcement was larger than that of the samples reinforced with 2.0% medium/long steel fibres. That would mean that the CTE improved rapidly with a slight increase in CEBC when the dosage of short fibres increased from 1.5% to 2.0%, and thus exhibiting better compressive toughness. For double-hybrid samples, the degradation in CTE appeared in the cases where short fibres replaced 1.0% 10- and 13-mm fibres, and their CTI presented a similar downtrend, which could be explained by the reason of the larger strength attenuation in comparison with the original fibre-sized samples. However, unlike the strength variations, F05M10L, F10M05L and ternary-hybrid (F05SML) samples showed better compressive energy absorption ability and toughness. In particular, the CTE of F05SML samples at 28-day age increased by 702.8% and 10.1%, respectively, compared with control and F15L samples, while the CTI increased by 108.0% and 5.8%, respectively. All these improvements were attributed to the positive synergistic function of the multiscale

fibre hybridization on the compressive behaviour after cracking, which jointly mitigated the propagation of cracks in two (10/13 mm) and three (6/10/13 mm) length scales [145, 151, 152]. Hence, the use of 1.5% ternary fibre hybridization endowed DUHPC with excellent compression energy absorption and toughness properties, while having a good mixture consistency, even with slightly reduced compressive strength.

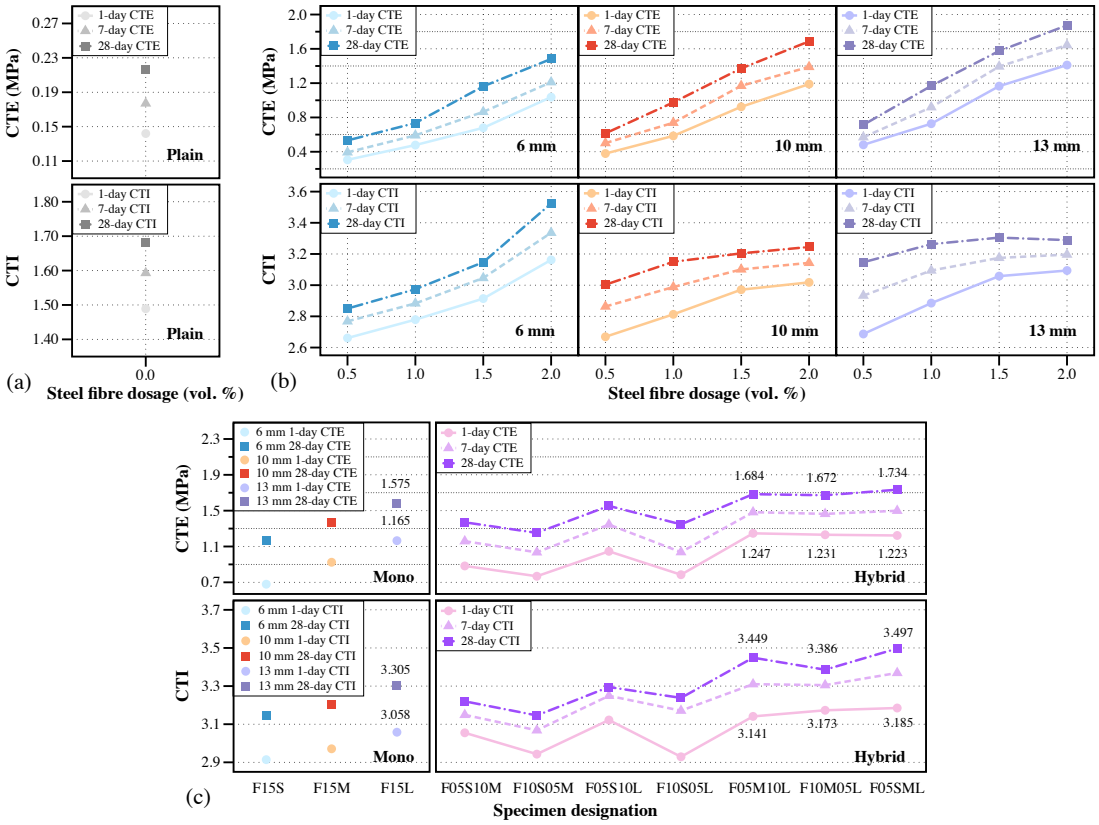

Fig. 4.8. Compressive total energy absorption and toughness index of (a) control; (b) mono and (c) hybrid FR-DUHPC samples after 1, 7 and 28-day curing.

Fig. 4.9(a) shows the variations in the 28-day static MOE of mono (0.5-2.0%) and hybrid (1.5%) FR-DUHPC samples. The static MOE is also obtained based on the linear section of compressive stress-strain curves, and 83-90% of the ultimate stress is considered as the upper limit of the elastic section of DUHPC in the

current study [157, 158]. It could be observed that the MOE of mono FR-DUHPC samples gradually increased with steel fibre length and volume addition. As an illustration, the MOE was increased from 35.8 to 39.9 GPa for F05S and F20S samples, and was continuously increased to 42.1 GPa for F20L samples, which was attributed to the improvement of fibre length and dosage on the compressive strength reported above. It was noteworthy that in the case of fibre hybridization, the F05SML (HSF7) samples demonstrated the comparable MOE of 41.1 GPa when compared with longer steel fibre reinforcements, such as F15L, F05M10L and F10M05L. This might be attributed to the homogenous micro-structure with multiscale hybrid fibre reinforcement in effectively bridging the micro-, meso- and macro-cracks, leading to a more linear elastic part under compression load [151]. In addition, the relationships between 28-day compressive strength and MOE of mono and hybrid FR-DUHPC were contrasted with the developed fitting curve obtained from Chapter 3, as illustrated in Fig. 4.9(b). It was further manifested that the enhancement in compressive strength caused a logarithmic improvement in static MOE (MOE = 14,152·lnf_c - 44,028) with a great goodness of fit of 0.973.

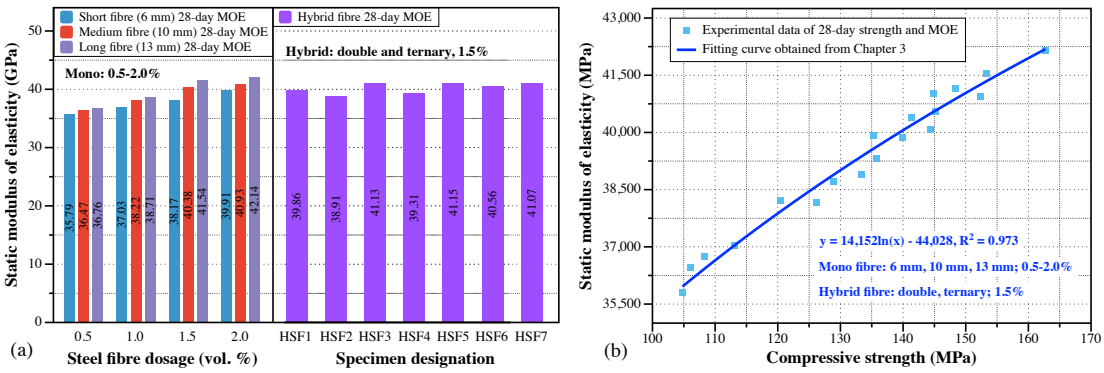

Fig. 4.9. (a) 28-day static MOE and (b) its relationship with compressive strength of mono and hybrid FR-DUHPC samples.

4.4.2 Flexure behaviour

Fig. 4.10 illustrates the development of the flexural strength with curing age and fibre dosage when steel fibres with different lengths are separately mixed into DUHPC mixtures. The strength of DUHPC with any length of mono reinforcement was improved with curing age and fibre dosage, and the increase was significant when the fibre length increased from 6 to 10 and 13 mm under the same addition. For instance, the flexural strengths of control samples at three testing ages were 9.3, 11.7 and 12.9 MPa, respectively, and they increased to 13.7, 16.2 and 17.9 MPa for F05M DUHPC samples and continued to increase to 29.4, 35.3 and 39.6 MPa when 2.0% medium fibre was mixed. F20L samples illustrated the highest 28-day strength of 42.2 MPa, which improved by 227.1%, 32.3% and 6.6%, respectively, as compared to the control, F20S and F20M samples. Similar to the variation trend of compressive strength, when the fibre addition exceeded 1.5%, introducing more fibres into the mixture did not prominently improve the flexural strength. Especially for the mixtures reinforced with long fibres, the 1, 7 and 28-day strengths at 2.0% reinforcement were only 2.6%, 2.5% and 3.9% higher than the same-age strengths at 1.5% fibre reinforcement, which was still related to the observed fibre agglomeration. It should be noticed that under the identical fibre dosage (0.5-2.0%), the incorporation of longer steel fibres into DUHPC mixtures contributed to more positive effect on flexure rather than compression, as manifested from the contrast between Figs. 4.5(d) and 4.10(d). For example, little difference in compressive strength of DUHPC reinforced with any single length

of fibres was observed at 0.5% fibre addition, as reported in the previous section, whereas the flexural strength improved from 14.8 to 17.9 MPa (by 20.9%), and then to 22.7 MPa (by 26.8%) as the fibre length increased. This means that the use of 10- and 13-mm steel fibres is more beneficial for DUHPC structures/units that are mainly subjected to bending loads during their serviceability.

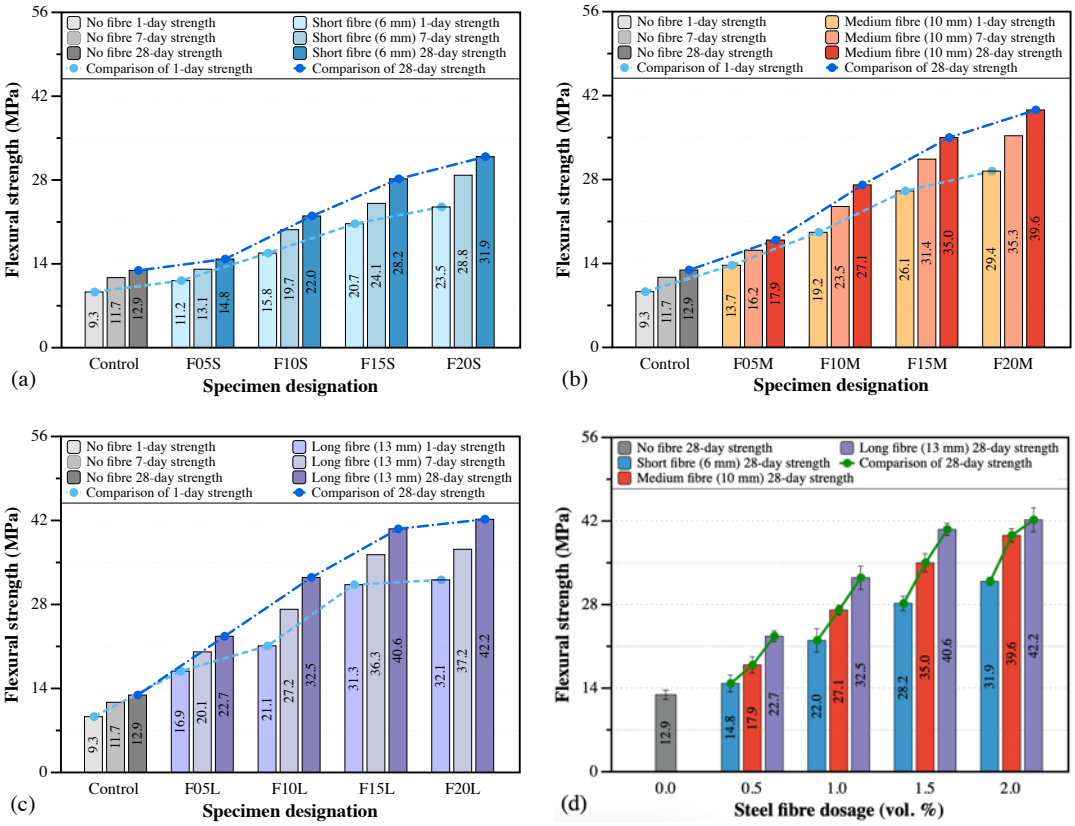

Fig. 4.10. Flexural strength of mono FR-DUHPC samples after 1, 7 and 28-day curing: (a) 6-mm fibre; (b) 10-mm fibre; (c) 13-mm fibre and (d) 28-day strength comparison regarding control samples.

Fig. 4.11 illustrates the impacts of hybrid fibre reinforcement (1.5 Vol-%) on the flexural strength of DUHPC at three ages. The attenuation in flexural strength also occurred on DUHPC mixtures where longer fibres were partially substituted by shorter ones at all ages, and the largest decrease was up to 18.7% (F10S05L,

33.0 MPa). It should be pointed out that the decrease in compressive strength of the identical sample was obtained as 12.4%, as reported above, which further demonstrated that the flexural behaviour of DUHPC was more sensitive to fibre size than the compression. Under the double-hybrid condition, mixing medium-length steel fibres instead of partial long ones exhibited the least negative impact on the flexural strength, such as the 28-day strength dropped from 40.6 (F15L) to 38.6 (F05M10L) and 37.5 MPa (F10M05L) with a decrease of 4.9% and 7.6%, respectively. For the ternary-hybrid samples, even though the flexural strength at each curing age was attenuated to some extent (the 28-day strength decreased by 11.6%) due to the addition of 6-mm fibres in comparison with F15L samples, their ultimate strength was higher in comparison with F15M samples. The ternary hybridization could mitigate the lower efficiency of short fibres in inhibiting the crack propagation, and weaken the stress between fibres and cement matrix by virtue of the quantity and dimension advantages, thus delaying the formation and development of the multiscale cracks [139, 159].

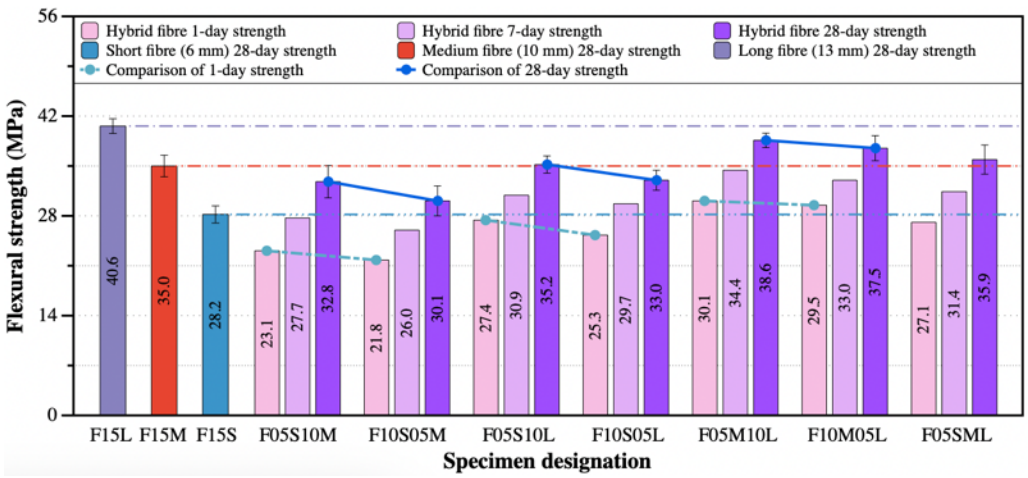

Fig. 4.11. Effects of hybrid fibre reinforcement on flexural strength of DUHPC.

Fig. 4.12 illustrates the typical flexural load-midspan deflection relationships of DUHPC samples reinforced with mono and hybrid steel fibres after 28 days of curing, and the correlation curve for control samples is also depicted. Similar to the compressive stress-strain behaviour, the incorporation of any length, dosage and mixing method (mono and hybrid) of steel fibres could transform the sudden fracture of DUHPC into ductile failure under flexural-tensile load, as compared to control ones with no fibre. The presence of steel fibres rendered the samples to sustain the continuous action of the bending load and reach the ultimate bearing capacity after the crack initiation (corresponding to the cracking strength, which would be discussed and analyzed in detail in the following section). Then, with the gradual increase in the width of the matrix cracks and the midspan deflection of the samples, the stress between the cracks redistributed and the load borne by the fibres became larger by virtue of the anchorage and friction between the matrix and embedded fibres, thus retarding the crack propagation. For mono FR-DUHPC samples, the higher fibre additions and longer fibre lengths contributed to markedly higher flexural bearing capability and better ductility (Table 4.5). In this section, the expression $i = \Delta_{0.85}/\Delta_{crack}$ proposed by Cohn et al. [160] was utilized to calculate the flexural deflection ductility index of FR-DUHPC prismatic samples, where i is the ductility index, $\Delta_{0.85}$ is the deflection value corresponding to 85% of the peak load in the descending part of the curve, and Δ_{crack} is the first yield deflection value of prismatic samples. In addition, it could be observed that in the descending part of the curve beyond the peak load, the visible zigzag

patterns appeared on the curves of all samples (except for 2.0% 10- and 13-mm FR-DUHPC samples), and the tearing sounds could be heard during the loading process, which was in line with the test results concluded by Wu et al. [152]. However, as the total number of bridging fibres across the fracture surface as well as the anchorage length increased, the amplitude of the foregoing zigzag patterns mitigated evidently, manifesting that the restraint effect of steel fibres on flexural-tensile cracks was more efficient and the cracks' development was more stable. For hybrid FR-DUHPC samples depicted in Fig. 4.12(d), as expected, the use of shorter steel fibres as a partial substitute for longer ones led to a reduction in peak load and a degradation in ductility (Table 4.5), and the phenomenon of steel fibres been pulled out suddenly and frequently was more likely during the deflection softening process, especially for hybrid samples with more 6-mm fibres. It is noteworthy that the ductility index of samples F05M10L was greater than that of samples F15L or even F20L, further demonstrating the positive synergistic effect of the multiscale fibre hybridization on the flexural behaviour after cracking.

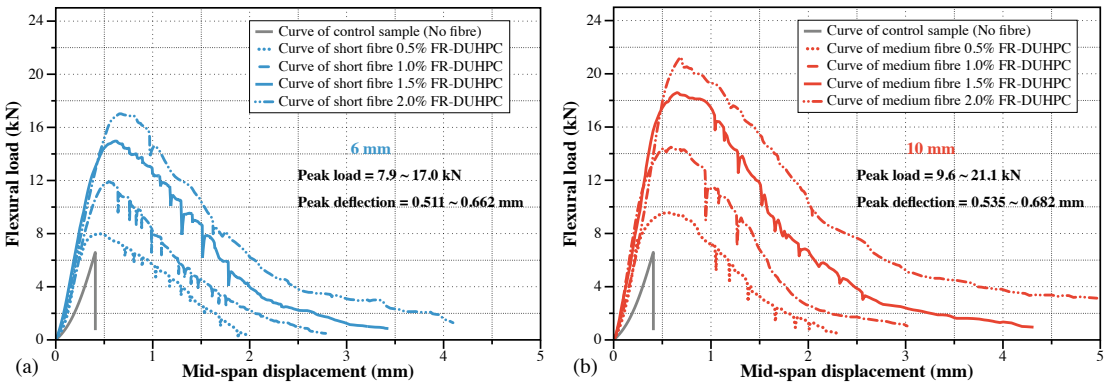

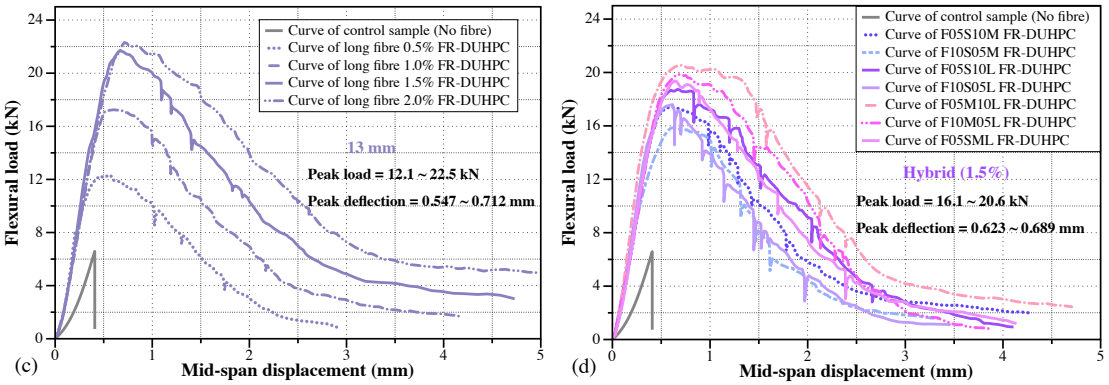

Fig. 4.12. Typical 28-day flexural load-deflection curves of (a-c) mono and (d) hybrid FR-DUHPC samples.

Table 4.5

Deflection ductility index of mono and hybrid FR-DUHPC samples.

Mix	Ductility	Mix	Ductility	Mix	Ductility	Mix	Ductility	Mix	Ductility
F05S	2.46	F05M	3.59	F05L	3.87	F05S10M	3.93	F05M10L	5.25
F10S	2.70	F10M	3.75	F10L	3.96	F10S05M	3.74	F10M05L	4.24
F15S	2.99	F15M	3.96	F15L	4.29	F05S10L	4.23	F05SML	3.94
F20S	3.08	F20M	4.18	F20L	4.55	F10S05L	3.68	Control	1.00

Figs. 4.13 and 4.14 together show the impacts of fibre dosage and hybridization on the 28-day flexural cracking strength and toughness of mono and hybrid FR-DUHPC samples. The cracking strength was considered as the flexural stress when the strain gauge ruptured, and the toughness, FT_{δ}, $FT_{3\delta}$, $FT_{5.5\delta}$ and $FT_{10.5\delta}$, were, respectively, referred to the total area under the flexural load-deflection curves shown in Fig. 4.12 as the mid-span displacement reached 1, 3, 5.5 and 10.5 times the cracking deflection (δ_{cr}) corresponding to the cracking strength. Accordingly, the toughness indexes, FTI_5, FTI_{10} and FTI_{20}, were parameters by dividing the $FT_{3\delta}$, $FT_{5.5\delta}$ and $FT_{10.5\delta}$ by FT_{δ} revealing the energy consumption

capacity of DUHPC after cracking, which were given by the Chinese national standard CECS13-89 [149]. It could be observed that the cracking strength of DUHPC with any mono fibre reinforcement was enhanced prominently with fibre dosage. Compared with the 28-day flexural strength (12.9 MPa) for reference samples listed in Table 4.3, the contributions of three fibres to cracking strength at 0.5% dosage were comparable. However, with the increase in fibre dosage, longer steel fibre reinforcement exhibited a better effect on improving the cracking strength. In addition, the clear variation of the ratio between cracking and peak strength indicated that gradually increasing the fibre volume addition rendered DUHPC to exhibit more prominent deflection-hardening behaviour, i.e., there was still much room for the enhancement in flexural strength of DUHPC after the crack initiation. For samples with 1.5% hybrid reinforcement, introducing 10-mm fibres instead of partial 13-mm ones had a little impact on cracking strength, but a mildly increase could be found when they were partially replaced by 6- and 10-mm fibres in the ternary hybridization. Additionally, the aforementioned strength percentage varied within the range of 50-60%, and gradually increased with the substitution using shorter steel fibres.

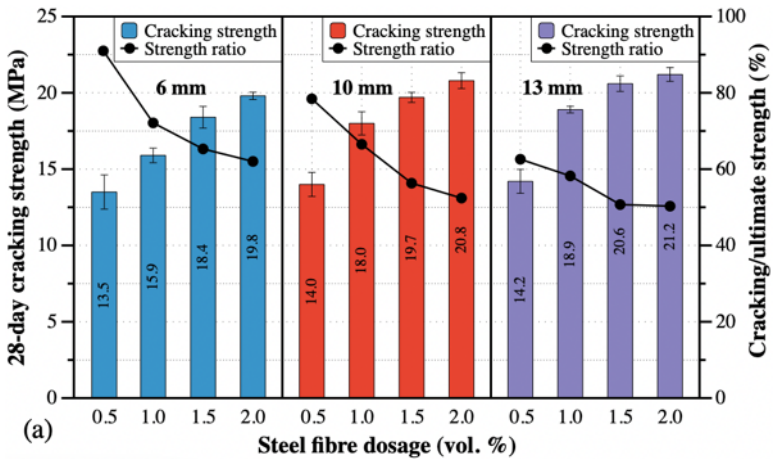

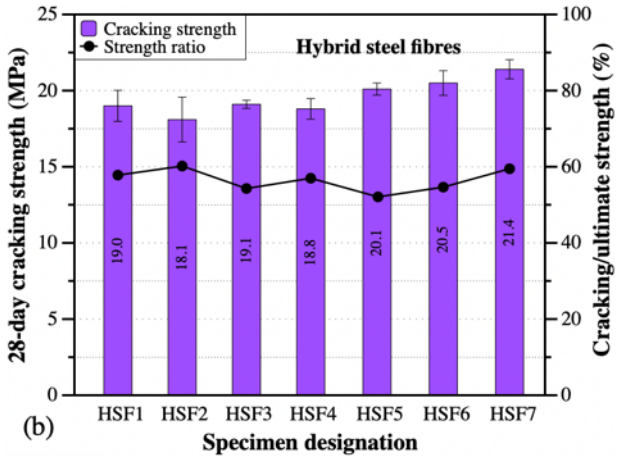

Fig. 4.13. Flexural cracking strength and its ratio to the ultimate strength of (a) mono and (b) hybrid FR-DUHPC samples after 28-day curing.

As indicated in Fig. 4.14, the changes in flexural toughness and toughness index of DUHPC with mono fibre reinforcement demonstrated a roughly similar trend to those of flexural cracking strength. It was worth noting that since 6-mm fibres had small length and rather low efficiency in restricting the cracks development, they were incapable to render the reinforced samples exhibiting better ductility at lower fibre incorporation beyond cracking. Therefore, the flexural toughness $FT_{10.5\delta}$ and toughness index FTI_{20} in the cases of the fibre additions of 0.5% and 1.0% were calculated as zero. So did these two parameters of samples with 0.5% 10-mm fibre reinforcement. As could be observed in Fig. 4.14(a) that longer steel fibres demonstrated a more remarkable toughening effect at the deflection points of $5.5\delta_{cr}$ and $10.5\delta_{cr}$, especially for DUHPC samples with higher fibre dosages (1.0-2.0%). For example, the toughness at the deflection point of $10.5\delta_{cr}$ was 38.0 kN·mm when 1.5% 13-mm steel fibres were introduced, and the corresponding index FTI_{20} was 25.8. The toughness value was approximately 40.7% and 82.7% higher than the cases when 1.5% 10- and 6-mm fibres were separately blended,

and FTI_{20} was approximately 36.5% and 65.4% higher than the corresponding samples. In the cases of fibre hybridization, as shown in Fig. 4.14(b), the use of shorter fibres to substitute partial longer ones reduced the flexural toughness and energy consumption ability to some extent. Under the same fibre dosage of 1.5%, F05M10L (HSF5), F10M05L (HSF6) and F05SML (HSF7) cases exhibited slightly lower and much higher flexural toughness as respectively compared to F15L and F15M samples. Meanwhile, due to the reduced amount of longer steel fibres, the above three hybrid FR-DUHPC samples had better fibre dispersibility and mixture workability, according to the observation shown in Fig. 4.2.

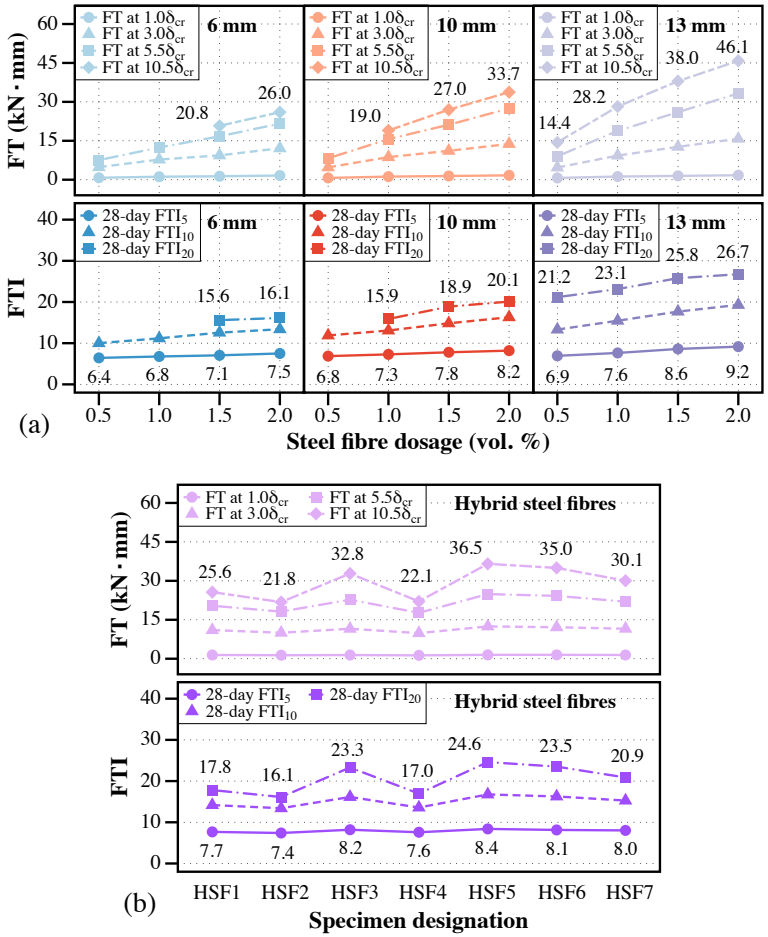

Fig. 4.14. Flexural toughness (FT) and toughness indexes (FTI) of (a) mono and (b) hybrid FR-DUHPC samples after 28-day curing.

4.4.3 Split-tension behaviour

The development of split-tensile strength with curing age and fibre dosage when steel fibres with different lengths are separately mixed into DUHPC mixtures is depicted in Fig. 4.15. The strength development of DUHPC with any mono fibre reinforcements were similar to the variation trend of the flexural strength. As the addition of steel fibres increased from 0.5% to 2.0%, the split-tensile strength of short, medium and long FR-DUHPC at 28 days was, respectively, improved by 10.9-57.8%, 20.3-82.8% and 32.8-89.1%, compared with control samples. From the above it can be found that the strength improvement of 13-mm fibres was weakened at the high-volume dosage. This trend can be more clearly observed from Fig. 4.15(d). That is, the 28-day splitting-tensile strength of F05L and F10L samples was improved by 10.4% and 7.8% compared with F05M and F10M ones, respectively, while these improvements were reduced to 2.8% and 3.4% when the fibre addition added to 1.5% and 2.0%. Moreover, the slowdown in the growth rate of split-tensile strength also occurred after the fibre addition exceeded 1.5%, for any single length of steel FR-DUHPC samples.

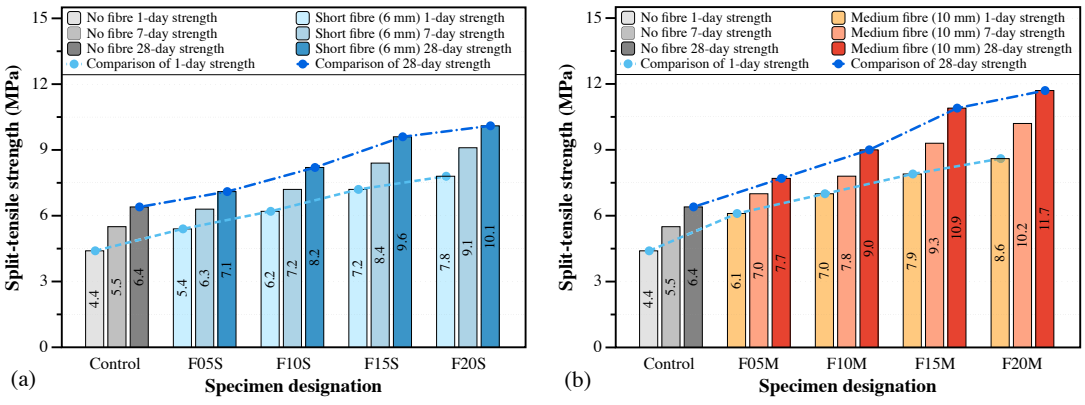

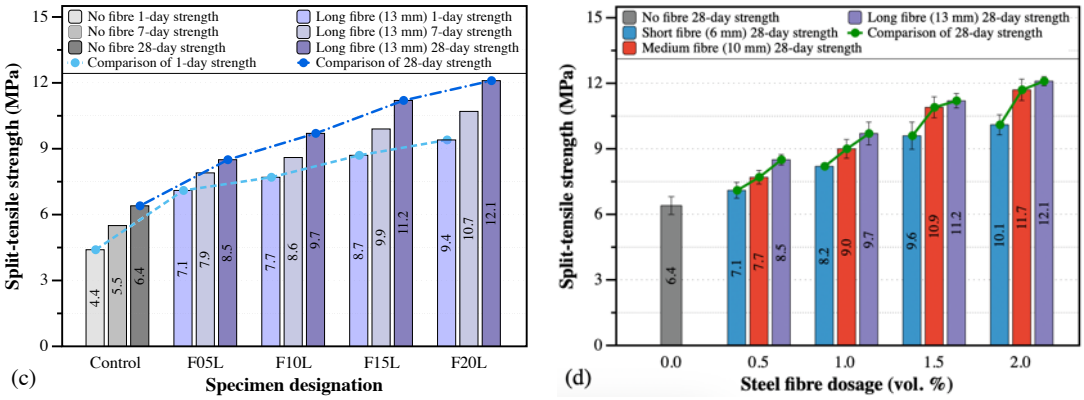

Fig. 4.15. Split-tensile strength of mono FR-DUHPC samples after 1, 7 and 28-day curing: (a) 6-mm fibre; (b) 10-mm fibre; (c) 13-mm fibre and (d) 28-day strength comparison regarding control samples.

Fig. 4.16 also depicts the impacts of hybrid fibre reinforcement (1.5 Vol-%) on the split-tensile strength of DUHPC at three testing ages. Similar strength attenuation could be found when longer (10- and 13-mm) steel fibres were partially replaced with 6-mm short ones, owing to the poorer efficiency of short fibre reinforcement in constraining the cracks propagation. However, it is interesting that the samples with 10-mm steel fibres substituting partial longer ones (F05M10L and F10M05L) demonstrated comparable or even slightly higher split-tensile strength than the original samples (F15L). In addition, the ternary-hybrid fibre-reinforced samples also exhibited satisfactory strength at all ages, in contrast to the three samples mentioned above. All these improvements in split-tensile strength were ascribed to the combined strengthening effect from the hybrid fibre reinforcement, which jointly mitigated the cracks development in two (10/13 mm) and three (6/10/13 mm) length scales [145, 151, 152].

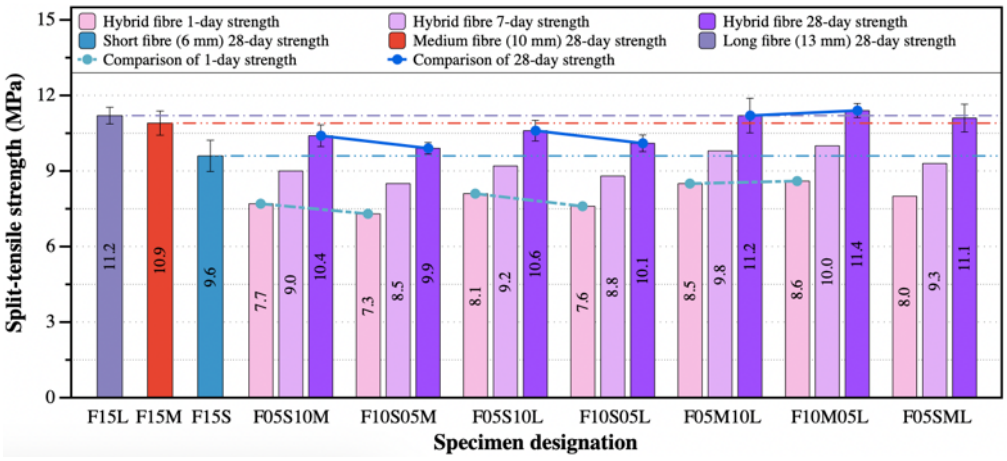

Fig. 4.16. Effects of hybrid fibre reinforcement on split-tensile strength of DUHPC.

Fig. 4.17 illustrates the typical split-tensile load-displacement curves of DUHPC samples reinforced with mono and hybrid steel fibres after 28 days of curing, and the correlation curve for control samples is also presented. Since the test samples were cylinder, their bearing surface was developed from the line to the plane after reaching the peak load. The failure of samples was continuously transformed in split-tension and compression, resulting in obvious fluctuation and undulation in the descending section of the foregoing curves. As exhibited in Fig. 4.17(a-c), although the inclusion of 0.5 Vol-% steel fibres of any length could enhance the maximum bearing capability of DUHPC under splitting- tensile load, its effect on the improvement of brittle failure after the initial crack was not significant, and the reinforced samples had comparable splitting stiffness as compared to the control case. This was mainly due to the lower constraint efficiency of short fibres for rapid cracks propagation and the insufficient toughening amount of longer fibres at the constant volume dosage. However, as the fibre addition increased, the ductile failure became conspicuous, and the samples exhibited obvious tension

hardening behaviour and enhanced splitting stiffness at higher fibre dosages (1.5-2.0% for 6- and 10-mm FR-DUHPC and 1.0-2.0% for 13-mm FR-DUHPC). In addition, longer fibres were more effective for improving the foregoing ductility, as indicated by the progressively extended vertical displacement corresponding to the peak load (from 0.735-0.784 to 0.795-0.842 and 0.817-0.844). For hybrid FR-DUHPC cases, all the samples exhibited visible tension hardening and ductile failure characteristics except for the samples with more 6-mm fibre substitution (F10S05M and F10S05L), which exhibited a larger bearing capacity decline after peak load.

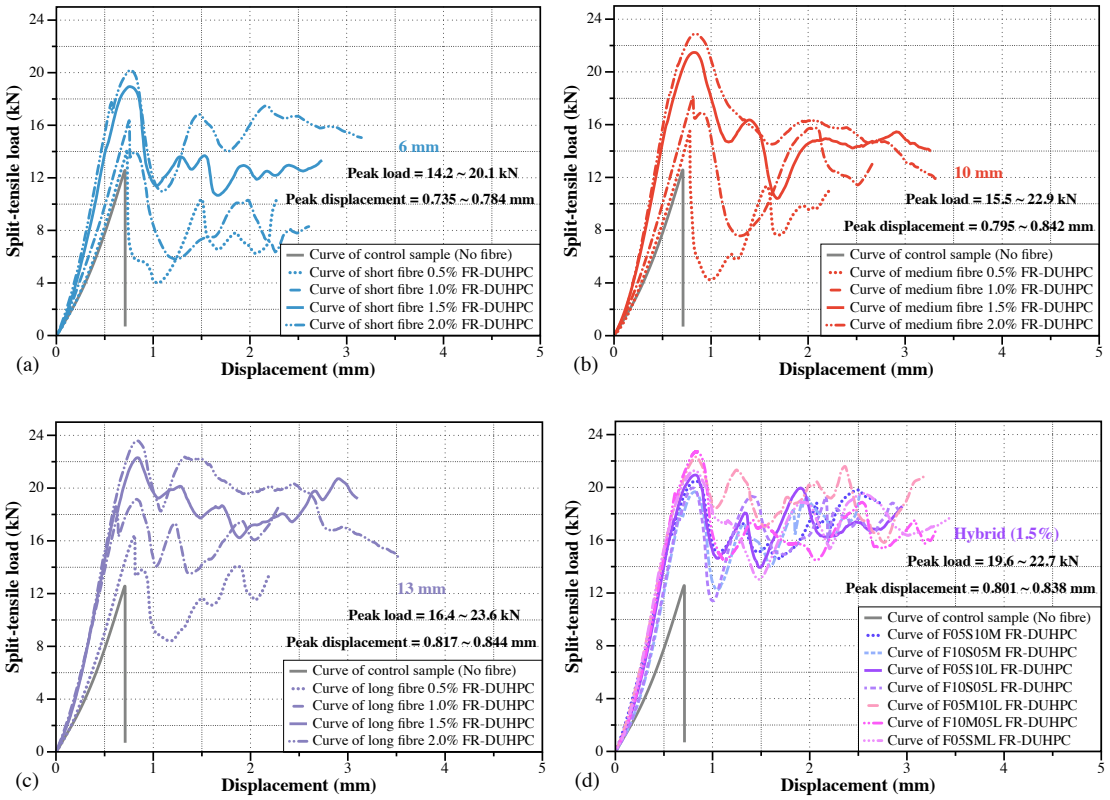

Fig. 4.17. Typical 28-day split-tensile load-displacement curves of (a-c) mono and (d) hybrid FR-DUHPC samples.

4.4.4 Discussion

As analyzed above, compared with control samples without fibre reinforcement, the incorporation of any length, dosage and mixing method (mono/hybrid) of steel fibres could improve the static mechanical performance (strength, toughness and energy absorption behaviour) of DUHPC and meanwhile transform the failure mode from the brittleness to ductility, especially at higher fibre volume dosages and longer fibre lengths.

For mono FR-DUHPC samples, steel fibres contributed greater positive impact to the strength in flexure and split-tension than the compression, and this effect was prominent once the longer fibres were mixed, at the same volume addition. As an illustration, compared with control samples, the 28-day strength increments in compression were 39.0%, 55.6% and 68.8% when 1.5% short, medium and long steel fibres were separately incorporated. For flexure and split-tension, the aforementioned increments were 118.6%, 171.3%, 214.7% and 50.0%, 70.3%, 75.0%, respectively. In addition, the improvement effect of steel fibres with larger quantity and longer size on flexural ductility and toughness of DUHPC after the crack initiation was likewise evidently stronger than that on compression-related properties, which could be intuitively observed from the contrast between the Figs. 4.7(a-c) and 4.12(a-c), as well as the Figs. 4.8(b) and 4.14(a). This means that the utilization of any length of steel fibres (better to mix longer ones at higher addition) is very beneficial for DUHPC structures and components since they are mainly subjected to flexural-tensile load during their serviceability.

In the case of fibre hybridization, the addition of shorter steel fibres as a partial substitute for the initial-sized ones reduced the mechanical properties of DUHPC to some extent. Moreover, the attenuation of the flexural behaviour was more evident when 6-mm steel fibres were introduced with volume substitution of 1.0%, which was manifested by the attenuated cracking/ultimate flexural strength, as well as the degraded deflection hardening, toughness and energy consumption property. Even so, F05M10L/F10M05L and F05SML samples presented slightly lower and much higher flexural toughness as respectively compared to F15L and F15M samples, and also these samples presented comparable compressive and split-tensile strength when compared to F15L cases, whereas better compressive toughness and energy absorption ability. To find out its cause, the improvements were attributed to the positive synergistic effect of multiscale fibre hybridization on the mechanical behaviour of DUHPC after cracking, which jointly alleviated the cracks propagation in two (10/13 mm) and three (6/10/13 mm) length scales [145, 151, 152]. Shorter steel fibres with better dispersion could effectively fill the inherent voids of the cementing slurries and reduced/restrained the emergence of micro-cracks, while the longer ones powerfully bridged/held the matrix on both sides of the cracks after the micro-cracks developed into the macro-crack, which improved the post-cracking behaviour of DUHPC.

In this study, another non-negligible factor that caused the length and dosage of steel fibres to possess a more significant improvement effect in the flexural and split-tensile properties of the developed DUHPC came from its fabrication method.

Take the prism FR-DUHPC samples under static bending tests as an illustration, they were vibration-compacted in three layers using surcharges to obtain the final form, as introduced in Section 4.2.2. In other words, under the combined action of vibration and compaction, steel fibres tended to be aligned parallel to the direction of the compaction layer (Fig. 4.18), which was similar to the wall-effect of the self-compacting 3D-printing steel FR-UHPC as reported in Ref. [161]. This endowed the embedded steel fibres with a longer effective anchoring length when the matrix was cracked, and hence signally improved the flexural performance of DUHPC. Moreover, as compared to medium/long steel fibres, 6-mm short fibres were also likely to be distributed perpendicular and/or inclined to the casting layer since the thickness of each layer was around 13 mm. Therefore, under the same volume addition, the use of short steel fibres manifested a lower improvement effect on flexural-tensile performance. In addition, it was noteworthy that the split-tensile strength of FR-DUHPC samples with the identical mix proportion at the same testing ages was approximately 27-50% of the flexural strength (less than the relevant strength ratio of self-compacting FR-UHPC), and the enhancement of the split-tensile strength with fibre dosage and length was not as significant as that of the latter. The primary reason also came from the preparation method of DUHPC and the different loading directions of the two test methods as shown in Fig. 4.4. As can be seen from Fig. 4.4(b), the cylinder samples under compression load would not only undergo the splitting-tensile failure, but also might appear the detachment of adjacent compaction layers (exhibited in Fig. 3.19), owing to the

insufficient interlayer bonding and fibre reinforcement. Nevertheless, the layered consolidation had a litter effect on the flexural property of the prismatic samples under the Z-axis loading, and therefore resulted in a lower increase in split-tensile strength than that in flexure.

Hence, after comprehensively considering the main applications and preparation technologies of the developed DUHPC, as well as the impact of the distribution, dosage, length and mixing method of steel fibres on its mechanical properties, the mixtures with hybrid medium and long steel fibres as well as with hybrid short, medium and long ones were suggested to be utilized in the practical application of DUHPC structures/members. Moreover, the length of steel fibres introduced was not recommended to exceed 13 mm due to the easy agglomeration of longer steel fibres and the lower moisture content of DUHPC. Furthermore, it should be pointed out that although the water-binder ratio of the developed DUHPC in this study (w/b = 0.16) was similar to that of self-compacting UHPC (w/b = 0.16~0.20), the moisture content of DUHPC mixtures was significantly reduced owing to the lower content of the cementitious materials (approximately 860 kg/m^3). Under the combined effect of more addition of aggregates (approximately 1400 kg/m^3), the barren appearance of dry concrete was exhibited. This characteristic of DUHPC enabled it to be rapidly demoulded upon the formation, or even without formwork operation. The prepared mixtures could be used in concrete structures and units with special requirements for early strength behaviour by virtue of the exhibited extremely high early (up to 133.2 and 32.1 MPa for compression and flexure at 1

day of age) and long-term (up to 162.7 and 42.2 MPa for compression and flexure at 28 days) strengths, thereby effectively speeding up the construction progress.

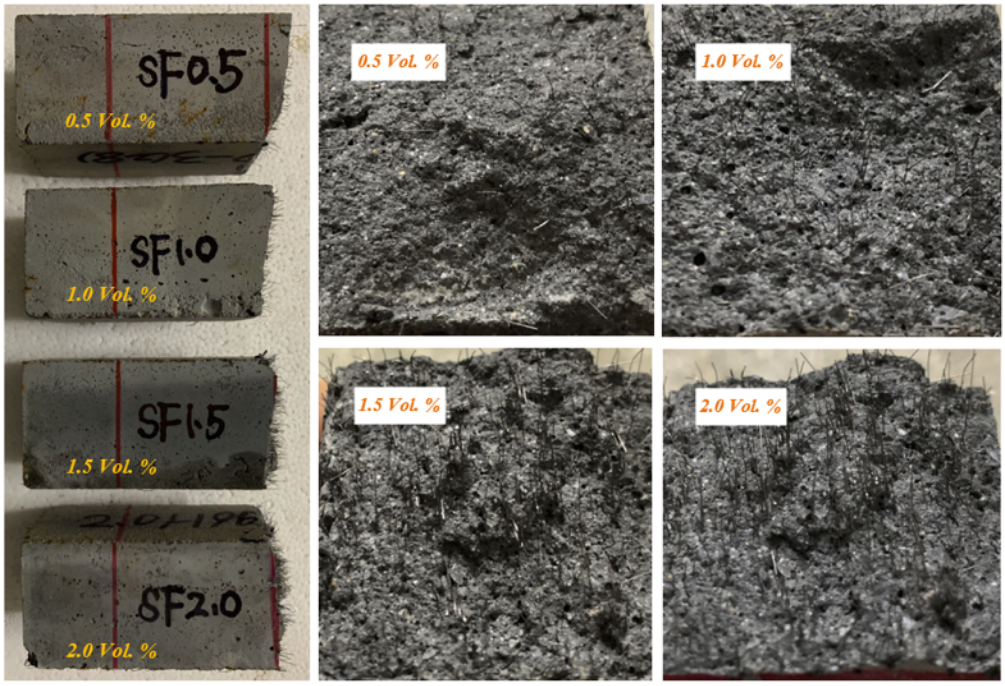

Fig. 4.18. Fibre distribution within the fracture surface of 0.5-2.0% FR-DUHPC samples after bending tests.

4.5 Multivariate regression analysis

From the aforementioned analysis in Sections 4.4.1-4.4.3, the length and dosage of steel fibres as well as the curing age were the leading factors influencing the properties of FR-DUHPC. To further explore the functional relationships between the influencing factors and strength behaviour, this section introduces a multiple regression analysis method frequently used in the statistical analysis, which can establish linear/nonlinear mathematical correlations between multiple variables via taking the single variable as a response dependent variable (RDV) and other variables as independent variables (IVs). The conventional multivariate linear

functional relationship can be expressed as follows:

$$Y_i = \alpha + \beta_1 \cdot X_1 + \beta_2 \cdot X_2 + \cdots + \beta_k \cdot X_k,\ i = 1, \cdots, n,\ \textit{linear model 1} \quad (4.1)$$

where α and β are regression constants, X_k is the IV corresponding to the steel fibre length and dosage as well as the curing age (k = 3), and Y_i is the RDV corresponding to the compressive, flexural and split-tensile strengths in this study (n = 3). The values of the foregoing IVs are, respectively, 6, 10 and 13 (length), 0.005,0.01, 0.015 and 0.02 (dosage), and 1, 7 and 28 (age). Moreover, for the purpose of achieving a more accurate regressive functional results, Jin et al. [162, 163] also took the natural logarithm of the above conventional linear function or introduced mixed IVs, and the following nonlinear and mixed model relationships expressed in multivariate linear formats were proposed:

$$\ln(Y_i) = \alpha + \beta_1 \cdot X_1 + \cdots + \beta_k \cdot X_k,\ i = 1, \cdots, n,\ \textit{nonlinear model 2} \quad (4.2)$$

$$\ln(Y_i) = \alpha + \beta_1 \cdot \ln(X_1) + \cdots + \beta_k \cdot \ln(X_k),\ i = 1, \cdots, n,\ \textit{nonlinear model 3} \quad (4.3)$$

$$X_{ik}/Y_i = \alpha + \sum_{j=1}^{k} \beta_j \cdot X_{ij},\ i = 1, \cdots, n,\ j = 1, \cdots, k,\ \textit{mixed models from 4 to (k + 3)} \quad (4.4)$$

$$\ln(X_{ik})/Y_i = \alpha + \sum_{j=1}^{k} \beta_j \cdot \ln(X_{ij}),\ i = 1, \cdots, n,\ j = 1, \cdots, k,\ \textit{mixed models from (k + 4) to (2k + 3)} \quad (4.5)$$

As indicated in Eqs. (4.1)-(4.5), a total of 9 multivariate regression models were presented for each RDV, including 1 linear model, 2 nonlinear models and 6 mixed models. It is well known that the accuracy of regression results improves with the number of sample data and in order to ensure their accuracy, generally the number of the sample data should be no less than 36. Therefore, this section

only performs multivariate regression analysis on the strength behaviour of mono FR-DUHPC with the assistance of the SPSS statistical software to carry out the variance and residual analysis for each model and test the significance of each influencing factor. The detailed regression results of RDVs related to compressive, flexural and split-tensile strength are listed in Table 4.6, where R^2 is the goodness of fit, D-W value is the Durbin-Watson statistical result utilized to diagnose the autocorrelation of model residual deviations (the optimal range is 1.5-2.5 and preferably close to 2.0), and X_L, X_C and X_A are the abbreviations of IVs of the length and dosage of steel fibres and the curing age, respectively.

Table 4.6

Regression results of strength behaviour for mono FR-DUHPC.

Models		f_c - related			f_r - related			f_{ts} - related		
(No.)		RDV	R^2	D-W	RDV	R^2	D-W	RDV	R^2	D-W
Linear	1	f_c	0.927	1.712	f_r	0.937	1.559	f_{ts}	0.946	1.168
Non-linear	2	$\ln(f_c)$	0.932	1.693	$\ln(f_r)$	0.933	1.466	$\ln(f_{ts})$	0.946	0.802
	3	$\ln(f_c)$	0.943	2.133	$\ln(f_r)$	0.975	2.594	$\ln(f_{ts})$	0.963	2.174
Mixed	4	X_L/f_c	0.940	1.270	X_L/f_r	0.879	1.428	X_L/f_{ts}	0.961	0.699
	5	X_C/f_c	0.969	1.827	X_C/f_r	0.930	1.384	X_C/f_{ts}	0.961	1.530
	6	X_A/f_c	0.979	1.420	X_A/f_r	0.890	1.430	X_A/f_{ts}	0.973	1.246
	7	$\ln(X_L)/f_c$	0.931	1.717	$\ln(X_L)/f_r$	0.959	1.959	$\ln(X_L)/f_{ts}$	0.974	1.896
	8	$\ln(X_C)/f_c$	0.982	2.201	$\ln(X_C)/f_r$	0.945	1.638	$\ln(X_C)/f_{ts}$	0.976	1.431
	9	$\ln(X_A)/f_c$	0.976	1.165	$\ln(X_A)/f_r$	0.896	1.195	$\ln(X_A)/f_{ts}$	0.967	0.892

As indicated in Table 4.6, the overwhelming majority of the nonlinear and mixed multivariate regression models illustrated comparable or better fitting than the

linear model, although the R^2 of the linear one for all RDVs had been greater than 0.9. The largest R^2 values of regression models corresponding to compressive, flexural and split-tensile strengths were 0.982, 0.975 and 0.976. After considering the optimum D-W value range reported above, the best-fit multivariate regression models in predicting the above three strength behaviour were identified as the mixed models 8, 7 and 7, respectively, and the expressions are as follows:

$$\ln(X_C)/f_c = 0.029 + 0.006\cdot\ln(X_L) + 0.019\cdot\ln(X_C) + 0.002\cdot\ln(X_A), \text{ model 8} \quad (4.6)$$

$$\ln(X_L)/f_r = -0.129 + 0.001\cdot\ln(X_L) - 0.053\cdot\ln(X_C) - 0.009\cdot\ln(X_A), \text{ model 7} \quad (4.7)$$

$$\ln(X_L)/f_{ts} = -0.135 + 0.058\cdot\ln(X_L) - 0.069\cdot\ln(X_C) - 0.021\cdot\ln(X_A), \text{ model 7} \quad (4.8)$$

The R^2 and D-W values of the presented three expressions were, respectively, 0.982 and 2.201, 0.959 and 1.959, and 0.974 and 1.896. Fig. 4.19 also shows the histogram and cumulative probability of the standardized residuals of these best-fit regression models. As can be observed that the standardized residuals of compressive, flexural and split-tensile strength-related RDVs basically obeyed the normal distribution, and the zero residual values all demonstrated the highest frequency. Besides, by contrasting the cumulative probability distribution between sample observations and theoretical normal hypothesis, as shown in Fig. 4.19(b, d and f), all residuals of RDVs-related models were basically evenly distributed on both sides of the 45-degree diagonal of the graph, which demonstrated the tenability of the normal distribution hypothesis of sample residuals.

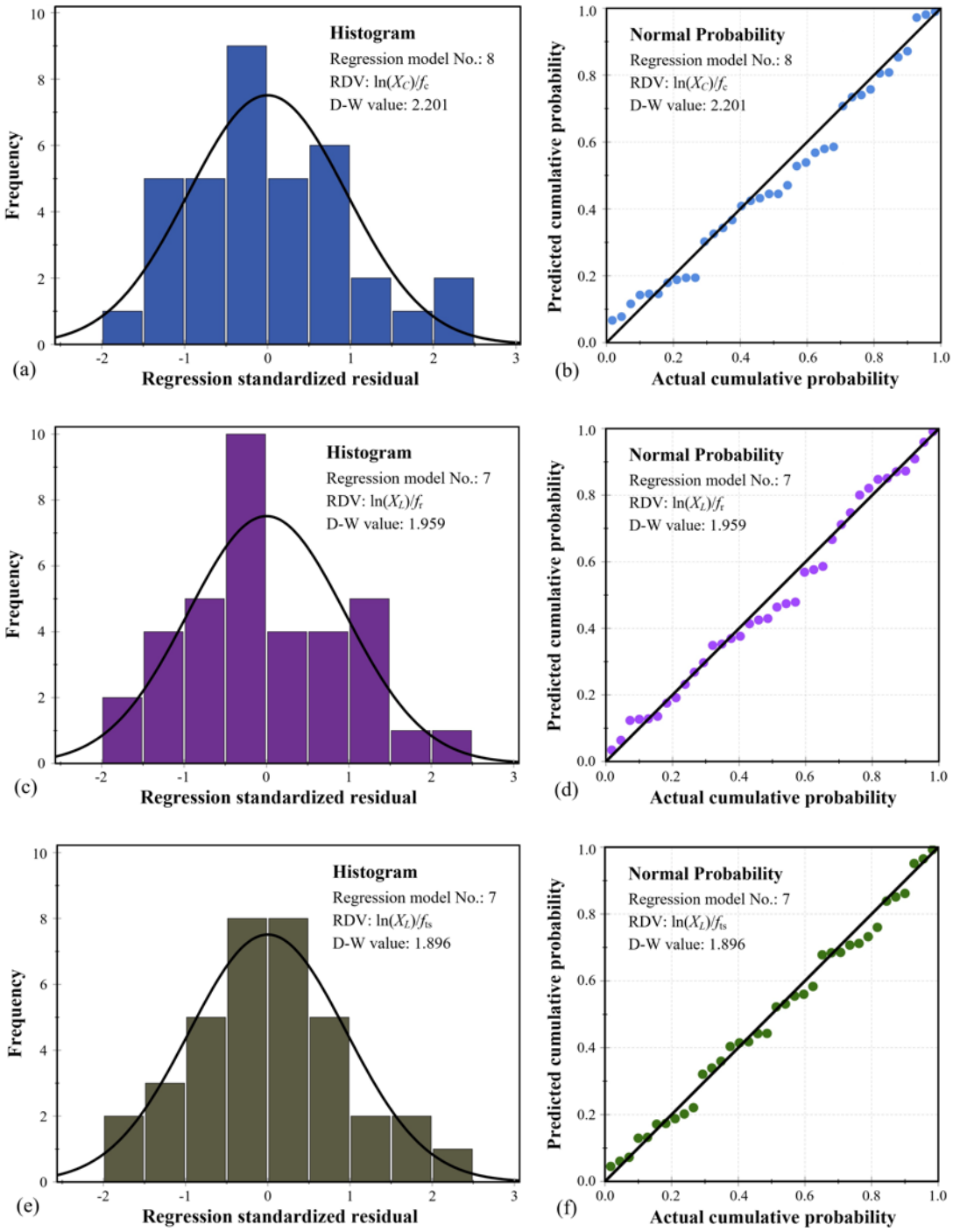

Fig. 4.19. Standardized residual and normal probability of (a-b) compressive, (c-d) flexural and (e-f) split-tensile strengths related using best-fit models.

In addition to the normal distribution test for the standardized residuals of the regression models, it is also necessary to test the model's overall significance and the impact degree of various influencing IVs. Table 4.7 illustrates the typical

results of ANOVA and the impact of the individual factor (fibre length, dosage and curing age) on the strength behaviour of FR-DUHPC based on Model 1 (linear regression). As can be observed that the F value of Model 1 for various strengths was larger than $F_{0.05}$ of 2.901 and $F_{0.01}$ of 4.459, manifesting that the regressive model was overall significant and the multivariate regression relationship existed between the evaluated RDVs and the selected IVs. Additionally, by examining the impact of each individual factor on target RDVs, i.e., the T-test, all IVs showed a significantly positive influence on compressive, flexural and split-tensile strengths by virtue of the corresponding P values were less than 0.05. Meanwhile, the steel fibre dosage with higher T values was found with a more significant impact on all strengths than the other two factors.

Table 4.7

ANOVA and individual influencing factor results based on Model 1.

RDVs	f_c			f_r			f_{ts}		
Factors	F value	T value	P value	F	T	P	F	T	P
ANOVA	135.52	---	---	158.94	---	---	186.10	---	---
Length	---	7.41	0.00	---	9.97	0.00	---	9.70	0.00
Dosage	---	16.73	0.00	---	17.66	0.00	---	17.11	0.00
Age	---	8.47	0.00	---	8.10	0.00	---	13.09	0.00

Considering the accuracy of the multivariate regression results improved with the number of data and Jin et al. [163] likewise pointed out that the mutual internal correlations might be existed among the multiple IVs, the impact of experimental

compressive strength as an IV introduced into multivariate regression analysis was hence evaluated. Table 4.8 detailly presented the updated regression results of flexural and split-tensile strength related RDVs, where X_{fc} is the abbreviation of the IV of compressive strength.

Table 4.8

Regression results of flexural tensile strength for mono FR-DUHPC (considering X_{fc}).

Models		f_r - related			f_{ts} - related		
(No.)		RDV	R^2	D-W	RDV	R^2	D-W
Linear	1#	f_r	0.977	1.703	f_{ts}	0.965	1.243
Non-linear	2#	$\ln(f_r)$	0.946	1.491	$\ln(f_{ts})$	0.956	0.776
	3#	$\ln(f_r)$	0.976	2.363	$\ln(f_{ts})$	0.976	1.744
Mixed	4#	X_L/f_r	0.916	1.886	X_L/f_{ts}	0.981	1.192
	5#	X_C/f_r	0.963	1.260	X_C/f_{ts}	0.969	1.701
	6#	X_A/f_r	0.890	1.419	X_A/f_{ts}	0.973	1.200
	7#	X_{fc}/f_r	0.813	1.557	X_{fc}/f_{ts}	0.592	1.081
	8#	$\ln(X_L)/f_r$	0.969	1.956	$\ln(X_L)/f_{ts}$	0.981	1.761
	9#	$\ln(X_C)/f_r$	0.956	1.981	$\ln(X_C)/f_{ts}$	0.976	1.562
	10#	$\ln(X_A)/f_r$	0.901	1.155	$\ln(X_A)/f_{ts}$	0.967	0.893
	11#	$\ln(X_{fc})/f_r$	0.957	2.060	$\ln(X_{fc})/f_{ts}$	0.958	1.640

It can be observed that the total number of the mixed model was increased from 6 to 8 due to the introduction of the foregoing X_{fc}. Compared with the R^2 values of the original regression models exhibited in Table 4.6, the updated regression models exhibited a better fitting effect. For the flexural and split-tensile strength indexes, the most evident enhancement in R^2 value were found to linear Model 1

and nonlinear Model 4, which were increased from 0.937, 0.879 (flexure) and 0.946, 0.961 (split-tension) to 0.977, 0.916 (flexure) and 0.965, 0.981 (split-tension), respectively. After comprehensively considering the degree of fitting and the ideal range of D-W values, the best-fit multiple regression models in predicting the foregoing strength behaviour were all identified as the mixed model 8#. The updated best-fit models exhibited below had the identical RDV formats as the original regression model 7, with the consideration of the compressive strength effect as an additional IV. Fig. 4.20 intuitively shows the comparisons between the experimental and predicted RDV values related to flexural and split-tensile strength via utilizing Model 7 and Model 8#. It could be observed that Model 8# outperformed Model 7 in predicting the flexural and split-tensile strength values under different IV conditions. The points of the contrast between the predicted and measured values were more closely spread out on both sides of the diagonal of the graph with higher R^2 values. Therefore, the proposed multiple regression equations (4.9) and (4.10) considering the effects of steel fibre length (6-13 mm), dosage (0.5-2.0%), curing age (1-28-day) and concrete compressive strength could be reliably utilized to estimate the flexural and split-tensile strength of mono steel FR-DUHPC within a given range of each IV. This was an effective method for predicting the flexural tensile performance of DUHPC structures/units that were mainly subjected to flexural tensile loads during the serviceability.

$$\ln(X_L)/f_r = -0.120 + 0.001\cdot\ln(X_L) - 0.048\cdot\ln(X_C) - 0.006\cdot\ln(X_A) - 0.002\cdot\ln(X_{fc}), \text{ model } 8^{\#} \quad (4.9)$$

$$\ln(X_L)/f_{ts} = 0.431 + 0.076\cdot\ln(X_L) - 0.042\cdot\ln(X_C) - 0.015\cdot\ln(X_A) - 0.104\cdot\ln(X_{fc}),\ \text{model } 8^{\#} \quad (4.10)$$

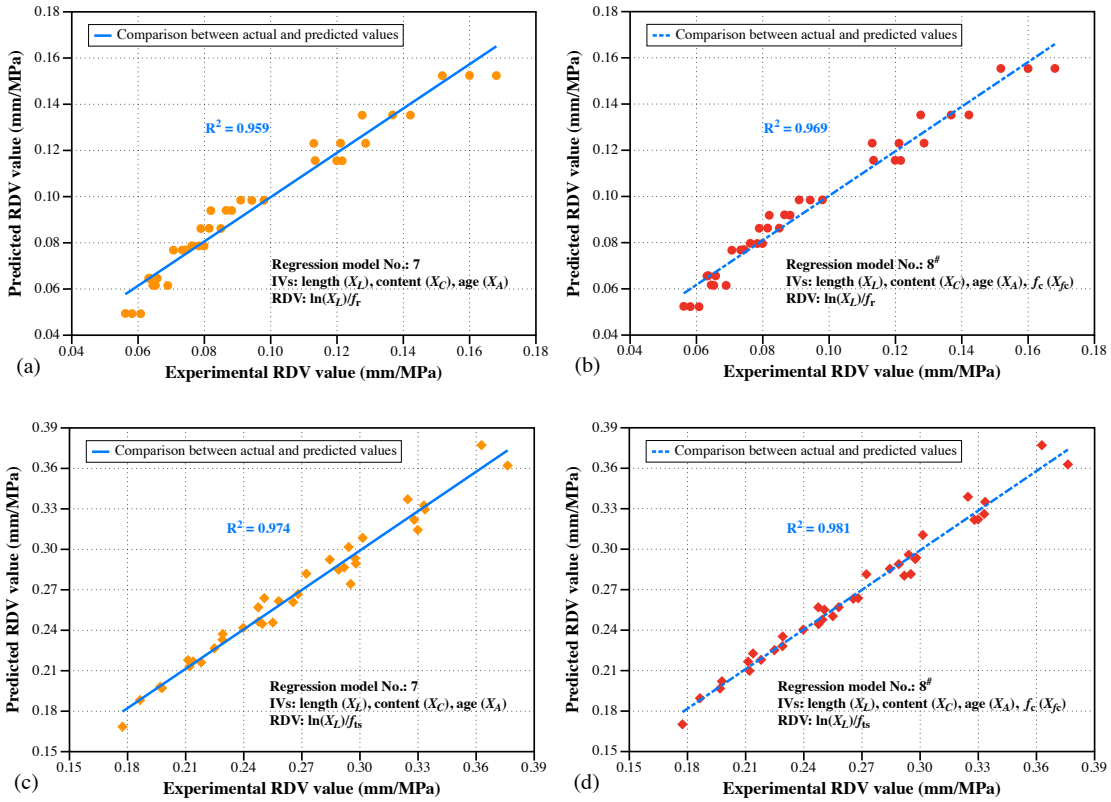

Fig. 4.20. Comparisons between the experimental and predicted results of (a-b) flexural and (c-d) split-tensile strengths related using Model 7 and Model 8#.

4.6 Conclusion

In this chapter, the static mechanical properties of DUHPC with mono and hybrid steel fibre reinforcements were experimentally studied. Then, the multivariate regression analysis was carried out on mono steel FR-DUHPC cases to explore the functional relationships between the influencing factors (steel fibre length, volume dosage and curing age) and the above strength behaviour. Based on the analysis and discussion presented above, the main findings can be obtained as follows:

1) Compared with reference samples without fibre reinforcement, the single incorporation of any length of straight steel fibres enhanced the compressive strength, total energy absorption, toughness and elastic modulus of DUHPC. Under the same fibre dosage, longer fibres exhibited better strengthening and toughening effect. In the case of fibre hybridization, the use of shorter fibres replacing partial initial-sized ones decreased the compressive strength, but F05M10L, F10M05L and F05SML samples exhibited better energy absorption ability and toughness. The relationship between the compressive strength and elastic modulus (28-day age) followed the logarithmic distribution developed in Chapter 3.
2) The variations in flexural and split-tensile strengths of DUHPC with mono fibre reinforcement indicated a similar uptrend to those of the compressive strength, but the improvement was more significant when the fibre length added from 6 to 10 and 13 mm. Therefore, the pronounced attenuation in flexural strength occurred in hybrid cases in which longer fibres were partially substituted by shorter ones at all ages. Additionally, the flexural cracking strength, deflection-hardening behaviour and flexural toughness were all improved remarkably with fibre dosage, and the longer ones exhibited more positive enhancement effect. Similarly, the replacement of longer steel fibres with more 6-mm ones evidently diminished the flexural toughness and energy absorption capacity of DUHPC after cracking.
3) After comprehensively considering the applications and preparation methods

of the developed DUHPC, as well as the impact of the distribution, dosage, length and mixing method of steel fibres on its mechanical performance, the mixtures with hybrid medium and long steel fibres as well as with hybrid short, medium and long ones were suggested to be used in the practical application of DUHPC structures/units. Moreover, the length of steel fibres incorporated was not recommended to exceed 13 mm in view of the easy agglomeration of longer steel fibres and the lower moisture content of DUHPC.

4) The proposed multivariate regression linear, nonlinear and most of the mixed models could well estimate the compressive, flexural and split-tensile strength of mono FR-DUHPC at a given range of steel fibre length (6-13 mm), volume dosage (0.5-2.0%) and curing age (1 day-28 days) with R^2 larger than 0.9 and D-W values close to 2.0. All the factors demonstrated a significantly positive impact on the foregoing strength behaviour. After the compressive strength was introduced into multivariate regression analysis as an additional IV, the updated best-fit models outperformed the original regression models in the prediction accuracy of both flexural and split-tensile properties.

Chapter 5

Mechanical Behaviour and Environmental Benefit of Eco-Friendly Steel FR-DUHPC Containing HVFA and Crumb Rubber

5.1 Introduction

The rapid development in industrialization and modernization has driven the economy forward, but the industrial and domestic wastes have also increased in large quantities, rendering environmental preservation an important challenge for modern human beings. Incorporating these wastes/by-products as renewable materials into concrete mixtures has been manifested to not only improve some properties of fresh/hardened concrete, but also achieve the strategic target of sustainable development [164-166].

FA, as a waste by-product of the high-temperature coal combustion in industrial production, is currently a major SCM to substitute partial cement introduced in concrete mixes. The use of FA can greatly reduce the adiabatic temperature rising of fresh concrete, increase the volume content of the slurry inside the mixture and effectively improve the interfacial behaviour between slurries and aggregate [133, 167]. Waste crumb rubber (CR), mainly derived from the aging and abrasion of rubber products, is an internationally recognized industrial solid black pollution. Acting as a high molecular polymer material, its chemical property is stable and thus difficult to degrade in the natural environment. The disposal of landfill and stockpiles adopted will not only occupy a large amount of land resources, but also affect the growth of vegetation, causing the irreversible effects on human health

and ecological system. Fortunately, the use of waste CR as a concrete aggregate can effectively mitigate the aforementioned severe environmental hazards while also imparting beneficial properties to the concrete, including increased flexibility, enhanced energy absorption ability and improved crack resistance [116, 165].

Rao et al. [39] studied the strength and abrasion resistance of RCC with partial cement being replaced by HVFA. The findings indicated that the utilization of FA with substitution ratios ranging 0-60% reduced the compressive/flexural strengths up to 90 days. The decrease in compressive strength also led to a degradation of abrasion resistance, both due to the poor early-age reactivity of FA introduced. Similar strength developments were also observed by Aghabaglou et al. [99], but meanwhile they found that all the strength values of RCC increased evidently when FA replaced partial aggregate, which was due to the increased amount of cementing slurries. Adamu et al. [18] studied the mechanical property, abrasion and impact resistance of RCC with inclusion of HVFA, CR aggregate and nano-silica. They concluded that the HVFA RCC exhibited decreased fresh density, degraded strength and abrasion/impact resistance compared with the control case, and the addition of CR substituting partial sand further escalated the above detriments. However, the nano-silica added could mitigate these adverse impacts by virtue of igniting the early reactivity of FA and densifying the ITZs between the matrix and rubber crumbs. Moreover, nano-silica also played a significant role in mitigating the severe degradation of RCC shrinkage, creep and fatigue behaviour caused by HVFA and CR incorporated [62, 63]. In addition to nano-silica, Fakhri et al. [36] introduced a certain amount of silica fume into rubberized RCC mixtures

and obtained the result of slightly enhanced compressive strength of RCC with 20% substitution of fine aggregate by waste rubber particles, and Kolase et al. [82] observed that the use of PP fibres could increase the flexural/tensile strength, fatigue life and collapsible load of RCC slabs with FA substitution up to 45%.

As reviewed above, researchers have carried out some experimental studies to weaken the adverse impact on the mechanical properties of dry concrete caused by the addition of HVFA and rubber crumbs. However, the strength behaviour of the upgraded concrete, especially the early age properties, is still not desirable, which is a major hurdle in the adaptation, popularization and expansion of the practical applications of such concrete material. The current chapter is aimed at investigating the mechanical performance and environmental benefit of steel FR-DUHPC with inclusions of HVFA and waste CR, based on the sustainable FR-DUHPC developed in Chapter 3. The research demonstrates the feasibility of future use of HVFA and CR in DUHPC/DHPC (dry high performance concrete) structures (RCCP and RCCD) and units (DCC roof tiles, sewer pipes and load-bearing piles). In the case of satisfying the strength and service requirements, the detrimental impact of the solid wastes can be effectively alleviated, leading towards eco-friendly construction as well as sustainable environment.

5.2 Experimental programme

5.2.1 Raw materials

In this experimental investigation, Portland cement, silica fume, GGBS, FA, silica sand, CR, steel fibre, superplasticizer and water were used for the preparation of

FR-DUHPC mixes. The cement used complied with Chinese national standard GB175-2020 [168] with specific surface area of 315 m^2/kg and initial/final setting times of 50/320 min. The use of silica fume, FA and GGBS as a partial substitute for cement could improve the properties of concrete by virtue of their compound pozzolanic effect [110, 129]. The main chemical compositions of these cementing materials are indicated in Table 5.1. What needs extra illustration here is that the FA characterized with micro-spherical appearance can improve the workability of fresh concrete, and silica fume with high reactivity can provide an early-strength benefit, which are all conductive to DUHPC with lower moisture content and high early-strength requirements. As for CR aggregates, 20-80-mesh rubber particles obtained by shredding waste tyres were utilized to substitute partial natural silica sand (composed of coarse, medium and fine sand) with aggregate sizes ranging 0.15-1.18 mm (20-70 mesh). The physical characteristics of rubber particles are listed in Table 5.2. Anti-rusty copper-coated straight steel fibres with a length of 10 mm, an aspect ratio of 83.3 mm and tensile strength of more than 4 GPa were used to improve the mechanical properties of DUHPC mixing with HVFA and CR aggregate. In terms of superplasticizer, it was a common additive preparing HPC or UHPC aimed to reduce the viscosity of concrete mixtures, and was particularly important for the studied DUHPC with lower moisture content and the addition of steel fibres. The appearances of silica fume, FA, GGBS, CR and steel fibres are exhibited in Fig. 5.1.

Table 5.1

Main chemical compositions of cementitious materials for FR-DUHPC.

Components (wt, %)	Cement	Silica fume	FA	GGBS
Aluminium oxide (Al_2O_3)	3.15	0.69	29.09	21.71
Silicon dioxide (SiO_2)	20.42	93.91	53.36	34.43
Calcium oxide (CaO)	68.09	1.85	8.27	33.16
Ferric oxide (Fe_2O_3)	4.46	0.56	3.49	2.65
Magnesium oxide (MgO)	2.16	0.64	1.37	5.66
Sulphur trioxide (SO_3)	1.13	<0.01	0.99	0.58
Loss on ignition (LOI)	0.52	0.30	2.48	1.01

Table 5.2

Physical characteristics and composition of CR aggregate.

Properties	Specific gravity	Bulk density (kg/m^3)	Screenings (%)	Moisture content (%)	Metal content (%)
Value	0.61	314	0.014	< 0.5	0.029

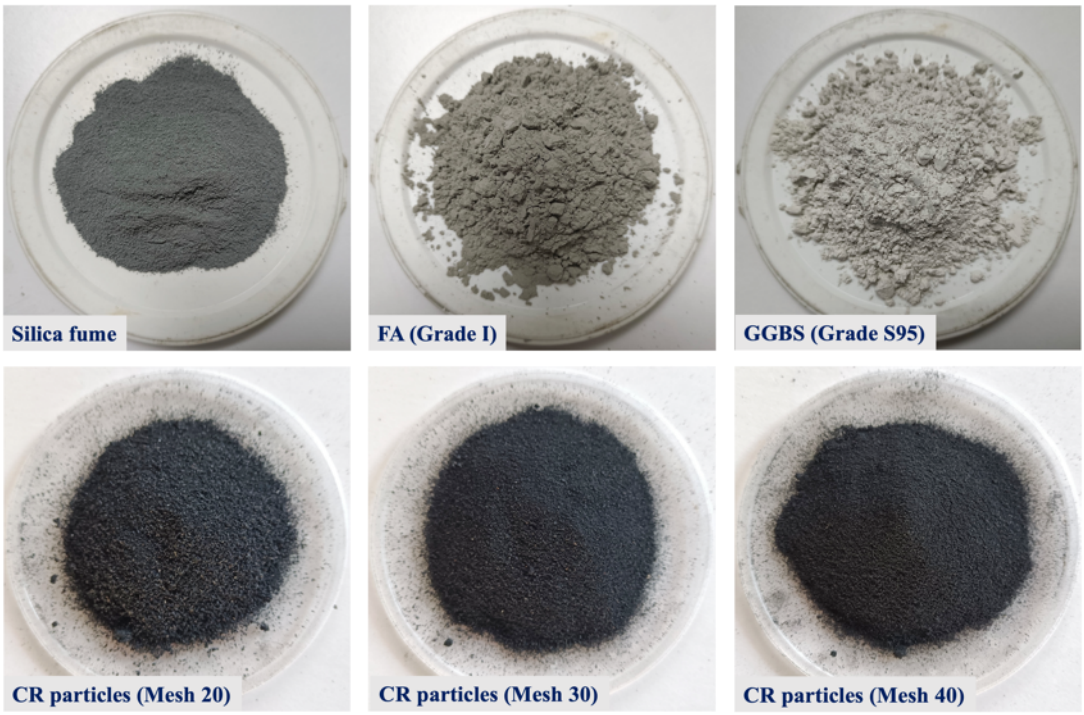

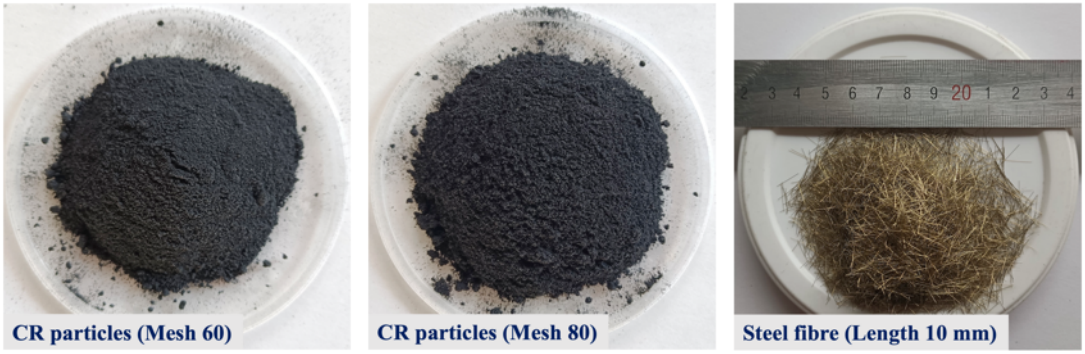

Fig. 5.1. Appearance of silica fume, FA, GGBS, CR particles and steel fibres.

5.2.2 Mix proportions

A summary of mix proportions for the studied FR-DUHPC is shown in Table 5.3. The contents of FA and CR particles were considered as the major variables to assess their impacts on FR-DUHPC properties as partial substitutes for cement and silica sand, respectively. In the group of D-FA mixtures, the inclusion of FA included five grades of cement mass substitution, respectively, were 20%, 30%, 40%, 50% and 60%. The incorporation of 20% FA as well as other constituent materials (the content was set to a fixed value) followed the mixing ratios and the optimal steel fibre dosage obtained in Chapter 3. The weight variations in the ratio of these materials to the cement were caused by the gradual decrease in cement consumption. In the group of D-R mixtures, the mixing amount of FA remained constant. Due to the addition of FA, which involved mass substitution of cement, the incorporation of CR also entailed mass replacement of silica sand, resulting in three distinct cases: 100% of coarse sand (D-RC10, accounted for 10% of the total mass of silica sand), 100% of coarse and 40% of medium sand (D-RCM25, accounted for 25% of total silica sand), and 100% of coarse and 70% of medium

sand (D-RCM35, accounted for 35% of total sand). It should be pointed out that since the use of CR to replace 100% of medium sand (accounted for 35% of total sand) as well as fine sand (accounted for 55% of total sand) would lead to obvious matrix defects in FR-DUHPC samples, the medium sand was partially substituted in this study and the mixing ratio of fine sand was not listed in the table. In addition, steel fibres with dosages of 0.5-1.5% were added to D-R mixes to evaluate their reinforcement effect.

Table 5.3

Mixture proportions of eco-friendly FR-DUHPC by weight.

Group	Sample	Cement	SLF	FA	GGBS	Silica sand		CR		Water	Fibre
						CSS	MSS	CCR	MCR		(Vol-%)
D-FA	D-FA20	1.00	0.15	0.31	0.08	0.25	0.92	--	--	0.25	1.5
	D-FA30	1.00	0.18	0.55	0.09	0.30	1.09	--	--	0.29	1.5
	D-FA40	1.00	0.22	0.89	0.11	0.36	1.33	--	--	0.36	1.5
	D-FA50	1.00	0.29	1.43	0.14	0.47	1.71	--	--	0.46	1.5
	D-FA60	1.00	0.40	2.40	0.20	0.65	2.40	--	--	0.65	1.5
D-R	D-RC10	1.00	0.29	1.43	0.14	0.00	1.71	0.47	0.00	0.46	0.5-1.5
	D-RCM25	1.00	0.29	1.43	0.14	0.00	1.01	0.47	0.70	0.46	0.5-1.5
	D-RCM35	1.00	0.29	1.43	0.14	0.00	0.54	0.47	1.17	0.46	0.5-1.5

Note: “SLF” denotes silica fume; “CSS” and “MSS” denote coarse and medium silica sand, respectively; “CCR” and “MCR” denote coarse and medium crumb rubber, respectively; and “Vol-%” denotes volume fraction.

5.2.3 Preparation and curing regime

The step by step preparation procedures and curing method of the studied FR-DUHPC were basically the same as those introduced in Chapter 3. During the preparation, all the powdery cementing materials as well as aggregates (including CR aggregate for D-FA-R mixtures) were firstly dry mixed in a concrete mixer for about 3 mins, followed by 4 mins of introducing steel fibres with small increments to prevent the fibre accumulation or agglomeration. Then, water with pre-blended superplasticizer was added to dry ingredient whilst mixing simultaneously. The duration of the wet stirring upon water addition was controlled at 6-8 mins, and the whole mixing was completed when a satisfactory mixture consistency was observed and the fibres were evenly distributed. Once the mixing was completed, three cubic and three beam samples were cast layer by layer by using a vibrated-compaction method, in which a vibrating table was under the variform moulds and a surcharge was placed on the surface of the fresh mixture. It was noteworthy that prior to the batch casting of D-FA-R mixtures, trial and error methods were used to determine the optimum vibration time considering different CR contents. It should be noted that the shaking table should keep a low frequency and the duration could be shortened appropriately to minimize the tendency of the uneven distribution of the matrix aggregate structure caused by the floating of lightweight rubber particles to the top of the compaction layer. Upon vibrated-compaction, all the D-FA and D-FA-R mixtures were covered with plastic film for 3 h to obtain the initial strength, followed by moist/steam cured in an insulated water tank at a

temperature of 50 ℃ for the first day. The samples were then demoulded and left to cool before further cured in normal-temperature water until the testing ages. Fig. 5.2 exhibits the typical FR-DUHPC samples during the curing and the cases of severe initial defects in concrete matrix due to excessive CR addition reported in Section 5.2.2. Finally, a total of 336 FR-DUHPC with 120 HVFA and 216 CR samples were prepared and cured for the assessment of density and mechanical properties at various ages.

Fig. 5.2. Water curing and typical FR-DUHPC samples containing CR aggregate.

5.2.4 Test setup

To study the hardening behaviour of the eco-friendly FR-DUHPC, two mechanical tests after 1, 7, 28 and 60-day curing were performed as per Chinese standards GBT50081-2019 [148] and CECS13-89 [149]. For compression behaviour of the studied concrete including the compressive strength, contributions of pozzolanic effect, stress-strain relationship and MOE, cubic samples of dimensions 40 mm × 40 mm × 40 mm were tested through using a servo-hydraulic test machine with a 500 kN capacity. During each test, the compression load was applied vertically to the compaction surface of concrete samples at a constant rate of 0.2 mm/min,

and was finally terminated when the residual bearing capacity was approximately 10% of the peak load. In terms of the flexural performance including the flexural strength, contributions of pozzolanic effect, load-displacement relationship and deflection hardening, beam samples of sizes 40 mm × 40 mm × 160 mm were tested via using a universal test machine with a 100 kN capacity. Similar to the compression test, a displacement-controlled load was applied vertically to the outermost compaction surface of the prismatic sample at a rate of 0.05 mm/min and would terminate when either the midspan displacement reached 5 mm or the bending capacity reduced to 10% of the peak load. Fig. 5.3 exhibits the setup of uniaxial compression and four-point bending tests. Two symmetrically arranged laser LVDTs were fixed on the support pad on both sides of cubic and prismatic samples to record and transmit the axial displacement and midspan deflection in real time. In addition, strain gages affixing to the bottom tension area of the prism samples were employed to measure the flexural cracking strength of the studied concrete. Once the strain gages ruptured in tension due to the initial crack of test samples, the corresponding cracking load was recorded and saved via National Instruments (NI, cDAQ-9189) measurement system.

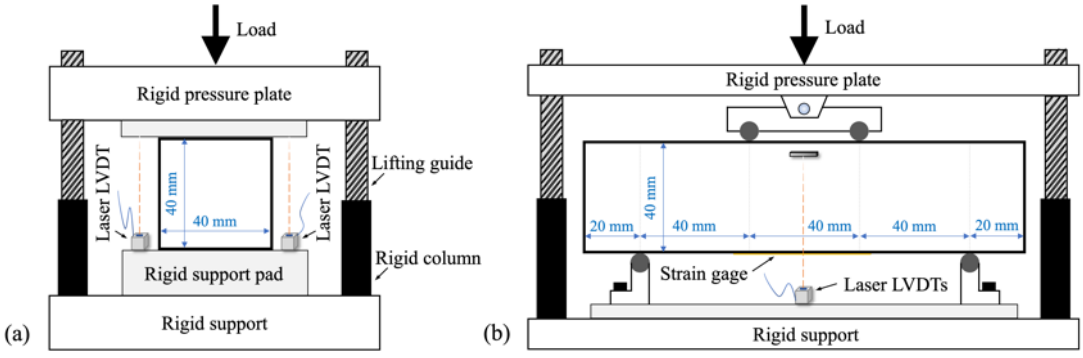

Fig. 5.3. Schematics of (a) uniaxial compression and (b) four-point bending test.

To further study the microstructure morphology of hardened D-FA-R mixtures, Scanning Electron Microscopy (SEM) technology was employed via using JSM-7800F Field Emission Scanning Electron Microscope. The SEM thin pieces of sizes 10 mm × 10 mm × 5 mm were collected from the undamaged FR-DUHPC samples after the compression test at 60 days. The surface of the thin pieces was first polished using grit papers of grades 300-1000 μm. Then, the pieces were placed into ETD-2000 vacuum instrument for drying and its surface was sputtered with a gold coating to increase the pieces' conductivity during the observation.

5.3 Results and discussion

5.3.1 FR-DUHPC incorporating HVFA

Table 5.4 exhibits the average density and strength values (respectively achieved from six and three identical samples) of FR-DUHPC samples incorporating HVFA at four ages, in which f_c and f_r are, respectively, the uniaxial compressive and flexural strength in the unit of MPa.

Table 5.4

Density and mechanical test results of FR-DUHPC incorporating HVFA.

Sample	Density (kg/m^3)				f_c (MPa)				f_r (MPa)			
	1-d	7-d	28-d	60-d	1-d	7-d	28-d	60-d	1-d	7-d	28-d	60-d
D-FA20	2417	2421	2429	2413	120.6	126.8	134.0	142.1	26.3	29.6	33.2	37.3
D-FA30	2382	2393	2397	2372	106.6	115.2	125.1	136.6	24.2	27.6	31.4	36.3
D-FA40	2321	2332	2347	2363	92.0	102.3	115.8	131.4	21.4	25.1	29.6	35.1
D-FA50	2306	2310	2298	2328	76.7	87.7	106.6	126.7	18.0	22.0	27.7	34.2
D-FA60	2278	2299	2275	2295	56.8	69.5	94.7	110.1	13.3	17.7	24.8	29.9

5.3.1.1 Density

The variations in density of FR-DUHPC samples with partial cement substituted by FA are presented in Fig. 5.4. The density was obtained when the concrete sample was in the saturated surface dry state prior to the mechanical tests, and was the average of six samples to be tested in compression and bending. It could be found that the curing age exhibited a marginal impact on FR-DUHPC density under the same FA content, but the density tended to decrease with FA addition, which was manifested in that the average density diminished from 2420 to 2287 kg/m^3 as the FA content gradually increased to 60%. Generally, the inclusion of FA would increase the volume content of cementing paste inside the mixture and improve the workability of fresh concrete. However, the lower FA specific gravity reduced the mass of the mixture per unit volume after cement was substituted by equivalent weight, and thus causing a certain decrease in the density of hardened FR-DUHPC. Additionally, during the vibrated compaction, the fresh mixture with higher FA additions was observed to be susceptible to bulging, resulting in poor concrete compactness and a reduction in density.

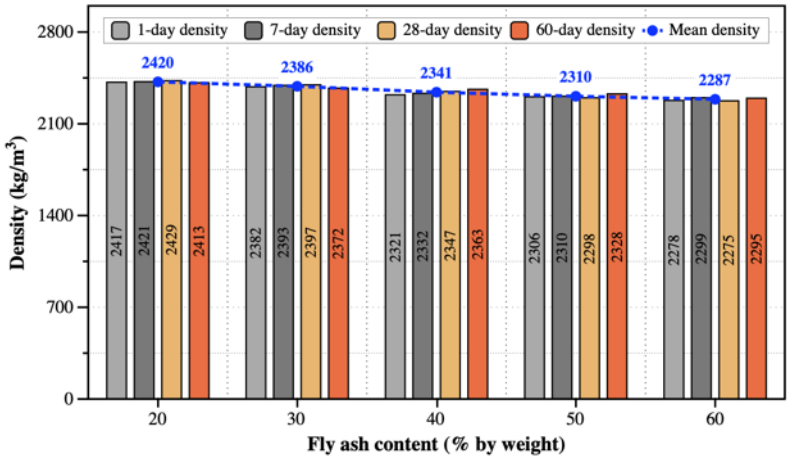

Fig. 5.4. Effect of FA substitution level on hardened density of FR-DUHPC.

5.3.1.2 Compressive performance

The compression test results of FR-DUHPC samples with various FA additions at four curing ages are exhibited in Fig. 5.5. The columns represented the mean strength values obtained from three samples of the identical mixture. As could be observed that the compressive strength of FR-DUHPC enhanced gradually with curing age, but reduced evidently with FA substitution level for cement, especially for samples with more addition of FA at earlier ages. For instance, the 1- and 7-day strength values of samples with 20% FA content were, respectively, 120.6 and 126.8 MPa, whereas those of the samples with 50% and 60% FA contents, respectively, diminished to 76.7 and 87.7 MPa (decreased by 36.5% and 30.8%), as well as 56.8 and 69.5 MPa (decreased by 52.9% and 45.2%). The reason was that the rate of cement hydration and the number of hydration products, which dominated the early strength of FR-DUHPC mixtures, were gradually retarded and reduced with the increase in FA substitution for cement, while the secondary hydration of FA lagged behind could not timely compensate the strength loss caused by the reduction of cement addition [123, 167]. Moreover, compared to self-compacting concrete, the lower cement content of dry concrete mixture by nature was another non-negligible factor that caused an evident diminishment in early compressive strength under higher FA additions. However, these samples showed faster kinematics of strength development in the middle and later periods owing to the gradually-activated FA pozzolanic reaction, indicated by the blue line of strength increment in the figure, which effectively alleviated the early strength

loss. Compared with the reductions of 36.5% and 30.8% as well as 52.9% and 45.2% at earlier ages obtained above, the compressive strengths of the identical samples at 60 days were only decreased by 10.8% and 22.5%, respectively.

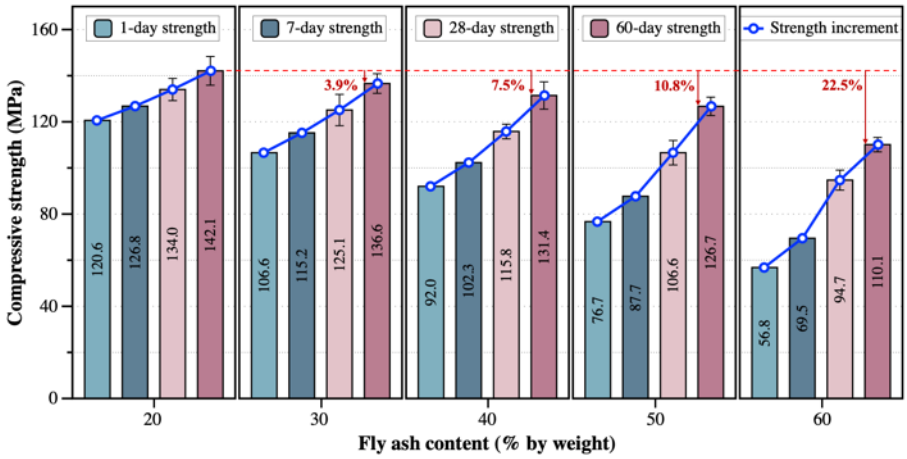

Fig. 5.5. Effect of FA substitution level on compressive strength of FR-DUHPC.

The variation in strength gain in compression at various time intervals is intuitively listed in Table 5.5. It could be clearly observed that with the increase in FA content, the improvements of 28- and 60-day compressive strength with respect to 1-day strength (expressed by 28-d^1 and 60-d^1 in the table) were remarkably higher than those of 7-day strength (expressed by 7-d^1 in the table). The comparisons of the values of 28-d^7 and 60-d^7 exhibited the same strength enhancement trend. For the percentage of strength gain at the current periods based on the prior ages, i.e., 7-d^1, 28-d^7 and 60-d^{28}, the strength improvement of samples with 50% and 60% FA contents at 28 days was apparently higher than that at 7 days, while the 60-day strength gain diminished to a certain extent with samples D-FA60 being the most pronounced (from 36.3% to 16.3%). This might be attributed to the fact that the incorporation of high substitution level of FA signally diluted the cement

concentration in the mixes, resulting in a decrease in the amount of $Ca(OH)_2$, the primary hydration product of cement, which influenced the secondary hydration process of FA in the later periods [169]. Moreover, the use of silica fume with high early reactivity might be another reason for consuming $Ca(OH)_2$ and therefore affecting the mixture's later strength gain [170].

Table 5.5

Compressive strength increment at different time intervals.

Sample	f_c (MPa)				Increment (%)					
	1-d	7-d	28-d	60-d	7-d^1	28-d^1	28-d^7	60-d^1	60-d^7	60-d^{28}
D-FA20	120.6	126.8	134.0	142.1	5.1	11.1	5.7	17.8	12.1	6.0
D-FA30	106.6	115.2	125.1	136.6	8.1	17.3	8.6	28.1	18.6	9.2
D-FA40	92.0	102.3	115.8	131.4	11.2	25.9	13.2	42.8	28.4	13.5
D-FA50	76.7	87.7	106.6	126.7	14.3	39.0	21.5	65.2	44.5	18.9
D-FA60	56.8	69.5	94.7	110.1	22.4	66.7	36.3	93.8	58.4	16.3

In order to better quantitatively analyze the contribution of pozzolanic effect of FA to the FR-DUHPC strength at various ages, three parameters (SP_{Con}, SP_{FA} and R_{FA}), which were devised from Pu's research [171] and commonly utilized in the impact analysis of various pozzolan materials [172, 173], are introduced. In this investigation, the modified SP_{Con} (specific strength of FR-DUHPC) represents the contribution of unit cement, silica fume and GGBS to concrete strength, and is calculated by the equation below:

$$SP_{Con} = F / P_{CSG} \text{ (MPa)} \quad (5.1)$$

where F is the ultimate strength value of concrete samples and P_{CSG} is the mass percentage of cement, silica fume and GGBS to the total inclusion of cementitious materials. The modified SP_{FA} (specific strength of pozzolanic effect) represents the contribution of FA to concrete strength, and is expressed as follows:

$$SP_{FA} = SP_{Con} - SP_{CSG} \text{ (MPa)} \quad (5.2)$$

where SP_{CSG} is the specific strength of FR-DUHPC containing only cementing materials of cement, silica fume and GGBS, that is, the mass percentage is 100%. Subsequently, the contribution rate of pozzolanic effect of FA to concrete strength, R_{FA}, can be obtained through the equation below:

$$R_{FA} = (SP_{FA} / SP_{Con}) \times 100\% \quad (5.3)$$

It was noteworthy that the contribution of FA to FR-DUHPC strength reported here not only originated from its own pozzolanic effect, but also covered the compound pozzolanic and micro-aggregate filling effect due to the addition of FA. Using the compression results listed in Table 5.4 as well as the strength of the additionally prepared and tested FA-free samples, the development of compressive specific strength following the curing age is exhibited in Fig. 5.6. It can be clearly observed that the values of compressive SP_{Con} of the FA-mixed FR-DUHPC (expressed by red lines) were far greater than those of the FA-free ones (represented by blue lines), and the disparity between them developed prominently with FA addition. This disparity characterized the compressive SP_{FA} due to the incorporation of FA (expressed by purple areas), that is, the pozzolanic effect exhibited a significantly promoted contribution to compressive strength with FA addition and curing age.

The compressive R_{FA} at various ages is subsequently shown in detail in Fig. 5.7. It was indicated that although the R_{FA} of 20-50% FA content was similar at 1-day age, it exhibited a slight ascending trend (from 15.6% to 17.1%) with FA addition, which was different from what other researchers had stated [172, 174]. This was mainly owing to the accelerated early cement hydration and pozzolanic reaction rate through the used moist/steam curing, which effectively alleviated the adverse impact caused by the delayed secondary hydration of FA [110]. However, as the FA content continued to increase to 60%, the foregoing R_{FA} attenuated to 10.4% due to the severe dilution of the cement and the rapid consumption of hydration products such as $Ca(OH)_2$. After 28 days of curing, FR-DUHPC with higher FA additions manifested a greater pozzolanic effect contribution, particularly for the cases where 50% and 60% of cement was replaced at 60 days, with contribution rates approaching 50%, respectively were 43.0% and 47.5%.

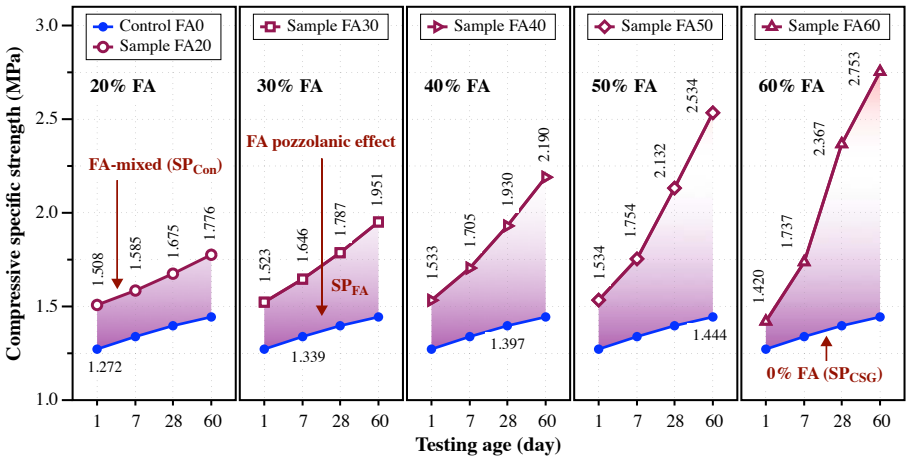

Fig. 5.6. Effect of FA substitution on compressive specific strength of FR-DUHPC.

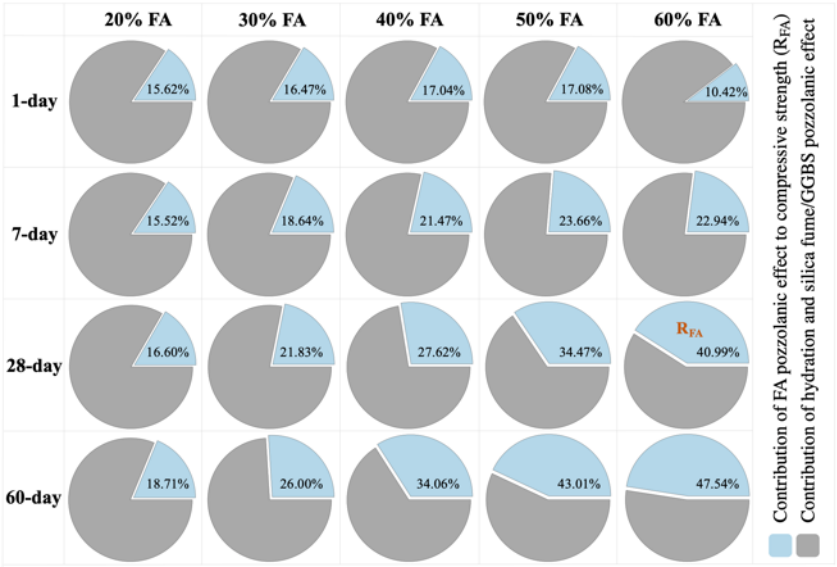

Fig. 5.7. Contribution rate of FA effect to compressive strength of FR-DUHPC.

Fig. 5.8 presents the typical compressive stress vs. strain curves associated with 20-60% FA-mixed FR-DUHPC mixtures after 28 and 60 days of curing. As shown by the figure, in addition to the difference in bearing capacity of the mixtures with different FA contents, their post-cracking curves all presented a similar downward trend, that is, the ductility and toughness were not signally affected by the change in FA addition (within the range of the evaluated contents). Furthermore, with the increase in FA addition, an attenuation trend in energy absorption performance (expressed by the total area under the curves) was noticed at 28 days of age, especially for the mix proportion containing 60% FA. However, the decline in the foregoing performance was apparently reduced with the extension of the curing to 60 days, and meanwhile the difference in the peak stress and strain capacity (strain at the peak stress) between each mixture was closed, respectively, from 95.6-134.9 MPa to 112.4-142.8 MPa, and from 0.0048-0.0052 to 0.0051-0.0053. All these improvements could be attributed to the excellent secondary hydration

of FA combined with compound pozzolanic effect, which developed prominently with the increase in FA substitution level for cement.

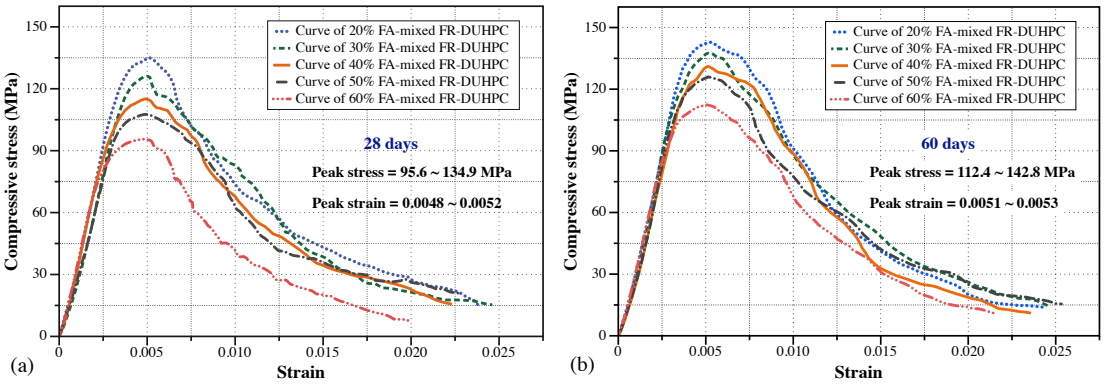

Fig. 5.8. Typical (a) 28-day and (b) 60-day compressive stress-strain relationships of FR-DUHPC incorporating various contents of FA.

The variations in MOE associated with 20-60% FA-mixed FR-DUHPC mixtures after 28- and 60-day curing are exhibited in Fig. 5.9(a). The MOE was calculated based on the compressive stress-strain relationships shown in Fig. 5.8, and 83-90% of the peak stress was considered as the due range of the elastic linear part for FA-mixed FR-DUHPC [157, 175]. Similar to compressive strength variations, the MOE increased with the curing age but meanwhile decreased gradually as the FA substitution level increased. In addition, a more evident increment in 60-day MOE was discerned for concrete mixtures with 50% and 60% FA contents, which was related to the remarkable improvement in compressive strength of the identical cases. The correlation between the compressive strength and MOE was further shown in Fig. 5.9(b) and compared with the fitting curve developed in the previous Chapter 3. As expected, the increase in compressive strength caused a

logarithmic enhancement in static MOE of 20-60% FA-mixed FR-DUHPC with R^2 greater than 0.96.

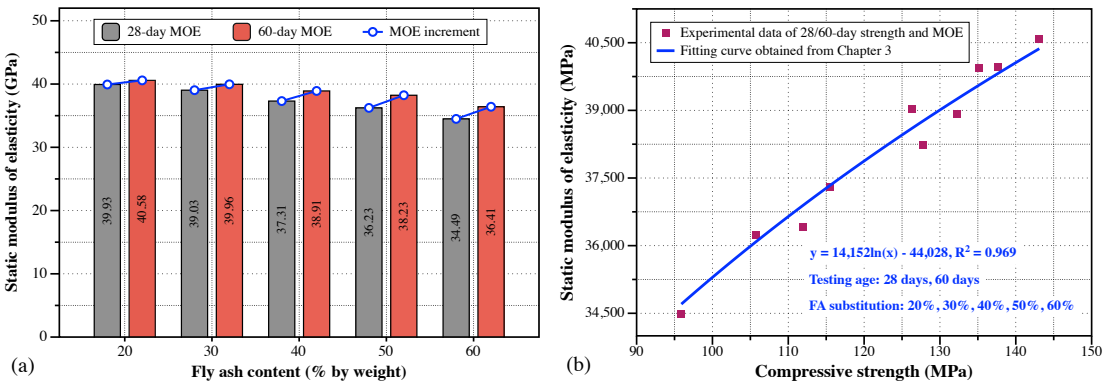

Fig. 5.9. (a) 28/60-day static MOE and (b) its relationship with compressive strength of FR-DUHPC incorporating various contents of FA.

5.3.1.3 Flexural-tensile performance

The four-point bending test results of FR-DUHPC samples mixed with different contents of FA at four ages are plotted in Fig. 5.10. Similar to the variation trend of compressive strength, increasing the FA content from 20% to 60% caused an attenuation in flexural strength at all testing ages up to 60 days, particularly for the mixtures with more cement substitution at earlier ages. However, owing to the excellent FA pozzolanic reaction, the flexural strength difference among different FA contents gradually diminished following the curing time, especially after 7-day age. The foregoing FA effect on flexural property can also be intuitively observed from Table 5.6, in which the strength increments at different time intervals are displayed. As shown in the table, compared with the 1-day strengths of mixtures with respective mix proportions, the flexural strength gains at 28 (28-d^1) and 60

(60-d^1) days were significantly stronger than those at 7 (7-d^1) days. Specifically, the strength gains, respectively, increased by 1.1-1.6 times for 28-d^1 and 2.3-2.8 times for 60-d^1 as the FA addition increased. Additionally, for the strength gain at the current periods with respect to the prior ages, the improvements in 50-60% FA-mixed mixtures at 28 days were notably stronger than that at 7 days. However, owing to the addition of high substitution level of FA severely diluted the cement concentration in the mixes, an evident weakening from 40.2% to 20.8% occurred to 60-d^{28} for D-FA60 mixture, which was consistent with that in compression. It should be pointed out that for the identical FR-DUHPC mixtures at the same ages, the strength attenuation in flexure due to the increasing FA addition was invariably weaker than that in compression, and meanwhile the positive contribution of FA to the flexural strength gain was stronger. For example, the compressive strength values of 30-60% FA-mixed samples at 60 days were, respectively, reduced by 3.9%, 7.5%, 10.8% and 22.5% in comparison with 20% FA content (presented in Fig. 5.5), while the flexural strength values were, respectively, decreased by 2.7%, 5.9%, 8.3% and 19.8% in the same situation. Moreover, the flexural strength gain 60-d^{28} for D-FA50 and D-FA60 samples (23.7% and 20.8%) was higher than their compression (18.9% and 16.3%, exhibited in Table 5.5) and presented a smaller reduction in comparison with the strength gain 28-d^7. The better positive effect of FA on flexural strength behaviour concluded above is beneficial for dry concrete structures and components that are primarily subjected to flexural-tensile loads during their applications.

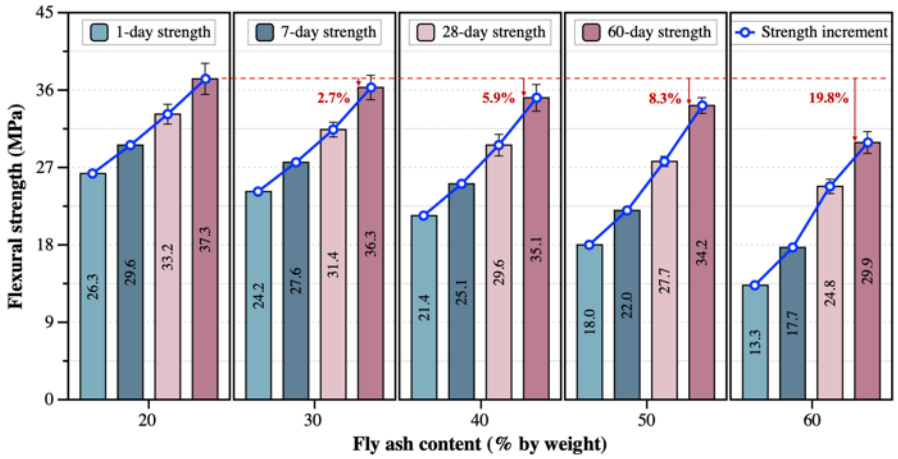

Fig. 5.10. Effect of FA substitution level on flexural strength of FR-DUHPC.

Table 5.6

Flexural strength increment at different time intervals.

Sample	f_r (MPa)				Increment (%)					
	1-d	7-d	28-d	60-d	7-d^{1}	28-d^{1}	28-d^{7}	60-d^{1}	60-d^{7}	60-d^{28}
D-FA20	26.3	29.6	33.2	37.3	12.7	26.2	11.9	41.9	25.9	12.5
D-FA30	24.2	27.6	31.4	36.3	14.3	30.1	13.8	50.1	31.3	15.3
D-FA40	21.4	25.1	29.6	35.1	17.2	38.1	17.8	63.8	39.8	18.6
D-FA50	18.0	22.0	27.7	34.2	22.3	54.1	25.9	90.6	55.8	23.7
D-FA60	13.3	17.7	24.8	29.9	33.4	86.9	40.2	125.9	69.4	20.8

Fig. 5.11 indicates the development of the flexural specific strength following the curing age, obtained by plugging the flexural strength values of FA-mixed (listed in Table 5.4) as well as additionally prepared and tested FA-free FR-DUHPC samples into Eqs. (5.1)-(5.2). It was illustrated that the values of flexural SP_{Con} of FA-mixed samples (expressed by red lines) were evidently greater than those of FA-free ones (expressed by blue lines), and the difference between SP_{Con} values of these two types of mix designs signally increased with FA addition and curing age. That is, the contribution of FA effect to the flexural strength (SP_{FA}, indicated by red areas) was significantly improved. Fig. 5.12 more intuitively exhibits the

above contribution in percentage, i.e., the contribution rate of FA effect to flexural strength (R_{FA}). As it could be found that owing to the adopted moist/steam curing accelerated the early-age cement hydration and pozzolanic reaction rate, the 1-day flexural R_{FA} was gradually increased from 10.5% to 18.1% as the FA addition raised from 20% to 50%. Although the flexural R_{FA} of D-FA60 samples reduced to a certain extent (11.2%) due to the severe dilution of cement introduction and the rapid consumption of hydration products, its value was still higher than that of D-FA20 samples. Then, with the extension of the curing, the R_{FA} of FA pozzolanic effect on flexural strength increased markedly with FA addition, which was similar to the variation trend of flexural strength and specific strength elaborated above. For example, the flexural R_{FA} of D-FA50 and D-FA60 samples was, respectively, 24.3% and 24.7% at 7- day age, while after 60 days it approximately doubled to 44.0% and 48.8%. In addition, by comparing the compressive R_{FA} of the identical mixes at the same curing ages (respectively 23.7% and 22.9% at 7 days, as well as 43.0% and 47.5% at 60 days) as illustrated in Fig. 5.7, the previous conclusion that the FA pozzolanic effect showed a better beneficial impact on improving the flexural strength behaviour was further confirmed.

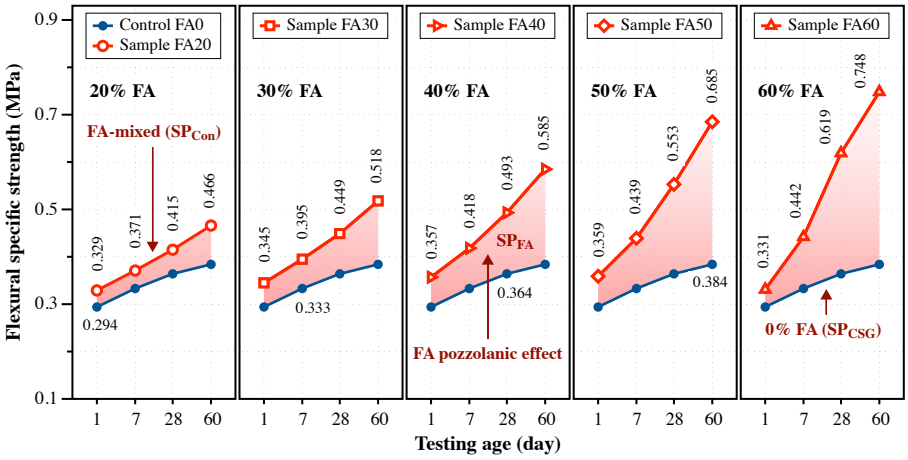

Fig. 5.11. Effect of FA substitution on flexural specific strength of FR-DUHPC.

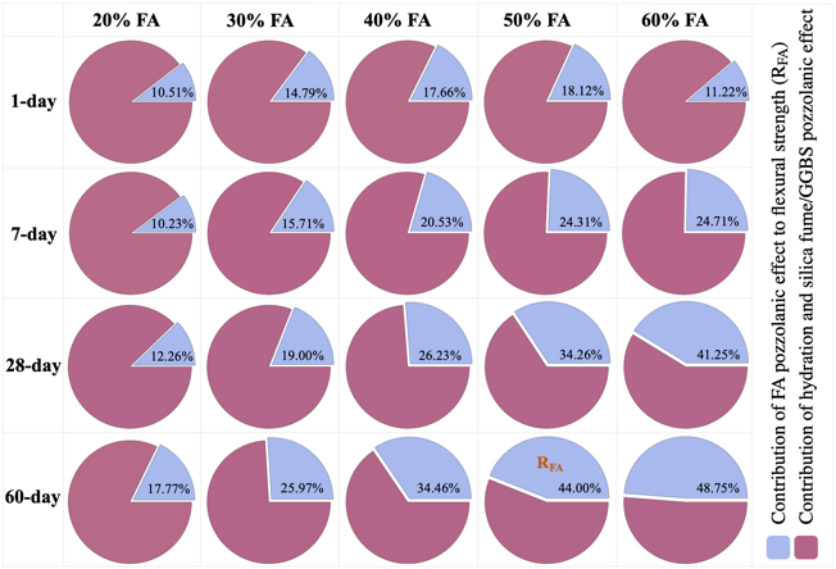

Fig. 5.12. Contribution rate of FA effect to flexural strength of FR-DUHPC.

Fig. 5.13 shows the typical flexural load vs. midspan deflection curves associated with 20-60% FA-mixed FR-DUHPC mixtures after 28 and 60 days of curing. As depicted in the figure, all of the studied samples exhibited desired ductility without fracture even when the residual bearing capacity diminished to around 10% of the peak load. In other words, the ductility was not greatly affected by the change in FA content. At 28 days of age, in addition to the large difference in the maximum bearing capacity, D-FA20 and D-FA60 samples also presented relatively better and poorer flexural toughness (represented by the area beneath the curves), respectively. However, after 60-day curing, the difference in peak load developed smaller (from 13.2-17.6 kN to 16.1-20.0 kN) and the samples showed comparable deflection capacity (deflection at the peak load, from 0.593-0.635 mm to 0.629-0.643 mm). Furthermore, the zigzag drop-off patterns similarly appeared on the softening section of the curves of all samples, heard with tearing sounds (steel fibres were pulled out from the matrix), which was consistent with the phenomena

mentioned in Chapters 3 and 4. But subsequently, the extent of drop-off tended to alleviate with the extension of curing, which might be attributed to the better bond-anchorage behaviour between the matrix and steel fibres by virtue of the fully activated FA pozzolanic effect.

Fig. 5.14(a) shows the variation in flexural cracking strength of 20-60% FA-mixed FR-DUHPC samples after 28 and 60 days of curing. The cracking strength was obtained by calculating the load corresponding to the tensile failure of the strain gauge affixing to the bottom area of the tested samples. For the evaluated mixes, the increase in FA addition also resulted in a certain reduction in flexural cracking strength, although at mid and late ages when the pozzolanic reaction was fully activated. Moreover, a notable improvement of 7.6% and 11.1% was, respectively, detected for mixtures incorporating 50% and 60% FA after 60-day curing. By contrasting the flexural strength at 28 and 60 days for samples with identical mix designs (as shown in Fig. 5.10), they all presented a robust deflection-hardening behaviour demonstrating an improved ability to resist the sustained higher load after the crack initiation, as shown in Fig. 5.14(b). In addition, it could be observed that with the curing age extended from 28 to 60 days, the ratio between flexural first-cracking and ultimate strengths decreased markedly, that is, there was more room for the enhancement of bearing capacity after the initial crack.

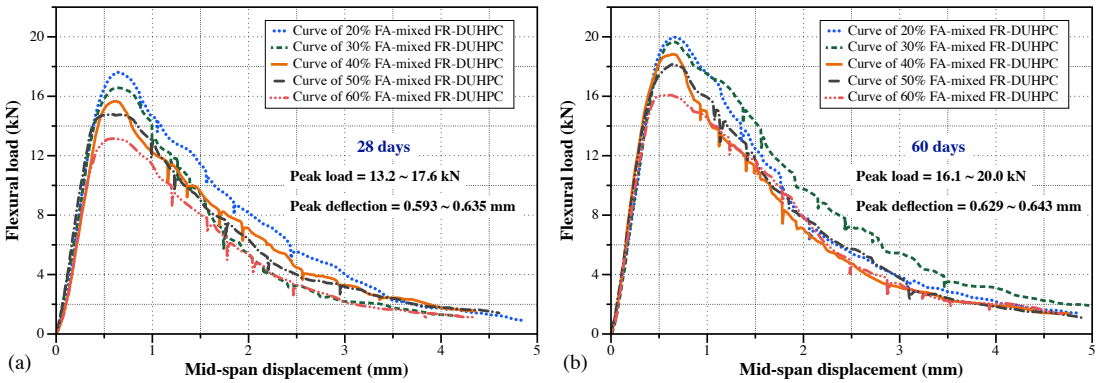

Fig. 5.13. Typical (a) 28-day and (b) 60-day flexural load-deflection relationships of FR-DUHPC incorporating various contents of FA.

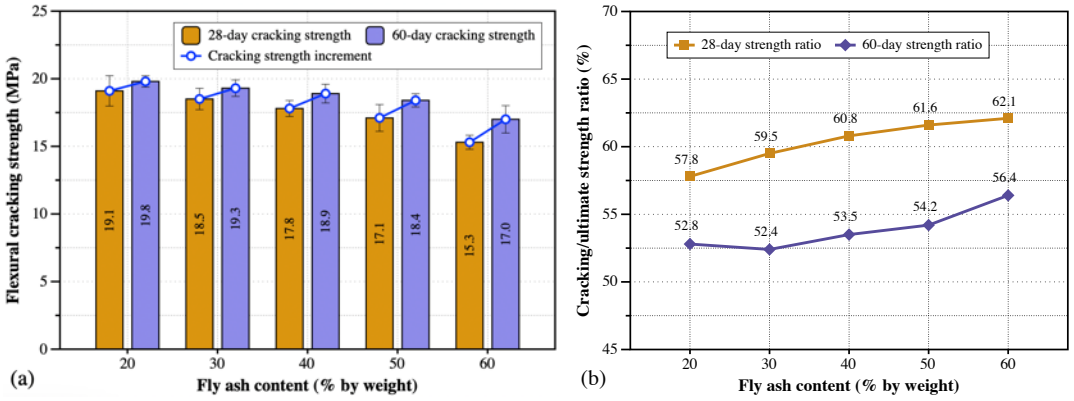

Fig. 5.14. (a) Flexural cracking strength and (b) its ratio to the ultimate strength of 20-60% FA-incorporated FR-DUHPC after 28- and 60-day curing.

5.3.1.4 Discussion

As summarized above, the compressive and flexural strengths of FR-DUHPC increased gradually with curing age but reduced significantly with FA substitution level for cement, especially for the mixtures with more FA at earlier ages. Other mechanical properties including the compressive MOE and flexural cracking strength demonstrated a similar variation trend. However, owing to the adopted moist/steam curing accelerated the early-age cement hydration and pozzolanic reaction rates of concrete mixtures, the contribution of FA effect to both strengths

at each age was significantly improved, particularly for the cases where 50% and 60% of cement was substituted after 28 days of curing. It was noteworthy that for identical FR-DUHPC samples at the same testing ages, the strength attenuation in flexure due to the increase in FA substitution was invariably weaker than that in compression, and the contribution of FA pozzolanic effect to flexural strength gain was prominent. This phenomenon could be further demonstrated via the variation in the compressive-flexural strength ratio at different ages, along with the fitting relationship between the two strengths, as shown in Fig. 5.15. It could be clearly observed that the strength ratio exhibited an evident downward trend with curing age and FA incorporation (indicated by blue lines), and meanwhile the power exponent in the fitting function was greater than 1.0 ($f_t = 0.167 \cdot f_c^{1.085}$, $R^2 = 0.955$). That is, the use of FA to substitute partial cement in FR-DUHPC mixes exhibited a more positive impact on improving the flexural strength behaviour of hardened mixtures, and higher FA contents exhibited a better effect. In addition, Fig. 5.16, in which the correlation of FA content and two strengths was presented, also illustrated the smaller decrease in flexural strength at all ages, manifested in that the negative slope of the flexural fitting curves was closer to zero. This is very beneficial for dry concrete structures and units that are mainly subjected to flexural-tensile loads during their service. However, it should be noted that the inclusion of 60% FA severely diluted the cement concentration in concrete mixes, leading to an evident reduction in hydration product amounts and a retardation in secondary hydration reactions. Consequently, both the early strength and the

strength development after 28-day curing were significantly decreased. The 60-day strength fitting curves (expressed by purple lines) exhibited in Fig. 5.16 also indicated a more visible strength diminishment occurred in the case where 60% of cement substitution was used. Thus, considering the sustainable development in resources as well as the impact of FA addition on the mechanical behaviour of FR-DUHPC at various ages, 50% cement substitution in line with the high-volume concept was determined to be the most appropriate FA addition in this study.

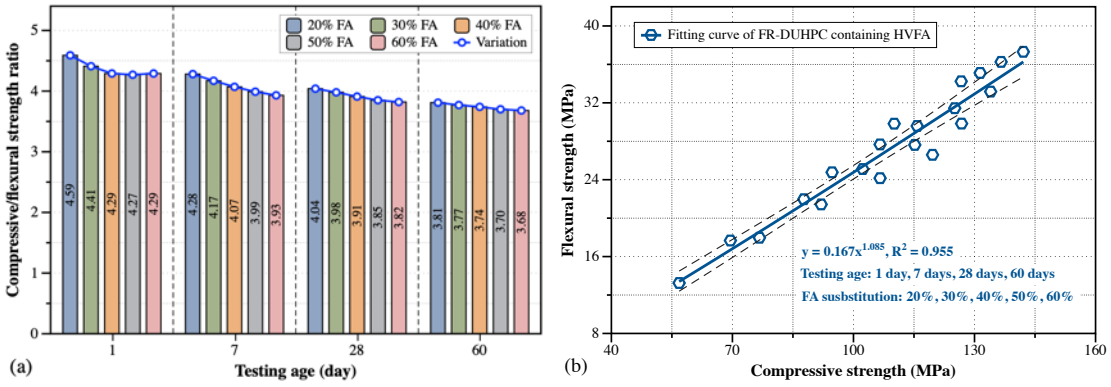

Fig. 5.15. (a) Strength ratio at various ages and (b) relationship between compressive and flexural strengths of FR-DUHPC incorporating various contents of FA.

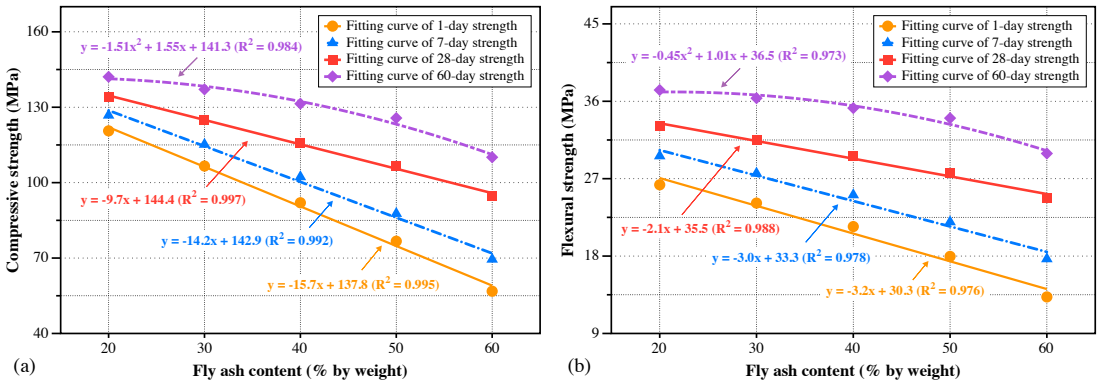

Fig. 5.16. Correlation between FA content and (a) compressive as well as (b) flexural strengths of FR-DUHPC.

5.3.2 FR-DUHPC incorporating HVFA and CR

On the basis of the mix ratio with optimal FA content concluded above, the performance of FR-DUHPC with partial silica sand substituted by CR particles were further studied, concerning different substitution levels and combinations. Table 5.7 shows the obtained mean density and compressive/flexural strength values at corresponding ages, in which the meanings of f_c and f_r are the same as those in Table 5.4.

Table 5.7

Density and mechanical results of FR-DUHPC containing HVFA and CR.

Sample	Fibre	Density (kg/m^3)				f_c (MPa)				f_r (MPa)			
	(%)	1-d	7-d	28-d	60-d	1-d	7-d	28-d	60-d	1-d	7-d	28-d	60-d
D-FA50-	0.5	2029	2035	2073	2074	33.3	35.1	43.2	52.0	7.3	8.3	11.4	15.0
RC10	1.0	2057	2070	2095	2081	37.7	40.6	52.9	65.7	8.9	10.4	14.7	19.4
	1.5	2086	2084	2098	2122	44.1	49.2	64.6	81.5	11.4	13.7	19.3	24.9
D-FA50-	0.5	1811	1794	1820	1823	19.4	20.5	26.4	32.2	3.7	4.4	6.2	8.4
RCM25	1.0	1841	1842	1856	1861	21.3	22.9	30.4	38.4	4.6	5.4	7.9	10.8
	1.5	1851	1864	1871	1878	24.1	25.6	36.3	45.9	5.9	6.9	10.5	13.8
D-FA50-	0.5	1659	1687	1699	1738	9.9	10.4	13.3	15.8	1.8	2.1	2.9	4.1
RCM35	1.0	1685	1721	1705	1761	10.9	12.0	15.2	18.2	2.2	2.7	4.0	5.4
	1.5	1728	1769	1788	1786	12.0	13.3	17.9	22.0	2.9	3.6	5.1	6.6

5.3.2.1 Density

The variations in density of 0.5-1.5% FR-DUHPC with partial silica sand replaced by CR are displayed in Fig. 5.17. The density of each mixture was considered as the average of six samples on each testing days upon curing. A regular increase

in hardened density was discerned with fibre addition due to the growing quantity of steel fibres with higher density, irrespective of the combination and level of CR substitution. However, compared with original FA50 DUHPC samples with 1.5% fibre reinforcement, the addition of CR aggregate caused a notable reduction in hardened density at all ages, especially for the mixtures with medium sand being partially substituted. Specifically, the density of D-FA50 samples was obtained as 2310 kg/m^3, while it reduced by 9.2% when all of the coarse sand was substituted (samples D-FA50-RC10), and was further dropped by 19.2% and 23.5% after 40% and 70% of medium sand were replaced (samples D-FA50-RCM25 and D-FA50-RCM35), respectively. This reduction might be attributed to the existence of two parallel effects, that is, the notably lower specific gravity of CR aggregate (listed in Table 5.2) reduced the mass of the mixture per unit volume, together with the entrapped air on the surface of CR aggregate facilitated the void formation inside the mixture and brought down the overall compactness [176, 177]. It should be noted that according to the definition of ACI 213.R3 guidelines [178] and Chinese standard JGJ51-90 [179], samples D-FA50-RCM25 and D-FA50-RCM35 can be classified as lightweight concrete (LWC) owing to their hardening densities less than 1920 kg/m^3, while samples D-FA50-RC10 can also be qualified as LWC by virtue of the average densities not exceeding 2100 kg/m^3 at three fibre dosages, according to the specification of Australian standard AS1379 [180].

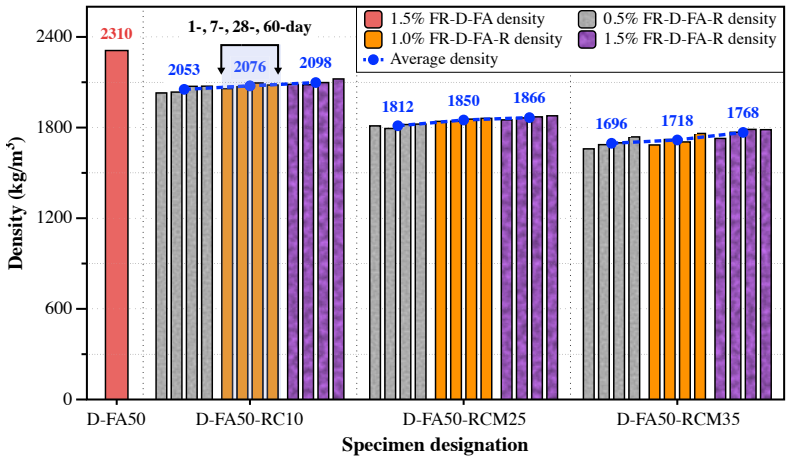

Fig. 5.17. Effects of CR substitution and fibre dosage on density of FR-DUHPC.

5.3.2.2 Compressive performance

The compression test results of 0.5-1.5% FR-DUHPC samples with partial quartz sand replaced by CR particles are shown in Fig. 5.18. The columns represented the average strength values obtained from three identical samples of each mix. Compared with control FA50 DUHPC samples with 1.5% fibre reinforcement, as shown in Fig. 5.5, an evident reduction in compressive strength of all ages with increasing CR substitution was noted at the same fibre dosage, and in particular, the strength signally deteriorated after the medium sand was partially replaced. For example, at 1.5% fibre reinforcement, original FA-mixed samples yielded 28- and 60-day compressive strength of 106.6 and 126.7 MPa, respectively, which diminished to 64.6 and 81.5 MPa (decreased by 39.4% and 35.7%) for D-FA50-RC10 samples, and further diminished to 36.6 and 45.9 MPa (reduced by 65.7% and 63.8%) as well as 17.9 and 22.0 MPa (reduced by 83.2% and 82.6%), for D-FA50-RCM25 and D-FA50-RCM35 samples, respectively. The evident reduction in strength was attributed to the weak bonding between cement paste and CR aggregate, which was induced due to the water repelled by CR aggregate during

mixing [181, 182] together with the low moisture content of dry concrete by nature, leading to increased thickness of the ITZ as depicted in Fig. 5.19(a). In addition, there was an incompatibility between the natural sand and rubber particles with lower bearing capacity but higher elasticity. As a result, after sand was partially substituted, CR aggregate was more easily deformed under compression load, which in turn accelerated the development of initial micro-cracks within concrete matrix [2, 183]. The aforementioned adverse impact would be more pronounced with partial medium sand substituted by finer CR aggregate. In addition, it can be noted that the compressive strength of the studied concrete enhanced gradually with fibre dosage and curing age, regardless of rubber addition and combination. However, the strength gain presented a visible decreasing trend with the increase in the addition of finer CR aggregate (indicated by blue lines). For example, the 60-day compressive strength of D-FA50-RC10 samples enhanced from 52.0 to 65.7 and 81.5 MPa as the fibre dosage increased, with increments of 26.4% and 56.7%, respectively. But the increments reduced to 19.3% and 42.6% as well as 15.2% and 39.2% after finer CR aggregate was added, that is, the improvement effect of steel fibres on the compressive strength was weakened. Reason for this phenomenon might be that at higher CR contents, more entrapped air attached to the finer rubber aggregate with a large specific surface area, which significantly deteriorated the compactness of the mixture, as reported in Section 5.3.2.1. This consequently resulted in poor anchorage between steel fibres and cement paste as well as CR aggregate, as shown in Fig. 5.19(b), hence weakening the restraint effect of fibres on concrete matrix under load.

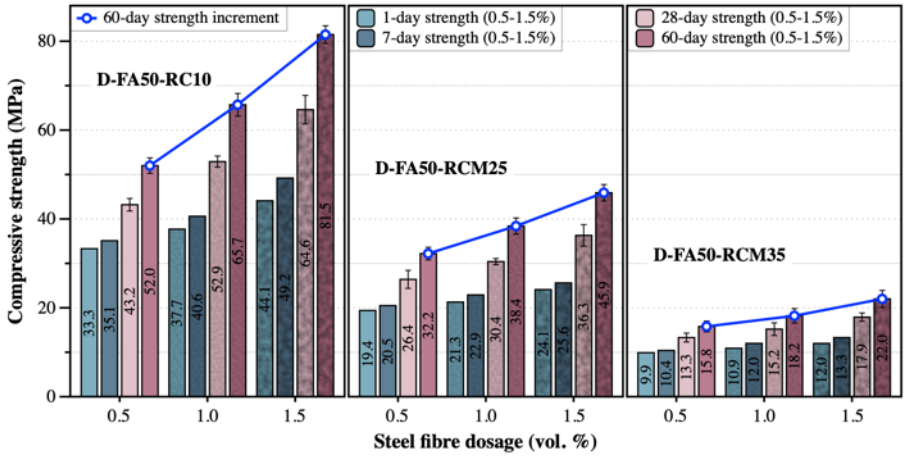

Fig. 5.18. Effects of CR substitution and fibre volume dosage on compressive strength of FR-DUHPC.

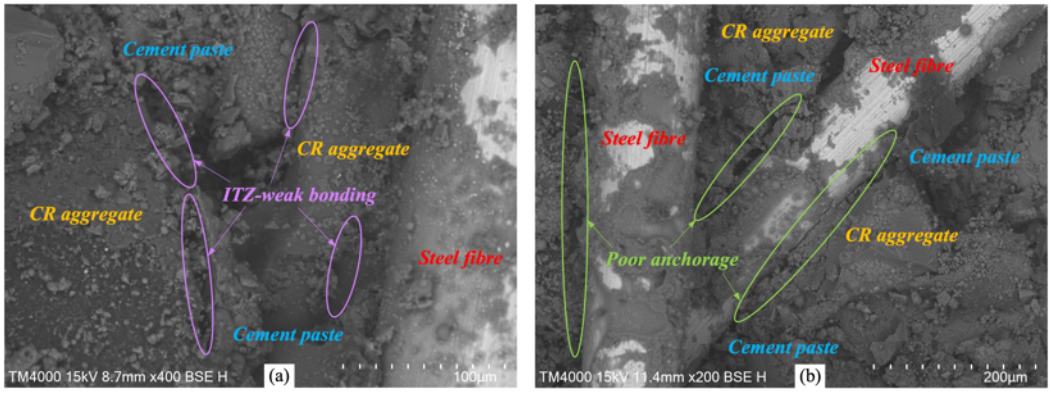

Fig. 5.19. Microstructure images in terms of ITZs between CR aggregate and (a) cement paste as well as (b) steel fibres of rubberized dry concrete based on SEM.

Fig. 5.20 shows the typical compressive stress vs. strain curves associated with 1.5% steel FR-DUHPC incorporating various contents of CR aggregate after 28- and 60-day curing, and the correlation curves for control 50% FA-mixed samples are also displayed for comparison. As depicted, the incorporation of CR particles to substitute partial natural sand caused a significant attenuation in bearing and strain capability of hardened mixtures, specifically indicated by the peak stress dropped from 107.6 and 126.0 MPa to 18.3 and 22.6 MPa and the peak strain

(strain at the peak stress) deteriorated from 0.0048 and 0.0051 to 0.0015 and 0.0016 at 28 and 60 days, respectively. Moreover, the compressive stiffness prior to the peak stress also tended to attenuate with the increase in CR substitution. However, despite this, all the samples exhibited excellent post-peak compressive performance regardless of CR addition and combination, that is, the ductility and toughness of the prepared rubberized concrete after cracking were not evidently degraded by the rubber incorporation. For example, at 60 days of age, although the ultimate bearing capacity of samples D-FA50-RC10 reduced by 34.9% (from 126.0 to 82.0 MPa), their residual stress value at the strain of 0.025 was greater than that of control samples, which might be attributed to the synergistic benefits of fibre toughening as well as energy absorption induced by rubber deformation. In addition, to further investigate the impact of fibre dosage on the stress-strain relationship of rubberized concrete, the typical compression curves of 0.5-1.5% fibre-reinforced samples were plotted, as shown in Fig. 5.21. It could be observed from the curves that all samples exhibited obvious ductile failure characteristics after the load exceeded their maximum bearing capacity, irrespective of the fibre dosage, rubber addition and combination used. As expected, both the peak stress and strain were increased with fibre dosage and this trend was pronounced at CR additions of 10% and 25%, in the ranges of 43.8-65.2 MPa and 0.0024-0.0035, 26.7-37.2 MPa and 0.0017-0.0024 at 28 days of age, and 52.3-82.0 MPa and 0.0028-0.0038, 32.5-46.5 MPa and 0.0018-0.0026 at 60 days of age, respectively for D-FA50-RC10 and D-FA50-RCM25 samples. Furthermore, the higher fibre

dosages endowed rubberized concrete with better ductility and energy absorption behaviour (expressed by the total area beneath the curves), which were mainly manifested in higher residual stress value at the same strain and a plumper post-peak curve contour. It was noteworthy that increasing the fibre addition from 0.5% to 1.5% contributed to better positive impact on ductility improvement rather than the load-carrying capacity for mixtures with 35% CR addition (D-FA50-RCM35), resulting in the difference of residual stress at the same strain upon cracking was almost evidently greater than that of the peak stress.

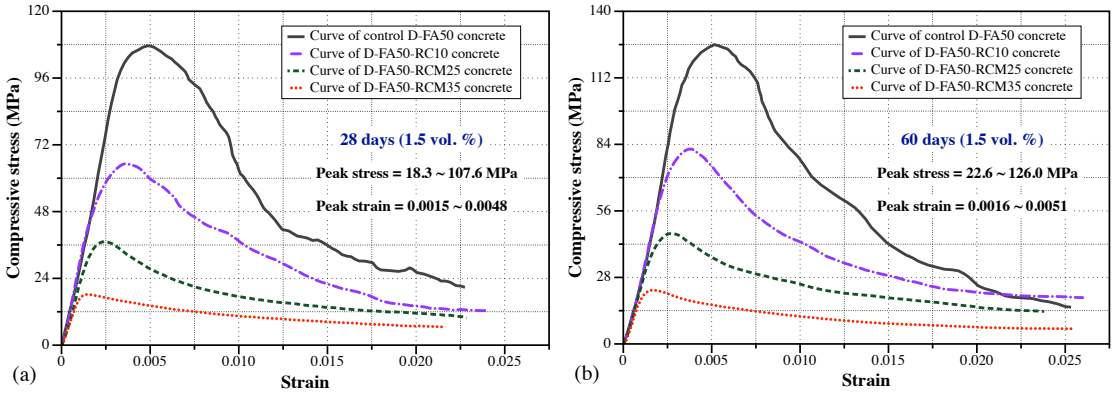

Fig. 5.20. Typical (a) 28-day and (b) 60-day compressive stress-strain relationships of 1.5% FR-DUHPC incorporating various contents of CR aggregate.

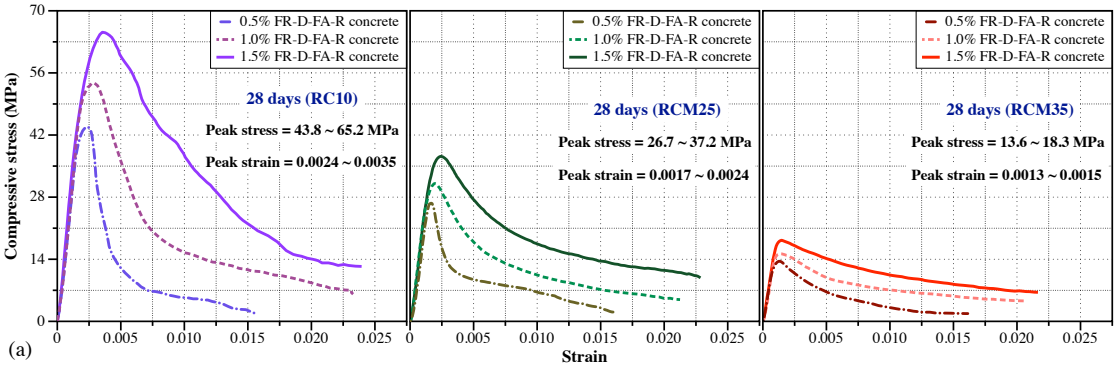

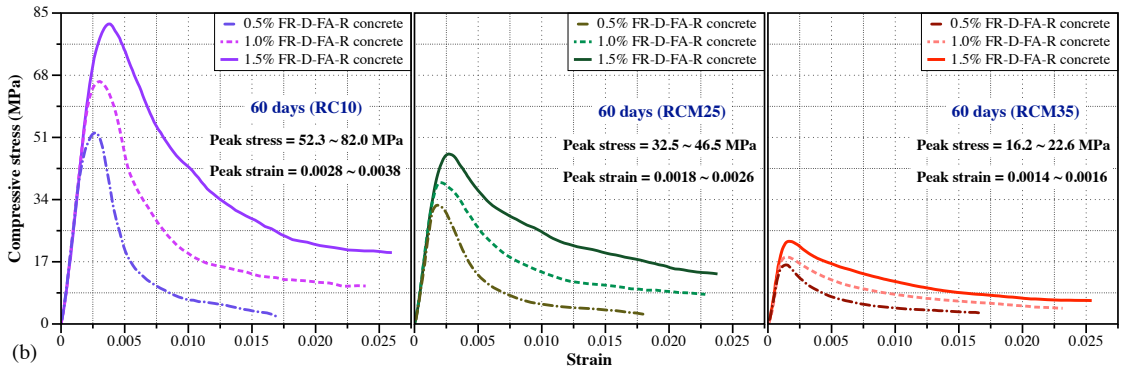

Fig. 5.21. Typical (a) 28-day and (b) 60-day compressive stress-strain relationships of 0.5-1.5% FR-DUHPC incorporating various contents of CR aggregate.

The variations in MOE associated with 0.5-1.5% steel FR-DUHPC incorporating various contents of CR aggregate after 28- and 60-day curing are depicted in Fig. 5.22(a). The MOE was also calculated based on the initial slope of compressive stress-strain curves plotted in Fig. 5.21, and the due range of the elastic branch was shrunk to 40-80% of the peak force due to the degraded and inhomogeneous microstructure of the rubberized mixtures as depicted in Fig. 5.19. As compared to the MOE of control samples (1.5% fibre reinforcement) without rubber particles exhibited in Fig. 5.9(a), a reduction in MOE was observed with the addition of CR aggregate, especially for mixtures with medium sand being partially substituted. For instance, the 60-day MOE reduced from 38.2 (control FA50 FR-DUHPC) to 33.1 (decreased by 13.4%) GPa when coarse sand was substituted, and it further diminished to 27.5 and 21.1 (decreased by 28.0% and 44.8%, respectively) GPa when 40% and 70% of medium sand was likewise substituted by CR aggregate (RCM25 and RCM35). This was due to the lower MOE of rubber aggregate than natural sand, along with the increase in rubber addition also notably deteriorated the compactness of the concrete matrix [182]. For rubberized samples reinforced

with different fibre dosages, the increase in fibre addition contributed to higher MOE at two ages, but the increment gradually mitigated with the addition of finer CR aggregate (indicated by blue lines), which was consistent with the variation trend of compressive strength. As an illustration, samples D-FA50-RC10 with 1.5% fibre reinforcement exhibited 16.6% and 14.9% increments in MOE after 28- and 60-day curing as compared to samples with 0.5% fibre reinforcement. However, samples D-FA50-RCM35 only demonstrated 9.4% and 8.2% increments in MOE under the identical conditions, which was related to the change in compressive strength and the evidently weakened fibre effect due to the higher CR addition. Furthermore, since the substitution of natural sand by CR (with notably different intrinsic properties) caused the evident changes in compressive behaviour of the studied mixtures, a new functional relationship between 28-/60-day compressive strength and MOE was developed (Fig. 5.22(b)). As depicted, the enhancement in compressive strength similarly led to a logarithmic increase in static MOE and a desired correlation (MOE = 8,698·lnf_c - 14,502) was derived with a goodness of fit of 0.992.

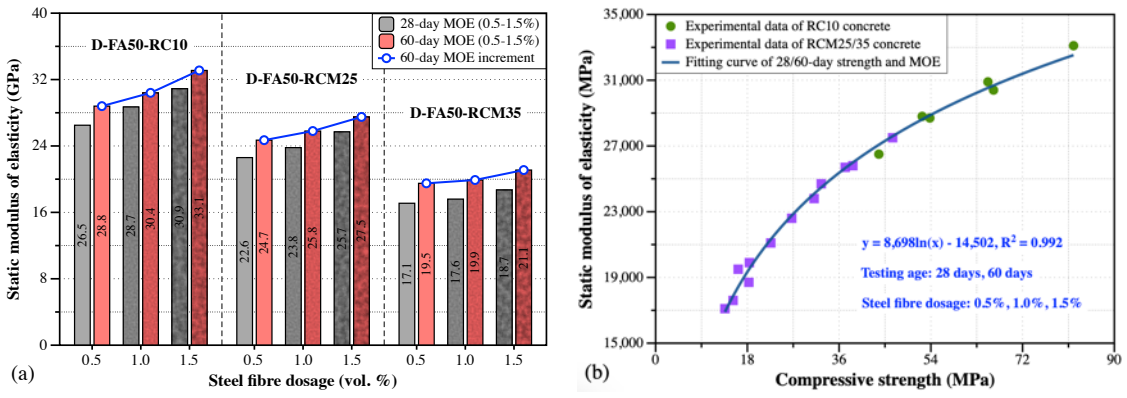

Fig. 5.22. (a) 28/60-day static MOE and (b) its relationship with compressive strength of 0.5-1.5% FR-DUHPC incorporating various contents of CR aggregate.

5.3.2.3 Flexural-tensile performance

The flexural strength results obtained on 0.5-1.5% steel FR-DUHPC mixes with various CR additions and substitution combinations are exhibited in Fig. 5.23. A similar variation trend of flexural strength to compression can be discerned when different contents of CR aggregate were incorporated into 1.5% fibre-reinforced mixtures. For instance, the flexural strength of D-FA50-RC10 samples at 28 and 60 days were, respectively, 30.3% and 27.2% lower compared with original mixes without CR, while for samples with partial medium sand being replaced (RCM25 and RCM35), the corresponding decline extended to 62.1% and 59.7% as well as 81.6% and 80.7%, respectively. The reduction also attributed to the ITZ debility of cement paste and CR aggregate within the matrix, and higher inclusions of the finer CR increased the possibility of micro-cracks' formation, causing these micro-cracks easier to penetrate into larger cracks during load application [176]. It was noteworthy that the foregoing adverse effect of CR addition was less serious on flexural performance with a smaller strength attenuation in comparison with the compression, which was in line with the findings reported by Sofi [184]. Moreover, under the same CR substitution, the fibre dosage and curing age all contributed to higher flexural strength and this positive impact was prominent for samples D-FA50-RC10 and D-FA50-RCM25. As an illustration, the strength at 60 days was enhanced by 28.4% and 27.8% as the fibre dosage increased from 1.0% to 1.5% for these two rubberized concretes. However, the strength was only enhanced by 22.2% when 70% of medium sand was substituted by CR aggregate (RCM35). The curing age exhibited a similar strength development impact. The primarily

reason was also that the workability and compactness of dry concrete mixtures with lower moisture content were significantly deteriorated after more finer rubber particles were introduced, which brought down the bonding performance between the fibres and matrix or rubber aggregate. Consequently, the fibres' reinforcement effect was weakened, although the mixtures were in the middle and later periods when the cement hydration was relatively adequate. As expected, the positive effect of fibre dosage on flexure was still better than that on compression, which calculated as 24.1% (RC10), 19.5% (RCM25) and 20.9% (RCM35) as the fibre addition increased from 1.0% to 1.5% after 60-day curing. This was attributed to the preparation of layered compaction of the developed concrete rendered steel fibres tend to be aligned parallel to the compacted direction, endowing fibres with more effective restraint on matrix cracking under flexural-tensile load, as reported in Chapter 3. All these benefits derived from the inclusion of CR aggregate and steel fibres increase the opportunities for utilizing the developed mixtures in dry concrete applications which are mainly subjected to bending loads during service.

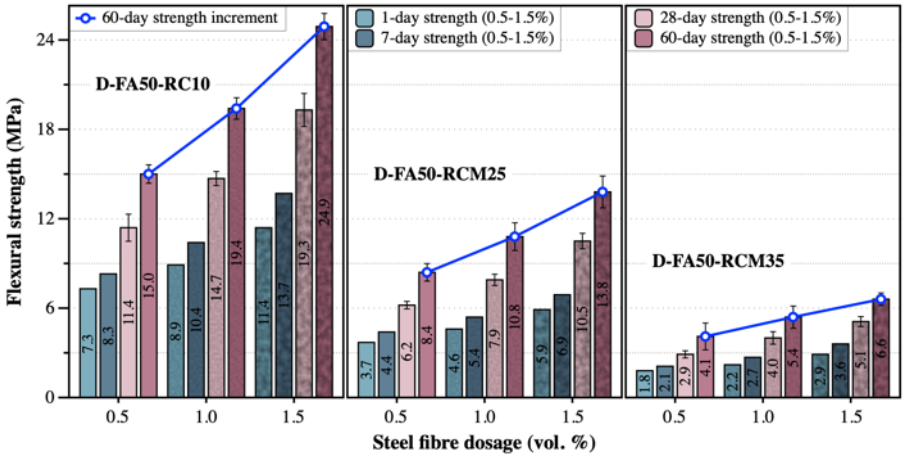

Fig. 5.23. Effects of CR substitution and fibre dosage on flexural strength of FR-DUHPC.

Fig. 5.24 shows the typical flexural load vs. midspan deflection curves associated with 1.5% FR-DUHPC containing various contents of CR aggregate after 28 and 60 days of curing, and the correlation curves for control 50% FA-mixed samples are additionally plotted for comparison. Although an evident attenuation in flexural bearing capacity of the hardened mixtures was noted (decreased from 14.8 and 18.2 kN to 2.8 and 3.6 kN at 28 and 60 days, respectively), the use of different percentages and combinations of CR substitution did not adversely affect their post-peak ductility. At 60-day age, as the midspan deflection extended to 4 mm, the residual bearing capacity of all rubberized samples was greater than that of the control one. In addition, the zigzag drop-off pattern appeared on the softening part of the control curves also mitigated apparently or even disappeared with CR addition, indicating that the development of flexural cracks tended to be stable. These improvements could be ascribed to the fact that the ability of CR aggregate to resist the large deformation and promote the energy absorption and dissipation of concrete matrix together with the toughening effect of fibres, and consequently, at large displacements the rubberized concrete still demonstrated greater flexural capacity than the mixes without CR [185]. Additionally, it could be found that the initial slope (flexural stiffness) of the curves' ascending part visibly decreased with the increase in rubber substitution, and the flexural strain capacity (deflection at the peak load) of samples containing 10% and 25% CR aggregate (RC10 and RCM25) was stronger than that of the control one. Specifically, the strain capacity value increased from 0.599 and 0.633 mm to 0.607 and 0.645 mm and then to

0.629 and 0.656 mm at 28 and 60 days, respectively. Alsaif et al. [185] and Turatsinze et al. [186] attributed this mechanism to the fact that the CR aggregate acting as the holes at the crack tip to mitigate the tip's sharpness and stress concentration, therefore effectively slowing down the kinetics of the micro-cracks' coalescence and propagation. The addition of steel fibres could further enhance the aforementioned benefits derived from rubber aggregate and help dry concrete structures/units with large surface area to better resist the durability deterioration caused by fatigue and shrinkage. In terms of rubberized samples reinforced with different dosages of fibres, they all showed excellent post-cracking behaviour at two ages, even for the cases with 35% CR addition and 0.5% fibre reinforcement, as shown in Fig. 5.25. As expected, the higher fibre dosage contributed to greater flexural load-carrying capacity and stiffness, as well as better strain capacity and toughness (represented by the area under the curves). As an illustration, the peak load increased from 8.0 and 4.5 kN to 13.5 and 7.4 kN, and the corresponding peak deflection extended from 0.552 and 0.558 mm to 0.645 and 0.656 mm at 60 days, respectively for D-FA50-RC10 and D-FA50-RCM25 samples. In addition, for samples containing 35% CR aggregate, the positive effect of fibre addition on flexural post-cracking behaviour was apparently better than that on load-carrying capacity, which was similar to the fibre effect on compressive ductility of identical samples analysed above. Furthermore, the zigzag drop-off pattern tended to be severe when less fibre reinforcement was employed, but they did not appear on the softening part of the curves for samples with higher CR contents (RCM25 and

RCM35), owing to the better synergistic effect between rubber and steel fibres.

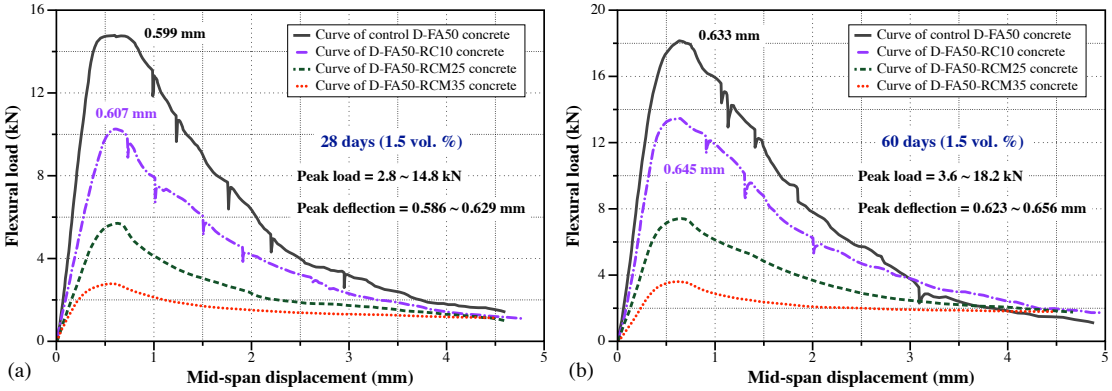

Fig. 5.24. Typical (a) 28-day and (b) 60-day flexural load-deflection relationships of 1.5% FR-DUHPC incorporating various contents of CR aggregate.

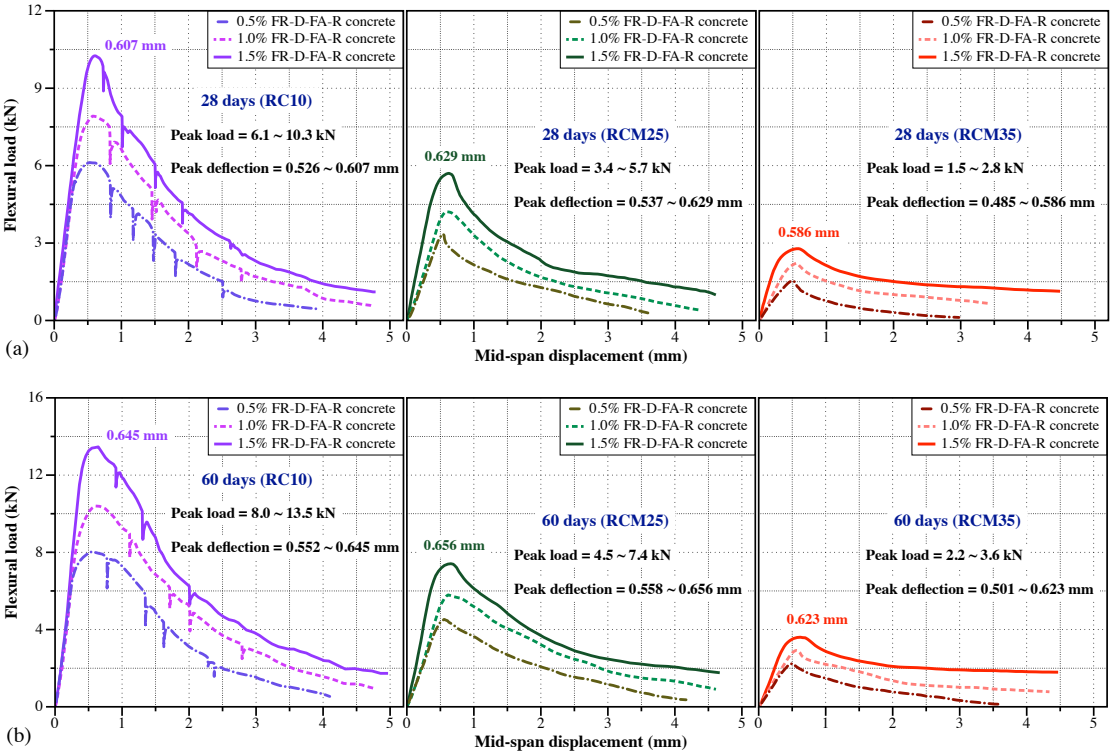

Fig. 5.25. Typical (a) 28-day and (b) 60-day flexural load-deflection relationships of 0.5-1.5% FR-DUHPC incorporating various contents of CR aggregate.

Fig. 5.26(a) illustrates the variations in flexural cracking strength of 0.5-1.5% FR-DUHPC containing various contents of CR aggregate after 28- and 60-day curing.

The cracking strength was obtained in the same approach as that of FA-mixed FR-DUHPC described in Section 5.3.1.3. As indicated by the figure, the increase in fibre dosage and the prolongation of curing age both exhibited evident positive impact on flexural cracking strength, while the increase in CR addition markedly weakened their effects (indicated by blue lines). For instance, the 60-day cracking strength enhanced by 22.1% and 24.9%, 18.2% and 19.2%, and 16.7% and 14.3% as fibre addition increased from 0.5% to 1.5%, respectively for samples with 10%, 25% and 35% CR additions. Such mechanical changes could be justified by the mechanism and explanation concluded previously regarding the variations in the flexural strength. By comparing the 28- and 60-day flexural strength values for samples with identical mix designs depicted in Fig. 5.23, all the fibre-reinforced rubberized mixtures exhibited a robust deflection-hardening behaviour indicating an improved ability to continuously undergo higher load after the crack initiation, as shown in Fig. 5.26(b). Compared with the flexural strength ratio (61.6% and 54.2%) of control FA50 concrete samples exhibited in Fig. 5.14(b), the addition of rubber aggregate also attenuated the ability of the assessed mixture to resist the sustained external loads after initial cracking, specifically, the strength ratio increased to 69.1% and 62.3%, 73.3% and 66.9%, and 76.8% and 71.1% as the CR addition increased at 28 and 60 days. Furthermore, although the higher fibre addition and longer curing age were both beneficial to better deflection-hardening behaviour, a more positive effect of increasing fibre dosage (0.5-1.5%) was noted on mixtures incorporating 35% CR substitution, with room for the improvement

increasing from 4.7% and 13.6% to 23.2% and 28.9% after 28- and 60-day curing, respectively.

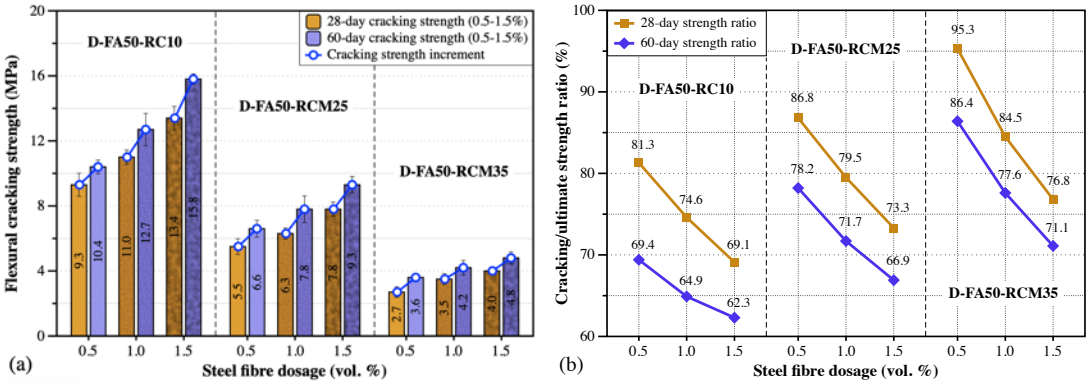

Fig. 5.26. (a) Flexural cracking strength and (b) its ratio to the ultimate strength of 0.5-1.5% FR-DUHPC incorporating various contents of CR aggregate after 28- and 60-day curing.

5.3.2.4 Discussion

As reported above, as compared to original FA50 1.5% FR-DUHPC, the addition of CR aggregate led to an evident reduction in density, compressive and flexural strengths at all ages, especially for the cases where the medium silica sand was partially replaced. The decrease in density was attributed to the existence of two parallel effects, that is, the lower specific gravity of CR aggregate decreased the mass of the mixture per unit volume, together with the entrapped air on the rubber aggregate which facilitated the void formation inside the mixture and brought down the overall compactness. It was therefore the mixtures' strength behaviour was notably affected. Fig. 5.27 depicts the correlations between the density and compressive/flexural strengths of the evaluated rubberized DUHPC with 0.5-1.5% fibre reinforcements. It could be noticed that the good relationships were existed

with R^2 greater than 0.83, and the increase in density caused a power functional enhancement in the two-strength behaviour. In addition, the samples D-FA50-RC10 exhibited a more visible strength gain with increasing density owing to the denser compactness, while the increment in flexural strength was greater than that in compression at the same unit weight. This finding was consistent with the development of flexural strength reported in Section 5.3.2.3, and could be further demonstrated from Fig. 5.28, in which the compressive-flexural strength ratio at different ages as well as the fitting relationship between the two strengths of the rubberized concrete are presented. Compared with the strength ratios (within the range of 3.70-4.27 up to 60 days) of the original FA50 1.5% FR-DUHPC exhibited in Fig. 5.15(a), lower ratio values appeared on rubberized samples at the same fibre addition, ranging from 3.27-3.91, 3.34-4.09 and 3.32-4.17, respectively for D-FA50-RC10, D-FA50-RCM25 and D-FA50-RCM35 samples. In addition, the power exponent within the functions was all greater than 1.0 ($f_t = 0.059 \cdot f_c^{1.384}$ for RC10; $f_t = 0.135 \cdot f_c^{1.202}$ for RCM25/35), indicating a faster kinetics of flexural strength development. Additionally, it could be found from Fig. 5.28(a) that the lower fibre dosage and larger CR addition all evidently weakened the foregoing flexural strength benefit, especially for the cases where the finer CR aggregate and 0.5% steel fibres were used. It was noteworthy that the mixes 0.5% FR-D-FA50-RCM25 as well as 0.5-1.5% FR-D-FA50-RCM35 could not be used for the construction of RCCP since their 28-day compressive strength was lower than the minimum strength requirement (27.6 MPa) as specified in the ACI guidelines

[187], but they were capable to fabricate DCC components such as masonry units and paving blocks with low strength requirements. For the mixes 1.0-1.5% FR-D-FA50-RCM25, it could even be used as the construction material for the heavy-duty pavements owing to the higher long-term strength. Furthermore, mixes 1.0-1.5% FR-D-FA50-RC10, which could be identified as high-strength LWC as per AS1379 [180], were able to be used in the construction of structural LWC by virtue of their 28-day compressive and flexural strengths respectively exceeding 50 and 14 MPa, and 60-day strengths exceeding 65 and 19 MPa.

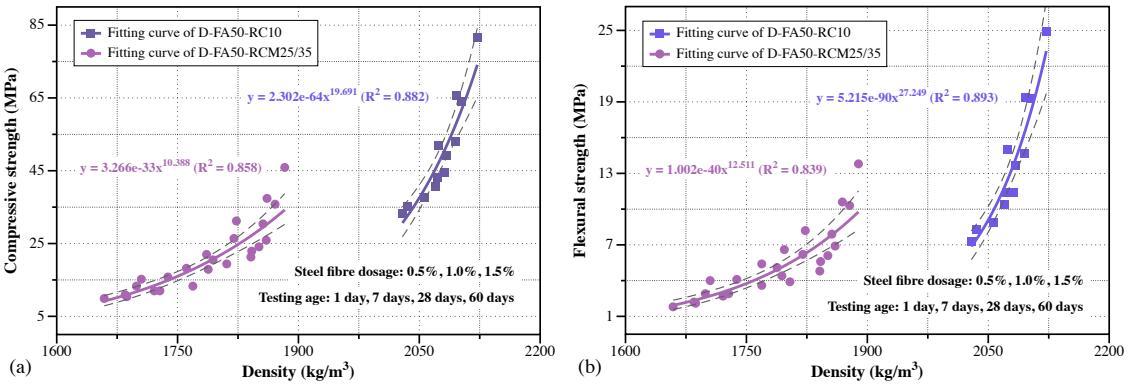

Fig. 5.27. Correlation between hardened density and (a) compressive as well as (b) flexural strengths of FR-DUHPC incorporating CR aggregate.

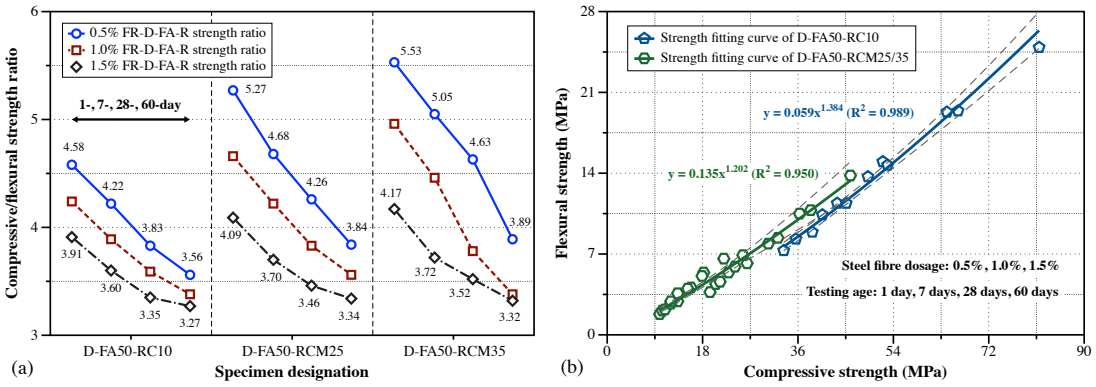

Fig. 5.28. (a) Strength ratio at various ages and (b) relationship between compressive and flexural strengths of FR-DUHPC incorporating CR aggregate.

5.4 Eco-friendly assessment

As reported above, the use of two environment-friendly raw materials (FA and CR) could evidently reduce the amount of cement and sand added in concrete mixes, which effectively mitigated the consumption of natural resources while improving the recycling of hazardous wastes. In this section, the eco-friendly benefit of the developed DUHPC containing various mixing amounts of FA and CR aggregate would be evaluated from two aspects of the cost and carbon footprint, so as to better demonstrate its sustainable characteristics.

5.4.1 Cost analysis

Fig. 5.29 gives the variation in estimated cost per cubic metre for each concrete mixture, where the cost is calculated on the basis of the mixture's mix proportions listed in Table 5.3 and the local market price for each raw material. As illustrated in Fig. 5.29(a), steel fibre, silica sand and silica fume were the three primary factors influencing the cost of 20-60% FA-mixed FR-DUHPC. As expected, the incorporation of FA to substitute partial cement could reduce the production cost of concrete due to the lower price of FA. The total cement cost per unit volume of concrete mixtures dropped from 279.6 to 107.5 CNY as the incorporation of FA increased from 20% to 60%, with a reduction of 61.6%. However, in the cases where CR aggregate were additionally incorporated, as shown in Fig. 5.29(b), the total expenditure per unit volume of rubberized concrete increased prominently with increasing substitution percentage of natural sand using CR aggregate. For example, the estimated cost, respectively, increased by 5.2%, 12.8% and 18.5%

when 10%, 25% and 35% of silica sand was substituted by rubber aggregate, as compared to original mixtures without CR at the same fibre reinforcement (1.5%). Besides, for mixes D-FA50-RCM35 with 1.5% fibre reinforcement, CR aggregate had become the second important factor influencing the concrete cost. This was mainly because the price of CR was significantly higher than that of natural sand owing to the operational process of the crushing, fibre separation and grinding of the waste tyres into fine rubber particles. In fact, most countries around the world used the processing methods of decomposition, crushing, pyrolysis and dumping to reduce the serious pollution of waste tyres on the environment, resulting in a huge amount of financial and resources losses. Thus, from the above perspective, the cost of CR aggregate (represented by purple columns) could be considered as zero, which was consistent with the viewpoint reported by Kazmi et al. [182]. In such instances, the total cost of rubberized dry concrete would change from the increase reported above to a decrease of 3.1%, 7.7% and 11.1%, respectively, as compared to original FA50 FR-DUHPC cost (2710.5 CNY). That is, the use of CR aggregate was capable of constructing/fabricating higher cost-effective dry concrete structures/components (including reduced raw material, maintenance and life cycle costs) with improved flexural stiffness and strain capacity along with enhanced resistance to fatigue and shrinkage. Moreover, as expected, steel fibre was likewise the major factor affecting the production cost of rubberized concrete owing to its higher material price. The increase in fibre dosage (0.5-1.5%) notably increased the total cost of rubberized concrete with fibre price accounting for

approximately 15.7-40.3%.

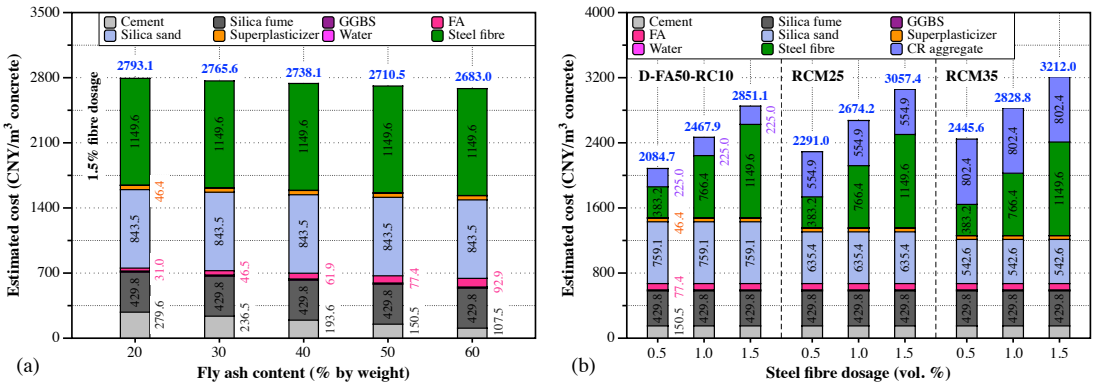

Fig. 5.29. Estimated cost of FR-DUHPC incorporating various contents of (a) FA and (b) CR aggregate.

5.4.2 Environmental impact analysis

The environmental impact of the developed DUHPC was evaluated with regard to the embodied CO_2 (ECO_2) emission and index for each concrete mixture. Fig. 5.30 exhibits in detail with regard to the ECO_2 emission values of a cubic metre concrete with different contents of FA and CR aggregate, using expression (5.4).

$$ECO_2\ emission = \sum_{i=1}^{n} \left(M_i \times ECO_{2_i}\right) \quad (5.4)$$

where i is the number of factors (including raw materials and curing) affecting the ECO_2 emission in the concrete mix, M_i is the content (kg/m^3) or duration (hour) of the foregoing i-th factor, and ECO_{2i} is the equivalent ECO_2 emission (CO_2-kg/kg) corresponding to the i-th factor, provided by references [188-190]. It should be noted that the recycle of waste rubber crumbs could effectively reduce the baneful effects on the natural environment and was also beneficial to the overall service life of dry concrete structures/units, therefore the value of ECO_{2i} of CR aggregate introduced was negative [190]. As depicted in Fig. 5.30(a), the addition of FA to

replace partial cement continuously reduced the carbon footprint per unit volume of dry concrete mixtures. Specifically, FA respectively contributed 0.3%, 0.5%, 0.8%, 1.0% and 1.3% of the total CO_2 emissions when the substitution level increased from 20% to 60%, while the value of ECO_2 emission of cement and the developed DUHPC decreased from 213.0 to 81.9 kg/m^3 and 479.1 to 351.1 kg/m^3, respectively, with a decrease of 61.6% and 26.7%. Generally, FA contributed to zero carbon footprint since it was the by-product of the coal combustion in power generation, and its ECO_2 originated from the energy consumption generated by filtration, extraction, grinding and drying operations [18]. Not surprisingly, steel fibre was still the major contributor to the environmental footprint of all mixtures, accounting for approximately 35.9-49.0% of the total CO_2 emissions. In terms of the rubberized concrete depicted in Fig. 5.30(b), it could be clearly seen that the ECO_2 emission value of all mixtures converted negative (negative ECO_2 emission) due to the inclusion of CR aggregate as a partial substitute for natural sand, with mixtures D-FA50-RCM25 and D-FA50-RCM35 being the most prominent (-710.2 and -1197.7 kg/m^3). That is, the use of rubber particles could greatly mitigate the consumption of natural resources and improve the environmental sustainability via reducing toxic chemicals entering the environment (air and soil). In addition, as for rubberized dry concrete with 0.5-1.5% fibre reinforcements, the higher fibre dosages contributed to greater ECO_2 emission and this effect was pronounced for the mixes containing 10% CR particles. Fig. 5.31 shows the variation in ECO_2 index of DUHPC, calculated as the ratio of the foregoing ECO_2 emission to 60-day compressive/flexural strength of the corresponding mixtures. As displayed,

the ECO_2 index in compression and flexure all prominently decreased as the FA content increased up to 50%, that is, the carbon footprint caused by the increase of unit strength tended to alleviate. This further supported the previous conclusion regarding the optimal content of FA substituting cement. For rubberized concrete with different steel fibre dosages, the values of the ECO_2 index were all negative, manifesting that the enhancement in both strengths of the studied mixtures had any adverse impact on the environment, especially when less steel fibres and more rubber crumbs were introduced.

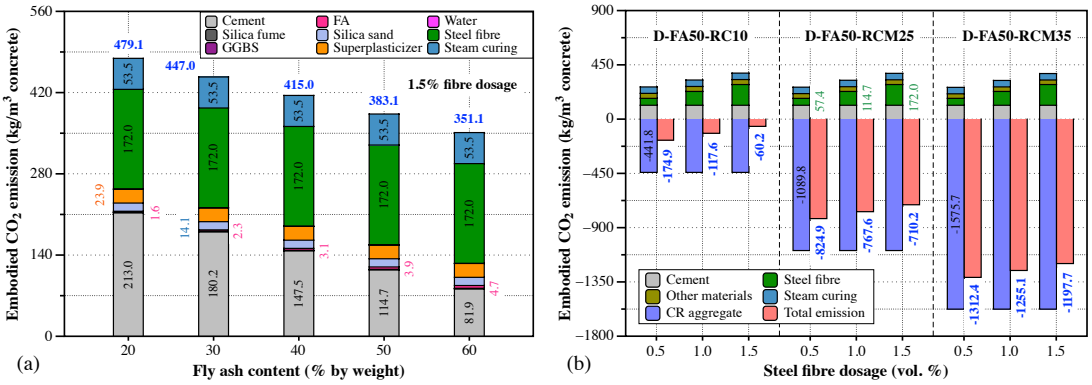

Fig. 5.30. Embodied CO_2 emission of FR-DUHPC incorporating various contents of (a) FA and (b) CR aggregate.

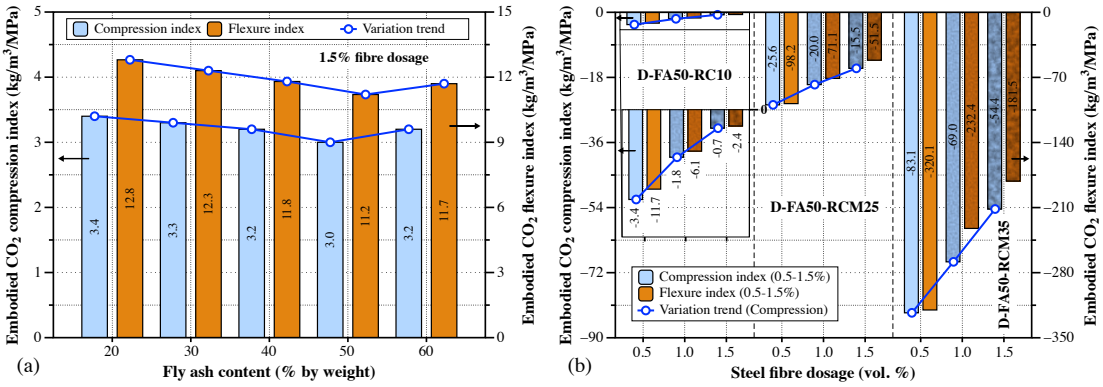

Fig. 5.31. Embodied CO_2 index of FR-DUHPC incorporating various contents of (a) FA and (b) CR aggregate.

Fig. 5.32 shows the correlation between ECO_2 emission and 60-day compressive strength of 20-60% FA-mixed FR-DUHPC, and compares its CO_2 footprint with other sustainable self-compacting UHPC [140-142, 188, 189, 191-193] and conventional dry concrete [79, 83, 105, 143, 194] summarized in the relevant literatures. As depicted, the enhancement in compressive strength led to a linear increment in ECO_2 emission with a satisfied goodness of fit of 0.915. Additionally, it could be clearly observed that the developed FR-DUHPC exhibited much lower CO_2 footprint as compared to the self-compacting UHPC under the condition of slightly lower or similar strength. Compared with the conventional dry concrete with fibre reinforcement, it demonstrated prominently higher strength behaviour with similar environmental impact. Therefore, the developed DUHPC is capable of constructing/manufacturing high-strength dry concrete structures/units while maintaining the fast-hardening, early-strength, and eco-friendly characteristics of conventional dry concrete.

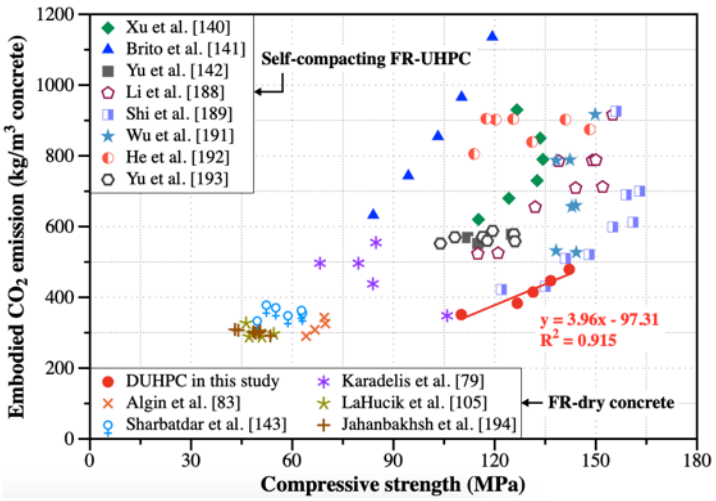

Fig. 5.32. Comparisons of embodied CO_2 emission of the developed 20-60% FA-mixed FR-DUHPC and other self-compacting FR-UHPC or FR-dry concrete.

5.5 Conclusion

This chapter focuses on assessing the mechanical behaviour and environmental benefit of the steel FR-DUHPC containing high-volume recycled waste materials (FA and CR), on the basis of the sustainable FR-DUHPC developed in Chapter 3. For this purpose, the mechanical property tests were performed on hardened mixtures with various substitution levels of FA and CR, as well as different fibre dosages. Afterwards, the eco-friendly assessment of these mixtures was carried out in terms of the cost and environmental impact analysis. In summary, the main conclusions are as follows:

1) The compressive/flexural strengths of FR-DUHPC enhanced gradually with curing age but reduced visibly with FA substitution level for cement, especially for mixtures with more FA at earlier ages. The compressive MOE and flexural cracking strength presented a similar variation trend. However, the strength loss in flexure was weaker than that in compression, and the contribution of FA effect to flexural strength gain was prominent.
2) Owing to the used moist/steam curing accelerated the early cement hydration and pozzolanic reaction rate of FR-DUHPC mixtures, the contribution of FA effect to both strengths at each age was evidently increased, particularly for the cases where 50% and 60% of cement were replaced after 28-day curing. Considering the sustainable development in resources and the effect of FA addition on the mechanical behaviour of FR-DUHPC at various ages, 50% of cement substitution conforming with the high-volume concept was determined

to be the suitable FA addition in this chapter.

3) Compared with the original FA50 FR-DUHPC with 1.5% fibre reinforcement, the use of CR aggregate resulted in a significant decrease in density, strength and MOE at all ages, especially for the cases where the medium sand was partially substituted. However, the adverse impact of rubber addition was less serious on flexural behaviour with a smaller strength attenuation.
4) For rubberized DUHPC with 0.5-1.5% fibre reinforcements, the mechanical properties enhanced gradually with fibre dosage and curing age, irrespective of CR substitution and combination. As expected, the positive effect of fibre dosage on flexure was still better than that on compression due to the used preparation of layered compaction rendered the steel fibres tend to be aligned parallel to the compacted layers, endowing fibres with more effective restraint on matrix cracking under flexural-tensile load.
5) In the case of 1.5% fibre reinforcement, the post-peak ductility of the studied mixtures under compression and bending loads was not evidently influenced by the increase in FA addition and the incorporation of CR aggregate, but was notably degraded with fibre dosage reduced from 1.5% to 0.5%. In addition, the stiffness of rubberized concrete attenuated prominently with CR addition, which was beneficial for dry concrete structures/units with large surface area to better resist the durability deterioration caused by fatigue and shrinkage.
6) The flexural behaviour benefits derived from the incorporation of steel fibres, FA and CR aggregate, as well as the eco-friendly benefits derived from the

cost saving, energy conservation and carbon emission reduction, render the developed LWC can be widely used in dry concrete applications with different strength requirements that are primarily subjected to bending load during the serviceability.

It was worth noting that in this section, the method of incorporating CR aggregate involved replacing silica sand of the same mass (mass substitution), resulting in an evidently higher amount of CR aggregate being incorporated as compared to the method of volume substitution. Hence, it could be predicted that incorporating CR aggregate at volumes ranging from 10% to 35% of the total silica sand volume would lead to the production of LWC with higher strength and improved properties at the same substitution levels adopted in this study.

Chapter 6

Repeated Impact Resistance of Steel FR-DUHPC: Effects of Fibre Length, Mixing Method, FA Content and CR Addition

6.1 Introduction

It is well known that the concrete-like brittle materials exhibit completely different mechanical responses under dynamic loads from those under static conditions, which evidently limits the application scenarios of such materials in engineering practice and increases the failure uncertainty of structural components during the service. Dry concrete, which contains the same raw material compositions but less water content as conventional cement-based self-compacting concrete, will inevitably be frequently suffered various types of dynamic loads in consideration of the usage scenarios of its structures and members [123]. For instance, airport runways need to withstand the repeated impacts from aircraft landings; overflow surfaces of concrete dams need to endure the cutting impact abrasion caused by flowing sandstones; and roof tiles need to resist the sustained impact load as well as varying speeds of hailfall.

Wang et al. [120, 121, 195] studied the compression behaviour and failure pattern of RCC under dynamic load via performing SHPB test considering material initial damage and sample size (diameters of 50, 75 and 100 mm). Furthermore, in their another research, the stress waves propagating between the interlayers were also investigated exhaustively under the same strain rate conditions, considering the layered compaction method commonly used in the construction of RCCD and

RCCP [94]. It was indicated that the impact of the strain rate effect on DIF of RCC strength was much weaker than that of self-compacting concrete, while the larger sample size contributed to higher dynamic strength, which was obviously contrary to the strength variation law under static loads. Moreover, the initial damage led to a more severe attenuation in the dynamic strength and toughness, especially at higher strain rates (≥ 60 s^{-1}), while its inherent stratification characteristic was beneficial to resist the propagation of stress waves within interlayers. Lin et al. [118] evaluated the seismic behaviour of a 132-meter-tall RCCD after Wenchuan M8 earthquake, focusing on its post-seismic hazard and structure integrity. Based on the spot survey and study, the dam's main structure remained intact with no visible cracking and failure despite the actual seismic load exceeding the design criteria upon which the dam was built, benefitted from the abutment reinforcement ensured the seismic stiffness throughout the dam, abutment and foundation. In terms of the seismic response analysis of RCCD using FEM, Ghaedi et al. [196, 197] numerically explored the effect of the flexible foundation and different sizes and shapes (circle, octagon and square) of galleries on the earthquake behaviour of Kinta RCCD in Malaysia, and Gharibdoust et al. [198] evaluated the influence of different base treatments (corresponded to different roughness) on the body cracking and base sliding of RCCD via employing the proposed pseudo dynamic testing method, followed by numerical verification on the above dam's properties through the sliding response analysis. In the analysis of the impact resistance of

dry concrete, Sharbatdar et al. [143] carried out the drop-weight impact test on RCC cylindrical samples (150 mm dia., 64 mm height) reinforced with four types of fibres. It was indicated that the samples reinforced with mono Kortta Emboss (2 kg/m^3) and steel (25 kg/m^3) fibres showed a better enhancement in multi-impact resistance (respectively, 2.7 and 2.9 times higher than the control case), and the inclusion of 30 kg/m^3 of steel fibres exhibited the best effect on preventing the rapid propagation of the multiple cracks from samples' cracking to complete rupture. Moreover, Hosseinnezhad et al. [199] and Adamu et al. [200] also used the same test method to examine the impact resistance of RCC containing RCA as well as CR particles and nano-silica material, respectively.

As reviewed above, a number of researches had been conducted for the dynamic property of dry concrete. However, the experimental research on its multi-impact resistance was undertaken in compliance with ACI guidelines, which focused on the anti-compression-impact performance of concrete material. Considering the characteristic of dry concrete structures/components that are mainly subjected to flexural-tensile load during serviceability, it is essential to investigate their flexural impact resistance under dynamic conditions. Hence, in this chapter, the foregoing impact performance of steel FR-DUHPC, which was developed in Chapter 3, was evaluated via performing a modified low-speed drop-weight impact test, drawing on the test method from other researchers for the fibre-reinforced self-compacting concrete [201-204]. The evaluation parameters include steel fibre length (6, 10

and 13 mm), mixing method (mono and hybridization), FA content (20-60% mass substitution for cement), and the addition of CR (10% mass substitution for silica sand).

6.2 Experimental programme

6.2.1 Materials and sample preparation

6.2.1.1 Raw materials and mix proportioning

In this experimental study, the raw materials utilized to prepare DUHPC tested samples consisted of Portland cement (P.C 42.5), silica fume, GGBS (Grade S95), FA (Grade I), natural quartz sand (fine, medium and coarse sand with aggregate size ranging 20-110 mesh), CR (20-40 mesh), straight steel fibre (diameter = 0.12 mm, tensile strength $\geq$ 4 GPa), high-performance superplasticizer and water. Fig. 6.1 exhibits the appearance of the main raw materials (FA, CR and steel fibre) that affect the impact resistance of FR-DUHPC concerned in this study, and the detailed mix proportions for the investigated mixes are exhibited in Table 6.1. In the group of D-F mixes, different steel fibre lengths (6, 10 and 13 mm) and mixing methods (mono and hybrid) were considered as the major affecting factors. For the designation of different mixes, F15 denotes the dosage of steel fibres, S, M and L, denote 6-mm short-length, 10-mm medium-length and 13-mm long-length steel fibre, respectively, and the item in the parenthesis indicates the fibre mixing regime. For example, F15S represents the mixture with 1.5% 6-mm mono steel fibre reinforcement, F10S05L denotes the mixture with 1.0% 6-mm and 0.5% 13-

mm double-hybrid steel fibre reinforcement, and F05SML corresponds to the mixture with 0.5% 6-mm, 10-mm and 13-mm ternary-hybrid fibre reinforcement. In addition, in the group of D-FA mixes, all the mixtures were reinforced with 1.5% 10-mm mono steel fibres, while the FA substitution content (20%, 30%, 40%, 50% and 60% by mass) for cement was considered as the primary influencing factor. In addition to the fibre dosage remained constant, the gradual increase in the mass ratio of other materials to cement resulted from the increase in FA addition substituting cement. Then, based on the optimal FA addition (50% substitution) concluded in Chapter 5, CR particles were introduced into FR-DUHPC mixtures as the completed replacement of coarse silica sand (20-40 mesh, accounted for 10% of the total mass of silica sand) to evaluate the influence of rubber aggregate on the impact resistance of the developed dry concrete, that is, the FA50-R-F15M mix. It should be pointed out that the mixes F15M and FA20-F15M, respectively classified in the groups D-F and D-FA, contained the same constituent materials' proportion, which was the optimal mixture proportion (including steel fibre dosage) obtained from the experimental study summarized in Chapter 3.

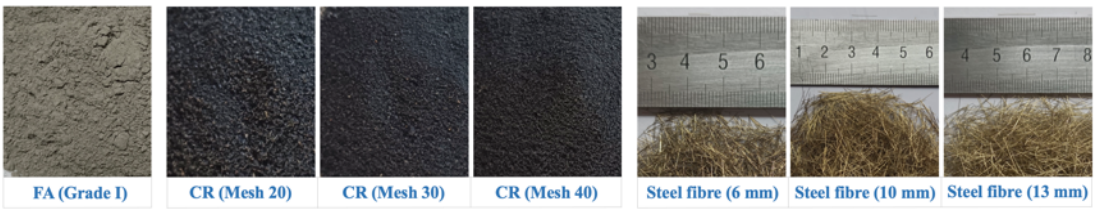

Fig. 6.1. Appearances of the major raw materials of FA, CR aggregate and steel fibre.

Table 6.1

Mixture proportions of studied FR-DUHPC by weight.

Group	Sample	Cement	SLF	FA	GGBS	Sand	CR	Water	Fibre (%)
D-F	F15S, F15M, F15L	1.00	0.15	0.31	0.08	2.84	--	0.25	1.5
	F05S10M, F10S05M, F05S10L, F10S05L, F05M10L, F10M05L, F05SML	1.00	0.15	0.31	0.08	2.84	--	0.25	1.5
D-FA	FA20-F15M	1.00	0.15	0.31	0.08	2.84	--	0.25	1.5
	FA30-F15M	1.00	0.18	0.55	0.09	3.36	--	0.29	1.5
	FA40-F15M	1.00	0.22	0.89	0.11	4.10	--	0.36	1.5
	FA50-F15M	1.00	0.29	1.43	0.14	5.28	--	0.46	1.5
	FA60-F15M	1.00	0.40	2.40	0.20	7.38	--	0.65	1.5
D-R	FA50-R-F15M	1.00	0.29	1.43	0.14	4.81	0.47	0.46	1.5

Note: “SLF” denotes silica fume and “%” denotes volume fraction.

6.2.1.2 Sample preparation and curing

The procedure of mixing FR-DUHPC with inclusions of various contents of steel fibres and FA, as well as CR aggregate was primarily the same as that reported in Chapter 5. Unlike the conventional self-compacting FR-UHPC, superplasticizer and water were added after the cementitious materials, aggregate (including CR particle) and steel fibres were uniformly dry-mixed in a concrete mixer. The use of the foregoing mixing sequence could somewhat alleviate the agglomeration or intertwining of steel fibres (especially for longer ones at higher dosages) in dry

concrete mixture with lower moisture content and a more viscous appearance. In addition, the real-time state of the fresh mixture should be paid attention to during wet stirring to prevent the workability from being deteriorated due to the increased water dissipation caused by the excessive mixing. Based on multiple preliminary mixing, a satisfied mixture consistency and a uniform distribution of steel fibres could be achieved via controlling the wet stirring duration within 6-8 mins. After the stirring of the fresh mixture was finished, prismatic beam samples having 40 mm × 40 mm × 160 mm were poured in three layers via utilizing a shaking table with a steel surcharge providing downward compaction to the mixture surface. The vibrated duration of each layer was controlled at 30-40 s, and the cementing paste derived from the vibrated compaction of the fresh mixture was conductive to the interfacial bonding between the layers. Once the moulding of the beam samples was completed, the plastic film was attached to the mixture's surface and 3 h later, the samples together with the moulds were put into an insulated water tank for further moist/steam curing (50 ℃) until 24 h. Subsequently, they were demoulded and cured for another 6 and 27 days in room-temperature water. Fig. 6.2(a) exhibits the detailed flow-process diagram of preparing FR-DUHPC reported above. Totally 288 beam samples, consisting of 6 identical ones of each mix at three ages, were moulded and cured. It should be noted that prior to the impact test, the bottom mid-span area of the beam samples was ground flat and tightly adhered with a 50-mm-length strain gauge to record the accurate flexural impact test data, as depicted in Fig. 6.2(b).

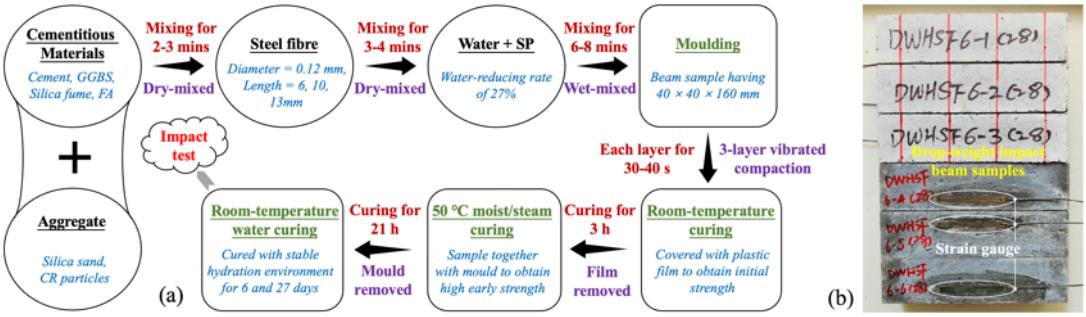

Fig. 6.2. (a) Detailed preparation flow and (b) typical FR-DUHPC beam samples prior to impact test.

6.2.2 Testing procedure

6.2.2.1 Drop-weight impact test

For the aim of investigating the flexural impact responses of the developed FR-DUHPC under low-speed impact loads, a modified instrumented impact testing machine with a free-falling weight as the main component was used, as depicted in Fig. 6.3. All beam samples were tested at the end of 1,7 and 28-day curing. Prior to the impact, a beam sample having a length of 160 mm was fixed on roller bearings with a spacing of 120 mm. Then, a concave steel gasket (thickness = 3 mm, width = 40 mm) was clamped at the centre of the upper surface of the beam sample to prevent the local damage under impact load. The horizontal distances between the edge of the steel gasket and support on both sides were all 40 mm. Two column sliding tracks were symmetrically fixed by the drop weight to ensure the hammer tup fall vertically and impact the mid-span of samples, while ignoring the dynamic friction between the falling weight and two sliding tracks. The impact load was induced by the falling weight with a steel dome-nosed tup falling freely from a pre-set height and hitting the steel sheet, and it was measured in real time

via a load cell mounted on the tup's rear part. The overall mass of the drop weight was 8.0 kg and the falling height was 120 mm, providing a constant strike velocity of 1.53 m/s and a kinetic energy of 9.4 J per hit. During the impact test, the drop weight was fallen repeatedly and the number of strikes causing the rupture of the strain gauge, which was affixed to the bottom tension area of the concrete sample, was considered the cracking resistance factor. It is noteworthy that the length of the applied strain gauge was 60 mm, which was greater than the mid-span impact bending area of the beam samples (40 mm). This consequently ensured that the strain gauge effectively captured the impact cracks, enabling the measurement of the cracking resistance factor to its maximum extent, as illustrated in Fig. 6.4(a). Furthermore, the number of strikes when the macro-cracks propagated to the top surface of the beam sample was designated as the final failure resistance factor, as shown in Fig. 6.4(b).

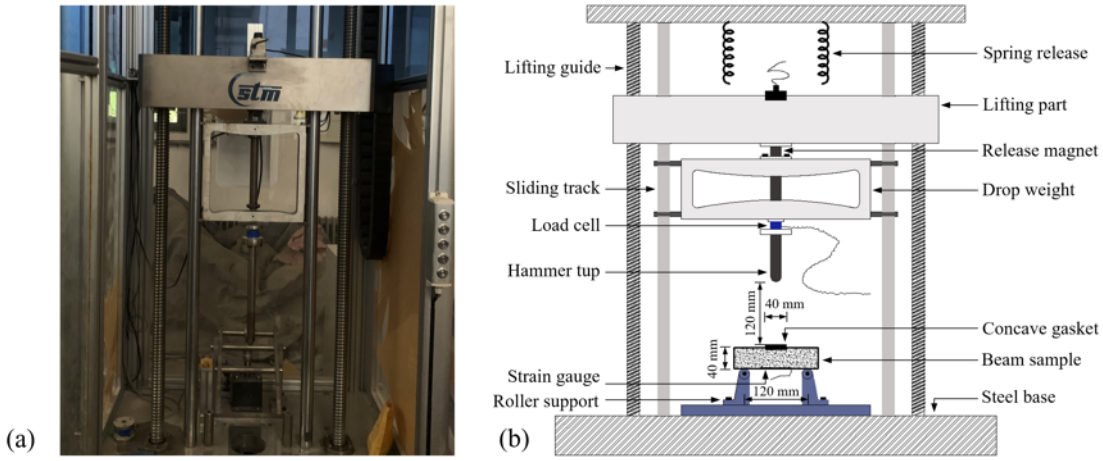

Fig. 6.3. Low-speed drop-weight impact test: (a) testing machine overview and (b) setup schematic diagram.

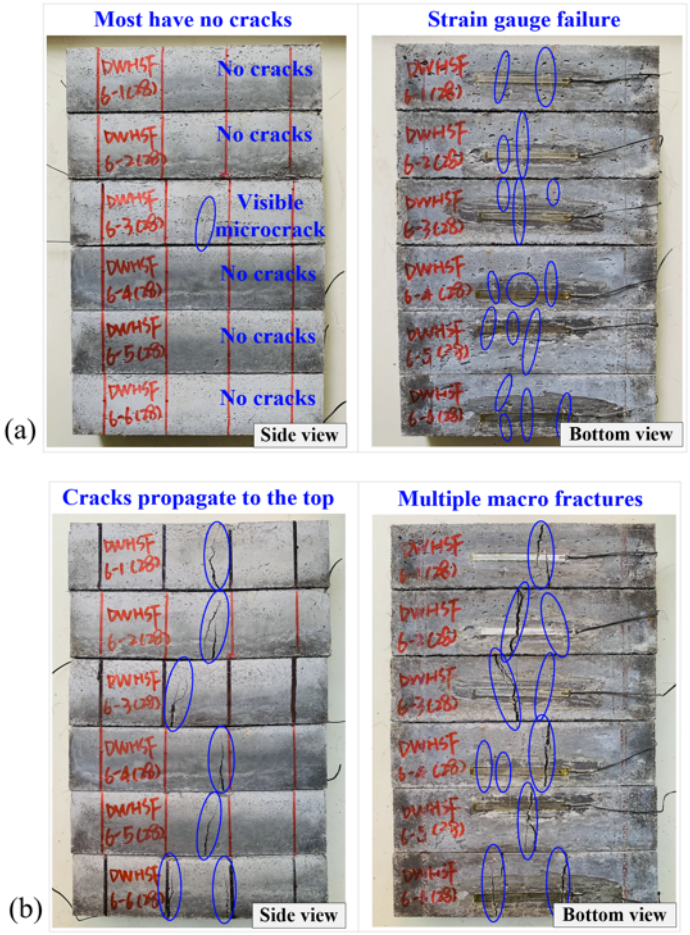

Fig. 6.4. Judgment basis for (a) initial cracking and (b) ultimate damage of samples.

6.2.2.2 Residual strength test

After the drop-weight impact tests, the four-point bending test, as per Chinese national standards GB/T50081-2019 [148] and CECS13-89 [149], was conducted on damaged FR-DUHPC beam samples to assess their residual bearing capacity (Fig. 6.5). During the test, a continuous compression load with a constant rate of 0.05 mm/min was applied to the beam sample using a 10-ton-capacity universal testing machine to ensure the quasi-static condition. Loading would be stopped when the sample reached its maximum bearing capacity, and the residual flexural strength could consequently be obtained by applying the equation [149]:

$$f_{rr} = PL/bh^2 \quad (6.1)$$

where f_{rr} is the residual flexural strength (MPa), P is the peak load (N), L is the clear span between the roller supports (= 120 mm), b and h are the width and depth of the beam sample (= 40 mm), respectively.

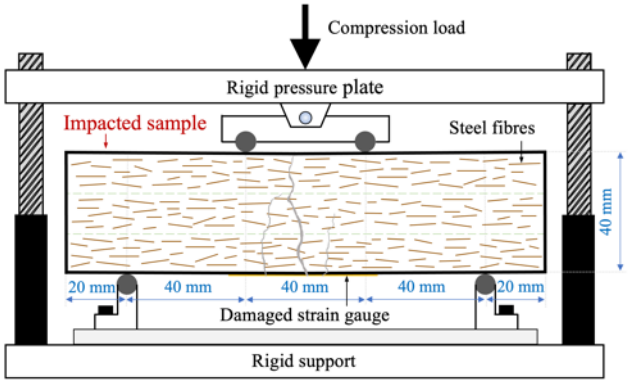

Fig. 6.5. Schematic of four-point bending residual strength test setup.

6.3 Results and discussion

6.3.1 Flexural impact behaviour

6.3.1.1 Cracking and ultimate failure resistance

As reported, low-speed drop-weight impact tests were performed on FR-DUHPC samples (1.5% steel fibre reinforcement) upon curing. Data from the impact tests is exhibited in detail in Tables 6.2 (mono/hybrid FR-DUHPC) and 6.3 (HVFA-/CR-mixed FR-DUHPC), in which N_c is the initial crack resistance factor and N_d is the ultimate damage resistance factor of the impacted samples. In order to minimize the experimental error caused by the strong dispersion of the drop-weight impact test data, 6 identical beam samples of each mixture were cast and moulded for testing and then their average was taken as the final result.

Table 6.2

Summary of drop-weight test results of mono/hybrid FR-DUHPC.

Samples		N_c (number)			N_d (number)			$(N_d-N_c)/N_c$ (%)		
(Mono/Hybrid)		1-d	7-d	28-d	1-d	7-d	28-d	1-d	7-d	28-d
Control (No fibre)		1 (0.00)	1 (0.00)	1 (0.00)	1 (0.00)	1 (0.00)	1 (0.00)	0	0	0
Single	F15S	1.0 (0.00)	1 (0.00)	1.3 (0.47)	1.8 (0.69)	3.0 (0.82)	4.8 (1.21)	80.0	200.0	269.2
	F15M	1.9 (0.83)	2.2 (0.69)	2.6 (0.74)	7.7 (1.25)	12.7 (1.60)	18.7 (3.35)	305.3	477.3	619.2
	F15L	2.5 (0.50)	2.8 (0.37)	3.2 (0.69)	16.5 (2.36)	21.0 (2.52)	28.5 (2.75)	560.0	650.0	790.6
Double	F05S10M	1.5 (0.50)	1.7 (0.75)	1.9 (0.62)	6.2 (1.57)	10.7 (2.21)	15.3 (5.62)	313.3	529.4	705.3
	F10S05M	1.3 (0.47)	1.3 (0.47)	1.5 (0.50)	3.7 (1.49)	5.8 (1.07)	8.5 (3.45)	184.6	346.2	466.7
	F05S10L	2.0 (0.58)	2.2 (0.37)	2.5 (0.96)	8.8 (1.34)	12.2 (1.86)	17.7 (2.36)	340.0	454.5	608.0
	F10S05L	1.3 (0.47)	1.3 (0.47)	1.6 (0.52)	5.0 (1.53)	6.2 (1.77)	9.2 (3.18)	284.6	376.9	475.0
	F05M10L	2.3 (0.47)	2.5 (0.50)	2.8 (0.37)	15.8 (3.08)	19.7 (2.28)	25.8 (3.80)	587.0	688.0	821.4
	F10M05L	2.2 (0.37)	2.3 (0.75)	2.6 (0.58)	13.0 (2.16)	17.3 (3.25)	22.2 (4.06)	490.9	652.2	753.8
Ternary	F05SML	1.7 (0.75)	1.8 (0.69)	2.0 (0.69)	7.7 (1.59)	11.5 (2.63)	14.8 (2.79)	352.9	538.9	640.0

Notes: items in parentheses denote standard deviation (SD) of measured parameters.

Table 6.3

Summary of drop-weight test results of HVFA-/CR-mixed FR-DUHPC.

Group	Samples	N_c (number)			N_d (number)			$(N_d\text{-}N_c)/N_c$ (%)		
		1-d	7-d	28-d	1-d	7-d	28-d	1-d	7-d	28-d
D-FA	FA20-F15M	1.9 (0.83)	2.2 (0.69)	2.6 (0.74)	7.7 (1.25)	12.7 (1.60)	18.7 (3.35)	305.3	477.3	619.2
	FA30-F15M	1.8 (0.37)	2.2 (0.37)	2.6 (0.94)	6.8 (1.34)	12.3 (1.70)	18.5 (3.04)	277.8	459.1	611.5
	FA40-F15M	1.7 (0.47)	2.0 (0.00)	2.5 (0.76)	5.8 (1.21)	10.5 (1.61)	18.0 (2.24)	241.2	425.0	620.0
	FA50-F15M	1.3 (0.47)	1.7 (0.47)	2.2 (0.69)	3.7 (1.11)	7.3 (2.49)	17.2 (1.68)	184.6	329.4	681.8
	FA60-F15M	1.0 (0.00)	1.3 (0.75)	1.8 (0.69)	1.5 (0.50)	4.2 (1.07)	15.3 (1.89)	50.0	223.1	750.0
D-R	FA50-R-F15M	1.0 (0.00)	1.0 (0.00)	1.2 (0.37)	1.3 (0.47)	1.8 (0.37)	3.8 (0.69)	30.0	80.0	216.7

Notes: items in parentheses denote standard deviation (SD) of measured parameters.

Fig. 6.6 shows the effect of steel fibre length and mixing method on the initial crack and ultimate failure of mono and hybrid FR-DUHPC under impact load. Compared with the reference mixture without fibre reinforcement, the use of any length and mixing method of steel fibres could significantly improved the flexural impact performance of the studied mixtures. For mono reinforcement, the optimal multi-strike resistance belonged to F15L mixtures, followed by F15M and F15S mixtures. The sequence was consistent with the result of static flexural behaviour as reported in Chapter 4. However, it should be noted that in the static test, the 1-28-day flexural strength values of 6-mm FR-DUHPC were no more than 50% different from those of 10- and 13-mm ones. But in the dynamic test, the impact behaviour of short fibre reinforcement was markedly weaker than that of the other two lengths of fibres. For example, the 28-day resistance factors of initial crack and ultimate failure of F15L samples were, respectively, 2.5 and 5.9, as well as 1.2 and 1.5 times the corresponding factors of F15S and F15M samples. In terms of hybrid FR-DUHPC, the use of any shorter steel fibres to replace partial longer ones in the mixes would lead to an evident reduction in N_c and N_d, and the more use of 6-mm fibres, the more severe the reduction was. As an illustration, samples F15M and F15L subjected to final failure after 18.7 and 28.5 drop-weight strikes, respectively, at the age of 28 days, while as the ratio of short steel fibres replacing the other two ones increased, the prepared samples could only withstand 15.3 and 8.5 (decreased by 18.2% and 54.6%), as well as 17.7 and 9.2 (decreased by

37.9% and 67.7%) impacts, respectively. It was reported by Wu et al. [152] that the impact energy required to damage UHPC was mostly formed with two parts, namely, the energy to destroy the concrete matrix along with the energy to pull out/break the toughening materials. In this study, although 6-mm steel fibres at the same dosage could shape a denser network microstructure within the matrix relying on their quantitative advantage, the insufficient anchoring length between fibres and matrix rendered it unable to effectively restrict the rapid development of impact cracks under drop load. Consequently, the mixtures with more addition of 6-mm fibres presented poor impact performance. Nevertheless, if the original toughening network was optimized via incorporating the same dosage of steel fibres with a slightly shorter length into the mixture (increased fibre quantity and decreased reinforcement spacing), the mixtures exhibited an acceptably reduced impact number. As an illustration, the impacts causing the cracking and failure of samples F05M10L at 28 days were, respectively, 2.8 and 25.8, approximately 12.5% and 9.5% lower than those of the original F15L samples. It was noteworthy that whichever mixing method was adopted, the longer fibres contributed to a better improvement in impact performance of the prepared mixtures with curing age, which manifested by the larger resistance factor difference in the histogram diagrams at different ages.

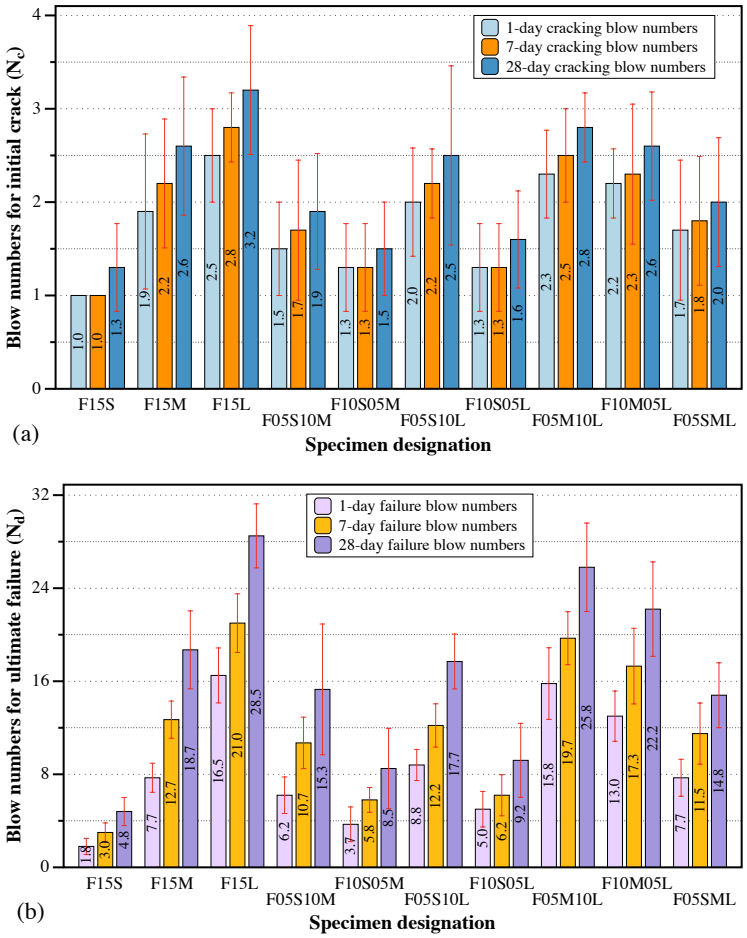

Fig. 6.6. Impact number of (a) initial crack and (b) ultimate failure of mono/hybrid FR-DUHPC after 1, 7 and 28-day curing.

Fig. 6.7 depicts the effects of FA content and CR addition on the initial crack and ultimate failure of mono FR-DUHPC under drop-weight impact load. For HVFA-mixed FR-DUHPC mixtures, the number of impacts at both initial cracking and ultimate failure gradually decreased with increasing FA content up to 28 days, but notably increased with curing age, especially for the mixtures incorporating higher FA additions. It should be noted that the cracking resistance factor (Fig. 6.7(a)) exhibited an evident reduction at all ages when FA content exceeded 40%, which was slightly different from the variations of static flexural property of identical FR-

DUHPC mixtures reported in Chapter 5 (significantly deteriorated when exceeded 50%). The same variation could also be observed for 1-day failure resistance factor shown in Fig. 6.7(b) (indicated by blue line). That is, the negative effect of cement dilution on the early/long-term impact cracking and early impact failure of FR-DUHPC was more evident. However, with the extension of curing time, the positive impact derived from FA secondary hydration effectively compensated for the foregoing adverse effect of cement dilution, rendering the failure resistance factor of mixtures with higher FA contents significantly improved. For example, the 1-day N_d of FA50-F15M and FA60-F15M samples was reduced by 52.0% and 80.5%, respectively, as compared to FA20-F15M samples, while at 28-day curing, the corresponding reduction was only 8.0% and 18.2%, respectively (indicated by green line in Fig. 6.7(b)). That is, the influence of FA incorporation on the long-term impact failure was basically the same as that on the static bending behaviour of identical samples. In the case of CR-mixed FR-DUHPC, i.e., the mixture FA50-R-F15M, the use of CR particles to substitute coarse sand significantly degraded the impact resistance of the studied concrete. At the age of 1 day, 7 and 28 days, the samples experienced initial cracking after 1.0, 1.0 and 1.2 impacts, which decreased by 23.1%, 41.2% and 45.5%, and then suffered final failure after 1.3, 1.8 and 3.8 impacts, which decreased by 64.9%, 75.3% and 77.9%, respectively, as compared to the control mixture FA50-F15M without CR addition. In a nutshell, the pozzolanic effect of FA exhibited a weaker impact on improving the impact

resistance (especially resistance to ultimate failure) of mixtures containing rubber aggregate. Moreover, the N_d at three ages was only increased by 30.0%, 80.0% and 216.7% in comparison with the corresponding N_c, which was far lower than 184.6%, 329.4% and 681.8% of control mixture. The palpable attenuation was due to the debilitated ITZ caused by the weak bonding along with poor anchorage between CR aggregate and cement paste as well as steel fibres, and the impact load greatly accelerated the development/propagation of micro-cracks to macro-perforate-cracks [2, 183].

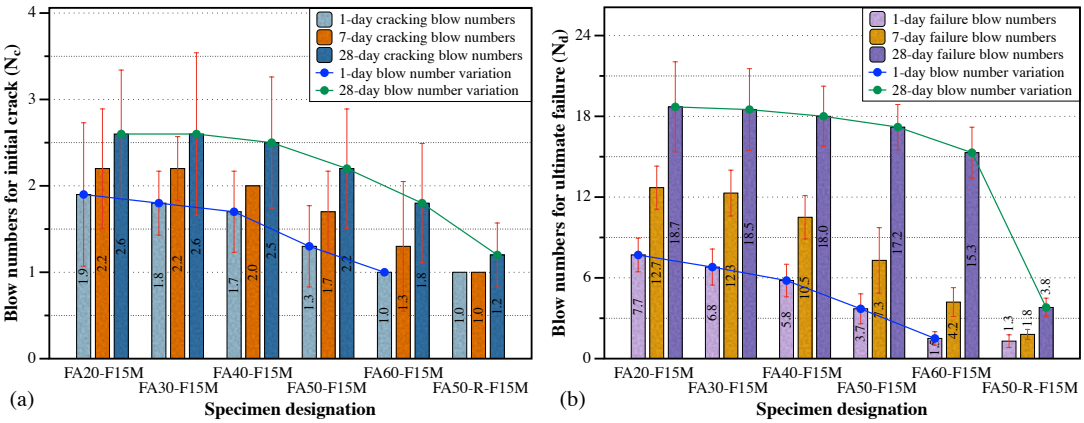

Fig. 6.7. Impact number of (a) initial crack and (b) ultimate failure of HVFA-/CR-mixed FR-DUHPC after 1, 7 and 28-day curing.

In order to more intuitively demonstrate the ability of the studied FR-DUHPC to continue to resist the impact until final damage after first cracking, the indicator of impact ductility ((N_d-N_c)/N_c) was adopted as depicted in Fig. 6.8. For mono fibre reinforcement shown in Fig. 6.8(a), longer fibre length and curing age contributed to better impact ductility up to approximately 8 times higher. It should be pointed out that the contribution of 13-mm fibres on mixtures' impact ductility seemed to

be prominent at an earlier age, but this positive impact gradually weakened with curing time (decreased ascending slope for F15M and F15L samples from 7 to 28 days). Reason for this phenomenon might be that at the initial stage of curing, the relatively poor bonding between steel fibres and matrix rendered the longer ones to more effectively withstand the repeated impacts of the falling weight by virtue of their anchorage length advantage. With the extension of curing age, 10-mm steel fibres demonstrated a more evident improvement benefitted from the quantitative advantage along with the enhanced bonding performance. For hybrid fibre-reinforced samples, an evident attenuation in impact ductility occurred in the cases where the 1.0% 6-mm fibres were introduced. Interestingly, for the mixtures with little or no 6-mm fibres (F05S10M, F05M10L and F10M05L), they presented almost or even better ductility than original mono reinforcements (F15M and F15L) at all testing ages. For instance, the 1- and 28-day impact ductility of F05M10L was, respectively, calculated as 587.0% and 821.4%, observably higher than the corresponding values of original F15M samples (560.0% and 790.6%). In other words, the optimized toughening network endowed the prepared mixtures with excellent multiple impact resistance both at the initial stage of curing and during service. In the cases where the FA content and CR addition were considered (Fig. 6.8(b)), the increase in FA content and the incorporation of CR aggregate both reduced the impact ductility of the studied mixtures up to 7 days. As expected, the flexural impact ductility at 28 days improved considerably with FA content by virtue of the continuous contribution of FA pozzolanic effect on matrix strength,

especially for mixtures with more FA. However, for CR-mixed FR-DUHPC, its 28-day impact ductility (217.6%) was apparently worse than that of the control one (FA50-F15M, 681.8%), indicating that the use of CR aggregate greatly weakened the secondary hydration effect of FA and led to an evidently degraded multiple impact resistance upon cracking.

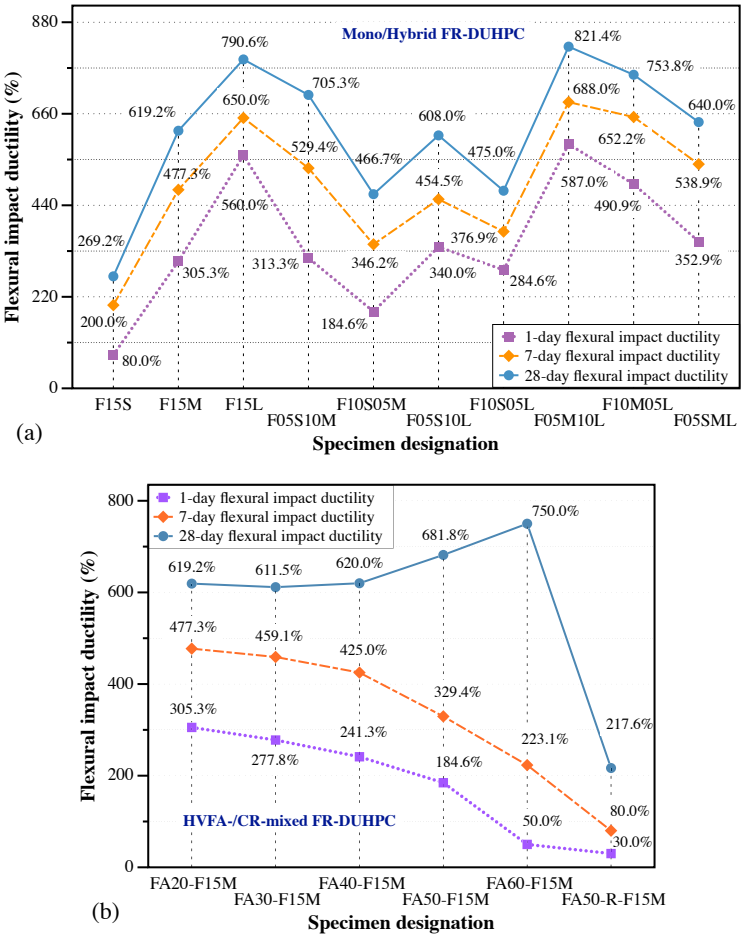

Fig. 6.8. Impact ductility of (a) mono/hybrid and (b) HVFA-/CR-mixed FR-DUHPC after 1, 7 and 28-day curing.

6.3.1.2 Impact force time history

The representative impact force time histories of FR-DUHPC after corresponding first cracking and final failure are shown in Fig. 6.9. The force was measured via

a load cell mounted on the rear part of hammer tup. As could be observed that the impact force time histories of the beam sample under drop-weight impact can be roughly divided into four phases. During the first phase, the tup with a certain mass fell freely from a fixed height and stroke the beam sample in a static state. The contact force reached its maximum value once the sample gained maximum acceleration along the hit direction. Then, the history entered the second phase, in which the beam sample deflected with the falling tup along the hit direction and continuously absorbed the impact energy. When the speed of the tup decreased to zero, the second phase ended, at which point the sample's deflection reached its limit and the energy was fully absorbed. Subsequently, the sample recovered partial deformation relying on its own stiffness along with the bearing support, and thus causing the tup rebound. This process corresponded to the third phase and ended with the tup separating from the impact surface. Finally, the concrete sample vibrated freely until the residual impact energy was completely dissipated (Phase IV). The overall time history was similar to that reported by Wei et al. [151], who prepared the large-scale beam specimens (168 × 168 × 2000 mm) to resist the impact of a drop hammer weighing 641.0 kg.

Compared with the impact force-time curve at initial cracking shown in Fig. 6.9(a), the prepared concrete samples still exhibited the same four-phase time history characteristics at ultimate failure (Fig. 6.9(b)), owing to the bridging effect of steel fibres on matrix cracks. However, its peak force value reduced to a certain extent due to the existence of the initial damage of beam samples, although the falling tup speed was constant during each hit. In addition, the formation and continuous

propagation/development of matrix cracks gradually deteriorated the stiffness of the impacted samples, which resulted in a notable diminishment in the secondary wave peak within the second phase. Moreover, the ability of the sample to recover its own partial deformation in the third phase attenuated evidently.

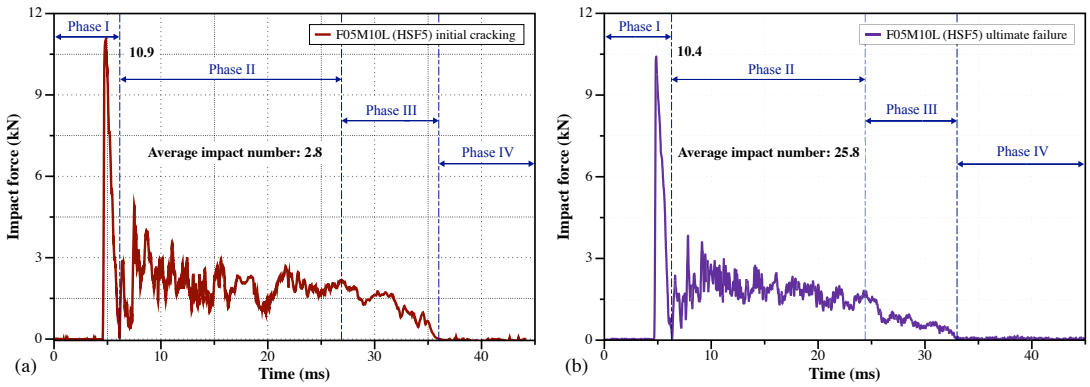

Fig. 6.9. Typical impact force-time curves at (a) initial cracking and (b) final failure of FR-DUHPC samples.

Fig. 6.10 exhibits the 28-day time histories of the impact force of mono/hybrid FR-DUHPC focusing on Phase I. For the peak force, it gradually increased from 9.2 to 10.5 kN with the use of longer steel fibres in the mono fibre reinforcement, as shown in Fig. 6.10(a). The peak force then reduced to some extent after samples were subjected to multiple impacts. Under the ultimate failure condition shown in Fig. 6.10(b), the less force drop was samples F15L and F15M, whereas the F15S samples exhibited the most reduction of approximately 12% comparative to the cracking peak force. That is, the concrete reinforced with longer fibres had better residual performance even after more impacts. For hybrid FR-DUHPC cases, the variations in peak force after initial cracking and final failure illustrated a similar attenuation trend to those of samples with mono fibre reinforcement. The evident

reduction occurred in cases with more 6-mm fibre addition, to approximately 10.4% and 13.4% for F10S05M (from 9.6 to 8.6 kN) and F10S05L (from 9.7 to 8.4 kN) samples, respectively. Conversely, the degradation in stiffness of F05M10L and F10M05L samples was not evident after being subjected to more hits. It should be pointed out that the peak force of hybrid FR-DUHPC at the above two cracking stages showed comparable, slightly higher/lower values than that of the original cases with single-type steel fibres. However, their static compressive and flexural strengths were slightly or significantly lower than those of the latter, as indicated in Chapter 4, which could be explained by the research finding that the concrete with hybrid reinforcement had a higher DIF under dynamic load [152].

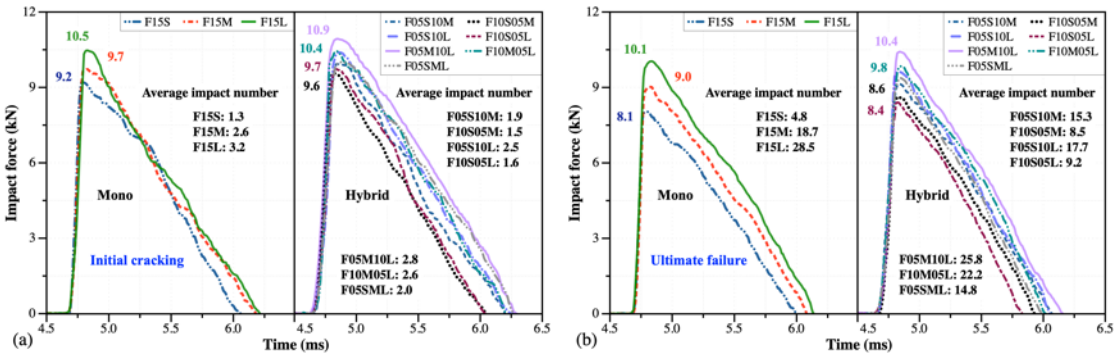

Fig. 6.10. Time histories of impact force of mono/hybrid FR-DUHPC at (a) initial cracking and (b) ultimate failure.

Fig. 6.11(a) shows the typical 28-day impact force time histories of FR-DUHPC with 50% of the cement substituted by FA (FA50-F15M). As displayed, the peak force at the cracking was 9.5 kN after samples were subjected to approximately 2.2 strikes. Subsequently, as the number of impacts increased to approximately 17.2, the peak force at the ultimate failure dropped to 8.7 kN, with a decrease of

8.4%. Compared with the original concrete samples (FA20-F15M) drawn as red lines, in addition to a slight decrease in the number of hits, HVFA-mixed samples demonstrated comparable peak impact force values and curve profile, which was attributed to the enhancement of matrix strength as well as the improvement of matrix-fibre anchorage benefited from the moist/steam curing and the following FA pozzolanic effect [110, 205]. However, after rubber particles were incorporated into FA50-F15M mixes to substitute partial silica sand (Fig. 6.11(b)), the 28-day peak force of CR-mixed FR-DUHPC at both initial cracking and final failure stages decreased notably with evidently reduced impact numbers (1.2 and 3.8 impacts), respectively, from 9.5 to 4.6 kN (reduced by 51.6%) and 8.7 to 2.7 kN (reduced by 69.0%). Additionally, the duration of force histories in Phases I, II and III was significantly shortened comparative to that shown in Fig. 6.9, and the secondary peak value after the peak force was also observably diminished. That is, the use of rubber aggregate attenuated the flexural stiffness of dry concrete and greatly weakened its capability to resist the cracking and postpone the final failure, even if the amount of CR incorporated was only 10% of the total mass of aggregate.

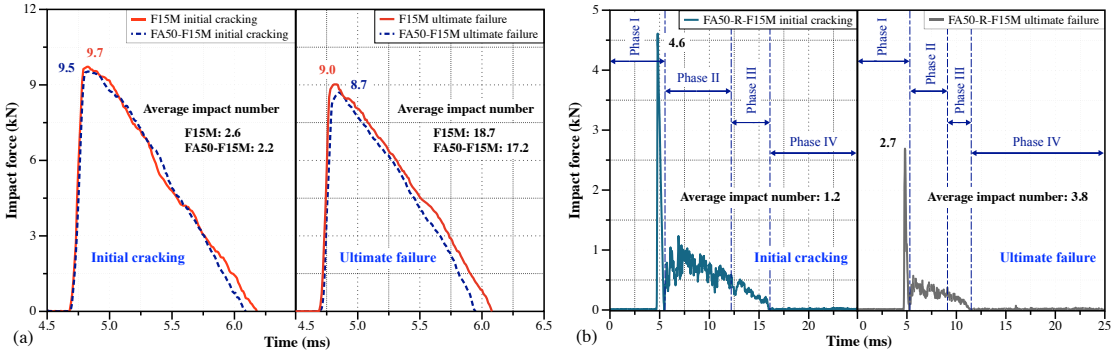

Fig. 6.11. Time histories of impact force of (a) HVFA50- and (b) CR-mixed FR-DUHPC at initial cracking and ultimate failure.

6.3.1.3 Failure patterns and cracks propagation

The typical failure patterns of mono/hybrid FR-DUHPC beam samples after drop-weight impact tests are displayed in Fig. 6.12. All beam samples remained intact after repeated impacts and presented obvious flexural-tensile responses within the mid-span area. It could be seen from Fig. 6.12(a-c), a relatively wide principal crack gradually extending from the bottom to the top appeared on beam samples with 6-mm fibre reinforcement. However, in addition to narrower principal cracks, the samples reinforced with longer fibres (F15M and F15L) were accompanied with many minor-cracks, and their tips were also bifurcated into several scattered micro-cracks like “tree branches”. Reason for this might be that the short fibres had low impact toughening efficiency under the repeated action of impact load. Once the initial crack appeared on matrix, it rapidly widened and propagated to the impact point and finally caused the samples to be damaged. It was reported by Hao et al. [206] and Holschemacher et al. [207] that the pull-out of steel fibres from the matrix was the primary failure mode of HPC under low-rate impact loads. Therefore, at a higher fibre additions, longer steel fibres could rely on their size advantage as well as the dense network to redistribute the flexural-tensile stress between the matrix and fibres, and thus effectively restrain the rapid development of impact cracks after cracking. In addition, the joint propagation of multiple minor-cracks contributed mixtures to absorbing and dissipating more impact energy. For the cases of hybrid reinforcement, the use of 6-mm fibres to replace any length of longer ones caused a reduction in the number of minor-cracks and a widening of the principal cracks, as shown in Fig. 6.12(d-e, h and k). However, the samples

reinforced with hybrid 10-/13-mm fibres exhibited similar failure patterns to F15M and F15L, and their bottom showed many minor/micro-cracks except for principal cracks (Fig. 6.12(f-g and i-j)). This was mainly attributed to the optimization of the original single fibre composition via fibre hybridization, in which more and longer steel fibres could bridge the impact cracks by virtue of their excellent anchoring performance with concrete matrix [204, 206, 207].

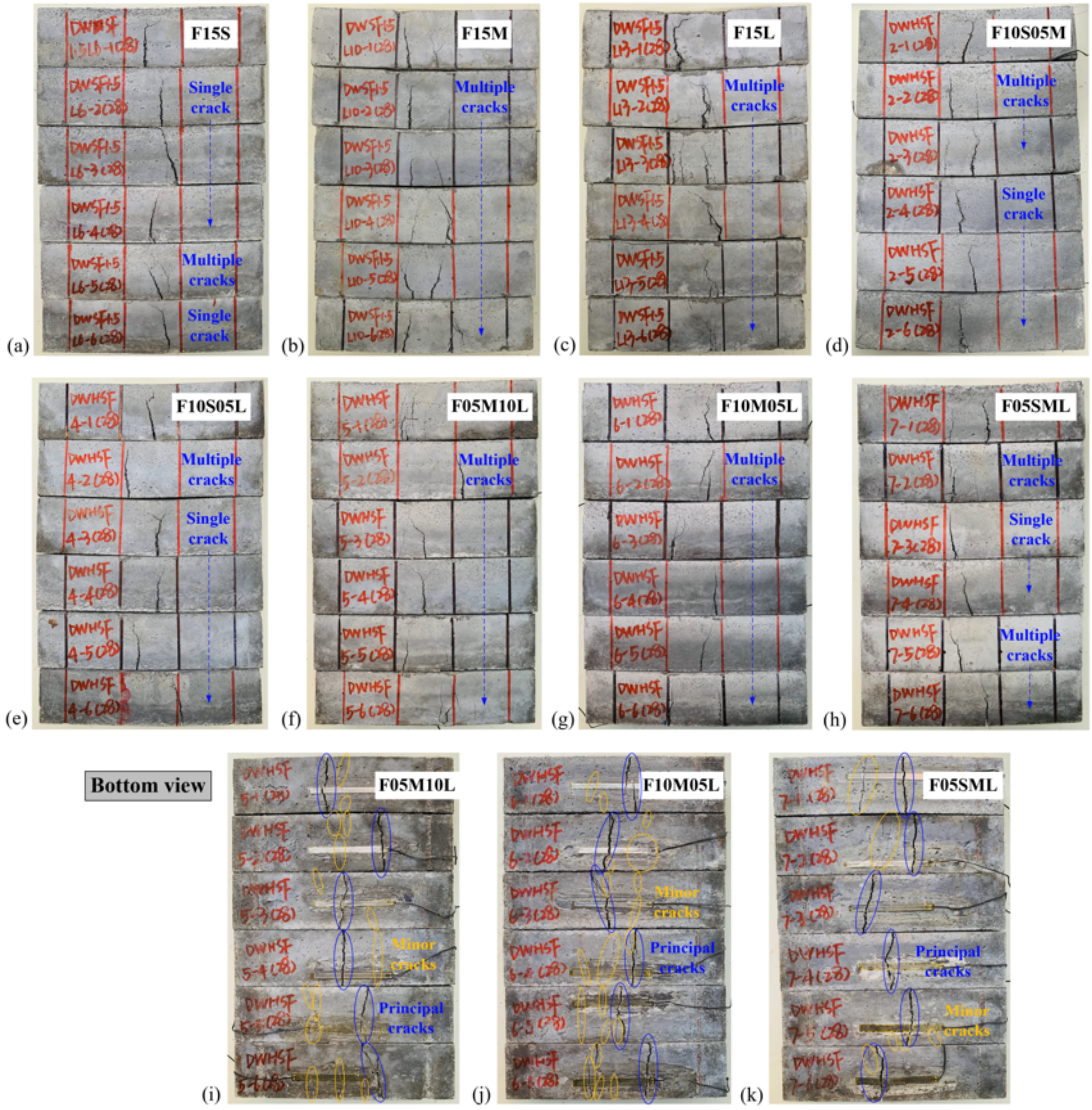

Fig. 6.12. Typical ultimate failure patterns of (a-c) mono and (d-k) hybrid FR-DUHPC beam samples after repeated drop-weight impacts.

Fig. 6.13(a and b), respectively, shows the final failure patterns of HVFA50- and CR-mixed FR-DUHPC after drop-weight tests. Compared with the original case (FA20-F15M) exhibited in Fig. 6.12(b), the width of the principal crack of HVFA50-mixed samples at failure was slightly wider, and the simultaneous appearance of the multiple minor-cracks accompanying the principal crack was reduced. That is, the relatively lagging secondary hydration (microstructure with obvious spherical FA particles as displayed in Fig. 6.13(c)) rendered the HVFA-mixed cases not to exhibit the most excellent impact resistance at 28-day age. After rubber particles were added to partially substitute silica sand, although the test samples remained intact at ultimate failure, its notably wider single crack rendered it to exhibit more serious bending deformation, and the crack width at/above the neutral axis also notably increased. Fig. 6.13(c) intuitively explains the reason for the attenuation in the impact performance of the prepared rubberized mixtures. That is, the matrix compactness and fibre anchoring were significantly deteriorated due to the weak ITZ between the cement paste and CR aggregate, together with the poor bonding between steel fibres and cement paste as well as CR aggregate. Under the action of the multiple impact load, steel fibres were more susceptible to being pulled out, so that they could not play a sufficient and effective toughening effect between the original/impact cracks.

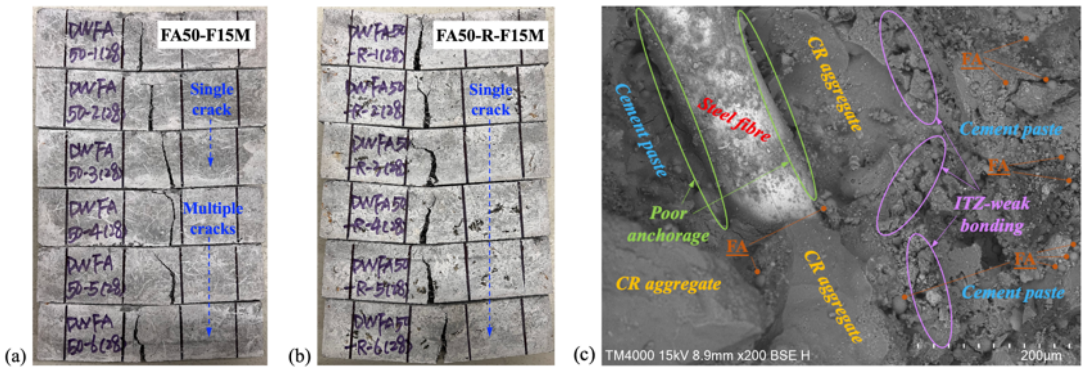

Fig. 6.13. Ultimate failure patterns of (a) HVFA50- and (b) CR-mixed FR-DUHPC beam samples after repeated drop-weight impacts along with (c) microstructure image of prepared CR-mixed dry concrete.

6.3.1.4 Residual flexural behaviour

Table 6.4 and Fig. 6.14 respectively list and depict the residual flexural strength values and their variations in mono/hybrid FR-DUHPC samples after final impact, in which f_r is the static flexural strength of identical undamaged samples obtained from Chapter 4 and f_{rr} is the residual flexural strength of damaged samples after dynamic tests. The ratios of dynamic residual to static flexural strength were also plotted to demonstrate the residual bending capacity. As can be observed that both the residual flexural strength and bearing capacity were improved signally with fibre length and curing age. Samples F15L, F05M10L and F10M05L showed the highest residual flexural strength and an excellent 28-day residual bearing capacity of more than 70% (indicated by the blue line). However, on the contrary, the samples with poor performance above were F15S, F10S05M and F10S05L, that is, the samples with more 6-mm fibre addition. Besides, the above samples also exhibited a relatively slow increase in residual strength (indicated by bottle green lines) in comparison with the static strength increment (indicated by light

green lines), whereas other samples showed comparable strength enhancement. Particularly necessary to be pointed out that the 28-day static strength of samples F05M10L and F05SML was respectively 38.6 and 35.9 MPa, approximately 4.9% and 11.6% lower than that of F15L samples, whereas the residual strength was approximately 4.8% and 20.7% lower. The main reason was that the anchoring disadvantages of 6-mm fibres, which were not prominent in static tests, rendered them to be easily pulled out from concrete matrix under impact, and hence could not effectively restrain the rapid propagation of micro-/macro-cracks. However, the longer fibres could firmly hold/bridge the matrix on both sides of the impact cracks by virtue of their quantity and anchorage length advantages, even though the concrete samples had suffered more impacts.

Table 6.4

Static and dynamic residual flexural results of mono/hybrid FR-DUHPC.

Samples	f_r (MPa)			f_{rr} (MPa)			f_{rr}/f_r (%)		
	1-d	7-d	28-d	1-d	7-d	28-d	1-d	7-d	28-d
F15S	20.7	24.1	28.2	8.8 (1.27)	11.4 (0.62)	14.9 (2.12)	42.5	47.3	52.8
F15M	26.1	31.4	35.0	15.9 (1.10)	20.2 (1.48)	25.1 (1.91)	60.9	64.3	71.7
F15L	31.3	36.3	40.6	20.5 (1.21)	25.3 (1.85)	31.4 (2.96)	65.5	69.7	77.3
F05S10M	23.1	27.7	32.8	13.3 (1.40)	17.4 (1.38)	22.5 (2.83)	57.6	62.8	68.6
F10S05M	21.8	26.0	30.1	11.6 (1.01)	14.7 (0.41)	18.3 (2.62)	53.2	56.5	60.8
F05S10L	27.4	30.9	35.2	16.5 (0.76)	19.9 (1.97)	24.7 (2.46)	60.2	64.4	70.2
F10S05L	25.3	29.7	33.0	12.2 (1.05)	16.3 (1.21)	20.0 (3.01)	48.2	54.9	60.6
F05M10L	30.1	34.4	38.6	19.6 (1.31)	24.2 (1.35)	29.9 (1.78)	65.1	70.4	77.5
F10M05L	29.5	33.0	37.5	18.5 (0.68)	22.7 (0.29)	27.6 (2.03)	62.7	68.8	73.6
F05SML	27.1	31.4	35.9	16.1 (1.74)	20.2 (1.41)	24.9 (2.79)	59.4	64.3	69.4

Notes: items in parentheses denote standard deviation (SD) of measured parameters.

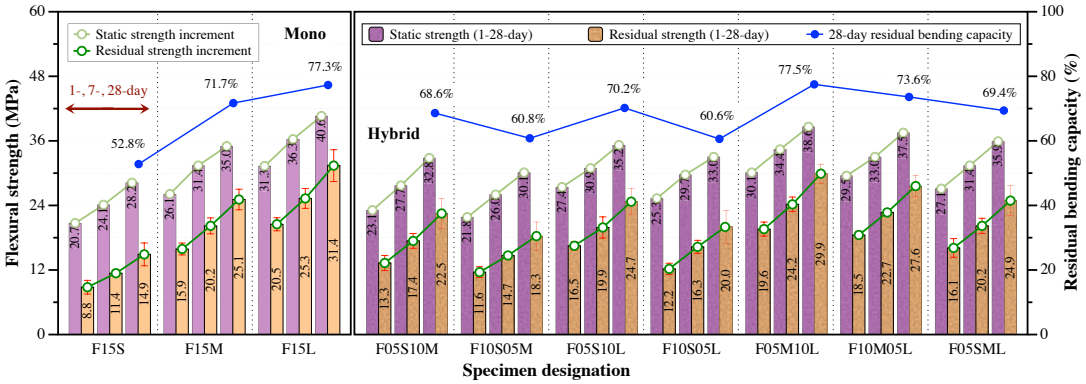

Fig. 6.14. Residual flexural strength and capacity ratio of mono/hybrid FR-DUHPC samples after impact tests.

Table 6.5 and Fig. 6.15 respectively list and depict the residual flexural strength values and their variations in HVFA-/CR-mixed FR-DUHPC beam samples after impact test, in which the meanings of f_r (obtained in Chapter 5) and f_{rr} are the same as those in Table 6.4. It could be observed that the residual strength and bending capacity significantly enhanced with curing age but gradually reduced with FA content at all ages (especially for samples with 50-60% of FA addition at early ages). Additionally, the growth rate of the early residual strength (indicated by bottle green lines) was evidently slowed down due to the continuous dilution of the cement concentration, but the subsequent long-term strength development was observably accelerated with FA addition owing to the progressive secondary hydration reaction. Compared to the static strength development at different ages (indicated by light green lines), the increment in residual strength of the identical samples exhibited insignificant difference. However, for the mixtures with higher FA additions, the attenuation in residual strength at the same ages was much greater than that in static strength. As an illustration, the 28-day static strength of concrete samples FA50-F15M and FA60-F15M was, respectively, 27.7 and 24.8

MPa, approximately 20.9% and 29.1% lower than that of F15L samples, but the residual strength was approximately 25.5% (18.7 MPa) and 36.3% (16.0 MPa) lower. In the case where rubber addition was considered, the incorporation of CR particles to substitute partial silica sand resulted in an evident attenuation in both residual strength and bearing capacity. As an illustration, the residual strength diminished by 46.8%, 47.6% and 43.9% at three ages, respectively, as compared to original FA50-F15M samples. It should be pointed out that the residual strength development of CR-mixed samples with curing age was far less than that of the foregoing original samples, and was likewise slower than its own static strength increment, specifically manifested by the increased residual capacity difference with curing age between these two mixtures (from 44.3% to 54.3% and 52.1% to 67.6%). That is, the inclusion of CR aggregate weakened the contribution of FA pozzolanic effect to strength improvement in the prepared FR-DUHPC, and this adverse impact was particularly prominent under dynamic impact load.

Table 6.5

Static and dynamic residual flexural results of HVFA-/CR-mixed FR-DUHPC.

Samples	f_r (MPa)			f_{rr} (MPa)			f_{rr}/f_r (%)		
	1-d	7-d	28-d	1-d	7-d	28-d	1-d	7-d	28-d
FA20	26.1	31.4	35.0	15.9 (1.10)	20.2 (1.48)	25.1 (1.91)	60.9	64.3	71.7
FA30	24.2	27.6	31.4	14.4 (0.99)	17.5 (1.62)	22.2 (2.17)	59.7	63.3	70.8
FA40	21.4	25.1	29.6	12.2 (1.39)	15.4 (1.21)	20.6 (1.96)	57.0	61.2	69.6
FA50	18.0	22.0	27.7	9.4 (1.13)	12.6 (1.06)	18.7 (2.05)	52.1	57.3	67.6
FA60	13.3	17.7	24.8	6.0 (1.33)	9.2 (1.46)	16.0 (1.93)	45.1	52.1	64.4
FA50-R	11.4	13.7	19.3	5.0 (1.47)	6.6 (0.88)	10.5 (1.02)	44.3	47.9	54.3

Notes: items in parentheses denote standard deviation (SD) of measured parameters.

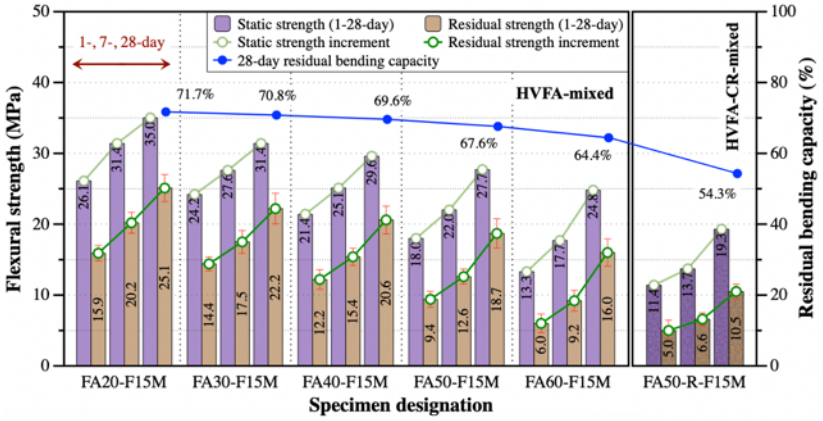

Fig. 6.15. Residual flexural strength and capacity ratio of HVFA-/CR-mixed FR-DUHPC samples after impact tests.

6.3.2 Weibull distribution analysis

As illustrated above, the prepared FR-DUHPC samples produced several initial cracks and eventually failed after being subjected to multiple drop-weight impacts. Hence, their failure mechanism was very similar to that within the bending fatigue test [201, 208]. Although the considerable efforts had been made in the sample preparation and experimental conduction to establish the same test conditions, the obtained data often varied and showed evident dispersion. In such instances, the statistical analysis method was highly necessary to investigate the foregoing scattered impact results. In this section, the two-parameter Weibull distribution, which was broadly utilized in the fatigue test data processing, was introduced to explore the flexural impact performance of the prepared FR-DUHPC after drop-weight impact tests. In considerations of the steel fibres possessed an excellent restraining effect on cracks propagation, as well as the concrete structures were normally used with multiple cracks during service, the used Weibull distribution hence focused on analyzing the impact numbers (N_d) of beam samples after final

failure. Besides, due to the poor impact resistance of CR-mixed FR-DUHPC with lower impact numbers, the statistical analysis was conducted on mono/hybrid and HVFA-mixed FR-DUHPC cases. The probability of survival function of the utilized two-parameter Weibull distribution can be expressed as follows [201, 209, 210]:

$$L_N(n) = \exp[(n/u)^{\alpha}] \quad (6.2)$$

where n is the specific impact number of the stochastic Weibull variable N (= N_d in this research) in drop-weight impact tests, α is the slope of the distribution curve (shape parameter), and u is the characteristic life (scale parameter). After taking two logarithms on both sides of the function simultaneously, the following expression can be obtained:

$$\ln[\ln(1/L_N)] = \alpha\ln(n) - \alpha\ln(u) \quad (6.3)$$

then, the expression can be simplified as follows after making $Y = \ln[\ln(1/L_N)]$ and $X = \ln(n)$:

$$Y = \alpha X - \alpha\ln(u) \quad (6.4)$$

hence, the linear relationships between X and Y can be tested to verify whether the ultimate failure blow numbers (N_d) of the prepared FR-DUHPC samples follow the two-parameter Weibull distribution. The impact numbers are first ranked in an ascending sequence, then the empirical survival function given below can be used to calculate the values of L_N [209, 211, 212]:

$$L_N = 1 - [i/(s + 1)] \quad (6.5)$$

where i is the sequence number of N_d, and s is the total number of the impacted samples for each mixture (= 6 in this study). Subsequently, the impact numbers

at ultimate failure (N_f) under different levels of reliability can be predicted utilizing the following expression combined with the corresponding Weibull distribution parameters [213]:

$$N_f = u[-\ln(R_l)]^{(1/\alpha)} \tag{6.6}$$

where R_l is the required levels of reliability functions. Fig. 6.16 demonstrates the correlations between the impact number N_d and empirical survival function value L_N of the prepared FR-DUHPC at 28 days of age, and the related regression parameters computed from the statistical analysis are collated in detail in Table 6.6. It could be clearly observed that the good linear relationships were existed between N_d and L_N of all FR-DUHPC cases with coefficient of determination (R^2) greater than 0.85. That is, the number of impacts causing the ultimate damage of mono/hybrid and HVFA-mixed FR-DUHPC under low-speed drop-weight impact followed the two-parameter Weibull distribution, even though the ultimate drop-weight blow numbers were not many within the range of 4.8-28.5 blows, as listed in Tables 6.2 and 6.3.

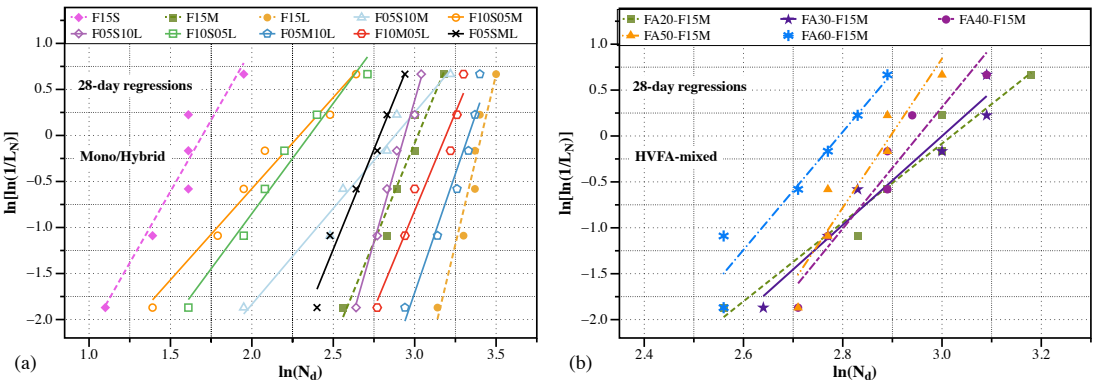

Fig. 6.16. 28-day linear regressions of ultimate failure impact numbers (N_d) for (a) mono/hybrid and (b) HVFA-mixed FR-DUHPC in Weibull distribution.

Table 6.6

Weibull regression parameters of the studied FR-DUHPC at final failure.

Mixes	28-day coefficients			Mixes	28-day coefficients			Mixes	28-day coefficients		
	α	$\alpha ln(u)$	R^2		α	$\alpha ln(u)$	R^2		α	$\alpha ln(u)$	R^2
F15S	3.10	5.26	0.909	F05S10L	6.15	18.06	0.987	FA20	4.29	12.97	0.955
F15M	4.29	12.97	0.955	F10S05L	2.40	5.64	0.972	FA30	4.84	14.53	0.953
F15L	7.38	25.17	0.934	F05M10L	5.16	17.19	0.952	FA40	6.62	19.54	0.922
F05S10M	2.09	6.01	0.971	F10M05L	4.26	13.59	0.955	FA50	8.11	23.50	0.894
F10S05M	1.98	4.54	0.974	F05SML	4.34	12.09	0.974	FA60	6.42	17.94	0.927

Fig. 6.17 exhibits the predicted failure impact number (N_f) of the evaluated FR-DUHPC under different levels of reliability at 28 days of age, plotted by utilizing Eq. (6.6) and the derived Weibull regression parameters shown in Table 6.6. For mono/hybrid cases illustrated in Fig. 6.17(a-b), longer steel fibres endowed the reinforced samples with better performance to withstand more falling impacts at the same reliability. Taking the 0.9 reliability level as an example, the N_f values of mono samples F15S, F15M and F15L were 2.7, 13.6 and 22.3, respectively, and those of hybrid F05S10M, F10S05M, F05S10L, F10S05L, F05M10L, F10M05L and F05SML cases were 7.6, 3.2, 13.1, 4.1, 18.1, 14.3 and 9.7, respectively. In terms of HVFA-mixed cases exhibited in Fig. 6.17(c), the increase in FA content resulted in a degradation in concrete resistance to multiple impacts at the same reliability, whereas the decrease was not evident benefitted from the continuous secondary hydration effect. For instance, the N_f values at 0.8 reliability level were 16.0, 15.1 and 12.9, respectively for FA20-, FA50- and FA60-F15M samples. In

a nutshell, the obtained curves derived from the conducted Weibull analysis can provide appropriate N_f values under different reliability levels, on the basis of eradicating costs and saving time, and can also preliminary calculate the relevant impact energy required for practical design requirements.

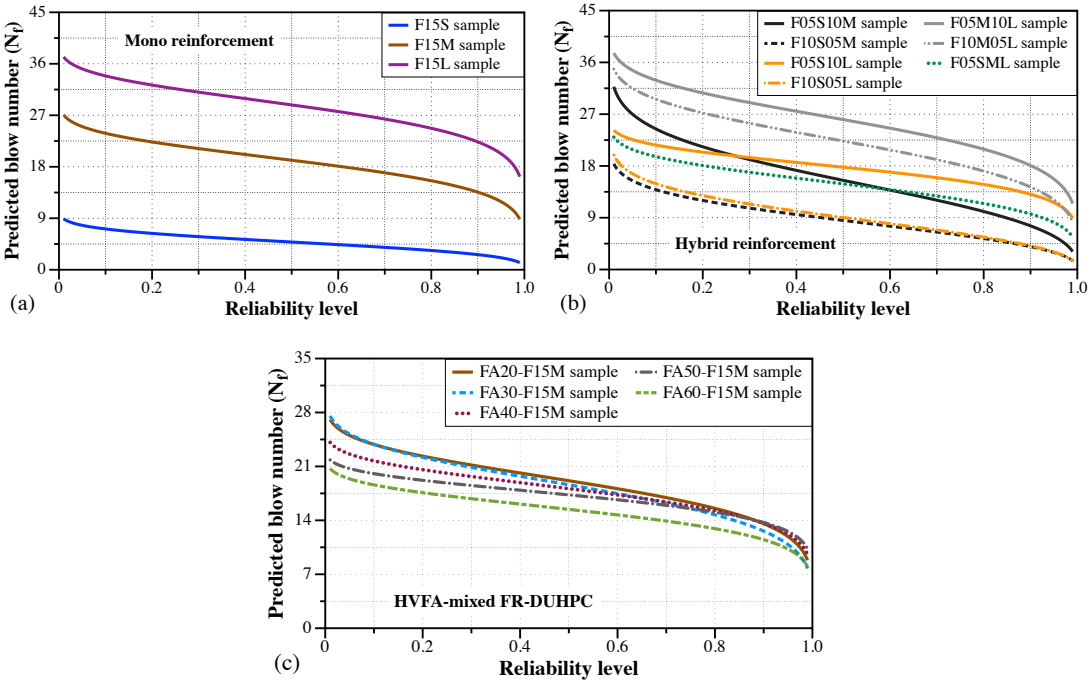

Fig. 6.17. Predicted 28-day impact numbers at ultimate failure of (a) mono; (b) hybrid and (c) HVFA-mixed FR-DUHPC in terms of different levels of reliability.

6.4 Conclusion

In this chapter, the modified low-velocity drop-weight impact test was carried out on steel FR-DUHPC beam samples to evaluate the effects of steel fibre length, mixing method, FA content and CR incorporation on the flexural impact resistance. Subsequently, Weibull statistical technique was adopted to analyze the ultimate failure impact number of mono/hybrid and HVFA-mixed samples in consideration of the large value variation. The primary findings from the current study are listed as follows:

1) The use of any length and mixing method of steel fibres remarkably increased the number of impacts at both initial cracking and final failure stages. Longer steel fibres endowed the prepared samples with better impact performance, whereas the 6-mm fibre reinforcement exhibited evidently decreased anti-impact number as well as deteriorated impact ductility, which was significantly weaker than its toughening effect under static conditions.
2) For HVFA-mixed samples, the number of impacts at initial cracking and final failure gradually decreased with FA addition up to 28 days, but the impact ductility improved considerably with curing age (especially for mixtures with higher FA contents) attributed to the continuous contribution of FA pozzolanic effect on matrix strength. However, as for CR-mixed samples, the addition of CR aggregate greatly weakened the foregoing FA effect and resulted in an evidently degraded multiple impact resistance upon cracking at all ages.
3) The peak impact force at first cracking and final failure gradually enhanced with the mixing proportion of longer fibres increased, but remarkably reduced after CR aggregate was added. The peak force of hybrid samples exhibited comparable or slightly higher/lower values than that of the original samples with single length of steel fibres, further demonstrating that the hybrid steel fibre reinforcement yielded a higher DIF under dynamic load.
4) All the beam samples remained intact after multiple impacts and presented obvious flexural-tensile responses within the mid-span area. As expected, 6-mm fibres were easily to be pulled out from concrete matrix under impact,

rendering the reinforced samples exhibiting a wide principal crack. However, longer fibres contributed samples to cracking with many minor-cracks as well as several scattered micro-cracks, which was conductive to absorbing and dissipating more energy during impact.

5) The good linear relationship existed between the final failure impact number and the probability of survival function of the studied FR-DUHPC cases with fitting coefficient greater than 0.85. That is, the impact number resulting in the ultimate failure of the mono/hybrid and HVFA-mixed FR-DUHPC under low-velocity drop-weight impact followed the two-parameter Weibull distribution. The impact energy value for practical structure design could be preliminarily computed utilizing the derived Weibull parameters under different levels of reliability.

Chapter 7

Conclusions and Recommendations

7.1 Conclusions

In this study, a promising building material named DUHPC was developed on the basis of retaining the advantages of traditional dry concrete. Compared with self-compacting UHPC, the developed DUHPC had a low cement addition but notably higher early strength. The cement and aggregate added could also be partially replaced by a variety of recycled materials to effectively mitigate the consumption of natural resources while improving the recycling of hazardous wastes. Relying on its higher strength and better toughness/ductility, the developed DUHPC could meet different requirements of various engineering applications, which markedly expanded the application field of dry concrete material in practice. Based on the analysis and discussions presented in the previous chapters, the primary findings can be summarized as follows:

- The various mechanical properties of DUHPC were improved significantly with steel fibre volume dosage at all ages. The fibre reinforcement demonstrated more positive impact to the flexural rather than the compressive performance, which was greatly beneficial for dry concrete structures/units that were mainly subjected to flexural-bending loads during their serviceability.
- The increase in initial curing temperature via using moist/steam curing regime caused an attenuation trend in various strengths of DUHPC, especially at 28-day period. However, its strength development kinematics improved signally

as the initial curing temperature increased at early ages. 50 ℃ moist/steam curing was suggested for consolidating the pre-fabricated DUHPC units based on the microstructure analysis performed.

- The development rate of flexural strength under the identical fibre dosage was faster than that of split-tensile strength attributed to the potential delamination failure. In the case of comprehensive consideration of the cost and mechanical performance of FR-DUHPC, volume fraction of 1.5% was considered to be the most suitable steel fibre addition in this study.
- Under the same fibre addition, longer steel fibres exhibited better effect on enhancing the compressive strength, total energy absorption, toughness and MOE of DUHPC. In the case of fibre hybridization, the utilization of shorter fibres substituting part of the initial-sized ones attenuated the compressive strength, but F05M10L, F10M05L and F05SML samples demonstrated better energy absorption ability and toughness.
- The enhancement in flexural and split-tensile strengths of DUHPC with mono steel fibre reinforcement was more prominent when the fibre length added from 6 to 10 and 13 mm. Thus, the pronounced attenuation in flexural strength occurred in hybrid FR-DUHPC cases in which longer fibres were partially substituted by shorter ones at all ages. The substitution of longer fibres with more 6-mm ones evidently deteriorated the flexural toughness and energy absorption capacity of DUHPC after cracking.
- The mixtures with hybrid 10- and 13-mm steel fibres as well as with hybrid 6-,

10- and 13-mm ones were suggested to be used in the practical application of DUHPC structures/components that were mainly subjected to static loads. In addition, the length of steel fibres added was not recommended to exceed 13 mm on account of the easy agglomeration of longer steel fibres and the lower moisture content of DUHPC.

- The proposed multivariate regression models could well estimate the flexural, compressive and split-tensile strength of mono FR-DUHPC at a given range of steel fibre length (6-13 mm), volume dosage (0.5-2.0%) and curing age (1 day-28 days) with R^2 larger than 0.9 and D-W values close to 2.0. After the compressive strength was introduced as an additional IV, the updated best-fit models outperformed the original models in the prediction accuracy of both flexural and split-tensile properties.
- The compressive/flexural strengths of FR-DUHPC enhanced gradually with curing age but diminished observably with FA substitution level for cement, especially for the mixtures with more FA at earlier ages. Owing to the utilized moist/steam curing, the contribution of FA effect to both strengths at each age was evidently increased, and 50% of cement substitution in line with the high-volume concept was determined to be the suitable FA addition in this study.
- The use of CR aggregate caused a significant decrease in density, strength and MOE at all ages, especially for the cases where the finer CR aggregate was introduced. The fibre dosage exhibited more positive impact on flexural behaviour of rubberized FR-DUHPC due to the adopted preparation method

rendered fibres tend to be aligned parallel to the compaction layers, endowing fibres with more effective restraint on matrix cracking under flexural-tensile load.

- The flexural behaviour benefits derived from the inclusion of steel fibres, FA and CR aggregate, as well as the eco-friendly benefits derived from the cost saving, energy conservation and carbon reduction, rendered the developed LWC can be widely utilized in dry concrete applications with different strength requirements that were mainly subjected to bending loads during service.
- The use of any length and mixing method of steel fibre significantly improved the impact performance of mono/hybrid FR-DUHPC, including the resistance factors of initial crack and final failure, impact ductility and residual bearing capability. Longer fibres endowed the prepared samples with better impact resistance, but 6-mm fibres exhibited insufficient toughening effect, especially when the dosage reached 1.0% and above.
- The resistance factor, peak impact force and residual bearing capability all gradually decreased with FA content up to 28 days, while the impact ductility improved notably with curing age attributed to the continuous contribution of FA pozzolanic effect. The use of CR aggregate greatly degraded the impact performance at all ages and weakened the positive impact of foregoing FA effect.
- Hybrid medium/long fibre reinforcement was proposed for DUHPC units that were mainly subjected to dynamic impact loads during service, while the FA

content used to substitute partial cement was not recommended to exceed 40% due to the evident deterioration in the early impact performance. CR aggregate was not proposed to be added to dry concrete mixtures since the impact load would greatly accentuate the initial matrix defects caused by the weak bonding with cement paste.

- The good linear relationships were existed between ultimate failure impact number and probability of survival function of all FR-DUHPC samples with R^2 greater than 0.85. That is, the number of impacts causing the ultimate failure of mono/hybrid and HVFA- mixed FR-DUHPC under low-velocity drop-weight impact obeyed the Weibull distribution. The impact energy value for structural design could be preliminarily computed using the derived Weibull parameters under different reliability levels.

7.2 Recommendations for future work

The developed FR-DUHPC in this study not only possesses the characteristics of fast hardening, low cement addition and rapid demoulding of conventional dry concrete, but also has the advantages of ultra-high strength, excellent ductility and energy absorption ability of UHPC. The current research has been dedicated to investigating the static and dynamic mechanical properties of the developed FR-DUHPC, therefore the suggestions for the following issues are elaborated for future studies:

- The current research on the mechanical behaviour of FR-DUHPC is basically carried out on specimens prepared/fabricated in the laboratory. However, the

concrete mixtures with good performance under laboratory conditions may not be desirable in the practical engineering applications. It is hence necessary to carry out more mechanical performance investigations for actual applications, and the raw material composition and structural configuration are needed to be optimised.

- The addition of steel fibres can markedly improve the various properties of the developed DUHPC. However, owing to the special appearance of its mixture, the distribution of steel fibres is much different from that in the self-compacting concrete, and the fibres may be distorted under the vibration and mechanical compaction. Efforts should be made to further explore the fibre reinforcement mechanism and the effect of fibre deformation on FR-DUHPC performance.
- The smart investigation of dry concrete is still in its infancy, that is, in the stage of the theoretical analysis and experimental exploration. At present, the main technologies for realizing the intelligentization of concrete are based on self-compacting concrete, and whether they are equally feasible for dry concrete with low moisture content and completely different preparation methods need in-depth research. Additionally, considering the extensive use of dry concrete roof tiles in Australia, the development of smart photovoltaic tiles with partial properties of solar panels is also an important research topic in the future.
- The durability performance is particularly important for dry concrete in some cases since its structures and units may be damaged caused by the durability deterioration rather than the strength loss. Hence, research on the durability

performance (freeze-thaw resistance, fatigue resistance and impact abrasion resistance) of the developed FR-DUHPC incorporating high-volume recycled materials need to be focused.

- The layer-by-layer vibrated compaction used in the preparation of FR-DUHPC will inevitably influence the interlayer bonding strength of the mixture and the anchoring/reinforcement effect of steel fibres. Further researches need to be carried out to explore the impact of interlayer casting interval, thickness and vibrated compaction load/duration on the permeability and sorptivity, as well as the bond-slip performance between steel fibres and concrete matrix of the developed FR-DUHPC.
- The development of the new dry concrete material, as well as the study of its static/dynamic mechanical property, aims to lay the foundation for its practical application in structures. Hence, it is strongly necessary to continue conducting investigations on the static/dynamic property and durability performance of dry concrete units and structures manufactured with the developed DUHPC. This includes studying aspects such as the resistance to hailstone hit on roof tiles, the resistance to high-speed impact and abrasion damage on airport runways, and the resistance to microbiological and acid corrosion on sewer pipes.

References

[1] ACI 211.2. Guide for selecting proportions for no-slump concrete. American Concrete Institute, 2002.

[2] Ling T-C. Effects of compaction method and rubber content on the properties of concrete paving blocks. Construction and Building Materials, 2012, 28(1):164-175.

[3] Aghaeipour A and Madhkhan M. Mechanical properties and durability of roller compacted concrete pavement (RCCP) - A review. Road Materials and Pavement Design, 2019:1-24.

[4] Sukontasukkul P and Chaikaew C. Properties of concrete pedestrian block mixed with crumb rubber. Construction and Building Materials, 2006, 20(7):450-457.

[5] Marchand J, Hornain H, Diamond S, Pigeon M, and Guiraud H. The microstructure of dry concrete products. Cement and Concrete Research, 1996, 26(3):427-438.

[6] Chhorn C, Hong S J, and Lee S W. Relationship between compressive and tensile strengths of roller-compacted concrete. Journal of Traffic and Transportation Engineering (English Edition), 2018, 5(3):215-223.

[7] Li M, Guo X, Shi J, and Zhu Z. Seepage and stress analysis of anti-seepage structures constructed with different concrete materials in an RCC gravity dam. Water Science and Engineering, 2015, 8(4):326-334.

[8] Rooholamini H, Hassani A, and Aliha M R M. Evaluating the effect of macro-synthetic fibre on the mechanical properties of roller-compacted concrete pavement using response surface methodology. Construction and Building Materials, 2018, 159:517-529.

[9] Zhang S, Ghouleh Z, He Z, Hu L, and Shao Y. Use of municipal solid waste incineration bottom ash as a supplementary cementitious material in dry-cast concrete. Construction and Building Materials, 2021, 266:120890.

[10] Chidiac S and Zibara H. Dry-cast concrete masonry products: properties and durability. Canadian Journal of Civil Engineering, 2007, 34(11):1413-1423.

[11] Pacheco-Torgal F, Lourenco P B, Labrincha J, Chindaprasirt P, and Kumar S, Eco-efficient masonry bricks and blocks: Design, properties and durability. 2014:

Woodhead Publishing.

[12] Hesami S, Modarres A, Soltaninejad M, and Madani H. Mechanical properties of roller compacted concrete pavement containing coal waste and limestone powder as partial replacements of cement. Construction and Building Materials, 2016, 111:625-636.

[13] Yang L and Shi J J. Experimental study on the impact of rainfall on RCC construction. Journal of Construction Engineering and Management, 2010, 136(5):477-483.

[14] Hong Y, Du C, and Jiang S. Design theory and practice of high RCC gravity dam under complex conditions. 2014, Science Press, Beijing (in Chinese).

[15] Ouyang J, Chen X, Huangfu Z, Lu C, Huang D, and Li Y. Application of distributed temperature sensing for cracking control of mass concrete. Construction and Building Materials, 2019, 197(10):778-791.

[16] Noorzaei J, Bayagoob K, Thanoon W, and Jaafar M. Thermal and stress analysis of Kinta RCC dam. Engineering Structures, 2006, 28(13):1795-1802.

[17] Debbarma S, Ransinchung G, and Singh S. Feasibility of roller compacted concrete pavement containing different fractions of reclaimed asphalt pavement. Construction and Building Materials, 2019, 199:508-525.

[18] Adamu M, Mohammed B S, and Liew M S. Mechanical properties and performance of high volume fly ash roller compacted concrete containing crumb rubber and nano silica. Construction and Building Materials, 2018, 171:521-538.

[19] Modarres A and Hosseini Z. Mechanical properties of roller compacted concrete containing rice husk ash with original and recycled asphalt pavement material. Materials and Design, 2014, 64:227-236.

[20] Topličić-Ćurčić G, Grdić D, Ristić N, and Grdić Z. Properties, materials and durability of rolled compacted concrete for pavements. Zaštita materijala, 2015, 56(3):345-353.

[21] Chan-Gi, Park, Jong-Whan, Yoon, Wan-Young, Kim, Jong-Pil, and Won. Mechanical and durability performance of roller-compacted concrete with fly ash

for dam applications. International Journal of Concrete Structures and Materials, 2007, 1(1):57-61.

[22] Saluja S, Kaur K, Goyal S, and Bhattacharjee B. Assessing the effect of GGBS content and aggregate characteristics on drying shrinkage of roller compacted concrete. Construction and Building Materials, 2019, 201:72-80.

[23] Deghfel M, Meddah A, Beddar M, and Chikouche M A. Experimental study on the effect of hot climate on the performance of roller-compacted concrete pavement. Innovative Infrastructure Solutions, 2019, 4:54.1-54.12.

[24] Kartal M and Contadakis M. Three-dimensional earthquake analysis of roller-compacted concrete dams. Natural Hazards and Earth System Sciences, 2012, 12(7):2369-2388.

[25] Harrington D, Abdo F, Adaska W, Hazaree C V, Ceylan H, and Bektas F. Guide for roller-compacted concrete pavements. 2010.

[26] Widoanindyawati V and Pratama M M A. The influence of compression applied during production to the compression strength of dry concrete: An experimental study. Procedia Engineering, 2014, 95:465-472.

[27] Peyvandi A and Soroushian P. Structural performance of dry-cast concrete nanocomposite pipes. Materials and Structures, 2015, 48(1-2):461-470.

[28] Peyvandi A, Soroushian P, Balachandra A M, and Sobolev K. Enhancement of the durability characteristics of concrete nanocomposite pipes with modified graphite nanoplatelets. Construction and Building Materials, 2013, 47:111-117.

[29] Mohamed N, Soliman A M, and Nehdi M L. Full-scale pipes using dry-cast steel fibre-reinforced concrete. Construction and Building Materials, 2014, 72:411-422.

[30] Park Y, Abolmaali A, Mohammadagha M, and Lee S. Structural performance of dry-cast rubberized concrete pipes with steel and synthetic fibers. Construction and Building Materials, 2015, 77:218-226.

[31] Chidiac S and Mihaljevic S. Performance of dry cast concrete blocks containing waste glass powder or polyethylene aggregates. Cement and Concrete Composites, 2011, 33(8):855-863.

[32] Amhudo R L, Tavio T, and Raka I G P. Comparison of compressive and tensile strengths of dry-cast concrete with ordinary portland and portland pozzolana cements. Civil Engineering Journal, 2018, 4(8):1760-1771.

[33] Willis W. Ernest. An introduction to dry-cast concrete. The Aberdeen Group, 1969.

[34] Uygunoğlu T, Topcu I B, Gencel O, and Brostow W. The effect of fly ash content and types of aggregates on the properties of pre-fabricated concrete interlocking blocks (PCIBs). Construction and Building Materials, 2012, 30:180-187.

[35] Chi M and Huang R. Effect of circulating fluidized bed combustion ash on the properties of roller compacted concrete. Cement and Concrete Composites, 2014, 45:148-156.

[36] Fakhri M and Saberi. K F. The effect of waste rubber particles and silica fume on the mechanical properties of roller compacted concrete pavement. Journal of Cleaner Production, 2016, 129:521-530.

[37] Najimi M, Sobhani J, and Pourkhorshidi A. A comprehensive study on no-slump concrete: from laboratory towards manufactory. Construction and Building Materials, 2012, 30:529-536.

[38] Rao S K, Sravana P, and Rao T C. Experimental studies in ultrasonic pulse velocity of roller compacted concrete pavement containing fly ash and M-sand. International Journal of Pavement Research and Technology, 2016, 9(4):289-301.

[39] Rao S K, Sravana P, and Rao T C. Investigating the effect of M-sand on abrasion resistance of fly ash roller compacted concrete (FRCC). Construction and Building Materials, 2016, 118:352-363.

[40] Rao S K, Sravana P, and Rao T C. Abrasion resistance and mechanical properties of roller compacted concrete with GGBS. Construction and Building Materials, 2016, 114:925-933.

[41] Lopez-Uceda A, Agrela F, Cabrera M, Ayuso J, and López M. Mechanical performance of roller compacted concrete with recycled concrete aggregates. Road Materials and Pavement Design, 2018, 19(1):36-55.

[42] Meddah A, Beddar M, and Bali A. Use of shredded rubber tire aggregates for roller

compacted concrete pavement. Journal of Cleaner Production, 2014, 72:187-192.

[43] Lessard J-M, Omran A, Tagnit-Hamou A, and Gagne R. Feasibility of using biomass fly and bottom ashes in dry-cast concrete production. Construction and Building Materials, 2017, 132:565-577.

[44] Liu S, Li Q, Rao M, and Wang L. Properties and microstructure of roller compacted concrete with high volume low quality fly ash. Materials Science, 2017, 23(3):273-279.

[45] Lessard J-M, Omran A, Tagnit-Hamou A, and Gagne R. Feasibility of using biomass fly and bottom ashes to produce RCC and PCC. Journal of Materials in Civil Engineering, 2016, 29(4):04016267.

[46] Yerramala A and Babu K G. Transport properties of high volume fly ash roller compacted concrete. Cement and Concrete Composites, 2011, 33(10):1057-1062.

[47] Abu-Khashaba M I, Adam I, and El-Ashaal A. Investigating the possibility of constructing low cost roller compacted concrete dam. Alexandria Engineering Journal, 2014, 53(1):131-142.

[48] Mardani-Aghabaglou A, Andiç-Çakir Ö, and Ramyar K. Freeze-thaw resistance and transport properties of high-volume fly ash roller compacted concrete designed by maximum density method. Cement and Concrete Composites, 2013, 37:259-266.

[49] Jacobsen S. High volume fly ash RCC for dams/mixture optimization and mechanical properties. Special Publication, 2001, 202:331-348.

[50] Vivek S, Narayanan R S, and Dhinakaran G. Comparative study on flexural behaviour of RCC beam and SCC ternary beams with mineral admixtures. Construction and Building Materials, 2017, 152:57-64.

[51] Shen L, Li Q, Ge W, and Xu S. The mechanical property and frost resistance of roller compacted concrete by mixing silica fume and limestone powder: Experimental study. Construction and Building Materials, 2020, 239:117882.

[52] Mehta A and Ashish D K. Silica fume and waste glass in cement concrete production: a review. Journal of Building Engineering, 2019:100888.

[53] Modarres A, Hesami S, Soltaninejad M, and Madani H. Application of coal waste in

sustainable roller compacted concrete pavement-environmental and technical assessment. International Journal of Pavement Engineering, 2018, 19(8):748-761.

[54] Ashteyat A M, Rjoub Y S A, Murad Y, and Asaad S. Mechanical and durability behaviour of roller-compacted concrete containing white cement by pass dust and polypropylene fibre. European Journal of Environmental and Civil Engineering, 2019, (12):1-18.

[55] Ramezanianpour A A, Mohammadi A, Dehkordi E R, and Chenar Q B. Mechanical properties and durability of roller compacted concrete pavements in cold regions. Construction and Building Materials, 2017, 146:260-266.

[56] Ghahari S, Mohammadi A, and Ramezanianpour A. Performance assessment of natural pozzolan roller compacted concrete pavements. Case Studies in Construction Materials, 2017, 7:82-90.

[57] Omran A, Harbec D, Tagnit-Hamou A, and Gagne R. Production of roller-compacted concrete using glass powder: Field study. Construction and Building Materials, 2017, 133:450-458.

[58] Rad S A M and Modarres A. Durability properties of non-air entrained roller compacted concrete pavement containing coal waste ash in presence of de-icing salts. Cold Regions Science and Technology, 2017, 137:48-59.

[59] Panesar D and Chidiac S. Ultrasonic pulse velocity for determining the early age properties of dry-cast concrete containing ground granulated blast-furnace slag. Canadian Journal of Civil Engineering, 2007, 34(5):682-685.

[60] Liu Y, Zhuge Y, Chow C W, Keegan A, Ma J, Hall C, Li D, Pham P N, Huang J, and Duan W. Cementitious composites containing alum sludge ash: An investigation of microstructural features by an advanced nanoindentation technology. Construction and Building Materials, 2021, 299:124286.

[61] Liu Y, Zhuge Y, Chow C W K, Keegan A, Pham P N, Li D, Oh J-A, and Siddique R. The potential use of drinking water sludge ash as supplementary cementitious material in the manufacture of concrete blocks. Resources, Conservation and Recycling, 2021, 168:105291.

[62] Adamu M, Mohammed B S, and Liew M S. Effect of crumb rubber and nano silica on the creep and drying shrinkage of roller compacted concrete pavement. International Journal of Geomate, 2018, 15(47):58-65.

[63] Adamu M, Mohammed B S, Shafiq N, and Shahir Liew M. Effect of crumb rubber and nano silica on the fatigue performance of roller compacted concrete pavement. Cogent Engineering, 2018, 5(1):1436027.

[64] Adamu M, Mohammed B S, and Shafiq N, Nano silica modified roller compacted rubbercrete-An overview, in Engineering Challenges for Sustainable Future. 2016, ROUTLEDGE in association with GSE Research. p. 483-487.

[65] Jebli M, Jamin F, Malachanne E, Garcia-Diaz E, and El Youssoufi M S. Experimental characterization of mechanical properties of the cement-aggregate interface in concrete. Construction and Building Materials, 2018, 161:16-25.

[66] Anastasiou E, Liapis A, and Papayianni I. Comparative life cycle assessment of concrete road pavements using industrial by-products as alternative materials. Resources, Conservation and Recycling, 2015, 101:1-8.

[67] Ninomiya Y, Kuroiwa Y, and Takao N. A study on concrete paving with limestone aggregate and limestone powder. Cement Science and Concrete Technology, 2013, 67(1):266-273.

[68] Rao S K, Sravana P, and Rao T C. Experimental Investigation on pozzolanic effect of fly ash in roller compacted concrete pavement using manufactured Sand as fine aggregate. International Journal of Applied Engineering Research, 2015, 10(8):20669-20682.

[69] Boussetta I, El Euch Khay S, and Neji J. Experimental testing and modelling of roller compacted concrete incorporating RAP waste as aggregates. European Journal of Environmental and Civil Engineering, 2018:1-15.

[70] Fakhri M and Amoosoltani E. The effect of reclaimed asphalt pavement and crumb rubber on mechanical properties of roller compacted concrete pavement. Construction and Building Materials, 2017, 137:470-484.

[71] Debieb F, Courard L, Kenai S, and Degeimbre R. Roller compacted concrete with

contaminated recycled aggregates. Construction and Building Materials, 2009, 23(11):3382-3387.

[72] Poon C S and Chan D. Paving blocks made with recycled concrete aggregate and crushed clay brick. Construction and Building Materials, 2006, 20(8):569-577.

[73] Lam M N-T, Jaritngam S, and Le D-H. Roller-compacted concrete pavement made of Electric Arc Furnace slag aggregate: Mix design and mechanical properties. Construction and Building Materials, 2017, 154:482-495.

[74] Ling T-C and Poon C-S. Use of recycled CRT funnel glass as fine aggregate in dry-mixed concrete paving blocks. Journal of Cleaner Production, 2014, 68:209-215.

[75] Adamu M, Mohammed B S, and Shafiq N. Flexural performance of nano silica modified roller compacted rubbercrete. International Journal of Advanced and Applied Sciences, 2017, 4(9):6-18.

[76] Meddah A, Bensaci H, Beddar M, and Bali A. Study of the effects of mechanical and chemical treatment of rubber on the performance of rubberized roller-compacted concrete pavement. Innovative Infrastructure Solutions, 2017, 2(1):17.

[77] Mohammed B S, Hossain K M A, Swee J T E, Wong G, and Abdullahi M. Properties of crumb rubber hollow concrete block. Journal of Cleaner Production, 2012, 23(1):57-67.

[78] Madhkhan M, Azizkhani R, and Harchegani M T. Effects of pozzolans together with steel and polypropylene fibers on mechanical properties of RCC pavements. Construction and Building Materials, 2012, 26(1):102-112.

[79] Karadelis J N and Lin Y. Flexural strengths and fibre efficiency of steel-fibre-reinforced, roller-compacted, polymer modified concrete. Construction and Building Materials, 2015, 93:498-505.

[80] Hazaree C, Ceylan H, and Wang K. Influences of mixture composition on properties and freeze–thaw resistance of RCC. Construction and Building Materials, 2011, 25(1):313-319.

[81] Lin Y, Karadelis J N, and Xu Y. A new mix design method for steel fibre-reinforced, roller compacted and polymer modified bonded concrete overlays. Construction

and Building Materials, 2013, 48:333-341.

[82] Kolase P K and Desai A K. Experimental study on monotonic and fatigue behaviour of polypropylene fibre-reinforced roller-compacted concrete with fly ash. Road Materials and Pavement Design, 2019, 20(5):1096-1113.

[83] Algin Z and Gerginci S. Freeze-thaw resistance and water permeability properties of roller compacted concrete produced with macro synthetic fibre. Construction and Building Materials, 2020, 234:117382.

[84] Yildizel S, Timur O, and Ozturk A. Abrasion resistance and mechanical properties of waste-glass-fiber-reinforced roller-compacted concrete. Mechanics of Composite Materials, 2018, 54(2):251-256.

[85] Haghnejad M and Modarres A. Effect of freeze-thaw cycles on the response of roller compacted concrete pavement reinforced by recycled polypropylene fibre under monotonic and cyclic loadings. Road Materials and Pavement Design, 2020:1-17.

[86] Sobhan K and Mashnad M. Roller-compacted fiber concrete pavement foundation with recycled aggregate and waste plastics. Transportation Research Record, 2001, 1775(1):53-63.

[87] Graeff A G, Pilakoutas K, Neocleous K, and Peres M V N N. Fatigue resistance and cracking mechanism of concrete pavements reinforced with recycled steel fibres recovered from post-consumer tyres. Engineering Structures, 2012, 45(DEC.):385-395.

[88] Rooholamini H, Hassani A, and Aliha M. Fracture properties of hybrid fibre-reinforced roller-compacted concrete in mode I with consideration of possible kinked crack. Construction and Building Materials, 2018, 187:248-256.

[89] Mohammed H A. Design and evaluation of two-layer roller compacted concrete (Doctoral dissertation). University of Nottingham. 2018.

[90] ASTM C1176/C1176M. Standard practice for making roller-compacted concrete in cylinder molds using a vibrating table.

[91] ASTM C1435/C1435M. Standard practice for molding roller-compacted concrete

in cylinder molds using a vibrating hammer.

[92] Chhorn C and Lee S-W. Consistency control of roller-compacted concrete for pavement. KSCE Journal of Civil Engineering, 2017, 21(5):1757-1763.

[93] Zhang S, Wang X, Wang C, Song R, and Huo H. Compressive behavior and constitutive model for roller compacted concrete under impact loading: Considering vertical stratification. Construction and Building Materials, 2017, 151:428-440.

[94] Wang X, Zhang S, Wang C, Shang C, Cao K, and Wei P. Investigation into stress wave propagation across interlayers existing in roller compacted concrete (RCC) under impact loadings. Construction and Building Materials, 2018, 193:13-22.

[95] Li B, Wang Z, Jiang Y, and Zhu Z. Temperature control and crack prevention during construction in steep slope dams and stilling basins in high-altitude areas. Advances in Mechanical Engineering, 2018, 10(1):1-15.

[96] Zhang X, Li S, Li Y, Ge Y, and Li H. Effect of superficial insulation on roller-compacted concrete dams in cold regions. Advances in Engineering Software, 2011, 42(11):939-943.

[97] Jaafar M, Bayagoob K, Noorzaei J, and Thanoon W A. Development of finite element computer code for thermal analysis of roller compacted concrete dams. Advances in Engineering Software, 2007, 38(11-12):886-895.

[98] ASTM C1170/C1170M. Standard test method for determining consistency and density of roller-compacted concrete using a vibrating table.

[99] Mardani-Aghabaglou A and Ramyar K. Mechanical properties of high-volume fly ash roller compacted concrete designed by maximum density method. Construction and Building Materials, 2013, 38:356-364.

[100] Atiş C D. Strength properties of high-volume fly ash roller compacted and workable concrete, and influence of curing condition. Cement and Concrete Research, 2005, 35(6):1112-1121.

[101] Settari C, Debieb F, Kadri E H, and Boukendakdji O. Assessing the effects of recycled asphalt pavement materials on the performance of roller compacted concrete. Construction and Building Materials, 2015, 101:617-621.

[102] Rooholamini H, Sedghi R, Ghobadipour B, and Adresi M. Effect of electric arc furnace steel slag on the mechanical and fracture properties of roller-compacted concrete. Construction and Building Materials, 2019, 211:88-98.

[103] Mohammed B S and Adamu M. Mechanical performance of roller compacted concrete pavement containing crumb rubber and nano silica. Construction and Building Materials, 2018, 159:234-251.

[104] Yazici Ş, Mardani-Aghabaglou A, Tuyan M, and Üte A A. Mechanical properties and impact resistance of roller-compacted concrete containing polypropylene fibre. Magazine of Concrete Research, 2015, 67(16):867-875.

[105] LaHucik J, Dahal S, Roesler J, and Amirkhanian A N. Mechanical properties of roller-compacted concrete with macro-fibers. Construction and Building Materials, 2017, 135:440-446.

[106] Huang C-H, Lin S-K, Chang C-S, and Chen H-J. Mix proportions and mechanical properties of concrete containing very high-volume of Class F fly ash. Construction and Building Materials, 2013, 46:71-78.

[107] Naik T R, Kraus R N, Chun Y-m, Ramme B W, and Singh S S. Properties of field manufactured cast-concrete products utilizing recycled materials. Journal of Materials in Civil Engineering, 2003, 15(4):400-407.

[108] Rao S K, Sravana P, and Rao T C. Investigation on pozzolanic effect of Fly ash in Roller Compacted Concrete pavement. IRACST-Engineering Science and Technology: An International Journal (ESTIJ), 2015, 5(2):202-206.

[109]Wilson A and Abolmaali A. Performance of synthetic fiber-reinforced concrete pipes. Journal of Pipeline Systems Engineering and Practice, 2014, 5(3):04014002.

[110] Shao R, Wu C, Li J, and Liu Z. Development of sustainable steel fibre-reinforced dry ultra-high performance concrete (DUHPC). Journal of Cleaner Production, 2022, 337:130507.

[111] Angelakopoulos H, Papastergiou P, and Pilakoutas K. Fibrous roller-compacted concrete with recycled materials–feasibility study. Magazine of Concrete Research, 2015, 67(15):801-811.

[112] Liu G, Lu W, Lou Y, Pan W, and Wang Z. Interlayer shear strength of roller compacted concrete (RCC) with various interlayer treatments. Construction and Building Materials, 2018, 166:647-656.

[113] Zhu X, Guo Z, Yang W, and Cheng B. Effects of double expansion agents on the properties of interlayer in roller-compacted concrete. Construction and Building Materials, 2020, 262:120909.

[114] Madhkhan M and Arasteh A. Evaluation of bond strength in roller compacted concrete under various normal pressures. WIT Transactions on The Built Environment, 2006, 85:269-277.

[115] Liu D, Li Z, and Liu J. Experimental study on real-time control of roller compacted concrete dam compaction quality using unit compaction energy indices. Construction and Building Materials, 2015, 96:567-575.

[116] Thomas B S and Gupta R C. A comprehensive review on the applications of waste tire rubber in cement concrete. Renewable and Sustainable Energy Reviews, 2016, 54:1323-1333.

[117] Gencel O, Ozel C, Koksal F, Erdogmus E, Martínez-Barrera G, and Brostow W. Properties of concrete paving blocks made with waste marble. Journal of Cleaner Production, 2012, 21(1):62-70.

[118] Lin P, Huang B, Li Q, and Wang R. Hazard and seismic reinforcement analysis for typical large dams following the Wenchuan earthquake. Engineering Geology, 2015, 194:86-97.

[119] Kartal M E, Cavusli M, and Sunbul A B. Assessing seismic response of a 2D roller-compacted concrete dam under variable reservoir lengths. Arabian Journal of Geosciences, 2017, 10(22):488.

[120] Wang C, Chen W, Hao H, Zhang S, Song R, and Wang X. Experimental investigations of dynamic compressive properties of roller compacted concrete (RCC). Construction and Building Materials, 2018, 168:671-682.

[121] Wang X, Zhang S, Wang C, Liu F, Song R, and Wei P. Initial damage effect on dynamic compressive behaviors of roller compacted concrete (RCC) under impact

loadings. Construction and Building Materials, 2018, 186:388-399.

[122] Wieland M and Brenner R P. Earthquake aspects of roller compacted concrete and concrete-face rockfill dams. In Proc. 13th World Conf. on Earthquake Engineering, Vancouver, Canada. 2004.

[123] Shao R, Wu C, and Li J. A comprehensive review on dry concrete: Application, raw material, preparation, mechanical, smart and durability performance. Journal of Building Engineering, 2022, 55:104676.

[124] Xiao R, Jiang X, Zhang M, Polaczyk P, and Huang B. Analytical investigation of phase assemblages of alkali-activated materials in CaO-SiO2-Al2O3 systems: The management of reaction products and designing of precursors. Materials and Design, 2020, 194:108975.

[125] Xiao R, Zhang Y, Jiang X, Polaczyk P, Ma Y, and Huang B. Alkali-activated slag supplemented with waste glass powder: Laboratory characterization, thermodynamic modelling and sustainability analysis. Journal of Cleaner Production, 2021, 286:125554.

[126] Feng J, Yin G, Tuo H, and Niu Z. Parameter optimization and regression analysis for multi-index of hybrid fiber-reinforced recycled coarse aggregate concrete using orthogonal experimental design. Construction and Building Materials, 2021, 267:121013.

[127] Wang Q, Feng J J, and Yan P Y. An explanation for the negative effect of elevated temperature at early ages on the late-age strength of concrete. Journal of Materials Science, 2011, 46(22):7279-7288.

[128] Balabio C B, Sala G, and Amira A. Effect of temperature on the development of C-S-H during early hydration of C3S. Organometallics, 2010, 24(8):1996-1999.

[129] Shen P, Lu L, He Y, Wang F, and Hu S. The effect of curing regimes on the mechanical properties, nano-mechanical properties and microstructure of ultra-high performance concrete. Cement and Concrete Research, 2019, 118:1-13.

[130] Wang D, Shi C, Wu Z, Xiao J, Huang Z, and Fang Z. A review on ultra-high performance concrete: Part II. Hydration, microstructure and properties.

Construction and Building Materials, 2015, 96:368-377.

[131] Li S, Zhang Y, Pan Y, and Gao X. Effects of isothermal microwave heating on the strength and microstructure of ultra-high performance concrete embedded with steel fibers. Journal of Materials Research and Technology, 2021, 14:1893-1902.

[132] Liu G, Florea M V A, and Brouwers H J H. Characterization and performance of high volume recycled waste glass and ground granulated blast furnace slag or fly ash blended mortars. Journal of Cleaner Production, 2019, 235:461-472.

[133] Sun J, Zhang Z, and Hou G. Utilization of fly ash microsphere powder as a mineral admixture of cement: Effects on early hydration and microstructure at different curing temperatures. Powder Technology, 2020, 375:262-270.

[134] Zhang J, Chen T, and Gao X. Incorporation of self-ignited coal gangue in steam cured precast concrete. Journal of Cleaner Production, 2021, 292:126004.

[135] Yu R, Spiesz P, and Brouwers H. Mix design and properties assessment of ultra-high performance fibre reinforced concrete (UHPFRC). Cement and Concrete Research, 2014, 56:29-39.

[136] Long G, Gao Y, and Xie Y. Designing more sustainable and greener self-compacting concrete. Construction and Building Materials, 2015, 84:301-306.

[137] Zhang Y, Zhang J, Luo W, Wang J, Shi J, Zhuang H, and Wang Y. Effect of compressive strength and chloride diffusion on life cycle CO2 assessment of concrete containing supplementary cementitious materials. Journal of Cleaner Production, 2019, 218:450-458.

[138] Song Q, Yu R, Shui Z, Rao S, Wang X, Sun M, and Jiang C. Steel fibre content and interconnection induced electrochemical corrosion of ultra-high performance fibre reinforced concrete (UHPFRC). Cement and Concrete Composites, 2018, 94:191-200.

[139] Wu Z, Shi C, He W, and Wu L. Effects of steel fiber content and shape on mechanical properties of ultra high performance concrete. Construction and Building Materials, 2016, 103:8-14.

[140] Xu K, Huang W, Zhang L, Fu S, Chen M, Ding S, and Han B. Mechanical properties

of low-carbon ultrahigh-performance concrete with ceramic tile waste powder. Construction and Building Materials, 2021, 287:123036.

[141] Brito I d S, Rambo D A S, Martini S, Salvador R P, and Freitas M F d M. Flexural behavior of HPFRCC: Enhancing post-crack strength and toughness by magnetic alignment of the reinforcement. Construction and Building Materials, 2021, 269:121265.

[142] Yu R, Song Q, Wang X, Zhang Z, Shui Z, and Brouwers H. Sustainable development of ultra-high performance fibre reinforced concrete (UHPFRC): Towards to an optimized concrete matrix and efficient fibre application. Journal of Cleaner Production, 2017, 162:220-233.

[143] Sharbatdar M K and Rahmati F. Experimental evaluation of multi-functional effects of fibers on mechanical and performance properties of roller-compacted concrete pavements (RCCP). Construction and Building Materials, 2022, 316:125890.

[144] Al-Tameemi A A and A'mina K M. Influence of polypropylene fibers reinforcement on the mechanical properties of roller compacted concrete used in airports with partial replacement of cement by cement kiln dust. In Journal of Physics: Conference Series. 2021. IOP Publishing.

[145] Khan M, Cao M, and Ali M. Cracking behaviour and constitutive modelling of hybrid fibre reinforced concrete. Journal of Building Engineering, 2020, 30:101272.

[146] Scorza D, Luciano R, Mousa S, and Vantadori S. Fracture behaviour of hybrid fibre-reinforced roller-compacted concrete used in pavements. Construction and Building Materials, 2021, 271:121554.

[147] ACI 325.10R. Report on Roller-Compacted Concrete Pavement. American Concrete Institute, 2001.

[148] Chinese National Standard. Standard for test methods of concrete physical and mechanical properties, GB/T 50081 - 2019. Beijing, China, 2019.

[149] Chinese National Standard. Standard test methods for fiber reinforced concrete, CECS 13 : 2009. Beijing, China, 2009.

[150] Chinese National Standard. Test method of cement mortar strength (ISO method),

GB/T 17671 - 2021. Beijing, China, 2021.

[151] Wei J, Li J, Wu C, Liu Z, and Li J. Hybrid fibre reinforced ultra-high performance concrete beams under static and impact loads. Engineering Structures, 2021, 245:112921.

[152] Wu Z, Shi C, He W, and Wang D. Static and dynamic compressive properties of ultra-high performance concrete (UHPC) with hybrid steel fiber reinforcements. Cement and Concrete Composites, 2017, 79:148-157.

[153] Yu R, Spiesz P, and Brouwers H. Static properties and impact resistance of a green ultra-high performance hybrid fibre reinforced concrete (UHPHFRC): Experiments and modeling. Construction and Building Materials, 2014, 68:158-171.

[154] Yoo D-Y, Kim S-W, and Park J-J. Comparative flexural behavior of ultra-high-performance concrete reinforced with hybrid straight steel fibers. Construction and Building Materials, 2017, 132:219-229.

[155] Banthia N and Sappakittipakorn M. Toughness enhancement in steel fiber reinforced concrete through fiber hybridization. Cement and Concrete Research, 2007, 37(9):1366-1372.

[156] Khan M and Ali M. Improvement in concrete behavior with fly ash, silica-fume and coconut fibres. Construction and Building Materials, 2019, 203:174-187.

[157] Wang D, Shi C, Wu Z, Xiao J, Huang Z, and Fang Z. A review on ultra high performance concrete: Part II. Hydration, microstructure and properties. Construction and Building Materials, 2015, 96:368-377.

[158] Graybeal B A. Material property characterization of ultra-high performance concrete. United States. Federal Highway Administration. Office of Infrastructure …, 2006.

[159] Sahmaran M and Yaman I O. Hybrid fiber reinforced self-compacting concrete with a high-volume coarse fly ash. Construction and Building Materials, 2007, 21(1):150-156.

[160] Cohn M and Bartlett M. Computer-simulated flexural tests of partially prestressed concrete sections. Journal of the Structural Division, 1982, 108(12):2747-2765.

[161] Yang Y, Wu C, Liu Z, Wang H, and Ren Q. Mechanical anisotropy of ultra-high performance fibre-reinforced concrete for 3D printing. Cement and Concrete Composites, 2022, 125:104310.

[162] Jin R, Chen Q, and Soboyejo A B. Non-linear and mixed regression models in predicting sustainable concrete strength. Construction and Building Materials, 2018, 170:142-152.

[163] Jin R, Yan L, Soboyejo A B O, Huang L, and Kasal B. Multivariate regression models in estimating the behavior of FRP tube encased recycled aggregate concrete. Construction and Building Materials, 2018, 191:216-227.

[164] Wu H, Wang C, and Ma Z. Drying shrinkage, mechanical and transport properties of sustainable mortar with both recycled aggregate and powder from concrete waste. Journal of Building Engineering, 2022, 49:104048.

[165] Strukar K, Kalman Šipoš T, Miličević I, and Bušić R. Potential use of rubber as aggregate in structural reinforced concrete element - A review. Engineering Structures, 2019, 188:452-468.

[166] Gencel O, Oguz M, Gholampour A, and Ozbakkaloglu T. Recycling waste concretes as fine aggregate and fly ash as binder in production of thermal insulating foam concretes. Journal of Building Engineering, 2021, 38:102232.

[167] Singh N, Kumar P, and Goyal P. Reviewing the behaviour of high volume fly ash based self compacting concrete. Journal of Building Engineering, 2019, 26:100882.

[168] Chinese National Standard. Common portland cement, GB 175 - 2020. Beijing, China, 2020.

[169] Zou F, Hu C, Wang F, Ruan Y, and Hu S. Enhancement of early-age strength of the high content fly ash blended cement paste by sodium sulfate and C–S–H seeds towards a greener binder. Journal of Cleaner Production, 2020, 244:118566.

[170] Ashraf M, Iqbal M F, Rauf M, Ashraf M U, Ulhaq A, Muhammad H, and Liu Q-f. Developing a sustainable concrete incorporating bentonite clay and silica fume: Mechanical and durability performance. Journal of Cleaner Production, 2022, 337:130315.

[171] Pu X. Investigation on pozzolanic effect of mineral additives in cement and concrete by specific strength index. Cement and Concrete Research, 1999, 29(6):951-955.

[172] Madhkhan M and Katirai R. Effect of pozzolanic materials on mechanical properties and aging of glass fiber reinforced concrete. Construction and Building Materials, 2019, 225:146-158.

[173] Zhang D, Zhao J, Wang D, Wang Y, and Ma X. Influence of pozzolanic materials on the properties of natural hydraulic lime based mortars. Construction and Building Materials, 2020, 244:118360.

[174] Cao C, Sun W, and Qin H. The analysis on strength and fly ash effect of roller-compacted concrete with high volume fly ash. Cement and Concrete Research, 2000, 30(1):71-75.

[175] Shao R, Wu C, Li J, and Liu Z. Investigation on the mechanical characteristics of multiscale mono/hybrid steel fibre-reinforced dry UHPC. Cement and Concrete Composites, 2022, 133:104681.

[176] Thakur A, Senthil K, Sharma R, and Singh A. Employment of crumb rubber tyre in concrete masonry bricks. Materials Today: Proceedings, 2020, 32:553-559.

[177] Turatsinze A and Garros M. On the modulus of elasticity and strain capacity of self-compacting concrete incorporating rubber aggregates. Resources, Conservation and Recycling, 2008, 52(10):1209-1215.

[178] ACI 213.R3. Guide for structural lightweigth aggregate concrete. American Concrete Institute, 2003.

[179] Chinese National Standard. Technical specification for lightweight aggregate concrete, JGJ 51 - 90. Beijing, China, 1990.

[180] AS 1379. Specification and supply of concrete. Australian Standard, 2007.

[181] Mohammed B S, Adamu M, and Liew M S. Evaluating the effect of crumb rubber and nano silica on the properties of high volume fly ash roller compacted concrete pavement using non-destructive techniques. Case Studies in Construction Materials, 2018, 8:380-391.

[182] Kazmi S M S, Munir M J, and Wu Y-F. Application of waste tire rubber and recycled

aggregates in concrete products: A new compression casting approach. Resources, Conservation and Recycling, 2021, 167:105353.

[183] Xue J and Shinozuka M. Rubberized concrete: A green structural material with enhanced energy-dissipation capability. Construction and Building Materials, 2013, 42:196-204.

[184] Sofi A. Effect of waste tyre rubber on mechanical and durability properties of concrete - A review. Ain Shams Engineering Journal, 2018, 9(4):2691-2700.

[185] Alsaif A, Koutas L, Bernal S A, Guadagnini M, and Pilakoutas K. Mechanical performance of steel fibre reinforced rubberised concrete for flexible concrete pavements. Construction and Building Materials, 2018, 172:533-543.

[186] Turatsinze A, Granju J-L, and Bonnet S. Positive synergy between steel-fibres and rubber aggregates: effect on the resistance of cement-based mortars to shrinkage cracking. Cement and Concrete Research, 2006, 36(9):1692-1697.

[187] ACI 207.5R. Report on Roller Compacted Mass Concrete. ACI Manual of Concrete Practice, 2011.

[188] Li Y, Zeng X, Zhou J, Shi Y, Umar H A, Long G, and Xie Y. Development of an eco-friendly ultra-high performance concrete based on waste basalt powder for Sichuan-Tibet Railway. Journal of Cleaner Production, 2021, 312:127775.

[189] Shi Y, Long G, Zen X, Xie Y, and Shang T. Design of binder system of eco-efficient UHPC based on physical packing and chemical effect optimization. Construction and Building Materials, 2021, 274:121382.

[190] Long W, Li H, Wei J, Xing F, and Han N. Sustainable use of recycled crumb rubbers in eco-friendly alkali activated slag mortar: Dynamic mechanical properties. Journal of Cleaner Production, 2018, 204:1004-1015.

[191] Wu Z, Shi C, and He W. Comparative study on flexural properties of ultra-high performance concrete with supplementary cementitious materials under different curing regimes. Construction and Building Materials, 2017, 136:307-313.

[192] He Z, Shen M, Shi J, Yalçınkaya Ç, Du S, and Yuan Q. Recycling coral waste into eco-friendly UHPC: Mechanical strength, microstructure, and environmental

benefits. Science of The Total Environment, 2022:155424.

[193] Yu R, Spiesz P, and Brouwers H. Development of an eco-friendly Ultra-High Performance Concrete (UHPC) with efficient cement and mineral admixtures uses. Cement and Concrete Composites, 2015, 55:383-394.

[194] Jahanbakhsh P, Saberi K F, Soltaninejad M, and Hashemi S H. Laboratory investigation of modified roller compacted concrete pavement (RCCP) containing macro synthetic fibers. International Journal of Pavement Research and Technology, 2022:1-15.

[195] Wang X, Zhang S, Wang C, Song R, Shang C, and Fang X. Experimental investigation of the size effect of layered roller compacted concrete (RCC) under high-strain-rate loading. Construction and Building Materials, 2018, 165:45-57.

[196] Ghaedi K, Hejazi F, Ibrahim Z, and Khanzaei P. Flexible foundation effect on seismic analysis of Roller Compacted Concrete (RCC) dams using finite element method. KSCE Journal of Civil Engineering, 2018, 22(4):1275-1287.

[197] Ghaedi K, Jameel M, Ibrahim Z, and Khanzaei P. Seismic analysis of Roller Compacted Concrete (RCC) dams considering effect of sizes and shapes of galleries. KSCE Journal of Civil Engineering, 2016, 20(1):261-272.

[198] Gharibdoust A, Aldemir A, and Binici B. Seismic behaviour of roller compacted concrete dams under different base treatments. Structure and Infrastructure Engineering, 2020, 16(2):355-366.

[199] Hosseinnezhad H, Hatungimana D, and Ramyar K. Mechanical properties of roller compacted concrete containing recycled concrete aggregate. Revista de La Construcción, 2021, 20(2):277-290.

[200] Adamu M, Mohammed B S, Liew M S, and Alaloul W S. Evaluating the impact resistance of roller compacted concrete containing crumb rubber and nanosilica using response surface methodology and Weibull distribution. World Journal of Engineering, 2019, 16(1):33-43.

[201] Gupta T, Sharma R K, and Chaudhary S. Impact resistance of concrete containing waste rubber fiber and silica fume. International Journal of Impact Engineering,

2015, 83:76-87.

[202] Zhang W, Chen S, and Liu Y. Effect of weight and drop height of hammer on the flexural impact performance of fiber-reinforced concrete. Construction and Building Materials, 2017, 140:31-35.

[203] Yoo D Y, Yoon Y S, and Banthia N. Flexural response of steel-fiber-reinforced concrete beams: Effects of strength, fiber content, and strain-rate. Cement and Concrete Composites, 2015, 64:84-92.

[204] Yoo D Y, Banthia N, Kang S T, and Yoon Y S. Effect of fiber orientation on the rate-dependent flexural behavior of ultra-high-performance fiber-reinforced concrete. Composite Structures, 2016, 157:62-70.

[205] Onuaguluchi O, Ratu R, and Banthia N. Effect of sodium sulfate activation on the early-age matrix strength and steel fiber bond in high volume fly ash (HVFA) cement mortar. Construction and Building Materials, 2022, 341:127808.

[206] Hao Y, Hao H, and Chen G. Experimental investigation of the behaviour of spiral steel fibre reinforced concrete beams subjected to drop-weight impact loads. Materials and Structures, 2016, 49(1):353-370.

[207] Holschemacher K, Mueller T, and Ribakov Y. Effect of steel fibres on mechanical properties of high-strength concrete. Materials and Design, 2010, 31(5):2604-2615.

[208] Ali M, Soliman A, and Nehdi M. Hybrid-fiber reinforced engineered cementitious composite under tensile and impact loading. Materials and Design, 2017, 117:139-149.

[209] Chen M, Zhong H, and Zhang M. Flexural fatigue behaviour of recycled tyre polymer fibre reinforced concrete. Cement and Concrete Composites, 2020, 105:103441.

[210] Zhu X, Chen X, Liu S, Li S, Xuan W, and Chen Y. Experimental study on flexural fatigue performance of rubberised concrete for pavement. International Journal of Pavement Engineering, 2020, 21(9):1135-1146.

[211] Alsaif A, Garcia R, Figueiredo F P, Neocleous K, Christofe A, Guadagnini M, and Pilakoutas K. Fatigue performance of flexible steel fibre reinforced rubberised

concrete pavements. Engineering Structures, 2019, 193:170-183.

[212] Prasad N and Murali G. Exploring the impact performance of functionally-graded preplaced aggregate concrete incorporating steel and polypropylene fibres. Journal of Building Engineering, 2021, 35:102077.

[213] Murali G, Abid S R, Amran Y M, Abdelgader H S, Fediuk R, Susrutha A, and Poonguzhali K. Impact performance of novel multi-layered prepacked aggregate fibrous composites under compression and bending. Structures, 2020, 28:1502-1515.